

①

DTIC FILE C

PROCEEDINGS OF THE ATMOSPHERIC NEUTRAL DENSITY SPECIALIST CONFERENCE

AD-A225 249

HELD AT THE RAINTREE INN, AIRPORT
COLORADO SPRINGS, COLORADO
22 - 23 MARCH 1988

DTIC
FILE
MAR 30 1988
w l

APPROVED FOR PUBLIC RELEASE; DISTRIBUTION UNLIMITED

See p 1

REPRODUCED BY
U.S. DEPARTMENT OF COMMERCE
NATIONAL TECHNICAL INFORMATION SERVICE
SPRINGFIELD, VA 22161

90

SESSION CHAIRMEN

SESSION 1

Lt Col George R. Davenport
HQ 4th Weather Wing

SESSION 2

CAPT John L. Sullivan, USN
HQ USSPACECOM/J3S

SESSION 3

Dr Michael Gaposchkin
MIT Lincoln Laboratories

SESSION 4

Dr Joseph J.F. Liu
HQ AFSPACECOM/DOA

Accession For	
NTIS GRA&I	<input checked="checked" type="checkbox"/>
DTIC TAB	<input type="checkbox"/>
Unannounced	<input type="checkbox"/>
Justification	
Distribution/	
Availability Codes	
and/or	
Special	
A-1	

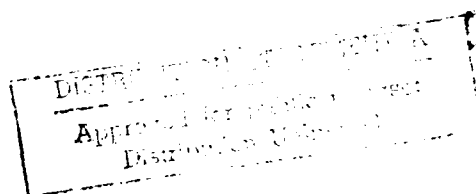


TABLE OF CONTENTS

Session Chairmen.....	ii
Introduction.....	vi
Schedule.....	ix
Opening Remarks - BGen Van Inwegen.....	1

Session 1

REQUIREMENTS

Chairman: Lt Col George R. Davenport
Headquarters Fourth Weather Wing

Air Weather Service Neutral Atmospheric Modeling Requirements.....	5
Captain Chris R. Tschan HQ AWS/DNXP	
Air Force Space Command Requirements for Neutral Atmospheric Density Specification and Prediction.....	24
Lt Col George R. Davenport HQ 4th Weather Wing	
Naval Space Surveillance Center Atmospheric Drag Requirements.....	34
Dr Stephen H. Knowles NAVSPASUR	

Session 2

OPERATIONS SUPPORT

Chairman: CAPT John L. Sullivan, USN
Headquarters United States Space Command/J3S

Space Control Operations - Meeting the Challenge.....	43
Captain Colette M. de la Barre HQ USSPACECOM/J3S	
MSFC's Modeling and Use of Orbital Density Results.....	53
Mr Dale Johnson NASA-MSFC/ED44	

A Summary of Civilian Neutral Density Modelers Utilizing Services from the Space Environment Services Center.....	60
Mr Gary Heckman NOAA R/E/SE2	
Options for Improving Drag Calculations at NAVSPASUR.....	62
Dr Paul W. Schumacher, Jr NAVSPASUR	
MIT Lincoln Laboratory Analysis of Satellite Drag.....	88
Dr E. M. Gaposchkin and A. J. Coster MIT Lincoln Laboratory	

Session 3

STATE-OF-THE-ART MODELS AND PROSPECTS

Chairman: Dr E. M. Gaposchkin
MIT/Lincoln Laboratories

Accuracy of Satellite Drag Models.....	120
Mr Frank A. Marcos Air Force Geophysics Laboratory	
MSIS Empirical Model Status and Directions for Improvement.....	140
Mr A. E. Hedin NASA/GSFC	
Measurements of Atmospheric Structure.....	154
Dr Jeng-Hwa Yee, Paul B. Hays, V. J. Abreu, W. R. Skinner, C. R. Cornish, and M. C. Luo The University of Michigan	
A Coupled Thermosphere/Ionosphere General Circulation Model.....	177
Dr Raymond G. Roble, E. C. Ridley, A. D. Richmond, and R. E. Dickinson National Center for Atmospheric Research	
EUV Monitoring and Geomagnetic Storm Forecasts Using the USAF-NOAA Solar X-Ray Imagers.....	241
Dr W. J. Wagner Space Environment Laboratory	

The Remote Atmospheric and Ionospheric Detection System.....	250
Dr A. B. Christensen, J. Pranke, G. G. Sivjee, and D. Kayser The Aerospace Corporation and, R. P. McCoy, K. D. Wolfram, R. R. Meier, L. J. Paxton, D. D. Cleary, D. K. Prinz, D. E. Anderson, Jr Naval Research Laboratory	

Session 4

SUMMARY AND RECOMMENDATIONS

Chairman: Dr Joseph J. F. Liu
Headquarters Air Force Space Command/DOA

Summary of the Neutral Density Conference.....	283
Dr H. Beat Wackernagel HQ AFSPACECOM/DOA	
Summary, Action Items, and Subsequent Events.....	285
Lt Col George R. Davenport HQ 4th Weather Wing	
Distribution List.....	A1-1

INTRODUCTION

Ever since the first man-made Earth satellite was launched in 1957, the scientific community has undertaken extensive and intensive studies of the atmospheric density at satellite altitudes. The critical impact of the neutral density upon orbital motion motivated research at various institutions and resulted in diverse models, developed for a wide range of space systems and mission applications.

Atmospheric neutral density research and neutral density model development continue at numerous government and private facilities. Each is attempting to resolve its own problems, but the issues to be addressed throughout the community remain closely related.

Many analytical and empirical atmospheric neutral density models have been developed over the last 25 years, and implemented in various operational, research, and development systems. These models are qualitatively equivalent but numerically different. In applications for example, the associated ballistic coefficients for a near-Earth satellite can be significantly different if the density models are different. Thus the orbital data can not be interchanged without experiencing loss of accuracy. This is a typical example of astrodynamic compatibility problems. This proliferation of incompatible models has created serious communication and data sharing difficulties; sophisticated conversion algorithms may be required to bring about compatibility between the space centers and their data users.

In recent years, the Air Force Space Command Directorate of Operations Analysis (formerly the Directorate of Astrodynamics) and a number of other professional organizations have conducted independent studies regarding the state-of-the-art atmospheric neutral density models and their respective performance in space systems. These studies have all concluded that, despite extensive research efforts, the scientific community has produced no significant improvement in either neutral density model accuracy or computational efficiency in the last two decades. The general agreement is that all available empirical neutral density models, those that input the measured 10.7 cm solar flux and a geomagnetic index, still exhibit an average error in the neighborhood of 15 percent and that the newer models tend to be more complex and thus are less efficient. In addition, the solar flux and geomagnetic indices are extremely difficult to predict. Therefore, the prediction of satellite orbits and positions remain inaccurate and unreliable.

Many government agencies, research institutions, and laboratories are expending tremendous effort to address the atmospheric neutral density development and are making encouraging progress. However, the problem is extremely complex, the focus of interest remains diverse throughout the scientific community, and research and development funds are becoming ever more limited. Therefore Air Force Space Command decided to sponsor this conference to offer a forum to coordinate and promote atmospheric neutral density research and development that is ultimately targeted at supporting space operations requirements.

Operational neutral density model users were invited to discuss their operational requirements and the difficulties that they have encountered, and atmospheric scientists were asked to present recent advances and prospects for improvement in the neutral density models. Cooperation and dialogue among members of the atmospheric neutral density operational and research communities is mutually beneficial and, in fact, synergistic. The scientific community needs relevance to justify continued research during this era of tight fiscal restraint, and they need data to develop and validate the advanced algorithms that will ultimately comprise improved models. The operational community has cited and validated requirements to specify and to predict the atmospheric neutral density at satellite altitudes with specific accuracy requirements as a function of altitude. Progress will continue only so long as the various agencies continue to provide mutual support.

The operators were invited from 4th Weather Wing (4WW), Air Force Space Command (AFSPACCOM), Air Weather Service (AWS), Air Force Global Weather Central (AFGWC), Naval Space Surveillance Center (NAVSPASUR), and United States Space Command (USSPACECOM); atmospheric scientists were invited from Air Force Geophysics Laboratory (AFGL), NASA Goddard Space Flight Center (GSFC), NASA Marshall Space Flight Center (MSFC), National Oceanic and Atmospheric Administration (NOAA), National Center for Atmospheric Research (NCAR), MIT Lincoln Laboratory (LL), and the University of Michigan (UM).

Topics for the presentations were selected to provide information and to generate discussion among the conference participants. The specific session topics included:

- o Examine the status of the current operational requirements and operational difficulties,
- o Assess the state-of-the-art atmospheric neutral density models and operational feasibilities,

- o Identify the available databases and additional data necessary for further improvements,
- o Address the operational standardization/compatibility issues;
- o Consolidate the near-term and long-term research and development activities, inter-agency cooperation/ collaboration and funding support, and
- o Generate and document recommendations and action items.

The conference was held at the Raintree Inn, Airport, in Colorado Springs, Colorado, on 22 and 23 March 1988, and was well attended.

JOSEPH J. F. LIU
GEORGE R. DAVENPORT
Co-Chairmen

ATMOSPHERIC NEUTRAL DENSITY SPECIALIST CONFERENCE

General Co-Chairmen

Dr Joseph Liu/DOA and Lt Col George R. Davenport/HQ 4WW

Raintree Inn - Airport, Colorado Springs, CO

AGENDA

22 March 1988, Tuesday

0800 - 0830 Registration
0830 - 0835 Welcome Attendees
0835 - 0845 Col Pfeffer/DOW
0845 - 0855 Col Sundberg/DOA

Session 1

REQUIREMENTS

Chairman: Lt Col Davenport/HQ 4WW

0855 - 0900 Chairman Opening Statement
0900 - 0930 "Air Weather Service Neutral Atmospheric Modeling
Requirements"
Captain Chris R. Tschan, HQ AWS/DNXP
0930 - 1000 "Air Force Space Command Requirements for Neutral
Atmospheric Density Specification and Prediction"
Lt Col Davenport, HQ 4WW
1000 - 1030 Coffee Break
1030 - 1100 Captain Patterson/Major Thedick, SAC*
1100 - 1130 "Naval Space Surveillance Center Atmospheric Drag
Requirements"
Dr Stephen H. Knowles, NAVSPASUR
1130 - 1200 Open Discussion
1200 - 1330 Lunch Break

*Did not attend Conference

Session 2

OPERATIONS SUPPORT

Chairman: CAPT Sullivan, USN, HQ USSPACECOM/J3S

1330 - 1335 Chairman Opening Statement
1335 - 1405 Captain Clausen, AFGWC*
1405 - 1435 "Space Control Operations - Meeting the Challenge"
Captain Colette M. de la Barr, J3S
1435 - 1505 "MSFC Modeling and Use of Orbital Density Results"
Mr Dale Johnson/Dr Robert Smith, MSFC
1505 - 1525 Coffee Break
1525 - 1555 "A Summary of Civilian Neutral Density Modelers
Utilizing Services from the Space Environment
Services Center"
Mr Gary Heckman, NOAA R/E/SE2
1555 - 1625 "Options for Improving Drag Calculations at
NAVSPASUR"
Dr Paul W. Schumacher, Jr, NAVSPASUR
1625 - 1645 "MIT Lincoln Laboratory Analysis of Satellite Drag"
Dr E. M. Gaposchkin and A. J. Coster, MIT Lincoln
Laboratory
1830 - 2100 Cash Bar, Dinner, and Social Activity

23 March 1988, Wednesday

0800 - 0820 Welcome Address - Brig General Van Inwegen

Session 3

STATE-OF-THE-ART MODELS AND PROSPECTS

Chairman: Dr Gaposchkin/LL

0820 - 0825 Chairman Opening Statement
0825 - 0855 "Accuracy of Satellite Drag Models"
Mr Frank A. Marcos, Air Force Geophysics
Laboratory

0855 - 0925 "MSIS Empirical Model Status and Directions for Improvement"
Mr A. E. Hedin, NASA/GSFC

0925 - 0955 "Measurements of Atmospheric Structure"
Dr J. H. Yee, University of Michigan

0955 - 1025 Coffee Break

1025 - 1055 "A Coupled Thermosphere/Ionosphere General Circulation Model"
Dr Raymond G. Roble, National Center for Atmospheric Research

1055 - 1125 "EUV Monitoring and Geomagnetic Storm Forecasts Using the USAF-NOAA Solar X-Ray Imagers"
Dr W. J. Wagner, Space Environment Laboratory

1125 - 1155 "The Remote Atmospheric and Ionospheric Detection System"
Dr Andrew R. Christensen, The Aerospace Corporation

1155 - 1225 Col Sundberg, DOA

1225 - 1400 Lunch Break

Session 4

SUMMARY AND RECOMMENDATIONS

Chairman: Dr Liu/DOA

1400 - 1410 Chairman Opening Statement

1410 - 1440 "Summary of the Neutral Density Conference"
Dr H. Beat Wackernagel, DOA

1440 - 1510 "Summary, Action Items, and Subsequent Events"
Lt Col George Davenport, HQ 4WW

1510 - 1540 Open Discussions - "Future Activities and Milestones"

1540 - 1600 Closing Remarks - Col Sundberg, DOA

GENERAL EARL VAN INWEGEN'S REMARKS
TO
NEUTRAL DENSITY SPECIALITY CONFERENCE

22 MARCH 1988

WELCOME ... I'M DELIGHTED TO HAVE THE OPPORTUNITY TO WELCOME YOU TO COLORADO SPRINGS AND TO SPACE COMMAND.

MAKING OPENING REMARKS ON THE SECOND DAY OF A CONFERENCE IS INDICATIVE OF THE SIGN OF THE TIMES. THE PRESS OF THE CURRENT BUDGET PROBLEM ... OF HAVING TO MINIMIZE THE OPERATIONAL IMPACT OF DOING LESS WITH LESS ...

AT LEAST I'M HERE ON THE SECOND DAY!!!

ACCEPTING THE FACT THAT WE WILL HAVE TO DO LESS WITH LESS IS A HARD BUT NECESSARY PILL TO SWALLOW. IT IS UP TO US ... ALL OF US ... TO MINIMIZE THE OPERATIONAL IMPACT OF HAVING LESS.

IN ASTRODYNAMICS WE HAVE AN OPPORTUNITY TO MAYBE NOT HAVE TO DECIDE HOW WE WILL DO LESS ... EVEN THOUGH WE GET LESS ... BECAUSE I BELIEVE THAT IF WE WORK TOGETHER AND FOCUS OUR EFFORTS, WE MIGHT BE ABLE TO DO MORE ... EVEN THOUGH OUR BUDGETS ARE SHRINKING IN REAL TERMS.

IN A VERY REAL SENSE, THAT IS THE PURPOSE OF THIS CONFERENCE ...

WHAT CAN WE DO BETTER BY WORKING TOGETHER?

WHAT CAN BE ACHIEVED IF WE COOPERATE?

THIS IS THE FIRST CONFERENCE WE, AIR FORCE SPACE COMMAND, HAVE SPONSORED AS PART OF THE NEW DIRECTION WE ARE TAKING IN DEALING WITH OPERATIONAL ASTRODYNAMICS.

WE HAVE THREE MAJOR UNDERTAKINGS IN OUR SPACE COMMAND OPERATIONS, DIRECTORATE OF OPERATIONS ANALYSIS ... WHICH MANY OF YOU MIGHT REMEMBER AS OUR DIRECTORATE OF ASTRODYNAMICS ... FOR 1988.

THE FIRST IS A COMPREHENSIVE REVIEW OF THE ERRORS IN OUR ASTRODYNAMIC ORBIT DETERMINATION AND PROPAGATION METHODOLOGIES.

IF WE CAN ACCURATELY CHARACTERIZE THE ERROR SOURCES AND THE IMPACT OF THOSE ERRORS ON OUR OPERATIONS ... WE HAVE THE KEY FOR GETTING STRONG SUPPORT FOR RESEARCH AND DEVELOPMENT IN ASTRODYNAMICS.

WITHOUT THAT FOUNDATION I BELIEVE IT WILL BE VIRTUALLY IMPOSSIBLE TO WIN IN THE BUDGET BATTLE.

OUR SECOND MAJOR INITIATIVE IS DEVELOPMENT OF AN ASTRODYNAMIC STANDARD FOR MILITARY SPACE OPERATIONS.

WE ALL STARTED WITH THE SAME PHYSICS, THE SAME DATA BASES, AND THE SAME MATH A NUMBER OF YEARS AGO. THINGS WERE SO MUCH SIMPLER THEN.

WHEN THERE WERE ONLY A FEW SATELLITE PROGRAMS AND THE TOTAL NUMBER OF MAN MADE OBJECTS IN ORBIT WERE NUMBERED IN THE HUNDREDS INSTEAD OF THE THOUSANDS AND TENS OF THOUSANDS, WE COULD TALK TO EACH OTHER.

SPACE HAS, HOWEVER, GROWN UP AND NOW IT IS COMPLEX. IN A NUMBER OF INSTANCES, THAT COMPLEXITY IS NOT AN ESSENTIAL CHARACTERISTIC ... IT IS MAN MADE.

WE ARE LOOKING IN OUR OPERATIONS ANALYSIS SHOP AT HOW TO STEP AWAY FROM SOME OF THAT COMPLEXITY. IN SO DOING WE HOPE TO IMPROVE PERFORMANCE AND REDUCE COST AT THE SAME TIME.

OUR THIRD MAJOR INITIATIVE IS A SERIES OF PROGRAMS, OF WHICH THIS CONFERENCE IS THE FIRST, TO TRANSFORM THE GOOD IDEAS FROM THE ERROR ANALYSIS AND STANDARDS DEFINITION EFFORTS INTO REALITY.

AS YOU KNOW, WE FIX THE POSITION OF AN INCREDIBLE NUMBER OF NON-COOPERATIVE ORBITAL OBJECTS EACH DAY USING A VARIETY OF SENSORS OF VARYING QUALITY. THIS HAS LED US AND OTHERS IN OUR BUSINESS TO MAKE A NUMBER OF APPROXIMATIONS TO BOOST COMPUTATIONAL SPEED, TO COMPENSATE FOR THE QUALITY OF OUR OBSERVATIONS, AND TO COMPENSATE FOR POOR INPUT DATA.

ONE INPUT DATA THAT HAS BEEN AND CONTINUES TO BE WEAK IS NEUTRAL DENSITY.

WE RECOGNIZE THAT CONSIDERABLE GOOD, HIGH QUALITY RESEARCH HAS BEEN PERFORMED ON THE NEUTRAL DENSITY PROBLEM OVER THE LAST TWENTY YEARS. THE CONTRIBUTIONS YOU HAVE MADE ON SPECIFIC PROBLEMS ARE PARTICULARLY NOTEWORTHY BECAUSE OF THE DIFFICULTIES ASSOCIATED WITH HIGH ATMOSPHERE RESEARCH. I APPRECIATE THE FACT THAT WE HAVE NOT FOUND A WAY TO KEEP A SENSOR IN THE 50 TO 250 KILOMETER ALTITUDE RANGE FOR ANY EXTENDED PERIOD OF TIME. THAT FORCES YOU TO WORK A TOUGH PROBLEM WITH VERY LIMITED DATA.

OUR PROBLEM IS THAT FOR MOST OF THAT TWENTY YEARS THERE HAS NOT BEEN A SIGNIFICANT IMPROVEMENT IN NEUTRAL DENSITY MODELING FOR MILITARY SPACE OPERATIONS ... AND YET, IN THE LOW ALTITUDE DOMAIN, NEUTRAL DENSITY IS ONE OF THE PRINCIPAL ... IF NOT THE PRINCIPAL ... SOURCE OF ORBIT PROPAGATION ERROR.

WE, THE SPACE OPERATORS ... AIR FORCE SPACE COMMAND AND THE UNITED STATES SPACE COMMAND NEED BETTER NEUTRAL DENSITY MODELS TO DO TODAY'S MISSIONS BETTER AND MAKE TOMORROW'S MISSIONS POSSIBLE.

SO ... WHAT DO WE DO IN AN ENVIRONMENT WHERE MONIES FOR RESEARCH AND DEVELOPMENT ARE GOING AWAY?

HOW DO WE DO MORE?

HOW DO WE DO MORE WITH LESS?

HOW DO WE PREPARE FOR THE FUTURE?

I BELIEVE THE KEY TO DOING MORE WITH LESS IS CLOSE COOPERATION AND COORDINATION BETWEEN THE RESEARCH AND DEVELOPMENT COMMUNITIES AND THE CUSTOMERS ... THAT'S US, THAT'S THE SPACE OPERATORS.

WITH SUCH CLOSE COOPERATION THE RESEARCH COMMUNITIES WILL BETTER UNDERSTAND THE OPERATIONAL PROBLEMS WE FACE:

HOW DO YOU ACHIEVE THE REQUIRED ACCURACY WITH LESS THAN PERFECT INPUT DATA?

HOW DO YOU HANDLE NON-COOPERATIVE OBJECTS?

7

HOW DO YOU MINIMIZE THE COMPUTATIONAL PROCESS SO WE CAN LIVE WITH AVAILABLE COMPUTERS?

AT THE SAME TIME, WE THE OPERATORS WILL BETTER UNDERSTAND HOW TO USE THE TOOLS YOU PROVIDE US.

WE WILL ALSO BE IN A STRONG POSITION TO PROMOTE, PARTICIPATE IN, AND SUPPORT CRITICAL RESEARCH AND DEVELOPMENT EFFORTS. WE MAY EVEN BE IN A POSITION TO PROMOTE NEW, DEDICATED HIGH ATMOSPHERE SENSORS TO ELIMINATE SOME OF THE PROBLEMS WE HAVE WITH THE DATA TODAY.

ONLY TIME WILL TELL. THIS CONFERENCE IS, HOWEVER, A CRITICAL FIRST STEP. IT WILL BE FOLLOWED BY A MAJOR INITIATIVE ON ASTRODYNAMIC STANDARDS ... SO WE ALL CAN WORK EFFICIENTLY AND EFFECTIVELY TOGETHER.

WE CAN NOT AFFORD AN "ASTRO TOWER OF BABLE" ... AND YET THAT IS ALMOST WHAT WE HAVE TODAY.

SOMETIME SOON WE WILL PUBLISH OUR ASTRODYNAMICS STANDARDS PACKAGE FOR YOUR REVIEW AND COMMENT. THAT WILL BE FOLLOWED BY A DETAILED REPORT ON ERROR BUDGETS IN ASTRODYNAMICS.

WITH THOSE INITIATIVES IN PLACE, WE SHOULD COLLECTIVELY BE ABLE TO DEFINE AND DEFEND IN THE BUDGET PROCESS THE CRITICAL ASTRODYNAMICS RESEARCH AND DEVELOPMENT. AND, IN SO DOING, SIGNIFICANTLY ENHANCE FUTURE MILITARY SPACE OPERATIONS.

AND ... AS I SAID IN THE BEGINNING ... I AM EXTREMELY PLEASED TO SEE YOU HERE TODAY. I SINCERELY WISH YOU SUCCESS AS YOU DRAW THIS CONFERENCE TO A CLOSE ... BECAUSE YOUR SUCCESS IS OUR SUCCESS.

BEFORE YOU LEAVE, PLEASE TAKE A FEW MOMENTS TO REFLECT ON THIS EFFORT AND THEN GIVE US FEED-BACK. IF YOU ARE NOT SURE WE ARE ON THE RIGHT TRACK, LET US KNOW. WE NEED YOUR GOOD IDEAS AND YOUR SUPPORT ... WE NEED YOUR COOPERATION.

CLOSE COOPERATION IS OUR ONLY HOPE TO DO MORE WITH LESS.

NOW, I WILL BE GLAD TO TAKE A FEW MINUTES IF YOU HAVE ANY GENERAL OFFICER TYPE QUESTIONS ...

SESSION 1

REQUIREMENTS

LT COL GEORGE R. DAVENPORT
CHAIRMAN

Air Weather Service Neutral Atmospheric Modeling Requirements

Capt Chris Tschan

Space Physics Programs

HQ AWS/DNXP

Scott AFB IL 62225-5008

1. Introduction

It became apparent at the Neutral Density Workshop held at the Air Force Geophysics Lab (AFGL) during October 1987, that many members of the research community were not familiar with the methods used by Air Weather Service (AWS) and AFGL to evaluate space environmental support requirements, seek solutions to operational shortfalls, and finally provide operational support. This paper provides the overview of AWS space environmental support and how the neutral modeling requirements established by the space system operators that AWS supports fit into this system (Figure 1). After providing an understanding of AWS space environmental support, the operational support requirements and our neutral modeling plan are presented.

2. AWS Space Environmental Support

AWS is one of only two US government agencies with the responsibility to provide basic, operational space environmental support (Figure 2). The other organization is the National Oceanographic and Atmospheric Administration (NOAA). AWS and NOAA try to complement each other's observational and modeling capabilities so that unnecessary duplication is minimized. For example, observations of the space environment made by AWS and NOAA systems are shared. Furthermore, the output of models run by NOAA is available to AWS, and plans are being made to make the output of models currently under development for AWS available to NOAA. This spirit of cooperation has served both organizations well.

Using the shared data base mentioned above, NOAA has the ability to provide operational space environmental support to civilian agencies and individuals. One such civilian agency which may require NOAA support is the National Aeronautics and Space Administration (NASA). Meanwhile, AWS uses this same shared data base to provide basic space environmental support to all Department of Defense (DOD) organizations. This does not mean that other DOD organizations in the Army, Navy, or Air Force do not tailor AWS space environmental support products to their particular space system; it simply means that the tailored support is based on a forecast, alert, or analysis which originated from AWS.

In order for AWS to provide support to a space system operator, operational space environmental support requirements must be stated. Then, based on these stated requirements, AWS can determine whether an operational shortfall exists. If the answer is yes and research is required to address the shortfall, then AWS generates a geophysical requirement (GR) (Figure 3). In response to the GR, AFGL will evaluate the relevant research (6.1) and exploratory development (6.2) that has either been completed or is in progress. Applicable 6.1

research and 6.2 development can either be monitored or financially supported by AFGL with the goal of getting this research to the stage where it has matured and is ready to be transitioned into an operational algorithm. If the research has matured to a point where operational shortfalls can be satisfied, then AWS begins the program acquisition process. The first step is to generate a statement of operational need (SON). The Space Environmental Technology Transition (SETT) SON defines AWS space modeling needs. The method used to develop an operational algorithm is the technology transition (T²) program designed to use 6.3 advanced development followed by 3400 operations and maintenance operational software development to make the bridge between 6.2 exploratory development and an AWS operational capability. The technology transition program is managed jointly by AWS and AFGL, with AFGL maintaining technical interaction with T² model developers (Figure 4) and evaluating progress on development of the required model. Headquarters AWS monitors the progress AFGL is making on model development and ensures that operational needs are addressed during development.

At this time there are two organizations providing space environmental support: the Air Force Global Weather Central (AFGWC) located at Offutt AFB NE, and 4th Weather Wing (4 WW) located at Peterson AFB CO (Figure 4). AFGWC currently provides all centralized space environmental support. All available ground-based and space-based measurements are used by AFGWC, as well as computer models of the near-Earth space environment. The space forecast products of the AFGWC support many space system customers, in addition to the US Space Command (USSPACECOM) community, whose needs we are addressing here.

In 1984, 4 WW became the main AWS organization with space environmental support in its charter. Currently, 4 WW tailors centralized support from AFGWC to the units it directly supports, such as USSPACECOM, Air Force Space Command (AFSPACECOM), and North American Aerospace Defense Command (NORAD). In the near future, this will change. A new centralized forecast facility dedicated to space environmental support is being built at Falcon AFB CO. This unit will be called the Space Forecast Center (SFC) and will be subordinate to 4 WW (Figure 5). Once SFC is fully operational, all the centralized space environmental support currently done at the AFGWC will be transferred to the SFC. In addition, all the new space environmental support models being developed will also run at the SFC. Moving all the centralized space support to Colorado has several advantages. Since US space operations are managed in Colorado, management of space environmental support (by 4 WW) and the actual centralized support (by the SFC) should be close to the management of space operations, in order to be responsive.

The major areas where AFGWC currently provide space environmental support are geomagnetic, ionospheric, and spacecraft (Figure 6). The basic space environmental data and model-produced fields are then tailored to meet the operational requirements of different space systems. In the ionospheric support area, for example, three-dimensional electron density fields may be converted to maps of critical frequencies for high-frequency communications systems operators. While the areas of current support are indicated by solid lines, the area where we intend to provide future support is the neutral thermosphere, indicated by dashed lines.

There are two types of neutral density support required by AWS customers. The first type involves forecasting the effects of the atmosphere on spacecraft

orbits, particularly for satellites in low-Earth orbit. The other requirement is to provide neutral variable specification at a point. At this time, AWS does not provide either type of neutral atmospheric support. Instead, AWS provides forecasts of both geomagnetic indices and solar radio flux at 10.7 cm. The F10.7 flux is a proxy indicator of the solar extreme ultraviolet (EUV) radiation, which results in dayside thermospheric heating. These indices are then used by space system operators as input into neutral models which they run for themselves. For NORAD this consists of Jacchia's 1964 model.

Data used by AWS to provide space environmental support is collected from ground-based and space-based sources (Figure 7). The ground-based data sources include five different data measurement networks. Likewise, the space-based measurement systems are shown in Figure 8. Note that at this time, there are no measurement systems capable of providing either remote or in-situ neutral measurements to AWS. That shortfall has several implications. First, there is no way for AWS to use neutral measurements either to initialize or to verify the planned neutral model. Further, as we attempt to build a comprehensive understanding of the near-Earth space environment through both measurements and model, there is at least 99 percent of this near-Earth space environment that we currently are not observing.

AWS is acquiring a series of space environmental models (Figure 9). While each model can function in a stand-alone mode, it is logical to couple the input and output fields of the models in a manner similar to the way these regions are coupled in nature. Currently, the AWS ionospheric model is operational but undergoing evolutionary upgrades. The magnetospheric model is under development and will become operational in fiscal year 1990 (FY90). Further, we expect to begin advanced development of the proposed neutral model in FY89. Work on integration of the models and development of a solar/interplanetary model is expected to begin in FY90. When all the individual models are completed and integrated, AWS will have the first known space model that couples the physics of these different regions in a dynamic manner all the way back to the driving source, the Sun.

To look now in more detail at the area of interest, a block diagram of the neutral atmospheric model is shown in Figure 10. The main data sources for the model are shown at the top. These input data are reduced to a form usable by the model. At the same time, the neutral model is capable of accepting input from both the magnetospheric and ionospheric models. The neutral model will produce output fields of density, winds, temperature, and composition. User-specific application software will then be developed to address specific customer support requirements.

3. AWS Neutral Modeling Requirements

Now that we have seen an overview of how AWS provides space environmental support, it's appropriate to look at the specific neutral atmospheric support requirements. Figure 11 provides these details by first showing the two groups of customers requiring support.

These requirements are quite simple. The USSPACECOM/AFSPACECOM/NORAD community requires forecasts of the neutral atmosphere out to 72 hours while other DOD space system operators require neutral atmospheric specification at particular locations or points.

The output variables for both customer groups are the same: neutral density, neutral winds, neutral temperatures, and neutral composition. The consolidated altitude range and accuracy goals of interest are also shown.

4. Neutral Modeling Status

An appropriate question following exposure to the neutral modeling requirements could be, "Where do we stand on this program?" These details are outlined in Figure 12. Frank Marcos, AFGL/LIS, is the manager for model development. To make maximum use of this position, he organized and ran the Neutral Density Workshop held at AFGL in October 1987. During this meeting, the state-of-the-science was reviewed and the science team formed. A subsequent meeting of the neutral modeling science team was held in Boulder CO in January 1988. The next logical step was to present the joint AWS-AFGL neutral modeling proposal to one of the operational groups stating neutral requirements, the USSPACECOM/AFSPACECOM/NORAD community. That's the purpose of this meeting.

Simultaneously, we intended to check for the existence of other neutral requirements or refinements to current requirements. Since we intend to begin development on this model early in FY89, we do not intend to incorporate major changes to the already stated operational requirements after May 1988 (Figure 13). For that reason, if any DOD space system operators see the need to revise or establish additional neutral model requirements, now is the time.

Since the proposed neutral model has been extensively compared with available data in the 250-500 km altitude range, this is the region where confidence is highest. Therefore, when the Phase I initial operating capability (IOC) is declared in FY91 (Figure 12), the proposed neutral model will supply reliable data in this altitude range. The proposed model will also be used to supply neutral data in the 500-1500 km altitude range, but confidence in the output variable will be lower. Values of density, temperature, and composition below 250 km during Phase I will be supplied by the mass spectrometer and incoherent scatter (MSIS) model.

Follow-on phases of neutral model development will extend the proposed neutral model down to 90 km as databases for verifying the model performance in the 90-250 km altitude range mature.

5. Conclusion

In summary, we have presented an overview of Air Weather Service space environmental support responsibilities. In addition, we have seen how operational shortfalls are addressed, the relationship between technical and operational space environmental support organizations, and the kinds of space environmental support provided by the Air Force Global Weather Central and later the Space Forecast Center. We have also reviewed the sources of data and overall modeling plan. In more detail, we looked at the neutral atmospheric customers, their requirements, and how AWS/AFGL jointly plan to satisfy these requirements.

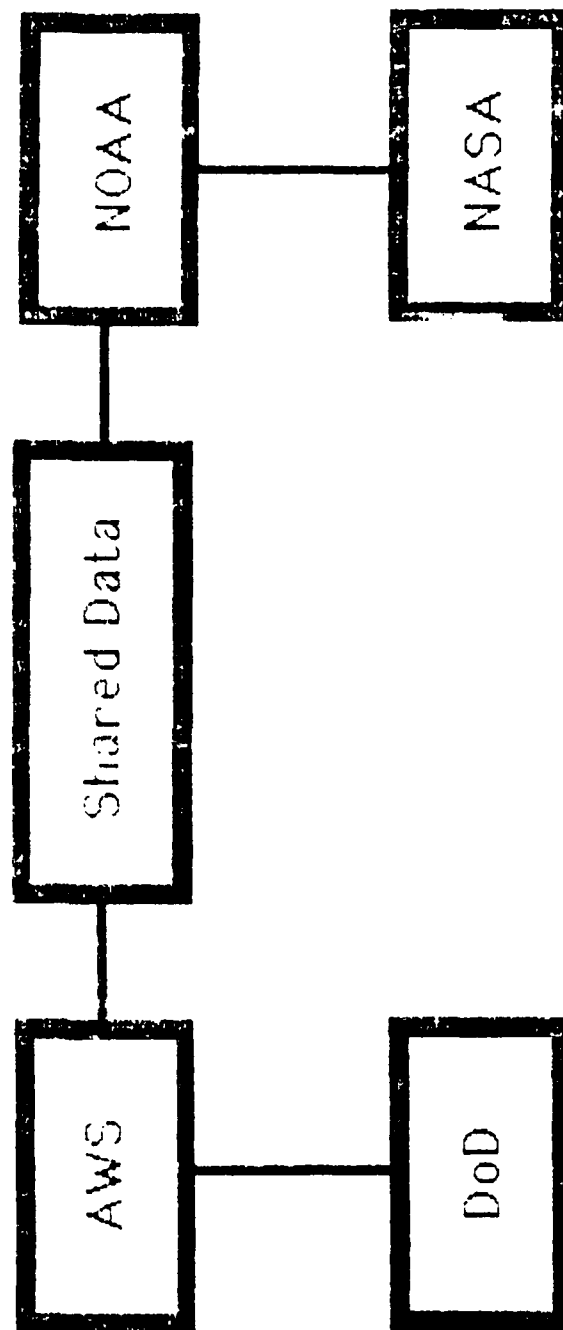
In conclusion, we know that an accurate neutral atmospheric model is needed to satisfy stated requirements and believe we've chosen the best approach

possible based on anticipated resources (Figure 14). However, if there are any DOD space system operators who need to refine these neutral requirements or levy additional requirements, now is the time to do so.

PURPOSE

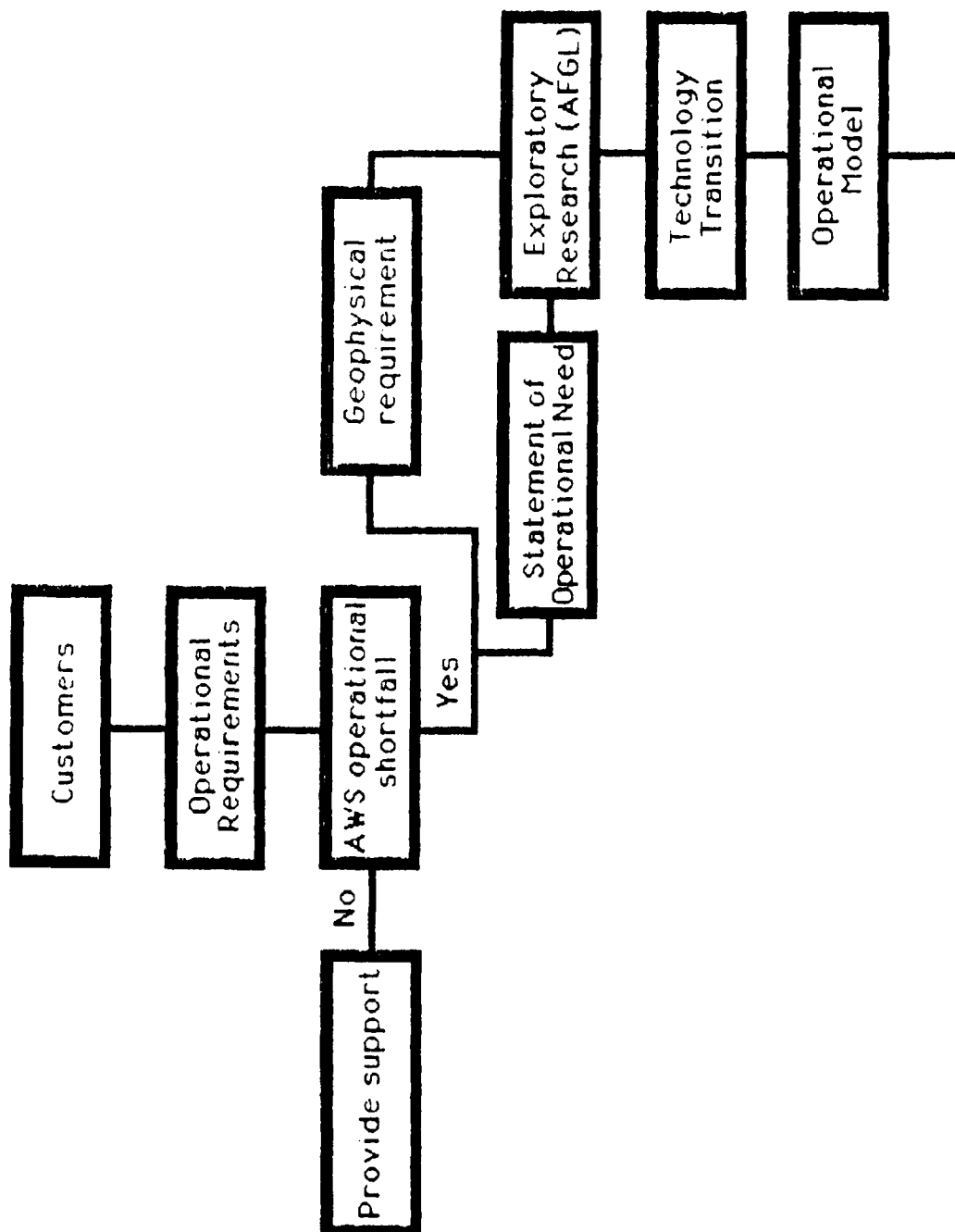
1. "Big picture" of AWS space environmental support.
2. Overview of the AWS/AFGL neutral modeling plan.
3. Check for refinements to operational requirements.

Space Support Responsibilities



Reproduced from
best available copy.

Operational Support Program



Support Relationships

Technical Support

Operational Support

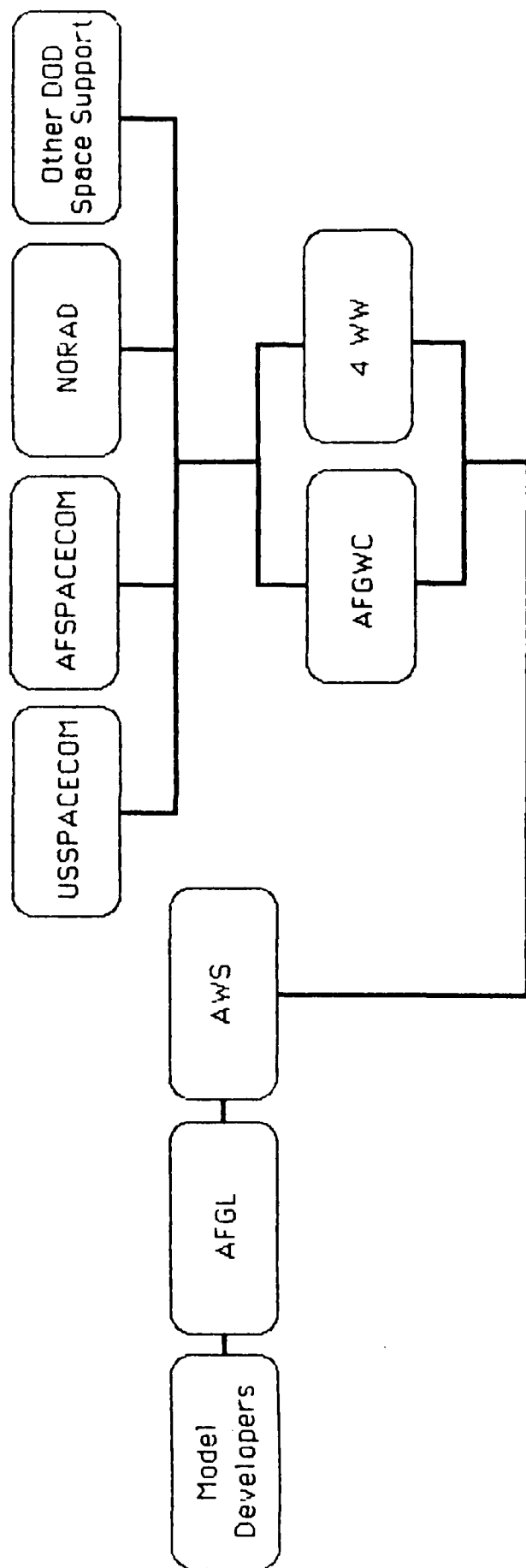
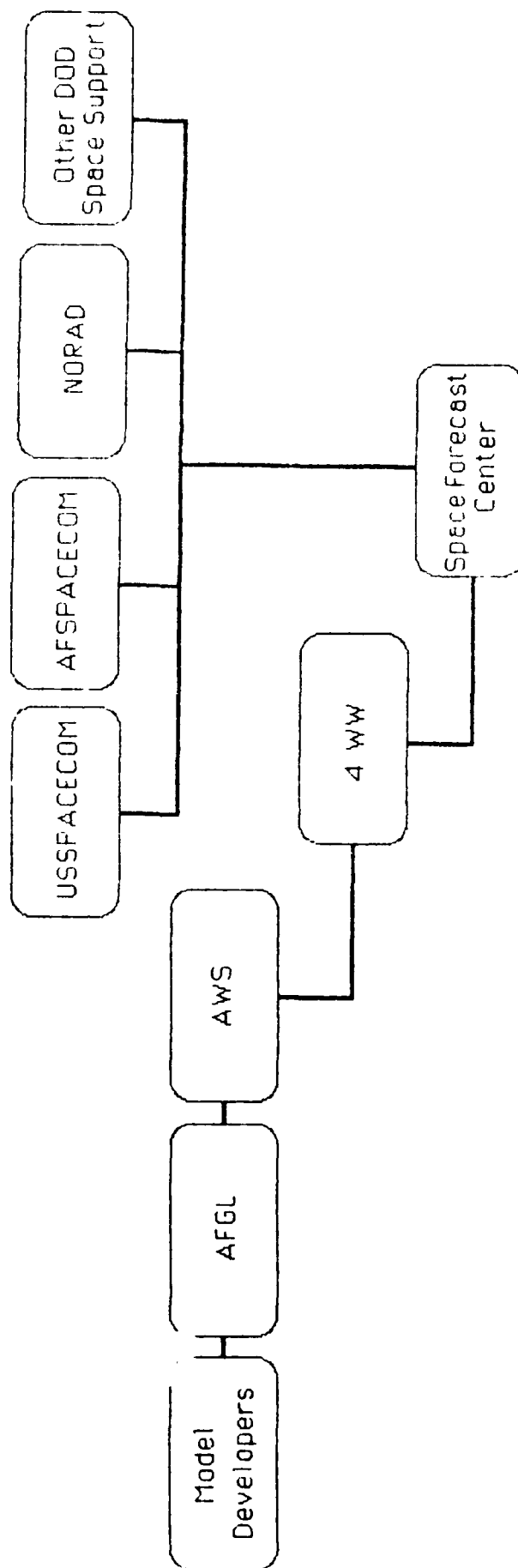


Figure 4

Future Space Environmental Support Relationships

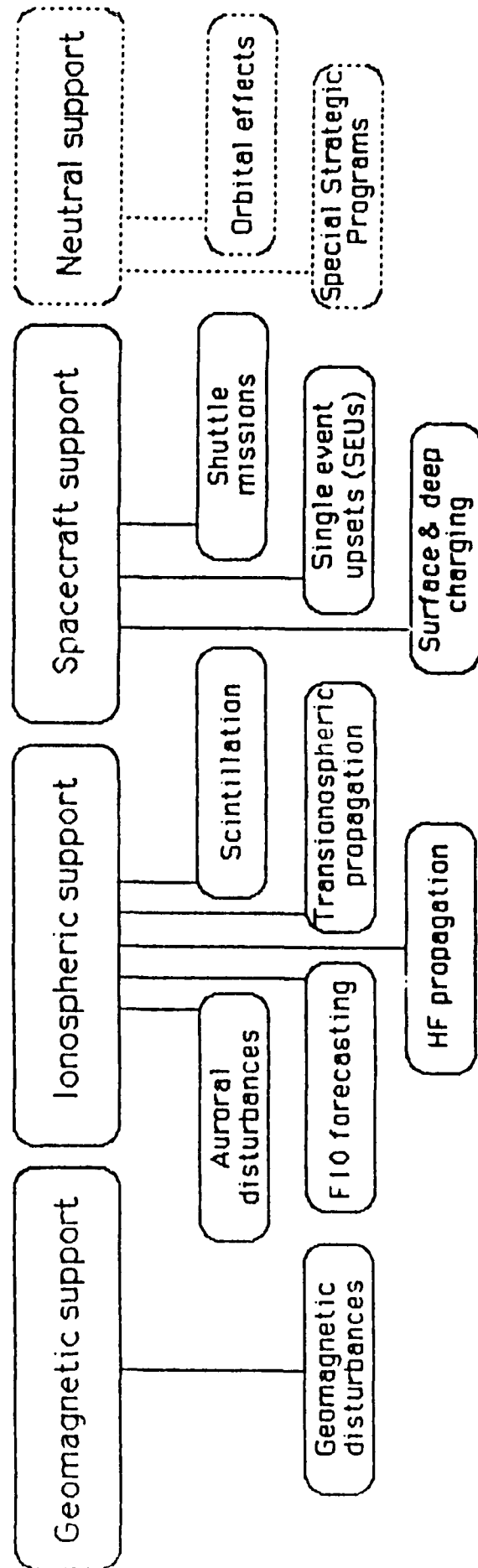
Technical Support

Operational Support



AFGWC/SFC Space Environmental Support Areas

Three main support areas and corresponding product areas



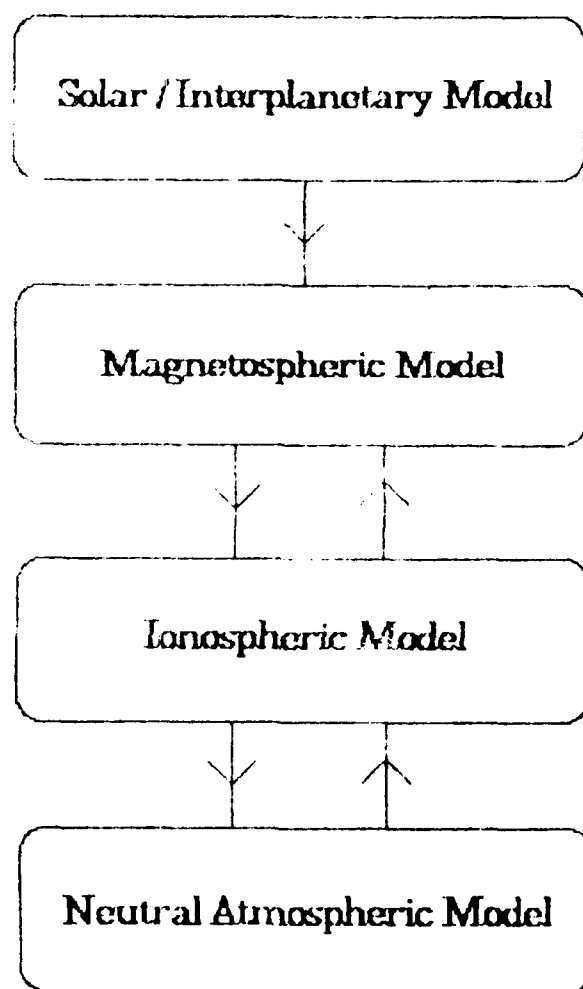
GROUND-BASED SPACE ENVIRONMENTAL DATA SOURCES

<u>INSTRUMENT</u>	<u>VARIABLES MEASURED</u>
Optical telescope (SOON)	Solar activity
Radio telescope (RSTN)	Solar radio output
Magnetometer	Geomagnetic activity
Polarimeter	Total electron content
Ionosonde	Bottomside electron density profile

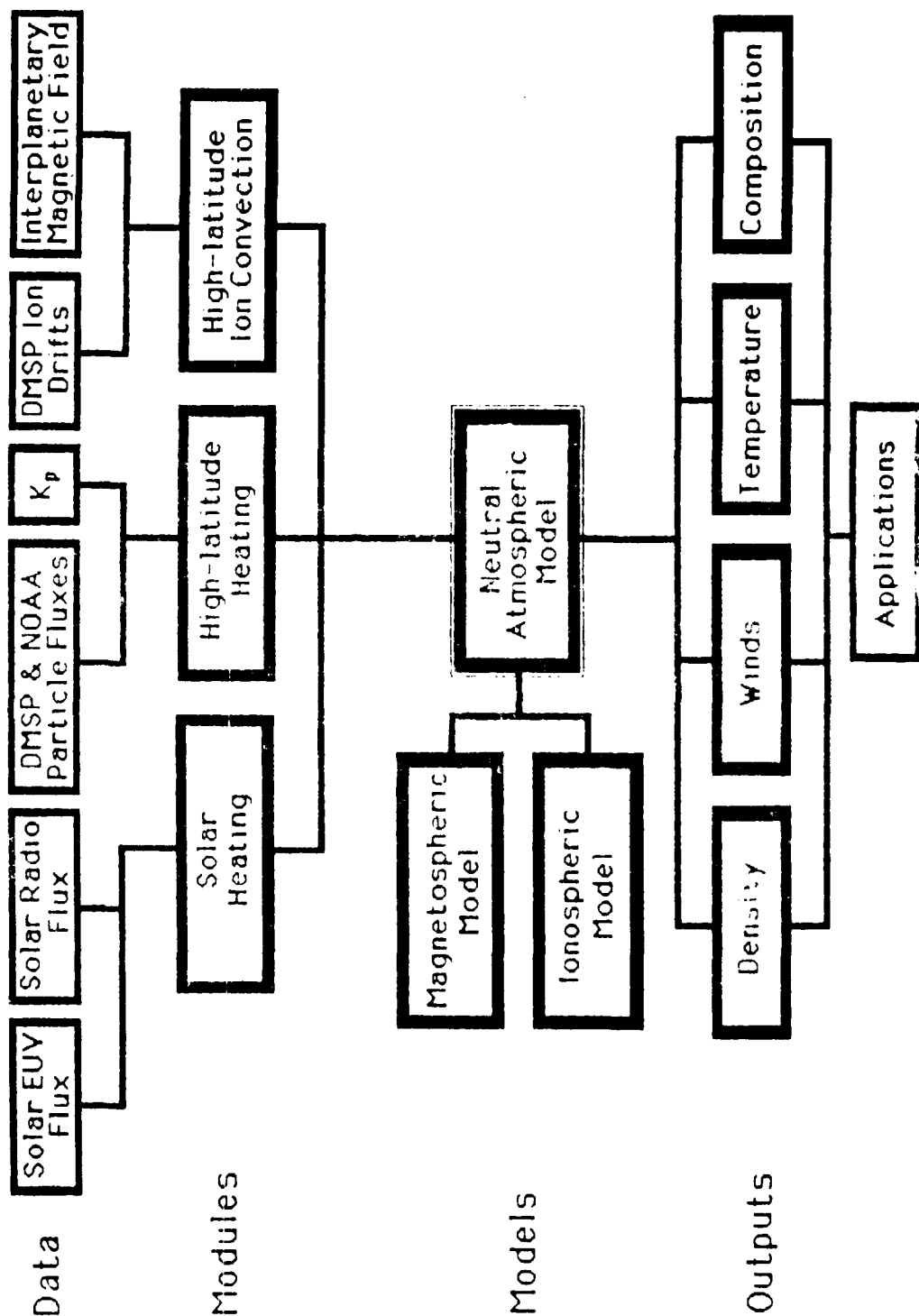
SPACE-BASED SPACE ENVIRONMENTAL DATA SOURCES

<u>INSTRUMENT</u>	<u>VARIABLES MEASURED</u>	<u>SPACECRAFT</u>
Solar X-ray sensor (SXI)	X-ray fluxes	GOES
Magnetometer (SSM)	Magnetic fields and currents	DMSP & GOES
Charged particle sensor (EP)	Geostationary particle fluxes	DOD & GOES
Charged particle sensor (SSJ/4)	Sun-synchronous particle fluxes	DMSP & NOAA
Visual auroral imager (OLS)	Auroral boundary location	DMSP
SSI/ES	Ion drift velocities	DMSP
SSI/ES	Ion and electron temperatures	DMSP
SSI/ES	Electron density irregularities	DMSP
Interplanetary sensor	IMF/solar wind	?
Neutral sensor	Neutral densities, winds, temperatures, and composition	?

Integrated Space Environmental Modeling System (ISEMS)



AWS Neutral Atmospheric Model



NEUTRAL ATMOSPHERIC MODEL REQUIREMENTS

Primary Customers:

- US SPACECOM, AF SPACECOM & NORAD
- Special Strategic Programs

Requirements:

- Accuracy
 - - Specification goal: 5%
 - - Forecasting goal: 10%
- Forecasting out to 72 hours
- Altitude range: 90 - 1500 km
- Neutral density, winds, temperatures, and composition

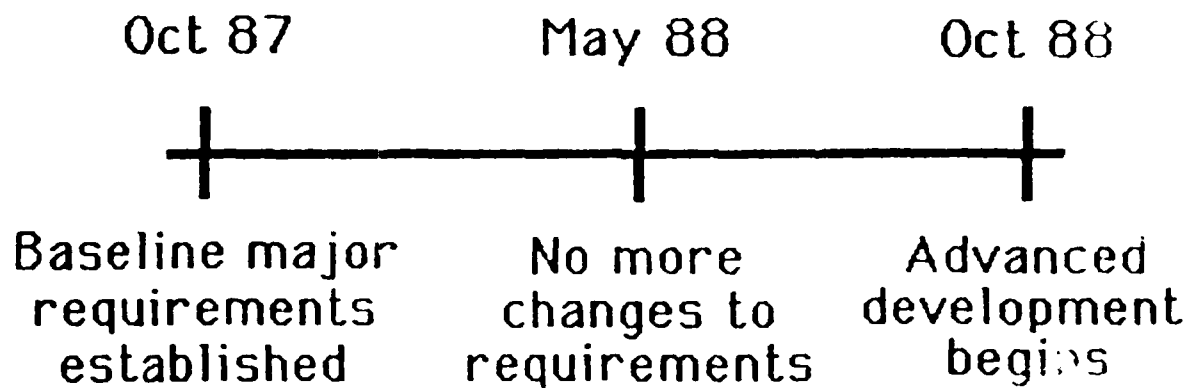
STATUS

- AFGL/LI technical manager
- AFGL Neutral Density Workshop (Oct 87)
- Science team formed (AFGL, AWS, NASA, NCAR, U of Mich)
- SPACECOM Neutral Density Conference (Mar 88)
- Advanced development expected to begin (FY89)

MILESTONES

- AFGL begins advanced development - FY89
- Operational software development begins - FY91
- Phase I Initial Operating Capability at SFC - FY91
- Phase II upgrade: 140 - 250 km specification capability - FY92
- Phase III upgrade: 90 - 140 km specification capability - FY93

TIMELINES



BOTTOM LINE

- AWS needs an accurate neutral atmospheric model.
- We need your operational requirements NOW !!!

Air Force Space Command Requirements for Neutral Atmospheric
Density Specification and Prediction

Lt Col George R. Davenport
Headquarters Fourth Weather Wing

The Air Force Space Command Deputy Director of Astrodynamics last stated the Air Force Space Command "Requirements for Atmospheric Neutral Density Predictions" in a 26 May 1986 letter to the 4th Weather Wing Aerospace Sciences Division. The requirement was for predictions of the neutral atmospheric density for 24 hours out to 72 hours, presumably to be updated every 24 hours, at all latitudes and longitudes for the 100 km to 1000 km altitude range. The upper limit of the altitude range is likely to be raised, possibly to 1500 km. The accuracy requirement is in the range of 5%.

Air Force Space Command also made several specific recommendations in the 26 May 1986 letter. The first recommendation is to "Create brand new models which utilize additional environmental input parameters." Additional model inputs might include the solar x-ray and solar extreme ultraviolet fluxes, auroral energy inputs, the solar wind, and measurements of the interplanetary magnetic field. The second recommendation is to "Get instruments in place for measuring and predicting new environmental parameters that may be needed." Such instruments might fly on the Defense Meteorological Satellite Program (DMSP) spacecraft, or they could include data from the NOAA Solar X-Ray Imager, the proposed NASA WIND/SIMPL libration point spacecraft, or a follow-on to the Navy's experimental Remote Atmospheric and Ionospheric Detection System (RAIDS). The third recommendation is to "Improve measurements and forecasts for currently used environmental parameters." These parameters are the geomagnetic indices and the 2800 MHz, 10.7 centimeter, solar radio flux measured daily from the Algonquin Observatory, the "Ottawa Flux" or "F10."

The Air Weather Service established Geophysical Requirement 2-87, "Neutral Atmospheric Specification and Prediction," to help the research community to understand shortcomings in generating products that describe the current and the future conditions of the neutral atmosphere to operational customers. Geophysical Requirement 2-87 includes Air Force Space Command requirements and recommendations as stated in the 21 May 1986 letter.

Currently Air Weather Service is just providing observed and predicted surrogate environmental parameters for each user to input into their own neutral atmosphere model. The Ottawa Flux and the geomagnetic indices are all that is available, so providing these parameters constitutes the current level of

support. This is analogous to providing an aircraft pilot with raw weather data for him to use to prepare his own flight route forecast.

The goal for the next few months is to update the Air Force Space Command requirement that was last stated almost two years ago. If appropriate, the U.S. Space Command, Air Force Space Command, and Navy Space Command should publish a formal Required Operational Capability (ROC) with supporting Statements of Operational Need (SONs). In the process of preparing and coordinating these requirements documents, the commands should stimulate similar stated requirements from other DOD agencies. For example, Strategic Air Command identified impacts of increased atmospheric density in their Statement of Operational Need for Military Space Flight Capability, which was validated on 22 September 1980. Although an old SON, it indicates that there is at least hope for support from other Air Force major commands.

BUSINESS CARD

LT COL GEORGE R. DAVENPORT

HEADQUARTERS 4TH WEATHER WING (MAC)
AEROSPACE SCIENCES DIVISION

4WW/DN

AIR FORCE SPACE COMMAND
AFSPACECOM/DOWA

UNITED STATES SPACE COMMAND
JSSPACECOM/J3W

NORTH AMERICAN AEROSPACE DEFENSE COMMAND
NORAD/NCW

AV 692-7750 (719) 554-7750

Reproduced from
best available copy.

AIR FORCE SPACE COMMAND REQUIREMENTS FOR
ATMOSPHERIC NEUTRAL DENSITY PREDICTIONS

STATED IN 21 MAY 1986 LETTER FROM THE
DEPUTY DIRECTOR OF ASTRODYNAMICS TO
4TH WEATHER WING AEROSPACE SCIENCES
DIVISION

AIR FORCE SPACE COMMAND REQUIREMENTS FOR
ATMOSPHERIC NEUTRAL DENSITY PREDICTIONS

PREDICTION: FROM 24 HOURS OUT TO 72 HOURS (UPDATED EVERY 24 HOURS)

ALTITUDES: 100 KM TO 1000 KM (UPPER LIMIT LIKELY TO BE RAISED)

ALL LATITUDES AND LONGITUDES

ACCURACY: IN THE RANGE OF 5%

AIR FORCE SPACE COMMAND RECOMMENDATIONS

"CREATE BRAND NEW MODELS TO UTILIZE ADDITIONAL ENVIRONMENTAL INPUT PARAMETERS"

AURORAL ENERGY INPUTS, SOLAR X-RAY AND EUV, SOLAR WIND,
INTERPLANETARY MAGNETIC FIELD

"GET INSTRUMENTATION IN PLACE FOR MEASURING AND PREDICTING NEW ENVIRONMENTAL PARAMETERS WHICH MAY BE NEEDED"

DMSP, SOLAR X-RAY IMAGER, WIND/SIMPL, RAIDS

"IMPROVE MEASUREMENTS AND FORECASTS FOR CURRENTLY USED ENVIRONMENTAL PARAMETERS"

OTTAWA 2800 MHZ, 10.7 CM SOLAR RADIO FLUX (F10)
GEOMAGNETIC INDICES

AIR WEATHER SERVICE GEOPHYSICAL REQUIREMENT 2-87
"NEUTRAL ATMOSPHERIC SPECIFICATION AND PREDICTION"

INCLUDES AIR FORCE SPACE COMMAND REQUIREMENTS
AND RECOMMENDATIONS

CURRENT AIR WEATHER SERVICE SUPPORT

PROVIDING OBSERVED AND PREDICTED SURROGATE ENVIRONMENTAL PARAMETERS
(OTTAWA FLUX AND GEOMAGNETIC INDICES) FOR USERS TO INPUT INTO THEIR
OWN MODELS

ANALOGOUS TO PROVIDING AN AIRCRAFT PILOT WITH RAW WEATHER DATA TO
USE TO PREPARE HIS OWN FLIGHT ROUTE FORECAST

GOALS

UPDATE THE AIR FORCE SPACE COMMAND STATED REQUIREMENTS
AND PUBLISH AS A FORMAL COMMAND NEED

STIMULATE SIMILAR STATED REQUIREMENTS FROM OTHER DOD
AGENCIES

SAC 07-79, STATEMENT OF OPERATIONAL NEED (SON) FOR
MILITARY SPACE FLIGHT CAPABILITY (U) 15 JUNE 1979

PARA 1B(4), PAGE 3

VALIDATED 22 SEP 80

... SOLAR ACTIVITY SHOULD ALSO BE CONSIDERED IN THE DESIGN OF A MILITARY SPACE FLIGHT SYSTEM (MSFS). MAJOR SOLAR EVENTS CAN DEGRADE SPACE-TO-GROUND COMMUNICATIONS (COMMAND AND CONTROL), AND CREATE POTENTIAL HEALTH HAZARDS FOR MANNED SPACE FLIGHT. MOREOVER, INCREASED SOLAR ACTIVITY CAN CAUSE INCREASES IN ATMOSPHERIC DENSITY FOR LOW ORBITING VEHICLES, THUS PROMOTING PREMATURE ORBIT DECAY. INCREASED SOLAR ACTIVITY CAN ALSO LEAD TO SPACECRAFT CHARGING; I.E., EXTRAORDINARY STATIC ELECTRIC POTENTIALS. THESE STATIC POTENTIALS HAVE DESTROYED CIRCUITRY IN SOME SPACECRAFT AND CAUSED ERRATIC OPERATION IN OTHERS. ...

Naval Space Surveillance Center Atmospheric Drag Requirements

Stephen H. Knowles

Naval Space Surveillance Center

Dahlgren, Va. 22448

The Naval Space Surveillance Center, with headquarters located in Dahlgren, Va., maintains a complete catalog of positions of earth-orbiting space objects as part of its operational responsibility as a component of the U.S. Space Command. As such, it has a need to know the atmospheric drag to an accuracy comparable to the nominal accuracy with which orbits are maintained. The accuracy of individual orbits in the NAVSPASUR catalog varies considerably in a way that depends on a number of parameters, including the altitude of the orbit, the tasking of the sensors, the stability of the thermosphere, etc. A nominal desired accuracy for near-earth orbits, however, is of the order of ± 1 to 3 miles. This accuracy is relatively coarse compared to precision orbit determinations that can produce accuracies of a few meters. Nevertheless, the inaccuracy associated with predicting the effect of atmospheric drag is usually the most important term contributing to orbit prediction degradation with time. Thus, improvements in drag compensation are of high importance in improving NAVSPASUR orbital prediction ability. This is of even more importance for the limited but

increasing number of orbits for which precision orbit prediction is required. A special important need exists for more accurate upper atmospheric modeling for the prediction of atmospheric re-entry. Present drag calculation accuracy requires near-real-time tracking, and accurate advance re-entry predictions are not possible

Atmospheric drag is a dissipative force. Its effects on different near-earth orbits, while quantitatively different, are qualitatively the same, namely, a decrease in the orbital energy. This energy decrease is exhibited most noticeable as a constant rate of decrease in the mean motion. This results in a change in the along-track position that is quadratic because of the integration involved. The mean motion effect results in the typically 5 times worse accuracy in determining along-track position which is the largest single uncertainty in most near-earth orbits. A second important effect is the reduction of eccentricity; orbits tend to circularize as a result of drag. Other elements describing the motion of the satellite within its plane are also perturbed, including a secular reduction in the semi-major axis.

Satellite drag is largely an affect of that region of the upper atmosphere known as the thermosphere, with a small contribution from the lowest part of the exosphere. The density and other parameters vary greatly over this region (Figure 1). The amount of along-track atmospheric effect is therefore highly dependent on perigee height. Figure 2 gives an indication of this relationship; above 1000 km. atmospheric drag can be

neglected for most purposes. Drag can be several tens of seconds per day for near-reentry situations, and more typically appears as an error in predicted arrival time of about ± 1 second.

At the present time, NAVSPASUR makes no correction for atmospheric drag from a model in computing our production orbits. The effect of drag is included empirically, however, by the inclusion of the first and second derivatives of the mean motion (\dot{n} and \ddot{n}) as orbital elements during the differential correction fitting process. Our differential correction is performed once per day; the orbital elements, including the drag terms, however, are the average over the data fitting span used in the differential correction. This can vary from 3 to 10 days for near-earth orbits, but is typically 3 days for most near-earth orbits that exhibit appreciable drag. The lack of explicit inclusion of a model has several effects, both advantageous and disadvantageous. In the first place, the correct mean atmospheric drag is automatically fitted for each orbit's parameters, without any necessity to include an error term from model inaccuracy. However, there is no ability to include dynamic behavior of the thermosphere. During the occurrence of major solar storms, this has resulted in situations wherein large numbers of orbits in our operation center have exceeded the tolerances that made them appear as 'UCTs' (uncorrelated targets), necessitating a large amount of labor by analysis staff to make them fit. Some of this problem can and should clearly be overcome by use of an atmospheric drag model to make the orbits measurable in terms of some physical parameter.

Hopefully this can be done in a way which will retain the empirical advantages of the present NAVSPASUR system while still improving the ability to respond to geophysical changes in the thermosphere density.

Currently available upper atmospheric models were largely developed in the early 1970's by Jacchia and others. The general consensus is that these models are capable of predicting density in the 100 to 1000 km. region to an accuracy of about 15%. Attempts to produce better accuracy than this have not so far met with success. There are several problems with attempting to produce improved accuracy. The present models are parametrized in terms of global parameters having to do with solar and magnetic field activity, specifically solar 10 cm. flux level and the Kp magnetic field index. These parameters as distributed are after-the-fact by up to several days and are averaged to some extent rather than instantaneous. In addition, they are global in the sense of having only one parameter to represent the overall atmospheric performance. The solar/geophysical indicators serve basically as indicators of energy inputs which increase the thermospheric/exospheric temperature and thus the atmospheric density. The relation between exospheric temperature and density is not simple (Figure 3).

As an operational orbit determiner/predictor, NAVSPASUR's most pressing need for improved treatment of drag is to account better for the effect of solar/geomagnetic disturbances ('storms') on the catalog. In order to compensate for this effect, real-time data inputs must be available, as solar storms

cannot be predicted accurately in advance. Conventional predictor indices do not serve for this purpose; an additional problem is that their inherent accuracy is considerably poorer during solar-geophysical storms than it is during quasi-steady-state conditions. At present there is no fast-response monitoring instrument to provide immediate notification of major solar events. Probably the best method to do this is a solar ultraviolet or X-ray detector; one is planned for circa 1990 as an adjunct to the next GOES launch by NOAA. There is also a case to be made for real-time monitoring of the upper atmospheric density at various locations around the earth. To a limited extent this can be accomplished by the tracking network itself, but not as presently constituted in real time. Various satellite systems have been suggested, including a series of 'dragsats' which would instantaneously measure the deceleration; this latter would provide the best current reading on the density of the thermosphere, although not providing a thorough sample of density at various altitudes. There is presently a fairly large amount of research underway to improve knowledge of the composition of the thermosphere; translating this into improved predictions of orbiting objects, is not straightforward. Some of the complexities involved are illustrated in Figure 4, which provides an indication of some of the processes controlling thermospheric structure and dynamics. It seems clear that, whatever improvement in thermospheric density modeling is decided upon, it will include provision for real-time data input and will be built

upon semi-empirical formulas rather than the theoretically
elegant series expansions of orbital mechanics.

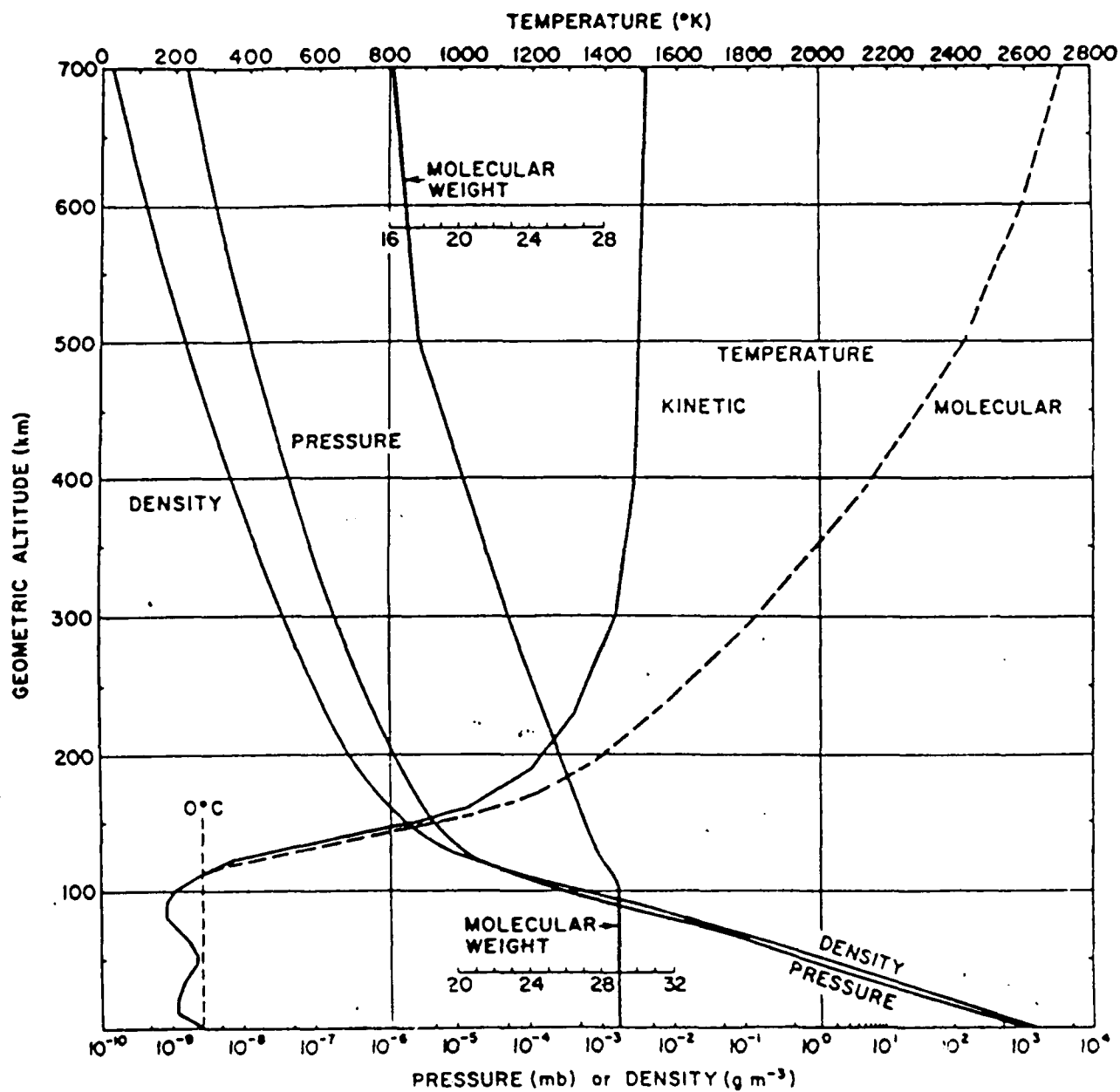


FIGURE 1

Profiles of thermosphere temperature, pressure, density and molecular weight under typical conditions

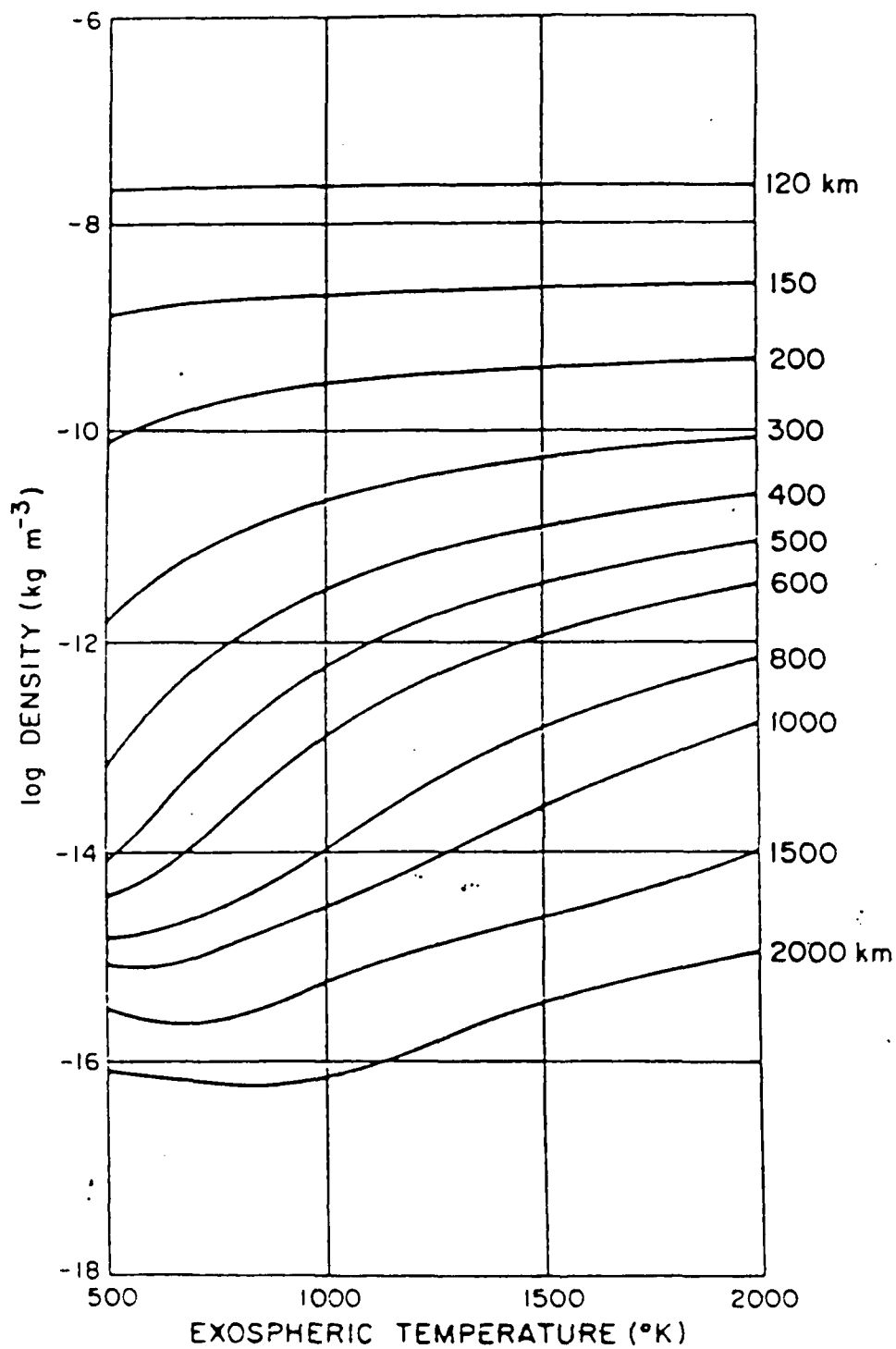


FIGURE 2
Relation between atmospheric density and temperature for various heights

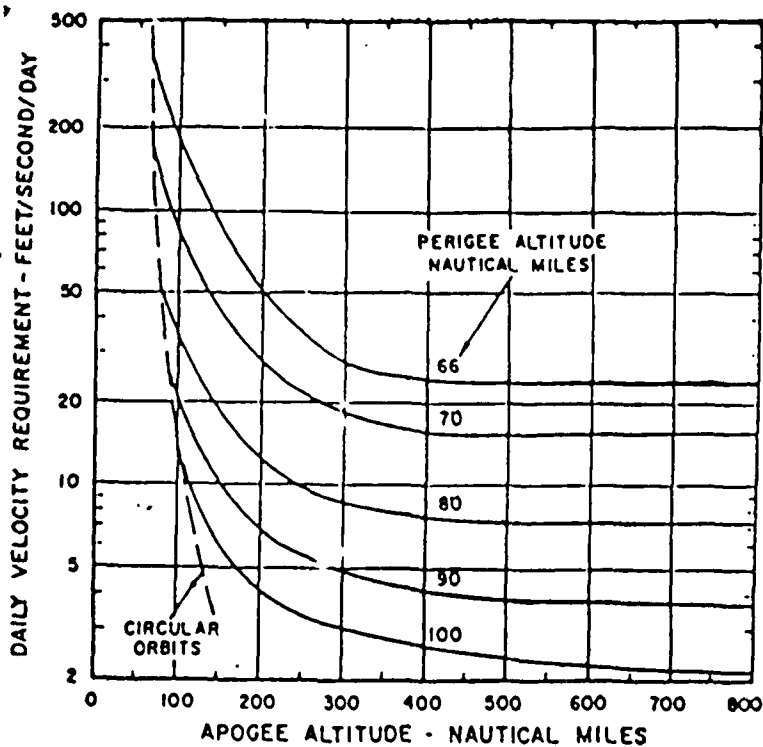


FIGURE 3

Velocity required to maintain orbital height as a function of altitude

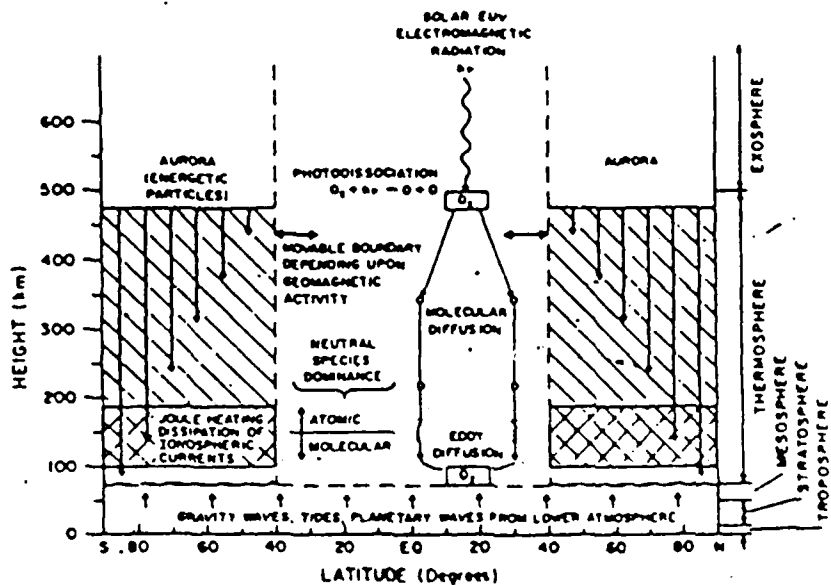


FIGURE 4

Principal processes and energy sources governing thermospheric structure and dynamics

SESSION 2

OPERATIONS SUPPORT

CAPT JOHN L. SULLIVAN, USN
CHAIRMAN

Space Control Operations - Meeting the Challenge

by

Capt Colette M. de la Barre

The mission of the USSPACECOM Space Control Operations Centers at the Cheyenne Mountain Air Force Station is space surveillance, satellite protection and negation. In recent years, the protection aspect of this mission has been expanding. The Strategic Defense Initiative Organization, Missile Test Ranges, and NASA require more accurate space surveillance support for many varied applications; however, the one that has received the most attention recently is prediction of close conjunctions between satellites and launch vehicles. In order to provide more accurate space surveillance products, USSPACECOM is demanding the most from its personnel and the spacetrack network. Since these resources are limited, USSPACECOM must look at other ways to meet the demands.

The Challenge

One of the challenges facing USSPACECOM is to provide more accurate predictions of close conjunctions between launch vehicles and orbiting space objects. According to the Outer Space Treaty of 1967, launch vehicle owner/operators are held liable if their launch vehicle collides with an orbiting payload. Although launch agency personnel are also concerned with avoiding orbiting debris to protect their launch vehicles, they usually resolve to avoid only payloads in order to minimize the impact on their launch opportunities. Since the prediction of the location of orbiting debris is much less accurate than payloads, the quality of USSPACECOM generated safe launch windows are significantly reduced when debris must be avoided. Moreover, the NASA Space Shuttle program management is not content to avoid only payloads due to the threat of orbiting debris to human life. NASA's requirements provide USSPACECOM with a tremendous challenge - to predict all catalogued space objects with significantly more accuracy.

Meeting the Challenge

Many factors enter into the accuracy of USSPACECOM space surveillance products including accuracy of spacetrack sensors, frequency of spacetrack observations, accuracy of orbit propagation models, and Space Control Operations Center personnel and computer work loads. An improvement in any of these areas would improve space surveillance products. An improvement in accuracy of orbit propagation models would have the greatest impact, because it would result in more accurate space surveillance products while reducing the time spent by USSPACECOM personnel and the spacetrack network on routine satellite maintenance. The resources saved could be put to use in other aspects of the Space Control Operations mission. Since the Space

Control Operations Centers don't control the accuracy of spacetrack sensors and satellite propagation models, but have control over sensor tasking and how often satellite orbits and space surveillance products are updated, USSPACECOM develops procedures to maximize space surveillance product accuracy while not stressing their computer system. These procedures result in increased personnel work load and increased tasking of the spacetrack network.

The accuracy of all space surveillance products depends on how accurately the Space Control Operations Centers can predict the location of a satellite. An accurate satellite prediction is generated by a good propagation model using good initial conditions. Good initial conditions are generated by obtaining frequent observations on the satellite from the spacetrack network and updating the satellite's orbit with those observations more often. Using this updated satellite orbital element set, a more accurate space surveillance product is generated by ensuring the time span over which the product is valid is not excessive. The following example shows how the USSPACECOM develops procedures and uses its personnel and the spacetrack network to generate the most accurate space surveillance product. To ensure the best accuracy of the impact location of a decaying satellite, the spacetrack sensors are tasked for observations on the satellite every time it comes within their field of view and the satellite's orbital element set is manually updated about every eight hours using these observations. The Tracking and Impact Prediction (TIP) for the satellite is updated at a minimum of eight times in 15 days with the final prediction being made within two hours of impact. If the model used to predict the satellite's position were more accurate, observations could be required less frequently by the spacetrack network, the satellite orbital element set would not need to be manually updated as often, and the TIP for the satellite would be accurate for a longer period of time. The result would be a significant decrease in resources required for TIPs.

USSPACECOM Atmospheric Density Models

USSPACECOM predicts the location of near Earth space objects using an analytical propagation model which includes a power density function (GPPF) and a numerical integration model which includes the Jacchia-SCC 64 (JSCC) empirical atmospheric density model (SPJSCC) [1]. Since USSPACECOM has catalogued over 18,900 orbiting space objects, and currently keeps track of over 7100 of which over 6300 are near Earth*, computation time is a real consideration in selecting which model to use. Since the SPJSCC model requires significantly more computer time than the GPPF, it is only used for special interest space objects including

* A near Earth satellite has an orbital period less than or equal to 225 minutes.

decaying satellites or less than one percent of all near Earth space objects. One of the most important differences between the models is the SPJSCC model includes the sun's effect on the Earth's atmospheric density and the GPPF doesn't [1]. Even though the JSCC model is more sophisticated than the power density function, it's predictions for density of the atmosphere are still reported to be 16 percent off from atmospheric measurements. Both models use a constant satellite ballistic coefficient [1].

Performance

The USSPACECOM Lost Satellite List and TIPs for decaying satellites were chosen as indicators of the performance of the USSPACECOM atmospheric density models. A near Earth satellite is considered lost by USSPACECOM when it has not been seen by the spacetrack network for more than two days. There are many factors that affect the number of satellites on the lost list and the TIPs for decaying satellites; however, a significant contributor is the geomagnetic disturbance level. Figure 1 shows the number of lost satellites from Oct 86 to Mar 88. Figure 2 shows the daily geomagnetic index (A_p) from Jan 86 to Mar 88. Analysis of the lost list during the two largest geomagnetic storms in 1988 (15 Jan 88 and 22 Feb 88) shows that the number of lost satellites doubled within six days after the storms (Fig. 3 and 4.) Since the satellites on the lost list are processed with the GPPF, and since the GPPF includes no solar effects, it is not surprising that the number of lost satellites increases significantly during high geomagnetic activity. It should also be noted that the average number of lost satellites over the 17 months studied is 178 which is not consistent with protecting the Space Shuttle and other launch vehicles from collision with orbiting space objects. An analysis of TIPs also shows that decay times for satellites are significantly affected by geomagnetic disturbances.

A TIP study was performed that analyzed how far off from actual decay time the two hour and 24 hour TIP times were for a five month period having no geomagnetic storms (Jan 86, Mar 86, Apr 86, Apr 87, and Jun 87) and a four month period having at least one geomagnetic storm with 24 hour geomagnetic disturbance index (A_p) greater than 80 (Feb 86, Sep 86, Jan 88, and Feb 88.) Table 1 shows the results of the TIP study. The two hour TIP times for the 25 satellites that decayed during the months with no geomagnetic storms were an average of 14 minutes off from their actual decay times while the 24 hour TIP showed a one hour and 46 minute difference. The 25 satellites that decayed during the months with large geomagnetic storms were found to be an average of 36 minutes off from their actual decay times for the two hour prediction and 3 hours and 42 minutes off for the 24 hour prediction. Since a decaying satellite can travel more than 6500 km in 14 minutes, even the two hour TIP during low geomagnetic storm levels is not very accurate. The TIP made 24 hours prior to impact is of little value.

Recommendations

USSPACECOM will continue to look at new ways to use personnel and the spacetrack network to improve space surveillance support. However, improvements to USSPACECOM atmospheric density models will do the most to improve space surveillance support. USSPACECOM needs a satellite propagation model that very accurately models atmospheric density during high and low solar activity without requiring more computation time than the GPPF. This model could be used for all near Earth space objects except special interest satellites. An improved version of SPJSCC is needed to process special interest satellites including decaying satellites. One may hypothesize that improvements in predicting the indicators of geomagnetic activity will significantly improve the products generated by the SPJSCC during high geomagnetic activity. However, improvements in modelling atmospheric density during low solar activity are also needed.

New Developments

Dr Joseph Liu and Dr Felix Hoots have developed some new semianalytic methods for propagating satellite orbits. These methods may be able to handle improvements in analytical and empirical atmospheric density models [2]. Mr Peter Kolodziejczyk is investigating ways to predict how satellite ballistic coefficient varies with satellite altitude [3]. He hypothesizes that an improved prediction model could absorb inaccuracies in atmospheric density models.

Conclusions

USSPACECOM requires improvements in near Earth atmospheric density models to meet the demands of future space surveillance support. Without improvements, USSPACECOM will continue to increase the burden on personnel and the spacetrack network. Since USSPACECOM resources are not without limit, the time will come when USSPACECOM will have difficulty meeting new space surveillance demands. Modelling atmospheric density simply enough to be used in a satellite propagation model which uses minimum computer time is no trivial problem. Improving atmospheric density predictions seems to increase the complexity of the mathematical model which increases the computer time required to propagate a satellite's orbit. A "Newton-size" solution is needed - Are there any Newton's out there?

REFERENCES

1. An Analysis of the Use of Empirical Atmospheric Density Models in Orbital Mechanics. Spacetrack Report No. 4, Air Force Space Command, February 1983.
2. Application of a Semianalytic Orbit Theory Using Observed Data. The Journal of the Astronautical Sciences, Vol XXXI, No 1, pp. 49-61, Jan - Mar 1983.
3. Kolodziejczyk, Peter P., Ballistic Coefficient Variation with Altitude for Earth Decaying Objects. Masters Thesis. Univ of Colorado, Dept of Electrical Engineering, 1987.

Near Earth Lost Satellites

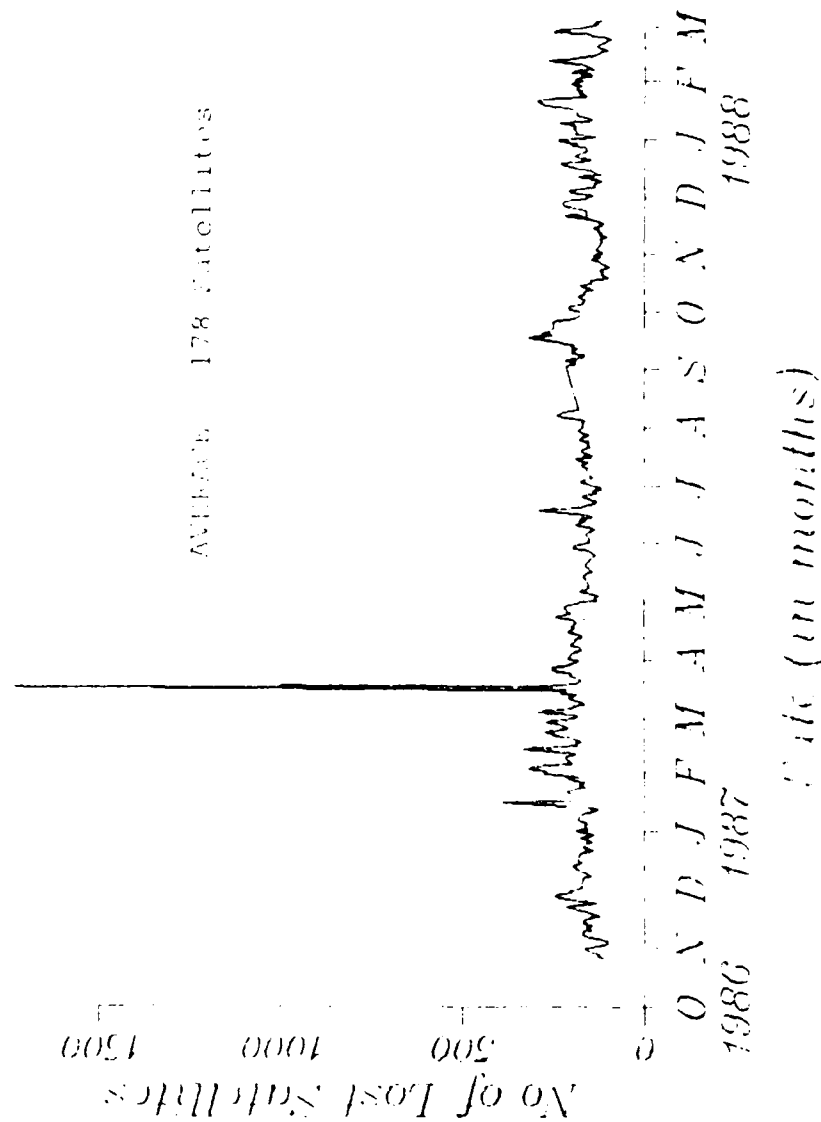


FIGURE 1 - Near Earth Lost Satellites

Geomagnetic Disturbances

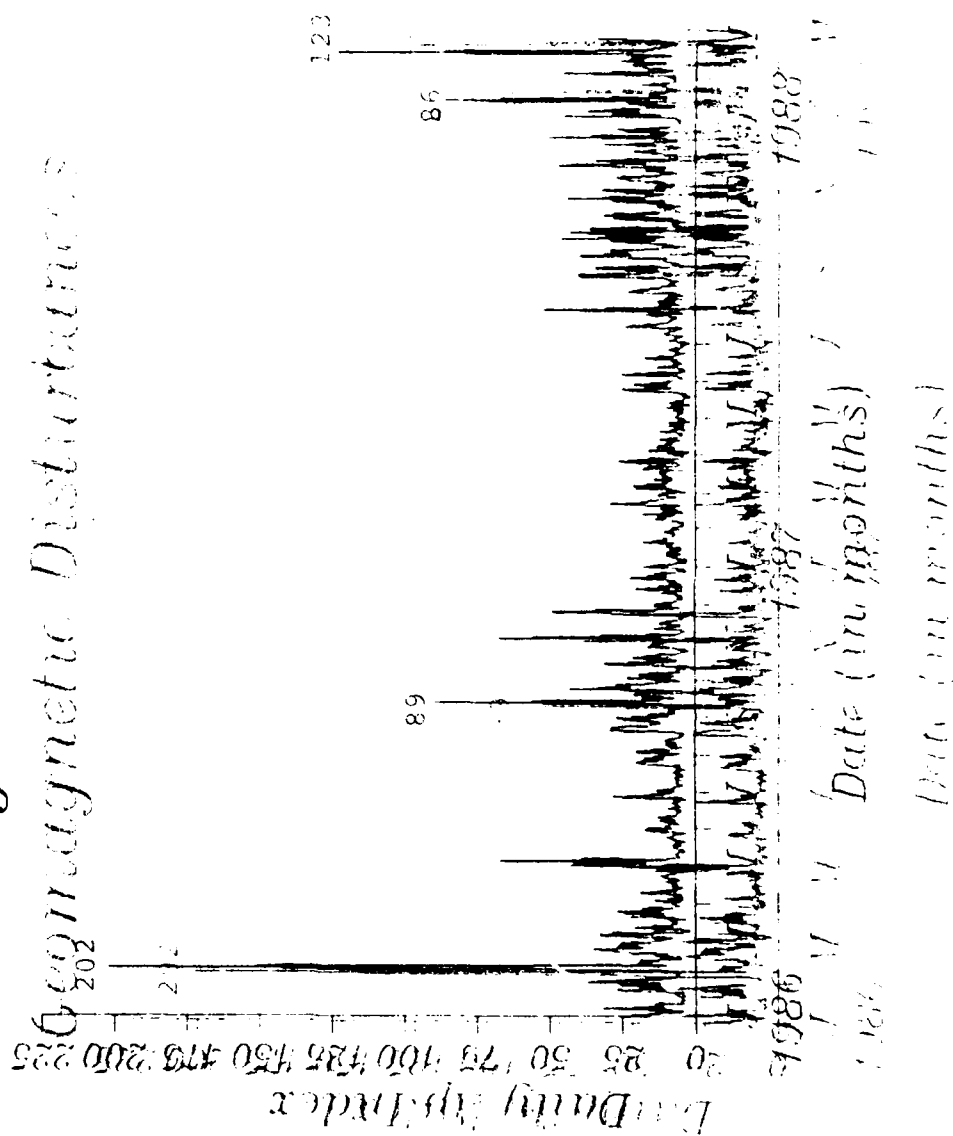


FIGURE 2 - Geomagnetic Disturbances

FIGURE 2 - Geomagnetic Disturbances

Near Earth Lost Satellites

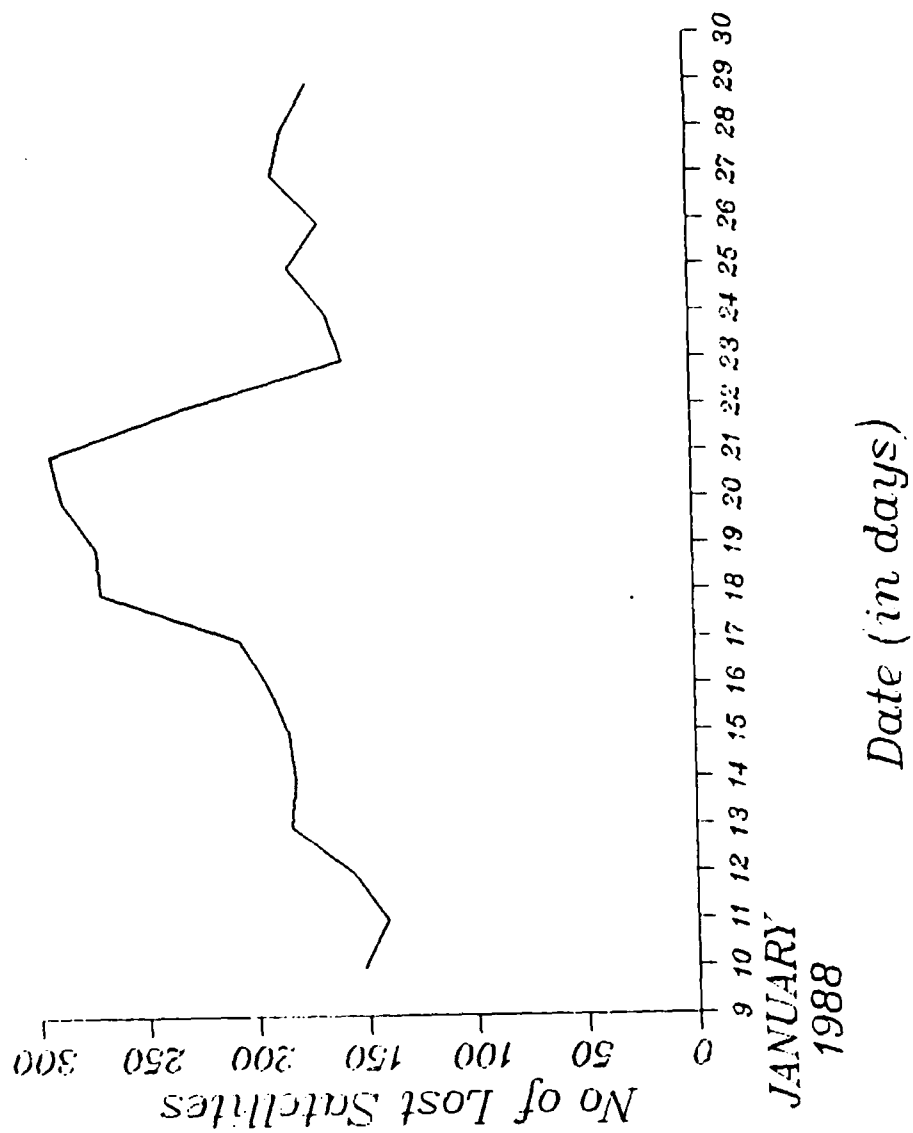


FIGURE 3 - Near Earth Lost Satellites during Jan 88
Geomagnetic Storm

Date (dd/mm)	No of Lost Satellites
1/3	100
2/3	120
3/3	150
4/3	180
5/3	200
6/3	220
7/3	230
8/3	210
9/3	180
10/3	150
11/3	120
12/3	100
13/3	80
14/3	60
15/3	40
16/3	20
17/3	10
18/3	5
19/3	10
20/3	20
21/3	30
22/3	40
23/3	50
24/3	60
25/3	70
26/3	80
27/3	90
28/3	100
29/3	110
30/3	120
31/3	130

... ..

**Table 1 - Predicted Decay Time
Versus Actual Decay Time**

	2 Hr	24 Hr
No Geomag Storms (Jan 86, Mar 86, Apr 86, Apr 87, Jun 87)	14 Min	1 Hr 46 Min
Geomag Storms (Feb 86, Sep 86, Jan 88, Feb 88)	36 Min	3 Hr 42 Min

50 satellites

14 Min > 6500 km

AFSPACECOM - ATMOSPHERIC NEUTRAL DENSITY SPECIALIST CONFERENCE

MARCH 22-23, 1988

SESSION 2: OPS SUPPORT

"MSFC'S MODELING AND USE OF ORBITAL DENSITY RESULTS"

by DALE JOHNSON, NASA-MSFC/ED44/(205) 544-1665

The Earth Science and Applications Division (ESAD) of NASA/MSFC provides orbital atmospheric support for the design studies of various planned NASA launch and space vehicles. Very little operational support is provided. Only as needed. Atmospheric models such as the MSFC/J70, now called the MSFC/Thermospheric Engineering Atmosphere Model (TEAM), are utilized in response to guidance, attitude and control studies which are needed by design engineers for vehicle response, precision orbit selection and positioning, attitude gyro saturation problems, etc. Atmospheric density is the key driver in these studies. A second area of density model support goes to the NASA lifetime prediction/orbital decay/satellite tracking program areas. Also atmospheric constituent input is used by those interested in material degradation and spacecraft glow problems. These atmospheric inputs and models are usually documented or baselined as the design criteria to use on selected NASA projects.

Some of the current orbital projects supported are: Space Station (document, JSC 30425), Space Telescope, OMV, and Tethered Satellite. Current orbital/middle atmosphere projects include: Space Shuttle, AOTV, AFE and NASP. ESAD generally supports projects on the drawing board, in the design stage, which are usually many years into the future. Comparisons of various atmospheric orbital models are also conducted by ESAD in order to determine and use the proper model for the proper application. See Figure 1.

A similar modeler/user density workshop was held at MSFC in November 1985, and has been documented as NASA CP-2460, entitled, "Upper and Middle Atmospheric Density Modeling Requirements For Spacecraft Design and Operations." I intend to highlight the key conclusions and recommendations as determined from this workshop. The workshop was called for because of a communications gap between the modelers and the engineering user communities. Once models or criteria were released, the modelers were unaware if the data and variations within the models were being used correctly or not. Likewise, the users could be unaware of

certain limitations and restrictions on the data or model. This could result in certain design and operational penalties. See Figure 2. There were eleven issues/user needs which surfaced and were concluded as a result of this workshop. These are presented in Figure 3.

The first five issues represent general recommendations and those dealing with middle atmospheric needs. The remaining six issues deal with thermospheric orbital density needs. #6 Better prediction of the input parameters used (i.e. solar flux and geomagnetic) in density models is needed in the short-or long-term. #7 The small-scale density structures are not accurately modeled. Perhaps some of the 15% density model uncertainty can be resolved using gravity wave theory, etc. #8 A need for more accurate thermospheric wind fields, especially at high latitudes, is needed. #9 Improvement of the theoretical Thermospheric General Circulation Models (TGCM) needs to be continued, and comparative studies done. Modelers need to be guided when using TGCM's. #10 For satellite drag studies the older Jacchia type model are generally preferred - since drag data went into these models. But with erosion and glow studies today, a need for a more accurate representation of the atmospheric constituents is needed (like the MSIS and Jacchia 1977 models). #11 The continuation of the routine middle and orbital atmospheric, solar and geomagnetic type measurements are still needed today for model improvements. In summary: The complexity of any density model does depend on the models application but the model also needs to be relatively simple and usable. Model accuracy needs improvement, and more measurements will help.

Since the November 1985 meeting there have been a few steps taken toward accomplishing some of these goals. An MSFC clearing house has been established concerning the GRAM model, which improves communications. Likewise, NASA and the USAF are more aware of what each is doing so that duplication of effort will be at a minimum. Use of the recent middle atmospheric data sources (i.e. satellite radiometry, limb scanners, lidar, MST radar, shuttle drag measurements) are currently being worked into the GRAM atmosphere. Funding for middle and orbital atmospheric measurements/research is still difficult to obtain today. NASA Headquarters has recently reorganized and has a Space Physics Division, which indicates some potential for orbital studies. The USAF/NASA NASP program is showing some receptiveness toward stratospheric and middle atmospheric programs which would aid NASP. The ENVIRONET (NASA-GSFC) currently has both the MSFC/TEAM and the MSIS-CIRA-86 models for its users. NASA/MSFC is currently evaluating the new geomagnetic storm model for TEAM,

and will be receiving a thermospheric wave model product from SAO by June. An abbreviated TGCM will be tested against the TEAM, MSIS, and J77. The AFGL Jac 70/Tidal model is also new, and will be evaluated. The MSFC orbital mechanics people have recently indicated a willingness to help compare density models with satellite data. The NASP Natural Environment Committee on May 11-12, 1988 will evaluate some density measurement programs like the mega lidar, and theoretical density perturbation studies, such as the thermospheric air glow data program. The up-coming CEDAR measurement program could use results from this theoretical study, for evaluation of emission data. Shuttle re-entry accelerometry data is also currently being backed out into density values along a 160-60 km altitude trajectory. The data sample will also aid GRAM in the middle atmospheric region by providing some quasi-horizontal gradient measurements of density.

Shown on Figure 4 is a schematic of the past history of the MSFC Global Reference Atmosphere Model (GRAM) and what future middle atmosphere and thermospheric plans are currently being accomplished. A GRAM-89 model is foreseen.

We feel that since orbital density models may be difficult to improve much beyond the current ~15% uncertainty limit, that efforts in enhancing/increasing the computer capability and more research in understanding more regarding errors in the drag coefficient, will also help this USAF operational problem.

ORGANIZATION: NASA - NSFC / ED44	MARSHALL SPACE FLIGHT CENTER MSFC's MODELING AND USE OF ORBITAL DENSITY RESULTS	NAME: DALE JOHNSON
CHART NO.:		DATE: MARCH 1988

THERMOSPHERIC ORBITAL MODELS USED BY NASA, ETC.

USED FOR: DESIGN & OPERATIONS - For Orbital and Re-entry/Launch

1. GUIDANCE & CONTROL - ATTITUDE: - (DENSITY)
 - Need response of operational systems
 - Satellite attitude control system problems - desaturation
 - Precision orbit positioning
2. MATERIALS DEGRADATION: - (CONSTITUENTS)
 - Deterioration of exposed surfaces
 - Drag coefficient
 - Spacecraft glow
3. SATELLITE LIFETIME PREDICTIONS/ORBITAL DECAY: - (DENSITY)
 - NORAD, NAVY, NASA, etc. Satellite tracking programs

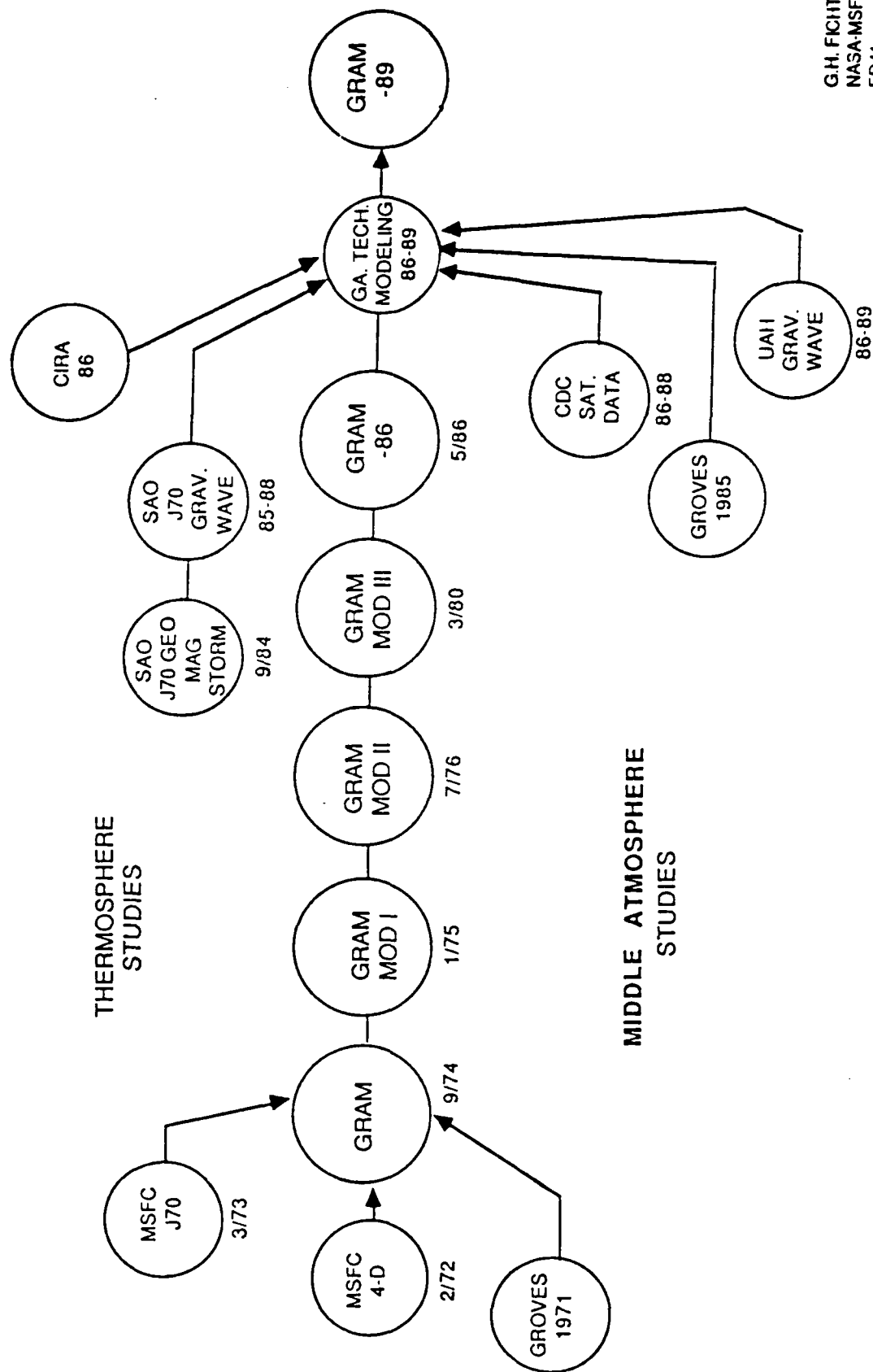
PROJECTS: (NASA)

1. ORBITAL: Space Station, Space Telescope, OMV, Tethered Satellite
2. ORBITAL/MIDDLE ATMOSPHERE: Shuttle, NASP, AOTV, AFE

ORGANIZATION: NASA - NSFC / ED44 CHART NO.:	MARSHALL SPACE FLIGHT CENTER NSFC's MODELING AND USE OF ORBITAL DENSITY RESULTS	NAME: DALE JOINSON DATE: MARCH 1988
<p>NOVEMBER 1985 DENSITY MODELERS/USERS MEETING:</p> <p>A COMMUNICATIONS GAP EXISTED BETWEEN MODELERS (DEVELOPERS/SUPPLIERS) AND ENGINEERING (USERS). Meeting called to develop a rationale and plan for possible solution.</p> <p><u>Modelers</u> were unaware of:</p> <ul style="list-style-type: none"> • How data was being used • How variations in natural environment parameters were being handled <p><u>Users</u> were unaware of:</p> <ul style="list-style-type: none"> • Limitations of and restrictions on data/models <p><u>Resulting in:</u> Design and Operational penalties</p> <p><u>CONCLUSION:</u></p> <ul style="list-style-type: none"> • Models must produce consistent/accurate values of atmospheric thermodynamic parameters from surface through exospheric levels for all lat/long/time/season/solar cycle phases. • System and mission planners use small-scale middle atmospheric variation statistics established by repeated runs of GRAM (ie. Shuttle, AOTV, AFE, Tethered Satellite) 		

ORGANIZATION: NASA - MSFC / ED44 CHART NO.:	MARSHALL SPACE FLIGHT CENTER MSFC's MODELING AND USE OF ORBITAL DENSITY RESULTS	NAME: DALE JOINSON DATE: MARCH 1988
<p>NOVEMBER 1985 UPPER & MIDDLE ATMOSPHERE DENSITY MODELING WORKSHOP CONCLUSIONS:</p> <p><u>ISSUES/USER NEEDS:</u> To Arrive at a More Efficient Time Model</p> <p><u>GENERAL:</u></p> <ol style="list-style-type: none"> 1. Better communications between modelers/users 2. Standardization - Prevent dup. of effort 3. Use new middle atmosphere data sources; 80-130/150 Km 4. Lack of Neutral Atmosphere Research Support 5. Comments/Recommendations to improve GRAM <p><u>THERMOSPHERIC:</u></p> <ol style="list-style-type: none"> 6. Better Prediction of Input Parameters - Solar/Geomagnetic Activity 7. Small-Scale Structures (in Space/Time) not Accurately Modeled 8. Need Better Representation of Wind-fields 9. Improve/Use Thermospheric GCM 10. Preference for old Jacchia Density Models - Need more accurate representation of constituent number densities 11. Continuation of "Routine" Measurements - of EUV, UV, Total Density, Constituent No. Density, 10.7cm Solar Flux, Ap (Kp), & Winds <p><u>MODEL SUMMARY:</u></p> <ol style="list-style-type: none"> 1. Hierarchy of Model Complexity - Depends on Applications 2. Need Increased Model Accuracy 3. Models must be Useable/Simple 4. Need More Measurements <p><u>CURRENT MODELING STATUS:</u></p> <ol style="list-style-type: none"> 1. GRAM Improvement Studies 2. Environet uses MSFC/TEAM & MSIS-CIRA-86 3. MSFC Thermospheric Geomagnetic Storm, and Wave Model Studies (in time) 4. Use of Rees abbreviated TtCM (using coefficients) 5. AFGL Jac70/Forbes Tide Model 6. InterModel Comparisons and Thermospheric Theoretical Airglow Studies 		

GRAM MODEL DEVELOPMENT HISTORY



G.H. FICHTL
NASA-MSFC
ED41
205-544-1626
FTS-824-1626
5-625-7-8

A Summary of Civilian
Neutral Density Modelers
Utilizing Services
from the Space Environment
Services Center
(Extended Abstract)

Presented at the
Air Force Space Command
Atmospheric Neutral Density Specialist Conference
Peterson AFB, Colorado
March 22-23, 1988

Gary Heckman
NOAA R/E/SE2
325 Broadway
Boulder, Colorado
80303

The Space Environment Services Center (SESC), located in Boulder, Colorado, is operated jointly by NOAA and the Air Weather Service to provide space environment services to meet national needs. The SESC provides forecasts, data, and guidance to the Department of Defense through the Global Weather Central and serves the civilian community directly. Among the services provided are forecasts and current values of indices required by civilian users to run operational and developmental neutral density models. Table 1 summarizes the users who are operating neutral density models and who utilize products from the SESC.

Table 1. Neutral density modelers who use SESC indices, forecasts or guidance

User	Type Model	Indices	Application	Altitude
Naval Astronautics Group	Modified Jacchia	10 cm K_p	Navigation satellite positioning	1000 km
Martin Marietta	MSIS	10 cm A_p	Thermal loading and payload fairing release during launches	80 km
NASA Marshall Space Flight Center	Jacchia	10 cm A_p	Projection of re-entry time and attitude control heights	Various
North American Rockwell-Johnson Space Center	Modified Jacchia	10 cm A_p K_p	Shuttle Drag Coefficient refinement	105-270 nm
Lincoln Laboratories	Various	10 cm A_p TED	Development and evaluation of models and inputs	Various

Notes:

10 cm is solar radio flux at 10 cm wavelength (2800 mHz).
 A_p and K_p are standard geomagnetic indices.
 TED is the total energy deposited in the upper atmosphere by precipitating particles as measured by the NOAA Satellite.

Options For Improving Drag Calculations At NAVSPASUR

Paul W. Schumacher, Jr.
Analysis & Software Department
NAVSPASUR, Dahlgren, Virginia
22 March 1988

Abstract

The main features of NAVSPASUR's catalog maintenance procedures are described. It is noted that the general theory used to propagate orbital elements forward in time does not at present include drag perturbations. Rather, observed changes in mean motion (inferred by differential correction) are used to estimate mean decay rates in semimajor axis and eccentricity. While producing the correct element trends for predictions over 2-3 days, this extremely simple "reduced-order" decay model has quantitative deficiencies which can lead to temporary mis-identification of satellites. Probably the best long-term remedy is to implement a new general theory which includes drag perturbations. However, this would require a long development and test/evaluation time. The present discussion examines a near-term alternative which can be pursued with modest effort, namely, refining the reduced-order decay model. On this approach one hopes merely to obtain more accurate mean decay rates than are now used. Some general analytical results are reviewed for the case of a locally exponential density profile. For more complicated profiles one can consider using numerical quadrature rather than literal expansions, even for catalog maintenance work, because the reduced-order equations are fairly simple. It does, of course, remain to be seen whether simple techniques of this type can be pushed far enough to effect any noticeable improvement in day-to-day operations.

Present NAVSPASUR Procedures

The catalog maintenance process at NAVSPASUR can be described very generally as follows. Upon receipt of observations and identification of the satellites, differential correction (D/C) is initiated to update the orbital elements to a new epoch. The parameters used in the D/C are nonsingular combinations of the classical elements designed to avoid geometrical indeterminacies at low eccentricity and low inclination. These parameters are akin to the so-called "equinoctial elements", but have the additional property of being valid even for retrograde equatorial orbits. The D/C also produces values for the parameters M_2 and M_3 , which are essentially rate of change and acceleration of mean motion respectively. These extra parameters are quite important at NAVSPASUR since they are the primary means by which orbital decay is detected and accounted for. Indeed, the D/C process itself is affected critically by these parameters. By an empirically derived formula, the values of M_2 and M_3 are used to determine the time-span of data over which the next day's D/C will be performed for that satellite. This so-called "fit span" can fall between 3 and 30 days, the shorter spans corresponding to higher decay rates. For exceptional satellites, operations analysts can manually specify fit spans outside this range. The importance of selecting a suitable fit span should be appreciated in light of the fact that drag perturbations are not well modelled at NAVSPASUR. Without accurate drag modelling, observations remote in time from the present are not significant for near-term predictions and should be ignored. The empirical fit span formula

provides this adjustment in a systematic way tuned to the characteristics and requirements of the NAVSPASUR system. Once the orbit has been differentially corrected and a new epoch established, the elements are propagated forward in time using the general theory of Brouwer [5] as modified by Lyddane [7] to handle low-eccentricity cases. This theory is notable for its accuracy in following gravitationally perturbed orbits, and has been implemented in a concise and efficient FORTRAN program at NAVSPASUR. However, the theory does not include any atmospheric perturbations.

With Brouwer elements available at a given time, conversion is made to the classical elements which in turn are used for a variety of purposes, including position predictions to be compared with future observations. Typically, predictions are needed for 2 to 3 days in the future, long enough that decay effects must somehow be included even though the general theory does not include them. The decay corrections now being used are applied to the classical elements themselves. In particular, mean motion is augmented with a term in M_2 . The quantity M_3 is available and could be included in the mean-anomaly polynomial, but it has been found that generally better predictions ensue when M_3 is not included, at least over 2 to 3 days. This effect has not been scrutinized; it seems to be due to better smoothing of unmodelled effects. In virtually all cases M_3 is very small. The observed mean motion rate M_2 is also used to estimate mean decay rates in semimajor axis a and eccentricity e .

The term \dot{a} is obtained by differentiating Kepler's Third Law in the form $n^2 a^3 = \text{constant}$. A minor refinement is to use the Brouwer "mean" mean motion M_1 rather than the osculating mean motion n in the calculation of \dot{a} . Subsequently, the mean eccentricity rate \dot{e} is computed in terms of \dot{a} by a formula to be explained later. These equations are examples of what might be called a "reduced-order" decay model: less than the full set of elements is included in the drag calculation, based (hopefully) on reasonable approximations.

The association of a single-station observation with a prediction is accepted based on a set of empirical tolerances (observed minus expected) in the values of time, direction cosine and Doppler shift for the satellite. Of particular interest is the tolerance in the time, which can vary from 2 to 30 seconds. This time tolerance is an empirical function of semimajor axis a , observed mean motion rate M_2 and time from epoch expressed as elapsed mean anomaly $M - M_0$. Low, rapidly decaying satellites far from the epoch call for the largest tolerance. As in the case of fit span, the importance of selecting a suitable time tolerance for association purposes should be appreciated. Since drag is poorly modelled in the system, too tight a tolerance would result in failure to associate the observation with any prediction. On the other hand, with an average of 45,000 observations being collected over a 24-hour span, it is likely that more than one prediction could be associated with an observation when the time tolerance is

relaxed. The dilemma is unavoidable as long as decay effects are poorly predicted. The empirical answer at NAVSPASUR has been to try to make sure that at least one association can always be made. In case of more than one possible association, the candidate with the smallest time difference is accepted.

There are obvious shortcomings in this strategy. A typical difficulty is that a sequence of closely spaced satellites may change their "parade order" under drag perturbations of the mean motions. This results in either unidentified or misidentified observations. The former call for some manual intervention to identify the satellite; the latter lead to manual D/C in which the analyst attempts to find and omit the offending observations from the input data. Some idea of the magnitude of this effort can be gained by noting that from 15 February to 15 March 1988 about 1500 manual identifications and about 4500 manual D/C's were required. Of course, these figures count occasions due to all causes, not just those due to decay uncertainties. Another effect of poor drag modelling is that the point of breakup in a separation event is poorly determined due to differential decay of the pieces. This sometimes makes it impossible to choose with reasonable certainty among many candidate "blast points". One might well anticipate an increasing future demand for precise locations of breakups, such as might be needed to distinguish accidents from deliberate and hostile actions. A third and very fundamental difficulty caused by poor decay modelling is that the final few orbits in the satellite's lifetime are poorly followed. Needless to say, this final phase is of great interest for many satellites.

Improving the Drag Calculations

The options for including accurate drag perturbations in NAVSPASUR calculations are just beginning to be examined afresh. In the past, when only some hundreds of satellites were being cataloged, there was no operational imperative to implement elaborate drag predictions. Even now, with more than 6500 objects in the catalog, there is still no operational imperative to include drag more accurately; that is, NAVSPASUR is presently quite successful in its operations. However, the analyst workload due to decay-related anomalies is significant. Moreover, that workload is an obvious, though as yet undocumented, function of atmospheric activity as measured by geomagnetic and solar flux (10.7cm) indices. (These indices are available daily at NAVSPASUR.) The nature of the satellite identification problem is such that it must get worse geometrically as the number of low-altitude satellites increases. Hence, it is only prudent to explore possible improvements before the matter does become imperative.

In the event that high accuracy in position were required, say, on the order of 10 meters, NAVSPASUR would have to resort to a special theory and simply bear the computational burden. The relatively few requests to date for arcs of such accuracy have always involved rather high-altitude satellites for which drag perturbations are either insignificant or not the limiting factor in the overall accuracy. Thus, no really accurate atmospheric model has ever been needed. But the choice of atmospheric model

would instantly become a crucial issue if high-accuracy low-altitude arcs were requested. With the choice made, though, including drag effects in the special theory is straightforward. For catalog maintenance, one can usually be satisfied with position accuracy on the order of 1 kilometer, for which a general theory will suffice. This is a fortunate circumstance; numerical integration, even at this accuracy, would be prohibitively time-consuming for catalog maintenance. Hence, the best prospect for improving NAVSPASUR catalog maintenance in the long run is to implement a general theory which accounts for drag. The theory of Lane and Cranford [4], currently used at NORAD/SSC, is certainly one candidate. The theory of Brouwer and Hori [1,6] was studied at NAVSPASUR more than twenty years ago, but finally was not developed for implementation due to lack (at that time) of a compelling need for it. Whatever general theory is selected, one can anticipate a long development and test/evaluation time for such a critical software component. If near-term results are desired and only modest effort can be allocated to the task, there is still an alternative worth exploring, namely, to refine the reduced-order decay model.

Drag models consisting of coupled equations for the elements a and e have been developed extensively by Sterne [3], King-Hele [2] and others. Typically, eccentric anomaly is used as the independent variable, and some averaging operation is used to obtain mean rates for these two elements. Considering only a and e is equivalent to assuming spherical symmetry of the atmosphere and

neglecting atmospheric rotation. Under these approximations, the orientation elements are not affected by drag, giving rise to the simple reduced-order system of two equations. (It will be assumed in this discussion that the perturbation of mean motion is an observed quantity and is available for input to the model.) Usually the two equations are solved to first-order. Then at the second order changes in the orientation elements can be considered, which arise due to atmospheric rotation, atmospheric oblateness and coupling with gravitationally - induced precessions of the orbit.

It may be found that numerical quadrature is a feasible way to obtain the first-order change in a and e , even for catalog maintenance applications. The equations are fairly simple and are valid for arbitrary density/height profiles. This approach does require a-priori knowledge of the ballistic coefficient for the satellite. Useful comments are found in the book by Sterne [3]. If the density/height profile is assumed to be exponential in the vicinity of some reference height, then analytical results are possible. The rate equations for a and e are found to contain cosine eccentric anomaly both in an exponential function and in algebraic factors. If the algebraic factors are developed in Fourier series and the equations are averaged over one revolution, the solution appears as an infinite series of modified Bessel functions. This is the approach taken by King-Hele [2] in his analysis of satellite lifetimes. There are a variety of ways to

evaluate the Bessel functions for both small and large values of the argument. Another way of treating the rate equations is to include the exponential function in the Fourier expansion. The Fourier coefficients will now be more complicated due to expanding the exponential function, but when each equation is averaged over one revolution only the leading coefficient remains. It turns out that the leading coefficient can be obtained explicitly without developing the rest of the expansion, and it can be arranged as an infinite series in the eccentricity. The series converges, but whether it converges fast enough to be useful is not known yet. A little inspection of this solution shows that the formula for mean decay rate of eccentricity currently used at NAVSPASUR is really a crudely truncated version of the Fourier series. Evidently, here is the place to begin refining the current model.

When first-order drag variations in a and e are available, one can address the second-order effects mentioned before. Of these, the easiest to illustrate is the coupling with gravitationally-induced mean rates in the node and perigee angles. The latter happen to be simple functions of a and e so the necessary partial derivatives are easy to obtain. Variations in node, perigee and inclination due to rotation of the atmosphere and atmospheric oblateness are more complicated. King-Hele [2] provides extensive discussion.

There is an altogether different type of analysis which may lead to a useful reduced-order model and which has not been thoroughly investigated. The concept is presented here in its "half-baked" form because several of its features have not been discussed in the literature. The analysis begins with a set of regularized equations of a type first proposed by Burdet [8]. The independent variable is true anomaly elapsed from the epoch, and the dependent variables consist of reciprocal radius, angular momentum, time, and a set of orthonormal unit vectors defining the osculating plane. In terms of these variables, the Cartesian position and velocity vectors have simple forms. The differential equations have the interesting property that they are rigorously linear for Keplerian motion. A further remarkable property appears when drag is modelled as any scalar function whatsoever multiplying the velocity vector. In that case all the equations except the one for angular momentum revert to their Keplerian forms. In principle, the only approximation enters in the solution for angular momentum. The rest of the system can be solved exactly using quadratures at most. Mittleman and Jezewski [9] examined the special, somewhat unrealistic, case in which angular momentum can also be obtained exactly. However, they did not discuss the more general property just noted.

Other Possibilities Related to Drag Modelling

It is worth mentioning a few topics that could be addressed if drag perturbations were being accounted for in a routine and accurate manner. As researchers attempt to model atmospheric phenomena more accurately, there is always the problem of observing and estimating the new parameters that arise. Satellite observations have been a prime source of observations for ionospheric and exospheric phenomena. Often the orbital effects of the phenomena would be detectable even though they are not significant for satellite operations. In this case, the possibility exists of using NAVSPASUR historical data to validate density models over extended past time. Complete observational archives have been maintained on magnetic tape since the inception of Naval Space Surveillance. The data is in the form of element sets and triangulated positions for every satellite observed by NAVSPASUR. Records extend over more than two complete solar cycles - almost thirty years. Although NAVSPASUR is not in a position to participate directly in such work, in principle the archives could be made available to researchers.

Another possibility of perennial interest is to estimate the ballistic coefficient of the satellite and from that infer values for the satellite mass or cross-sectional area. In using the reduced-order (a,e) model, the ballistic coefficient would be obtained by observing the decay in mean motion and inserting this value into the differential of Kepler's Third Law, producing the decay in semimajor axis. Then, given a suitable density profile, the ballistic coefficient in the reduced-order model is adjusted to match the calculated decay in semimajor axis to its known value. Information from other sources would then be needed to isolate any of the three parameters comprising the ballistic coefficient.

Another problem which has received scant attention is the rigorous derivation of the law governing the drag force magnitude. The law universally assumed nowadays is really just the definition of drag coefficient. It has little physical basis as a force law. It was originally derived by dimensional analysis of the variables judged to be significant in the inviscid flow of an incompressible fluid. This is hardly the flow regime encountered by a satellite. Of course, a proper critique of the drag law cannot be made until drag perturbations are being calculated very accurately.

Finally, if drag perturbations are being predicted well, one may hope to detect smaller effects now considered intractable to model. Examples might be differential rotation between the upper atmosphere and the solid Earth, and the orbital precession due to lift of a large-area satellite which has been attitude-stabilized in the direction of the sun. Naturally, it is doubtful whether simple reduced-order drag models would allow one to penetrate

References

1. D. Brouwer and G. M. Clemence, Methods of Celestial Mechanics, Academic Press, New York, 1961. See Chapter XVII.
2. Desmond King-Hele, Theory of Satellite Orbits in an Atmosphere, Butterworths, London, 1964.
3. Theodore E. Sterne, An Introduction to Celestial Mechanics, Interscience Publishers, Inc., New York, 1960. See Chapter 5.
4. NORAD Technical Publication SCC-008, "Mathematical Foundation for SCC Astrodynamics Theory", 6 April 1982.
5. D. Brouwer, *Astronomical Journal*, 1959, vol. 64, p. 378 ff; with erratum in vol. 65, p. 108.
6. D. Brouwer and G.-I. Hori, *Astronomical Journal*, 1961, vol. 66, no. 2, p. 39 ff.; and vol. 66, no. 6, p. 264 ff.
7. R. Lyddane, *Astronomical Journal*, 1963, vol. 68, no. 8.
8. Claude A. Burdet, *Journal für die Reine und Angewandte Mathematik*, 1969, band 238, p. 71 ff.
9. Don Mittleman and Don Jezewski, *Celestial Mechanics*, 1982, vol. 28, p. 401 ff.

OPTIONS FOR IMPROVING DRAG CALCULATIONS

AT NAVSPASUR

22 MARCH 1988

PAUL W. SCHUMACHER, JR.

NAVSPASUR ORBITAL CALCULATIONS

D/C PARAMETERS	BROUWER/LYDDANE	PREDICTION PARAMETERS
	GENERAL THEORY	(~ 48 HOURS)

$$\begin{aligned}
 &M + \omega + \Omega \\
 &\sqrt{\mu/a^3} \\
 &e \cos(\omega + \Omega) \\
 &e \sin(\omega + \Omega) \\
 &\sin \frac{I}{2} \cos \Omega \\
 &\sin \frac{I}{2} \sin \Omega
 \end{aligned}$$

$$\begin{aligned}
 &M, M_1 \\
 &\sqrt{\mu a} \\
 &\sqrt{\mu a(1-e^2)} \\
 &\sqrt{\mu a(1-e^2)} \cos I \\
 &\Omega \\
 &\omega
 \end{aligned}$$

$$\begin{aligned}
 &M = M_0 + M_1 t + M_2 t^2 + M_3 t^3 \\
 &\alpha = \alpha + \dot{\alpha} t \\
 &e = e + \dot{e} t \\
 &\cos I \\
 &\Omega \\
 &\omega
 \end{aligned}$$

M_2 } OBSERVED DECAY
 M_3 } IN MEAN MOTION

NO DECAY MODELLED

$$\begin{aligned}
 \dot{\alpha} &= -\frac{4}{3} \alpha \frac{M_2}{M_1} \\
 \dot{e} &= e(1-e^2) \frac{\dot{\alpha}}{\alpha}
 \end{aligned}$$

FIT SPAN = $f(M_2, M_3)$
 = 3 TO 30 DAYS

SATELLITE IDENTIFICATION

	NAVSPASUR ACCURACY (SENSOR + D/C ORBIT)	EMPIRICAL TOLERANCE FOR SAT. ID.
TIME AT FENCE PLANE	<0.25 SEC (SENSOR)	± 2 . TO 30. SEC. $f(\alpha, M_2, M-M_0)$
EAST/WEST DIRECTION COSINE ($\cos \theta$)	± 0.0002 ($\sim 40^\circ$ ZENITH)	$\pm 0.035 \sin \theta$ ($\sim 2^\circ$ ZENITH)
DOPPLER SHIFT	± 3 . TO 4. HZ.	± 110 . OR ± 310 . HZ.

TOTAL OBSERVATIONS PER DAY: 80,000+ RECEIVED
45,000 PROCESSED

TYPICAL DIFFICULTIES WHEN DRAG IS SIGNIFICANT

- (1) RAPID VARIATIONS IN DENSITY PROFILE INCREASE THE NUMBER OF UN-IDENTIFIED AND MIS-IDENTIFIED OBS.
MAIN REASON: PERTURBATIONS CAN CHANGE THE

"PARADE ORDER" OF SATELLITES WHEN
PREDICTED PASSES ARE CLOSELY SPACED.

- (2) "BLAST POINTS" OF SEPARATION EVENTS ARE POORLY DETERMINED DUE TO DIFFERENTIAL DECAY OF PIECES.

- (3) FINAL DECAY NOT ACCURATELY FOLLOWED.

OPTIONS FOR INCLUDING DRAG PERTURBATIONS AT NAVSPASUR

(1) FOR HIGH PRECISION (ACCURACY ~ 10M OR BETTER)

SPECIAL THEORY • NOT AN ISSUE YET

(2) FOR CATALOG MAINTENANCE (ACCURACY ~ 1KM OR BETTER)

GENERAL THEORY

• BROUWER/HORI (1961)

• LANE/CRAFORD (1965, 1969)

REDUCED-ORDER DECAY MODEL

• STERNE (1960)

• KING-HELE (1964 AND LATER)

USED NOW

$$\begin{cases} \dot{\alpha} = -\frac{4}{3}\alpha \frac{M_2}{M_1} \\ \dot{e} = e(1-e^2)\frac{\dot{\alpha}}{\alpha} \end{cases}$$

(3) FOR ASPADOC SUPPORT

TYPICAL REDUCED-ORDER DECAY MODEL

$$\frac{da}{dE} = -\delta \rho a^2 (1 + e \cos E) \sqrt{\frac{1 + e \cos E}{1 - e \cos E}}$$

$$\frac{de}{dE} = -\delta \rho a (1 - e^2) \cos E \sqrt{\frac{1 + e \cos E}{1 - e \cos E}}$$

WHERE DRAG = $\frac{1}{2} \rho V^2 A C_D$, OPPOSITE TO ORBITAL VELOCITY

$$\delta = \left(\frac{C_D A}{m} \right) \left(1 - \frac{r_{p0}}{V_{p0}} W \cos I \right)^2$$

- ASSUMES SPHERICALLY SYMMETRIC ATMOSPHERE
- NEGLECTS ATMOSPHERIC ROTATION, EXCEPT PARTLY AT PERIGEE

FOR "LOCALLY EXPONENTIAL" ATMOSPHERE:

$$\rho = \rho_{\text{REF}} \exp\left(\frac{r_{\text{REF}} - r}{H}\right) \quad \text{WHERE} \quad r = a(1 - e \cos E)$$

$$\frac{da}{dE} = -\delta \rho_{\text{REF}} \exp\left(\frac{r_{\text{REF}} - a}{H}\right) a^2 \exp\left(\frac{ae}{H} \cos E\right) (1 + e \cos E) \sqrt{\frac{1 + e \cos E}{1 - e \cos E}}$$

$$\frac{de}{dE} = -\delta \rho_{\text{REF}} \exp\left(\frac{r_{\text{REF}} - a}{H}\right) a(1 - e^2) \exp\left(\frac{ae}{H} \cos E\right) \cos E \sqrt{\frac{1 + e \cos E}{1 - e \cos E}}$$

$$I_n(z) = \frac{2}{\pi} \int_0^{2\pi} \exp(z \cos \phi) \cos n\phi \, d\phi$$

NOTE:

$$z = \frac{ae}{H}$$

SOLUTION IN MODIFIED BESSEL FUNCTIONS

- FIRST-ORDER IN ($\delta \rho_{\text{REF}}$)
- CHANGES IN ONE REVOLUTION ($E=0$ TO $E=2\pi$)

$$\Delta a = -\delta \rho_{\text{REF}} \exp\left(\frac{\Gamma_{\text{REF}} - a}{H}\right) \alpha^2 \left\{ \frac{\pi}{2} \sum_{k=0}^{\infty} \left[\sum_{\ell=0}^k \left(\frac{3/2}{k-\ell} \right) \left\{ \frac{1/2}{\ell} \right\} \right] \left[\sum_{m=0}^k \binom{k}{m} I_{k-2m}(z) \right] \frac{e^k}{2^k} \right\}$$

$$\Delta e = -\delta \rho_{\text{REF}} \exp\left(\frac{\Gamma_{\text{REF}} - a}{H}\right) \alpha(1 - e^2) \left\{ \frac{\pi}{2} \sum_{K=0}^{\infty} \left[\sum_{\ell=0}^K \left(\frac{1/2}{K-\ell} \right) \left\{ \frac{1/2}{\ell} \right\} \right] \left[\sum_{m=0}^{K+1} \binom{K+1}{m} I_{K+1-2m}(z) \right] \frac{e^K}{2^{K+1}} \right\}$$

EVALUATE $I_n(z)$ BY

- POWER SERIES
- ASYMPTOTIC SERIES
- RECURRENCE FORMULAE

SOLUTION IN FOURIER COSINE SERIES

- FIRST-ORDER IN ($\delta\rho_{\text{REF}}$)
- CHANGES IN ONE REVOLUTION ($E=0$ TO $E=2\pi$)

$$\Delta a = -2\pi\delta\rho_{\text{REF}} \text{EXP}\left(\frac{\rho_{\text{REF}} - a}{H}\right) a^2 \left[1 + F_1^{(0)}(a, e, H)\right]$$

$$\Delta e = -2\pi\delta\rho_{\text{REF}} \text{EXP}\left(\frac{\rho_{\text{REF}} - a}{H}\right) a(1-e^2) \left[F_2^{(0)}(a, e, H)\right]$$

$$F_1^{(0)} = \sum_{K=1}^{\infty} \left(\sum_{n=0}^{2K} \left[\sum_{\ell=0}^{2K-n} \binom{3/2}{2K-n-\ell} \left\{ \binom{1/2}{\ell} \right\} \frac{1}{n!} \left(\frac{a}{H}\right)^n \right] \binom{2K}{K} \frac{e^{2K}}{2^{2K}} \right)$$

$$F_2^{(0)} = \sum_{K=1}^{\infty} \left(\sum_{n=0}^{2K-1} \left[\sum_{\ell=0}^{2K-1-n} \binom{1/2}{2K-1-n-\ell} \left\{ \binom{1/2}{\ell} \right\} \frac{1}{n!} \left(\frac{a}{H}\right)^n \right] \binom{2K}{K} \frac{e^{2K-1}}{2^{2K}} \right)$$

OBSERVE: $\Delta e = \left[\frac{F_2^{(0)}}{1 + F_1^{(0)}} \right] (1-e^2) \frac{\Delta a}{a}$

MEAN INCREMENTS IN NODE AND PERIGEE RATES

$$\dot{\Omega} = - \frac{3J_2 R^2 \cos I}{2a^2(1-e^2)^2}$$

$$\dot{\omega} = + \frac{3J_2 R^2 (5\cos^2 I - 1)}{4a^2(1-e^2)^2}$$

VARY AS a^{-3} AND e^{-2} DECAY

$$\Delta \dot{\Omega} = \frac{\partial \dot{\Omega}}{\partial a} \Delta a + \frac{\partial \dot{\Omega}}{\partial e} \Delta e = \left[\frac{4e\Delta e}{1-e^2} - \frac{2\Delta a}{a} \right] \dot{\Omega}$$

$$\Delta \dot{\omega} = \frac{\partial \dot{\omega}}{\partial a} \Delta a + \frac{\partial \dot{\omega}}{\partial e} \Delta e = \left[\frac{4e\Delta e}{1-e^2} - \frac{2\Delta a}{a} \right] \dot{\omega}$$

- MOST PROMINENT SECOND-ORDER EFFECTS
- OUGHT TO INCLUDE ATMOSPHERIC ROTATION AND OBLATENESS AT THIS ORDER

A POSSIBLE REDUCED-ORDER DECAY MODEL (BURDET VARIABLES)

$$\hat{R}' = \hat{T}$$

$$\hat{T}' = -\hat{R} + \frac{1}{h^2 u^3} (\underline{P} \cdot \hat{N}) \hat{N}$$

$$\hat{N}' = -\frac{1}{h^2 u^3} (\underline{P} \cdot \hat{N}) \hat{T}$$

$$u'' + u = \frac{\mu}{h^2} - \frac{1}{h^2 u^3} [(\underline{P} \cdot \hat{R})u + (\underline{P} \cdot \hat{T})u']$$

$$(h^2)' = \frac{2}{u^3} (\underline{P} \cdot \hat{T})$$

$$t' = \frac{1}{h u^2}$$

$$(\quad)' \equiv d(\quad)/dx$$

X = TRUE ANOMALY FROM EPOCH

\hat{R} = UNIT RADIAL VECTOR

\hat{T} = UNIT TRANSVERSE VECTOR

\hat{N} = UNIT NORMAL VECTOR

\underline{P} = TOTAL PERTURBING ACCEL.

u = RECIPROCAL RADIUS

h = ANGULAR MOMENTUM

t = TIME

POSITION

$$\underline{r} = \frac{1}{u} \hat{R}$$

VELOCITY

$$\underline{v} = h(u \hat{T} - u' \hat{R})$$

IF DRAG IS MODELLED AS $\underline{P} = -s \underline{V} = -sh(u\hat{T} - u'\hat{R})$

THEN:

$$\left. \begin{aligned} \hat{R}' &= \hat{T} \\ \hat{T}' &= -\hat{R} \\ \hat{N}' &= 0 \end{aligned} \right\}$$

UNPERTURBED FORM

$$\left. \begin{aligned} u'' + u &= \frac{\mu}{h^2} \\ (h^2)' &= -\frac{2sh}{u^2} \\ t' &= \frac{1}{hu^2} \end{aligned} \right\}$$

RIGOROUSLY SOLVABLE IN QUADRATURES IF

$$s = ku^2 = \frac{k}{r^2}$$

(MITTLEMAN AND JEZEWSKI, 1982)

WHAT IF DRAG IS BEING ACCOUNTED FOR "VERY WELL"?

(1) VALIDATE DENSITY MODELS WITH NAVSPASUR ARCHIVE DATA

- TRIANGULATED POSITION OBS.
- ELEMENT SETS

(2) ESTIMATE VEHICLE PARAMETERS FROM $\left(\frac{C_D A}{m}\right)$

- CROSS SECTION
- MASS

(3) CRITIQUE DRAG LAW: $D = \frac{1}{2} \rho V^2 A C_D$?

(4) LOOK FOR SMALLER EFFECTS

- ATMOSPHERIC DYNAMICS
- LIFT PRECESSION OF SOLAR-ORIENTED SATS

M.I.T. Lincoln Laboratory Analysis of Satellite Drag

E. M. Gaposchkin and A. J. Coster

ABSTRACT

The use of atmospheric density models for the calculation of the drag force on satellites is evaluated. First, the variety of different roles that drag models play in the field of satellite tracking and space surveillance is discussed. Then, problems associated with determining the atmospheric drag on a satellite are presented. This is followed by a description of the current suite of atmospheric models. A subset of these models is selected for further quantitative consideration. This subset includes: Jacchia 1971 [CIRA 1972], Jacchia 1977, Barlier et al., 1977 [DTM], and Hedin 1983 [MSIS83]. These models are evaluated using precision tracking data on three spherical satellites. The satellites have perigee heights of 270 km, 780 km, and 1500 km. Cook's 1965 definition of C_d is used in this analysis. At the lower altitude, 270 km, all models performed equally well. At the higher altitudes, the models do not perform as well. Using our tracking data, an evaluation is also made of the atmospheric indices currently input to the models, the K_p and F10.7 cm flux, and of the precipitation index, which is not yet included in the models. Significant correlation is found with our data and the precipitation index. Based on this information, a suggested first revision to a version of the Jacchia 77 model is presented. In conclusion, drag data can still play an important role in understanding the thermosphere and in contributing unique data to monitor this next solar cycle.

I. INTRODUCTION

Atmospheric drag affects all satellites - in all altitude regimes - from low altitudes to beyond geosynchronous altitudes. For many satellites, the modelling of atmospheric drag is the largest error source in describing the force on the satellite. The focus of this paper is the use of atmospheric density models for calculation of the drag force on satellites. Atmospheric drag is viewed from the vantage point of satellite tracking. The data analysis presented in this paper comes from precision radar tracking data beginning in 1985 on two spherical satellites and from laser ranging data taken in 1986 on a third spherical satellite. The satellites have perigee heights of 270 km, 780

km, and 1500 km. These data were used to evaluate the following atmospheric density models: Jacchia 1971 [CIRA 1972], Jacchia 1977, Barlier et al., 1977 [DTM], and Hedin 1983 [MSIS83], using Cook's 1965 definition of C_d .

As introduction, Figure 1 illustrates several aspects of the atmospheric drag problem. First, observe the drag force equation. The drag force is a product of four factors: C_d , the ballistic coefficient; A/M , the area-to-mass ratio; ρ , the atmospheric density, and V , the speed of the satellite with respect to the atmosphere.⁵ Each of these quantities will be discussed in a later section of this paper. However, note here that none of these quantities is known precisely. An error made in the calculation of atmospheric drag can be related to an error made in determining any one of the above factors, and is more likely due to a combination of errors in all of them.

A second aspect of the atmospheric drag problem is suggested by the two separate terms for density listed directly below the drag force equation. Two terms are used because none of the standard atmospheric models predict reliable densities above 2000 km. This is despite the fact that drag effects are observed above this altitude. The reason is that, until recently, the primary interest in drag has been in the low altitude regimes. The majority of data used in building the atmospheric models comes from regions below 1000 km. Additional data is needed above 1000 km. Also, it is probable that the physical process of the two regions (above and below 2000 km) are different. In our analysis, we use an integrated atmospheric density model. Below 2000 km, the atmospheric density is determined from one of the conventional atmospheric models using inputs such as the F10.7 cm flux and the geomagnetic index, K_p . It is also assumed that the lower atmosphere is corotating with the solid earth. Above 2000 km, an empirically determined density fixed in inertial space is used.

Finally, in Figure 1, the size of the drag effect is suggested in a simplified model calculation. In this figure all satellites are assumed to be spheres with the same area-to-mass (A/M) ratio. The A/M is chosen to be $0.1 \text{ cm}^2/\text{gram}$ which is typical for satellite payloads. We calculate the time for drag to change the satellite position by 12 km. This is, in one sense, the orbit error committed ignoring drag altogether. It is found that for satellite COS 11796, which is a calibration sphere with perigee at about 300 km, there will be 12 km in error (along track) in 0.92 days or 13.6 revolutions. For LCS 4, another calibration sphere with perigee at about 800 km, there will be a 12 km error in 22.8 days or 323 revolutions. While for LCS 1, a calibration sphere with perigee at 2800 km there will be a 12 km

error in 38.9 days or 386 revolutions. Clearly, although the drag effect is far more noticeable at lower altitudes, there is significant drag observed at all altitudes.

II. USES OF DRAG MODELS

The primary uses of drag models are: precision orbit determination, mass determination or weighing of satellites, and investigation of geophysical phenomena. The first two uses, precision orbit determination and weighing of satellites, are considered time critical. Results must be available within hours to be of use. The last one, geophysical investigations, which includes the specific area of atmospheric physics, is less time critical. One can await a posteriori analysis to obtain an optimal estimate of the orbit. Table 1 summarizes the uses of atmospheric drag models and the different areas in satellite tracking that are involved in drag measurement.

Table 1. Uses of Drag Models

Precision Orbit Determination (Time Critical)

- Catalog Maintenance

- SOI

- Prediction/Forecasting

- ASAT Targeting/Threat Analysis

- Data Screening and Calibration

- Collision Avoidance

- Navigation of Satellites (e.g. Transit)

Weighing of Satellites (Time Critical)

- SOI

- Damage Assessment

- Decoying of Space Assets

- Space Debris Characterization

Geophysical Investigations

Atmospheric Physics

- Model Development

- Calibration of Other Sensors

- Synthesis with Other Data

Other Investigations

- Polar Motion and Earth Rotation

- Scientific Satellites Precision Orbits

- (MAGSAT, SEASAT, TOPEX)

A. Precision Orbit Determination

The main use of drag models is the determination of precision orbits. Because atmospheric drag is one of the largest forces on a satellite, accurate modelling of the atmosphere is required to obtain precision orbits. The ability to know precise satellite positions contributes to a variety of areas in satellite

tracking. For example, precision orbits on satellites are needed for catalog maintenance, SOI (Satellite Orbit Identification), collision avoidance, satellite navigation (e.g. Transit), ASAT targeting and threat analysis, and data screening and calibration.

Catalog maintenance requires knowledge of a satellite's orbital elements within a given accuracy. For data of a given quality, the best dynamical model of the orbit, one that includes the best model of atmospheric drag, will give the best, or most accurate, element set for a satellite. By maintaining an accurate catalog, one has available precision element sets for each satellite. A critical use of these element sets is Satellite Orbit Identification (SOI). Reliable and accurate orbits provide the most commonly used technique for the identification of satellites.

Another important use of precision elements is for the prediction and forecasting of satellite orbits. Prediction is needed for reasons such as acquiring more tracking data from a pencil beam radar, or determining when an orbit will decay, a requirement which stresses the atmospheric model at low altitudes. Predictions are also necessary for the manoeuvre planning and execution needed for orbit maintenance. Highly accurate and timely predictions of satellite position are also required to target within a given volume (ASAT targeting), or to assess the threat to an asset of another vehicle (threat analysis). In addition, orbit predictions play an important role in the testing of new surveillance systems. New systems, such as the space-based radar and the visible optical satellite tracking system, both currently under development, will need real-time precision predictions of position, up to 24 hours in advance, to interpret the sensor data properly. Finally, accurate predictions are needed by operational satellites. For example, the Navy Transit Navigation satellites are limited by the accuracy of drag models. At this time there are several Transit satellites which are surface force compensated and drag free. These satellites are expensive. Better drag models could alleviate the drag issues in a fundamental way.

Atmospheric models also play an important role in the calibration of satellite tracking data. One must be certain that the data has been validated, screened, and calibrated in order to have confidence in the inferences made based on tracking data. This is an ongoing data analysis function. Reliable and accurate orbit computation is needed to calibrate the data. Calibration computations are no more accurate than the precision of the orbit, which, in low altitudes, is limited by drag.

A final application for precision orbits is needed in the area of collision avoidance. There is a growing population of cataloged objects in space, almost 7000 in low altitude. The

possibility of collision, although small, is nevertheless real. Despite the small probability, the cost of a collision of one of our satellites, or even worse of our debris, with a foreign asset is so high that every step must be taken to eliminate such an occurrence. The precise and timely monitoring, i.e., maintenance of the catalog, is the only way to accomplish this.

B. Mass Determination of Satellites

The effects of all non-gravitational forces, e.g., drag and radiation pressure, are proportional to A/M . This fact is often used to measure A/M from the observed change in the satellite orbit. Given that information is known about the size (A) of a satellite from radar cross section (RCS) observations then, by measuring the drag force, the mass (M) of a satellite can be determined. This has been done, in fact, with more or less accuracy for some years. It hinges on knowing the density and the C_d contribution to the drag force equation. Hence it places a requirement on the accurate assessment of the atmospheric density.

The determination of a satellite's mass and size has important implications in the area of Satellite Orbit Identification (SOI). The combination of information concerning a satellite's mass and size (and perhaps its shape, attitude, and spin rate) is a second discrimination tool to be used in SOI, perhaps equally powerful to the information contained in the element sets. By monitoring this information, it can also be used to indicate if a change has taken place in either the orbit or in the operational status of the satellite. Such changes can be indicators of possible damage, in the event of an ASAT attack or collision.

Another use of weighing satellites is in the realm of decoying space assets. It is usual to view the decoy problem in terms of replicating the size, RCS, and optical characteristics of the asset in a decoy. However, with the ability to weigh the objects, the mass will also have to be replicated in order to be credible. Since the cost of space objects depends on the mass in orbit, such a requirement sharply reduces the attractiveness of decoying. Of course, issues such as response time and accuracy become paramount, since decoy strategies are manifold.

Finally, a further use of weighing satellites is in the low altitude regime where there is considerable debris. The debris population is continually changing. Debris is depleted by atmospheric drag and replenished by a variety of sources, including breakups and new rocket launches. An organized observation and analysis program is required to properly assess the hazard and the statistics of the population. A critical element of space debris characterization will be the measurement

of each particle's mass, which can be done with a good drag model and accurate tracking data.

C. Geophysical Investigations

Drag models used for operational tracking can provide significant insight into the basic physics of the Thermosphere. Excellent models have been derived from analysis of tracking data. Such tracking data can also provide basic information to test models. For example, drag data can be used to assess the models' performance and to determine basic constants within models. Drag data can also be used to calibrate other atmospheric sensors, such as instrumented satellites. Over the long term, one can hope to derive a complete thermospheric model based on physical principles, that combines observations of constituents from satellite instruments, with total density obtained from analysis of satellite drag.

Other geophysical investigations also depend on precision orbit computation. Currently, there are low altitude satellites used for measuring the earth's geopotential, its motion in space, its polar motion, and its rotation rate. Atmospheric drag is a significant error source in the analysis of these low altitude satellites. In addition, there are a number of low altitude geophysical sensors (e.g, MAGSAT, SEASAT, GEOSAT, TOPEX) that need to know the position of the satellite at the time of measurement. Again, improvement in drag modelling will lead directly to improvement in the analysis of this type of sensor data.

III. Outline of Drag Problems

The primary topic of this conference is Neutral Atmospheric Density Models. However, this emphasis is somewhat misplaced as the main interest is the calculation of satellite drag. The calculation of neutral density is only one piece of the problem. A number of other issues have to be addressed in order to achieve the desired capabilities.

As shown, the drag force per unit mass on a satellite, which is the force that is measured, is determined from

$$F = (1/2)C_d(A/M)\rho V_s^2 \quad (1)$$

where C_d is the ballistic coefficient, A/M the area-to-mass ratio, ρ is the atmospheric density, and V_s is the speed of the satellite with respect to the atmosphere. V_s can be written as the speed of the satellite, V_{sat} , and the speed of the atmosphere, V_{atms} . In our analysis, we assumed that the lower atmosphere co-rotates with the earth.

One of the main problems in determining the drag on a satellite is that none of the quantities in this product is known

without error. For example, there are fundamental unknowns in the physics of scattering. This issue is grouped in the definition of C_d which is given in Figure 2. C_d has to be determined for each satellite. It will be discussed in more detail in the following section.

The projected cross-section, A , in Equation 1 also has to be determined for the majority of satellites. In general, the cross section depends on a satellite's aspect angle. This is often difficult to calculate and probably will have to be observed. In our study we determined the atmospheric drag on selected spherical satellites so that questions of aspect did not arise. To calculate the area-to-mass ratio (A/M) in Equation 1, the true mass (M) must also be known. This is essential if drag measurements are to be used to predict absolute density.

The next term in Equation 1 is ρ , the atmospheric density. This value is usually predicted by the atmospheric models although the models themselves do not predict the density to better than 15% at low altitudes (less than 300 km). The model predictions get even worse with increasing altitude.

Finally, the last term in Equation 1 is the speed of the satellite with respect to the atmosphere. The speed of the satellite with respect to the earth is known with fairly high precision. However, this term also depends on the speed of atmospheric winds. It is clear from satellite experiments, drag analysis, and theoretical models that there are significant winds and gravity waves in the thermosphere. These winds can have a speed of several hundred meters per second, a speed which is comparable to satellite velocities. Therefore, any advance in the modelling of satellite drag must include information about winds.

Other problems related to the determination of atmospheric drag include the abundant evidence that sensible drag exists at all altitudes. From the standpoint of space surveillance, high altitude drag is not as serious as low altitude drag. The cumulative effects take months to be operationally significant. Yet the existence of this drag, not predicted by any of the current models, indicates a flaw in our understanding of the thermosphere. We cannot accept a model as comprehensive if it does not satisfactorily explain all the observed atmospheric phenomena.

Further difficulties in the determination of atmospheric drag can be found in the geophysical inputs to drag models. Recall that in the previous section we identified a number of important uses that were time critical, i.e., that need results within hours to be useful. Most of the present suite of models use geophysical parameters such as $F_{10.7}$ and K_p as measures of energy input to the atmosphere. These are surrogate parameters to

begin with. The reason is that direct measurements of the ionospheric current and the solar EUV flux are not available. The indices that are used have certain inherent problems. The K_p and A_p are planetary indices and so can not represent localized disturbances. The F10.7 cm flux, on the other hand, is used to represent the EUV solar flux, although it in itself has no direct influence on the atmosphere. The models also assume that we use data obtained after careful calibration and reduction by the geophysical agency, NOAA/USAF. Generally the final data values are available only after some weeks or months, and are not available for our time critical mission. We must, therefore, use predictions of these values based on incomplete information. A certain amount of error is associated with this approximation, and it needs to be quantified.

Table 2 summarizes the problem areas associated with determining atmospheric drag. In the following section we will explore one problem area in more detail.

Table 2. Summary of Problems Associated with Atmospheric Drag

- Physics
- Satellite Aspect
- Geophysical Input :
 - Accuracy and Prediction
 - Composition, Temperature, and Density Models
 - Winds and Super-Rotation
 - Gravity Waves
 - High Altitude Drag

IV. THEORY OF SCATTERING

One has to model the scattering mechanism to determine the ballistic coefficient C_d used in Equation 1. However, this process is not well understood. For example, we can not reliably predict how particles in free molecular flow scatter from a surface in space, nor is it known how that surface and the scattering change after long exposure in space.

A theory of scattering is summarized in Figure 2. It is a theory based on general principles. Verification of the theory is needed along with definition of several constants. Figure 2 gives the mathematical formalism for solar radiation pressure, neutral drag, and charge drag. These three effects have some common elements. It is instructive to consider them together.

In all three cases, the force on a general surface element depends on the scattering mechanism and the flux, the flux of neutral particles, photons, or charged particles. Two scattering mechanisms are indicated, specular and a Lambert's law "diffuse" scattering. Other scattering mechanisms are possible. These two are considered to be the limiting cases; one in which the scatterer completely "remembers" the information about the incoming flux vector momentum (specular), and the other in which no information is "remembered" (diffuse). In general, surfaces do not behave completely as specular or diffuse. A better model would be to assume a fractional part of both the diffuse and specular components on the satellite surface.

For neutral drag, the scattering interaction depends on the surface material of the satellite, and on the molecular weight and temperature, or thermal velocity, of each particle. The thermal dependence is theoretically modelled in terms of the ballistic coefficient. The molecular weight of the atmospheric constituent and that of the surface material of the satellite are modeled through an accommodation factor, δ . However, even if the chemical constituents of the atmosphere are known (using laboratory measurements from Herrero, 1983), the value of C_d can not be determined to better than 5% (Gaposchkin & Coster 1986).

V. PRESENT DRAG MODELS

Atmospheric density models for heights above 120 km have been derived from the analysis of satellite drag since the launch of Sputnik I. Satellite drag measures only the total density and contains no direct information about composition. Early models identified the fundamental dependence of the upper atmosphere on solar flux, geomagnetic index, diurnal, monthly and seasonal variations. Atmospheric models based on satellite drag data are typified by the COSPAR International Reference Atmosphere of 1972 (CIRA72), which is fundamentally based on the Jacchia 1971 model (Jacchia, 1972), and by the DTM 1978 model (Barlier et al., 1977).

Atmospheric composition can be inferred or measured using both ground-based incoherent backscatter radar measurements and satellites instrumented with mass spectrometers and accelerometers. This type of data has been used to construct the so-called Mass Spectrometer and Incoherent Backscatter (MSIS) models, typified by Hedin et al., 1977 a,b, 1983.

Jacchia attempted to merge drag and composition data into a combined model, Jacchia 1977. The Jacchia 1977 model has two modifications: a 1977 addendum, and a revision [Jacchia & Slowly, 1982]. An additional version of the Jacchia 1977 model known as the Jacchia-Bass model [Bass, 1980 a,b] was developed at the Air Force Geophysical Laboratory.

All models are relatively simple. They can be characterized as static diffusion models that only incorporate dynamics implicitly. The processes are, as yet, too complex to formulate a model based on physical principles alone.

The models we tested initially were the Jacchia 1977 and the MSIS 83 models. We also tested the Jacchia 1971 (CIRA72) model since it is a widely used standard, and the DTM 1978 model which was designed specifically to evaluate satellite drag. However, during the analysis, a number of issues concerning the Jacchia model arose that required testing of several variants. Finally, the results on seven models have been assembled. The development and testing of these models led to additional insights into the models and the scattering mechanisms used by the models.

The seven models are listed in Table 4. The four different versions of the Jacchia 1977 model evolved because of two revisions dealing with geomagnetic effects. The first was an analytic approximation to a geomagnetic effect described by Eq. 32 in the original 1977 Smithsonian Astrophysical Observatory Special Report No. 375 (Jacchia 1977). The second revision was described in Jacchia & Slowey, 1981 resulted from combining drag data with ESRO4 satellite data. These revisions are discussed in more detail in Gaposchkin and Coster 1986. J77' includes the analytic approximation, J77'' includes the Jacchia & Slowey 1981 revision, and J77''' includes both sets of revisions.

The J71, J77, J77', and DTM models are predominantly based on satellite drag measurements obtained in the region from 250 to 1000 km. In addition, the J77'' and J77''' models incorporate a considerable amount of satellite measured composition data from the ESRO 4 satellite at altitudes ranging 250 to 800 km and less than 40 degrees in latitude. The MSIS model is completely based on satellite mass spectrometer and ground-based incoherent scatter data, the latter used primarily to measure neutral temperatures. The majority of mass spectrometer data was obtained from the Atmospheric Explorer satellites in the altitude regions from 100 to 500 km.

Table 4. Seven Density Models Tested

J71	= Jacchia 71, aka CIRA 1972
DTM	= Barlier et al., 1978
MSIS83	= Hedin, 1983
J77	= Jacchia 77, as defined in SAO SR 375
J77'	= Jacchia 77 + analytical approximation
J77''	= Jacchia 77 + 1981 changes in AFGL report
J77'''	= Jacchia 77 + 1981 changes + analytical approx.

A timing test was performed on the different models. In the test, each model was called 4000 times in a variety of positions and hour angles. The results are presented in Table 5.

Table 5. Timing Test of the Atmospheric Models

J71	11.10 seconds
DTM	16.22 seconds
J77	35.38 seconds
J77'	41.98 seconds
J77''	33.26 seconds
J77'''	36.70 seconds
MSIS83	116.84 seconds (86.74)

The two times listed for the MSIS83 model refer to the how the geomagnetic A_p parameters were input. The MSIS83 program has the option of using either the daily value of the A_p or an array of 7 A_p indices, including the daily A_p index and different time averages of the 3-hr A_p indices. The shorter time listed for MSIS83 refers to program run with only the daily A_p value input. No significant difference was found between these two options. In our standard procedure, the array of A_p values as inputs to the MSIS83 model was used.

Our timing test shows that the MSIS 83 model is significantly slower than all of the Jacchia models. This result is in contradiction with the general consensus in the community which is that the J77 model is much slower computationally than both the J71 model and the MSIS model (Liu, et al., 1983, Afonso, et al., 1983). We assume this is because our implementation of the J77 model used a look up table similar to that used in the J71 program. Note also that the DTM model runs faster than all the models except for the J71 model.

We ran a computer simulation in which the ratios of the densities predicted by the JACCHIA 71, J77, J77', J77'', and MSIS 83 models were compared to those predicted by the J77'' model for the 300 km altitude. This simulation was done to see how much variance there is between the different models. The

J77'' model was selected as the standard model because it was found to be the best overall model in predicting satellite drag for our data set. All hour angles were sampled with latitude coverage between +60 to -60 degrees. The daily and average solar flux values were set at 74, and a Julian date of 46144 was used. The results for two different K_p values corresponding to a typical mean K_p value ($K_p = 2.5$) and to a high K_p value ($K_p = 5.0$) are presented in Table 6. In each case, twenty-five hundred data values were averaged.

Table 6. Comparison of Densities Derived by the Various Atmospheric Models to the J77'' Model at 300 Km

	$K_p = 2.5$		$K_p = 5.0$	
	Mean Ratio (Model/J77'')	Std. Dev. (%)	Mean Ratio (Model/J77'')	Std. Dev. (%)
1. Jacchia 71	1.082	6.5	1.16	9.1
2. Jacchia 77				
J77	0.886	6.3	0.81	8.7
J77'	0.872	7.3	0.81	9.4
J77''	1.000	0.0	1.00	0.0
J77'''	0.880	8.4	0.78	14.3
3. DTM 78	0.867	5.3	0.81	5.1
4. MSIS 83	0.934	9.3	0.93	10.2

Clearly the results show that at 300 km all of the models are in reasonable agreement. A 15% difference between the mean ratios of the models is apparent. It is known that atmospheric models can not predict densities better than 15% (a number which increases at higher altitudes). Space Command, however, would like a 5% prediction capability of drag.

In Gaposchkin & Coster (1986) we found that the J77, J77' and J77''' were clearly inferior to the J77'' in all cases. These models were not evaluated further.

VI. MEASUREMENTS OF SATELLITE DRAG

The rest of this paper is concerned with measurements of satellite drag and with what can be done with these measurements. In particular, we describe the measurements we made of atmospheric drag and how we used these measurements to evaluate the different atmospheric models. We were also able to use these measurements to evaluate different atmospheric indices, including those that are currently used as inputs and a new index that is not yet being used by the models. Following this, we will discuss a suggested first revision to the J77'' model based on a least squares fit of our measurements to the following terms: annual, semi-annual, seasonal-latitudinal, diurnal, K_p , PI.

Measurements of satellite drag were acquired by taking daily tracks of spherical satellites from Lincoln Laboratory and NASA facilities. Two satellite tracking radars that provide data with an accuracy of 1 meter [Gaposchkin 1985, 1986 a,b] are operated by Lincoln Laboratory. One radar is the Altair radar located on the Kwajalein Atoll, the other is the Millstone L-band radar located in Westford, Mass. A network of laser ranging stations that provide data on satellites equipped with cube corner reflectors is operated by NASA. The accuracy of this data is better than 2 cm [Gaposchkin et al., 1987].

Daily tracks of data on two satellites, LCS4 and COS1179, have been taken since the beginning of 1985. Daily tracks on the third satellite, EGS aka Agasii, have been taken since launch in 1986. Data from all of 1985 have been analyzed for the former satellites, as well as the initial two months of data on EGS in 1986. These satellites are described in Table 7 where the semi-major axis (a) and the perigee height (q) are given in km, the area-to-mass ratio (A/M) is given in cm²/gram, and the inclination (I) in degrees. The eccentricity is referred to as e.

Table 7. Satellites Used for Evaluation of Density Models

Cospar #	NSSC#	Name	a(km)	e	I(°)	q(km)	A/M
1980 37 A	11796	COS1179	7028	0.051	82.9	270	0.038
1971 67 E	5398	LCS#4	7207	0.008	87.6	780	0.285
1986 61 A	16908	EGS	7878	0.001	50.1	1500	0.045

Atmospheric density models were used in the orbit computation of these data sets to calculate atmospheric drag. The use of these models included the final data on the 10.7 cm solar flux and the geomagnetic index K_p (Solar Geophysical Data, 1985, 1986). A scale parameter (S) is introduced in the orbit determination program. S is a least squares fit parameter that is used for each orbital arc. S scales the entire drag model. It can be interpreted as an indication of the adequacy of the drag, and thus of the atmospheric model used to compute the drag. If S is less/greater than unity, then the atmospheric density predicted by the model is too large/small.

With a complete force model, and the scale factor, the orbital arcs are generally fit to the accuracy of the data (several meters). The orbital arcs are computed with one day spacing, using between two and four days of data. Any given pass of data will be in at least two orbit fits. This is used for data validation, as well as checking orbital consistency. The computed scale factors can be plotted as a function of epoch. These plots can then be used to give an indication of how the density model involved in the drag calculation may be deficient.

Figure 3 is an example of the scale factor data for satellite 11796 and for the J77'' model over a years time.

Scale factors were computed for each satellite and for each atmospheric model. In addition, scale factors were computed for both the specular and diffuse scattering case. These data are summarized in Table 8. The first term under each satellite is the average scale factor, \bar{S} , for that data set. The second term is the standard deviation, σ .

Table 8. Summary of Scale Factors

Diffuse

Satellite	11796	5398	16908
Model	\bar{S}/σ	\bar{S}/σ	\bar{S}/σ
J71			1.293/0.691
J77''	1.106/0.146	0.715/0.321	1.389/0.617
MSIS	1.177/0.138	0.753/0.345	1.665/1.220
DTM		0.878/0.255	1.344/0.570

Specular

Satellite	11796	5398"C"	5398"G"	16908
Model	\bar{S}/σ	\bar{S}/σ	\bar{S}/σ	\bar{S}/σ
J71	1.024/0.114	1.024/0.374	1.111/0.374	
J77''	1.108/0.153	0.876/0.333	0.950/0.333	1.919/0.839
MSIS	1.183/0.152	0.923/0.325	1.001/0.325	2.397/1.220
DTM	1.152/0.169	1.036/0.229	1.124/0.269	

The results for each satellite will now be discussed.

COS1179

COS1179 (NORAD Space Surveillance Center [NSSC]#11796) is known to be a sphere. Its mass, however, is not known from independent information. Therefore, an area-to-mass (A/M) ratio based on an average drag has been adopted. Because of this 11796 can only be used for a relative assessment of the atmospheric models. The scale factors for J77'' were computed assuming a diffuse scattering mechanism and are presented in Figure 3.

Throughout the time period analyzed, 11796 has a sufficiently large eccentricity that drag occurs mainly at perigee, where the scale height is about 7 km. Therefore, the orbit only samples the density at one geographic point each revolution. Figure 4 gives the latitude and solar hour angle of the perigee point for the interval analyzed. One can see that both latitude and hour

angle are completely sampled, and there is no simple correlation with the variation in S seen in Figure 3.

Scale factors were computed again for this satellite using the assumption of specular scattering. The mean values of the scale factors for these two cases are fairly similar as can be seen in Table 8. From the theoretical standpoint, a significant difference is not expected between the specular and diffuse cases because the drag at 295 km is primarily from oxygen and nitrogen. The mean molecular weight is approximately 16, which results in a value for the accommodation coefficient of nearly 1. The accommodation coefficient is the term used in the model for diffuse scattering. An accommodation coefficient of 1 results in the same value of C_d as that predicted by the model for specular scattering. The scale factors for the specular scattering are not significantly different.

As mentioned above, the absolute mean scale factors are not significant in this satellite. However, the fact that the scale factors differ by at most 5% indicates that all the models are in good agreement. The variation about the mean is smallest for the J77'' model, though all the models differ by 2% at most. On this basis one could marginally choose the J77'' as the best model. This difference is not believed to be significant. All models are equally good (or bad) at 275 km altitude for all latitude, hour angle, and geophysical data.

LCS4

LCS4 is a satellite built by Lincoln Laboratory. It is in a circular orbit at approximately 780 km altitude. Its physical characteristics, such as its area-to-mass ratio (A/M) and the composition of its outer surface (aluminum), are known. Because of its nearly circular orbit, the satellite does not provide a clear association of the position and the effect of drag. Nevertheless, the average drag can be discussed.

At this altitude the scale factors for all models are quite different. The orbital fits have been carefully scrutinized. The observed variability in S is believed to represent real variations in the atmospheric density at 780 km altitude that are not predicted by any of the models. In all cases, it can be seen that the scale factors are 20% to 30% less than unity, indicating that the predicted drag is too large by this factor.

At 780 km altitude the principal atmospheric constituents are hydrogen and helium. For these constituents, the difference between specular and diffuse scattering is quite large, resulting in diffuse ballistic coefficients 20% to 30% larger than specular ones. The mean scale factors, assuming the specular scattering mechanism, are approximately 0.9. The general agreement among the various models persuades us that:

- a) the specular scattering model is correct for the polished aluminum spherical satellite, and
- b) there may be a systematic overestimate of the density by as much as 12%.

The J71 model has the best mean value, and the DTM has the smallest variability. However, the differences may not be significant considering that the uncertainty in C_d may be as much as 5%.

A further issue arises due to an uncertainty about LCS4. LCS4 was one of two satellites fabricated by Lincoln Laboratory at the same time. Both were one square meter radar calibration spheres made of polished aluminum, identical in all but one respect. The records show that one sphere, the "G" sphere, failed on launch and never made it to orbit. The second, "C" sphere, became LCS4 upon launch. Both spheres were carefully measured, including the mass, which was given in the records as 38.186 kg for the "G" sphere, and 35.203 kg for the "C" sphere. The two spheres were unmarked, and virtually indistinguishable. One cannot rule out the possibility that they were interchanged during ground handling, and that the "G" sphere actually made it to orbit as LCS4. In this case all the recent density models are in better agreement with the data. To account for this, the scale factors can be multiplied by 1.085. Then assuming specular reflection the MSIS83 has a mean scale factor of virtually unity, and the J77'' is 0.95. Both of these values are within the uncertainty of the C_d . In any event the recent models are in acceptable average agreement at 780 km, although there are large variations in the density that are not modeled. It is true that the model with smallest variability for LCS4 is the DTM.

EGS

EGS (Experimental Geodetic Satellite) is a spherical satellite in a nearly circular orbit at 1500 km altitude, and equipped with laser cube corner reflectors. The laser ranging data, provided by NASA since launch in July 1986, has allowed the study of the density model at 1500 km. This is higher in altitude than any data used in constructing the models, and serves to measure how well the predicted densities of the models can be extrapolated. The EGS satellite has a known A/M that is given in Table 8 and a surface made of aluminum with holes for the laser cube corner reflectors.

Preliminary calculations on two months of data have been done using the MSIS83 and J77'' models. The scale factors were computed with both a diffuse and specular scattering mechanism. Since the atmosphere at 1500 km is mostly hydrogen, one would expect a significant difference in the result. In Table 8, we

see that for EGS the specular scattering assumption leads to scale factors of 1.9 and greater; the MSIS83 mean value is 2.39. The conventional diffuse scattering model gives an average scale factor of 1.39 for the J77'' and 1.67 for the MSIS83. A-priori one would choose the diffuse scattering for aluminum, and this is adopted. It is also concluded from this analysis that J77'' underestimates the density at 1500 km by about 30%, whereas the MSIS83 underestimates the density by about 60%. This is consistent with the results for LCS4, where the J77'' gives larger densities than MSIS83 at the 780 km altitude.

VII. EVALUATION OF ATMOSPHERIC INDICES

In addition to evaluating the atmospheric models, the derived scale factors can be used to determine how well the effects of the different indices are being modeled and to evaluate whether a new index is of value to future modelling efforts. This was done by correlating the series of derived scale factors with different series of atmospheric indices, including the daily F10.7 cm flux, the K_p , and the precipitation index (PI). The precipitation index is the only parameter we studied that is not currently being used as an input to any of the atmospheric models. It is an index which quantifies the intensity and spatial extent of high-latitude particle precipitation based on observations made along individual passes of the NOAA/TIROS weather satellites. It is measured in near real-time by the NOAA/TIROS weather satellites which are in circular sun-synchronous orbits at 850 km. (Foster, et al., 1986). We analyzed the power levels of the precipitation index.

The atmospheric parameters were averaged over the same time interval as the data used to compute the orbital arcs. For COS1179, 3 days of data were averaged for each parameter, while for LCS4, 4 days of data were averaged. Each series of atmospheric data was then correlated against the series of scale factors determined for both satellites using each of the four different atmospheric models. In certain cases, two series of scale factor data existed for each model corresponding to specular and diffuse scattering. This issue was discussed earlier. It was not significant when correlating the series of atmospheric parameters against the series of scale factors.

The results for each atmospheric parameter are presented in Tables 9 a,b, and c. In all cases, the correlation coefficients were computed from scale factors and geophysical data with the average subtracted, i.e. these data have zero mean. A correlation coefficient was determined for each atmospheric model and each satellite. A value of greater than 0.2 was considered to be significant correlation. The data discussed in these next sections represent the first six months of data in 1985 with one exception. The bracketed value in the J77'' columns for 11796 Diffuse represent the entire year of data for 1985.

TABLE 9a. Correlation Coefficients for F10.7 cm Flux

	11796		5398	
	Specular	Diffuse	Specular	Diffuse
J71	0.18		0.35	
J77"	-0.14	-0.15 (-0.02)	-0.07	-0.01
DTM 1978	0.02		0.12	0.12
MSIS 1983	0.04	0.06	0.11	0.02

TABLE 9b. Correlation Coefficients for K_p

	11796		5398	
	Specular	Diffuse	Specular	Diffuse
J71	0.21		-0.24	
J77	0.40	0.39 (0.27)	0.27	0.29
DTM	0.40		0.09	0.14
MSIS83	0.28		0.35	0.28

TABLE 9c. Correlation Coefficients for the Precipitation Index

	11796		5398	
	Specular	Diffuse	Specular	Diffuse
J71	0.42		-0.15	
J77''	0.48	0.46 (0.37)	0.36	0.40
DTM	0.53	0.28	0.19	
MSIS83	0.42	0.42	0.45	0.36

The results of the correlation between the series of daily F10.7 cm values and the series of determined scale factors are given in Table 9a. It appears that for the lower satellite the F10.7 cm flux is modeled fairly accurately. Problems that existed in the J71 model seem to have been corrected in the later models.

The results of the correlation between the K_p indices and the scale factors are given in Table 9b. The K_p index is used to model the influence of geomagnetic fluctuations in the atmosphere. There appears to be significant correlation between the K_p values and the series of scale factors determined for both satellites.

Figure 5 shows the correlation between the K_p data and the scale factors for the Jacchia 1977 S and the MSIS 1983 S models. S indicates specular scattering. The mean of each data set has been determined and subtracted from the series. The y- axis

therefore represents the data, with the mean subtracted, while the x-axis represents time. This data is presented here to illustrate the features in the data sets that are correlated.

Based on the data for the lower satellite, the MSIS model shows slightly less correlation with the K_p than does the Jacchia 1977 model, indicating that it better models the atmospheric response to changes in this index. We should point out that the MSIS model uses the A_p index instead of the K_p index. We computed the correlation between the A_p index and these data sets. The results were very similar to the results presented in Table 9b. Finally, the DTM model correlation with K_p at 275 km is similar to the others (0.40), but at 780 km it has a significantly smaller correlation (0.09).

The results of the correlation between the precipitation power index (PI) and the scale factors are given in Table 9c. As is evidenced in Table 9c, there is significant correlation between this index and the scale factors of the atmospheric models and both satellites. Of the parameters we investigated, the highest average correlation coefficients were seen with this index. Figure 6 illustrates in greater detail the correlation between the scale factor data and the precipitation index. The precipitation index is not used by any of the models to predict the atmospheric response to geomagnetic activity. Based on this data, we think that the precipitation index should be included in future atmospheric models. One should also note that there is significant correlation between the precipitation index and the K_p . The correlation coefficient between the K_p and prescription data sets is 0.47. Some of the correlation observed with the K_p could actually be leakage of the precipitation index correlation. Clearly this issue needs more data to be resolved.

VIII. REVISIONS TO THE JACCHIA 77" DENSITY MODEL

Model corrections were suggested by the fact that significant correlation of our scale factors and certain geophysical information were found. The scale factor information we determined can be used to suggest revisions to the models. A change in the scale factor can be shown to be directly equal to a change in the log of the atmospheric density. What we present here is a suggested revision to the J77" model based on a least squares fit of our scale factor data to the following terms : annual, semi-annual, seasonal-latitudinal, diurnal, K_p , and PI (precipitation index). We were able to investigate seasonal effects because we had a full year of data.

To determine the corrections to the model we chose the scale factors associated with the lower satellite 11796 computed using the J77" model. For each scale factor, an averaging time and values for the latitude, hour angle, solar declination, and geophysical index (PI, K_p , F10.7) were associated. The averaging

time was chosen so that it corresponds to the data span used in determining the scale factor, S. The geophysical indices were averaged over the same time interval. The values of latitude, hour angle, and solar declination were the values for the satellite at perigee during that time period.

Several functional forms were postulated and a joint least squares solution for the parameters was made. The formal statistics of each parameter were then assessed for significance. In this way the set of statistically significant parameters was found. For this series of S the results are given in Table 10. A mean value and slope were also recovered although not shown.

Table 10. 11796 Scale Factor Analysis

	$d S = d \log (\rho)$	
	Cosine	Sine
ANNUAL	(-0.0178 +- 0.0063)	(-0.0034 +-0.0107)
SEMIANNUAL	(-0.0026 +- 0.0047)	(-0.0629 +-0.0067)
LATITUDE	(0.0139 +- 0.0047)	(-0.0089 +-0.0040)
SEASONAL LATITUDINAL	(0.0022 +- 0.0154)	(0.0399 +-0.0087)
DIURNAL	(-0.0129 +- 0.0111)	(0.0035 +-0.0059)
PRECIPITATION INDEX	$((0.0009+-0.0005)+(0.0017+-0,0009)*\cos(\theta)^2))*PI$	

To understand the annual and semi-annual variations in S, the F10.7 cm flux, the 90 day mean F10.7 cm flux, and the scale factor S data were also analyzed for annual and semiannual variations. These coefficients are given in Table 11. The annual variations in the F10.7, the mean F10.7, and S are more or less in phase. The annual corrections in S might be expected, as there are known to be long period variations for a number of geophysical observations. For example, there are decade scale variations in weather, earth rotation, the ocean circulation, upper atmospheric circulation and climate. This variation probably cannot be predicted, and must be measured for each year and during each solar cycle.

TABLE 11. Annual and Semiannual Variation (Epoch = MJD 46325)

	ANNUAL		SEMIANNUAL	
	AMP	PHASE	AMP	PHASE
SCALE FACTOR	0.0181	-169.19	0.063	-92.37
PI	2.5820	162.50	1.519	-30.55
F10.7	1.5970	-120.40	3.690	147.60
[F10.7]	2.5200	-143.40	2.440	158.10
K _p	0.1807	51.05	0.094	-12.98

It is possible that the latitude, seasonal-latitudinal, and diurnal variation are all related to the shape of the diurnal variation (the diurnal bulge).

The most interesting result, is the dependence of S on the precipitation index, PI. The PI is not an input to any model at present. Our analysis indicates that it shows promise. In the model form, experiments were done with an hour angle dependence of the PI, but none was found significant. Recall that there is significant correlation between the PI and the K_p index. The correlation coefficient between these two data sets is 0.47. Both the K_p and PI are measures of the solar particle input energy to the atmosphere. What is unclear is how much of the information is common to both. Note, that we did not find a significant parametric dependence of S on K_p. However, when the dependence on PI was determined, and subtracted from S, the residual correlation of S'=S-dS with K_p was reduced to nearly zero. Recall that the correlation of S with K_p had been 0.27 (see Table 9b.) From this preliminary analysis it would seem that K_p and PI have somewhat different information to contribute. Furthermore the functional dependence of PI grows toward the equator ($0.0017 \cdot \cos(\theta)^2$) which is counter intuitive. Conventional wisdom holds that the influx of energy is in the auroral zone, and the effect of the thermosphere propagates equatorward decreasing in size. In fact the Jacchia 77" model has a $\sin(\theta)^3$ dependence on K_p, which is zero at the equator. A recent revision (Slowey 1984) gives a more detailed analysis of the geomagnetic effect and this is no longer true. Our model dependence may only indicate a flawed model assumption in the J77" model. The fact remains that there are still fundamental questions about the particle flux that should be answered.

With the seasonal terms removed, the correlation of scale factors with the precipitation index is reduced from 0.37 to 0.33. The correlation of the scale factors with the other geophysical parameters does not change. The K_p correlation, for instance, remained at 0.27. Apparently, the annual variation in the precipitation index is in phase with the error in the J77"

density model. This leads us to conclude that long term variation (seasonal) in the atmosphere may be controlled by the same phenomenon that influences the precipitation index.

The overall result of the scale factor analysis is summarized in Table 12. There are significant (10%) changes in the Jacchia 77 model suggested by this preliminary analysis. Most of the changes would be considered revisions, and they must be tested against other satellite data before taking them too seriously. The precipitation index model is new, and could be quite important. Here too, one must clearly understand the relation between K_p and PI before making any final model. We believe that we have only scratched the surface and that there is significant insight to be gained from this type of analysis.

TABLE 12. 11796 SCALE FACTOR ANALYSIS

1. Correlation of S with K_p is through cross correlation of K_p with PI. There is no direct correlation of K_p with scale factor.
2. Significant Model Corrections for Semiannual (6.3%), Latitude (1.6%), Seasonal Latitudinal (4.0%), and Diurnal (1.3 %) are appropriate for this satellite. The latitude correction could be the same as the diurnal correction.
3. Precipitation index predicts as much as 10 % change in density.
4. Precipitation index effect:

$$(0.0017 \cdot \cos(\theta)^2 + 0.0009) * PI * F(z)$$

is concentrated at equator and minimum at the pole. This is opposite to the geomagnetic K_p which depends on $\sin(\theta)^3$ in the J77" model.

5. Precipitation index effect seems planetary, not depending on hour angle.

IX. SUMMARY

We have tested atmospheric density models at 275 km, 780 km, and 1500 km. At the two lower altitudes, all models are in good agreement in the sense that they give the same average performance. They all exhibit significant departures from the actual density, and it is necessary to include "solve for" parameters in orbit determination to match the tracking data. As our analysis continues, the differences between models becomes more subtle, and a selection becomes more difficult. For example, the finding of Gaposchkin and Coster (1986) of a large

difference between the J77'' and the MSIS83 at 780 km is significantly reduced here. From the standpoint of computational speed the J71 is clearly superior, and the MSIS83 is deficient.

We are continuing work in five areas:

1. To extend the data for all three satellites, to avoid any biasing due to seasonal effects, and to improve the sampling.
2. To determine the mass of COS1179 and LCS4 using satellite orbit perturbations. It is at present routine to determine the mass of high altitude satellites from perturbations due to solar radiation pressure. This has not been possible until now for lower satellites because the effects of geopotential model errors dominated the solution. Recent geodetic solutions show promise of changing this situation. In this case we can hope to make some statement about the absolute densities at 275 km altitude, and clarify the ambiguity about the mass of LCS4.
3. Explore alternate indices or variables as input to the density models, such as the precipitation index.
4. Expand the source of accurate tracking data on these satellites, in order to increase the space and time resolution of the drag determinations.
5. Examine the accuracy of for sting drag, for prediction of satellite orbits.
6. Obtain data on other low altitude satellites.

X. CONCLUSIONS

1. No model does an adequate job of modelling the atmospheric density.
2. There is no agreement on what is the best model. We find that the differences between models, though measurable, are less than the agreement between the models.
3. There are real physical variations in the atmosphere that are not modeled by any of the current suite of atmospheric models. New model parameters are needed (e.g., winds, gravity waves, (Gross, 1985)).
4. The inclusion of the precipitation index in future atmospheric models should be investigated.

Significant correlation was observed between the precipitation index and the scale factors at 275 and 780 km.

5. Overall these models have at most 18% difference about the mean when averaged of all latitudes and hour angles below 800 km. However, the variance of the model differences exceed 16%.
6. The J71 continues to perform exceptionally well, and is the fastest overall. The MSIS83 is by a large factor, the slowest.
7. For our overall use, balancing accuracy, computer speed, and range of height, we use the J77''
8. The final conclusion is that satellite drag data can still play a role in understanding the thermosphere, and in contributing unique data to monitor the next solar cycle.

XI. RECOMMENDATIONS

OBTAIN NEW DRAG DATA WITH EXISTING FACILITIES

PRECISION RADAR DATA
CALIBRATION SPHERES (14 SATELLITES NOW AVAILABLE)
RECOVER MEAN DENSITIES
MODEL IMPROVEMENTS
MONITOR IN NEAR REAL TIME ATMOSPHERIC/GEOPHYSICAL INDICES
EXISTING DATA IS AVAILBALE (E.G., TRANSIT SATELLITES)

MAKE NEW MEASUREMENTS OF ENERGY INPUTS

CONTINUE PRECIPITATION INDEX MEASUREMENTS
OTHER INDICES NOW MAINTAINED
SATELLITE MEASUREMENTS OF EUV AND CORRLELATION WITH F10.7
CM FLUX, ETC.

WIND AND GRAVITY WAVES SHOULD BE INCORPORATED IN MODELS

LAUNCH DRAG SATELLITES (BALLOONS) SUPPORTED WITH HIGH ACCURACY TRACKING

NEW SATELLITE EXPERIMENTS ARE NECESSARY, SHOULD BE SIMULTANEOUSLY CALIBRATED WITH DRAG MEASUREMENTS.

REFERENCES

- G. Afonso, F. Barlier, C. Berger, F. Mignard, J. J. Walch, "Reassessment of the Charge and Neutral Drag of Lageos and its Geophysical Implications," preprint, 53 pp (Dec 1983).
- F. Barlier, C. Berger, J.L. Falin, G. Kockarts, and G. Thuillier, (1978), "A Thermospheric Model Based on Satellite Drag Data", Ann. Geophys., t.34, fasc. 1, 9-24, (1978).
- J.N. Bass, "Analytic Representation of the Jacchia 1977 Model Atmosphere", AFGL-TR-80-0037, Air Force Geophysics Laboratory, Hanscom AFB, MA , January 25, 1980, 14 pp, AD-A-085781. (1980a).
- J.N. Bass (1980b), "Condensed Storage of Diffusion Equation Solutions for Atmospheric Density Model Computations", AFGL-TR-80-0038, Air Force Geophysics Laboratory, Hanscom AFB, MA , January 25, 1980, 12 pp, AD-A-086863. (1980b).
- G.E. Cook (1965), "Satellite Drag Coefficients," Planet. Space Sci., 13, 929-946 (1965).
- J.C. Foster, J.M. Holt, R.G. Musgrove, and D. S. Evans, "Ionospheric Convection Associated with Discrete Levels of Particle Precipitation," Geophys. Res. Let., Vol. 13, 656-659, (1986).
- E.M. Gaposchkin, "Metric Calibration of the Millstone Hill L-Band Radar", MIT Lincoln Laboratory TR 721, 61 pp, AD-A-160362. (1985).
- E.M. Gaposchkin, "Calibration of the Kwajalein Radars," M.I.T Lincoln Laboratory TR 748, 79 pp, AD-B-104457. (1986).
- E.M. Gaposchkin, R.M. Byers, G. Conant (1986), "Deep Space Network Calibration 1985", M.I.T. Lincoln Laboratory STK-144, 211 pp, 11 December 1986.
- E.M. Gaposchkin and A.J. Coster, "Evaluation of Recent Atmospheric Density Models", Adv. Space Res., Vol. 6, No. 9, pp. 157-165, (1986).
- E.M. Gaposchkin, L.E. Kurtz, A.J. Coster, "Matera Laser Collocation Experiment", M.I.T. Lincoln Laboratory TR 780, 58 pp, 27 May 1987.
- S.H. Gross (1985), "Global Large Scale Structures in the F-Region, J. Geophys. Res., Vol. 90, No. A1, 553-558

A.E. Hedin, J.F. Salah, J.V. Evans, C.A. Reber, G.P. Newton, N.W. Spencer, C. Kayser, D. Alcayd, P. Bauer, L. Cogger, and J.P. McClure, 1977, A Global Thermospheric Model Based on Mass Spectrometer and Incoherent Scatter Data; MSIS 1, N2 density and temperature. J. Geophys. Res., Vol 82, pp2139-2147.

A.E. Hedin, C.H. Reber, G.P. Newton, N.W. Spencer, H.C. Brinton, and H.G. Mayr, 1977, A Global Thermospheric Model Based on Mass Spectrometer and Incoherent Scatter Data, MSIS 2, Composition. J. Geophys. Res., Vol 82, pp2148-2156.

A.E. Hedin, "A Revised Thermospheric Model Based on Mass Spectrometer and Incoherent Scatter Data: MSIS-83," J. Geophys. Res., Vol. 88, No. A12, 10170-10188, (1983)

F.A. Herrero (1983), "The Drag Coefficient of Cylindrical Spacecraft in Orbit at Altitudes Greater than 150 km", NASA, Technical Memorandum 85043, Goddard Space Flight Center, Greenbelt, MD, May 1983, 31 pgs

L.G. Jacchia (1972), "Atmospheric Models in the Region from 110 to 2000 km", in Cospar International Reference Atmosphere 19725, by Anon., Akademie-Verlag, Berlin. 1972, 227-338

L.G. Jacchia (1977). "Thermospheric Temperature, Density, and Composition: New Models", S.A.O. Special Report No. 375, Smithsonian Institution, Astrophysical Observatory, Cambridge, MA, March 1977, 106 pp

L.G. Jacchia and J.W. Slowey (1981). "Analysis of Data for the Development of Density and Composition Models of the Upper Atmosphere", AFGL-TR-81-0230, Air Force Geophysics Laboratory, Hanscom AFB, MA 01731, July 1981, 20 pp, AD-A-100420

J.F. Liu, R.G. France, H.B. Wackernagel (1983). An Analysis of the Use of Empirical Atmospheric Density Models in Orbital Mechanics, Spacetrack Report No. 4", Space Command, USAF, Peterson Air Force Base, CO 89014, Feb. 1983, 46 pp

J. Makhoul, "Linear Prediction: A Tutorial Review," Proc. IEEE, vol. 63, pp. 561-580, April 1975; correction in Proc. IEEE vol. 64, p. 285, Feb. 1976.

Slowey, J., 1984, Dynamic Model of the Earth's Upper Atmosphere, NASA Contractor Report 3855, Contract NAS834947, 18pp, September 1984.

Solar-Geophysical Data, 1985; U.S. Department of Commerce, Boulder, CO, USA 80303

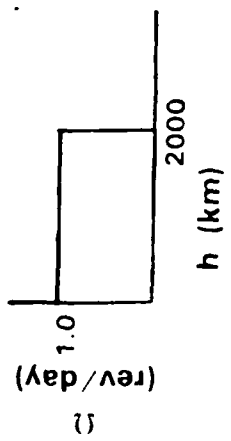
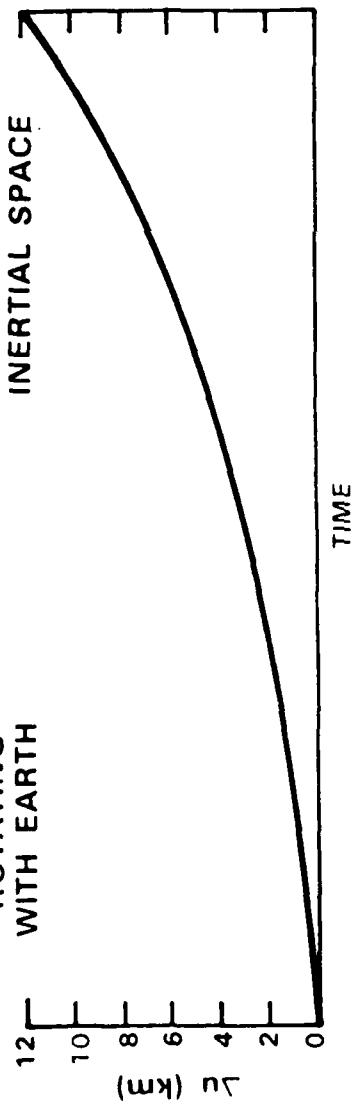
DRAG EFFECT FOR $(A/M) = 0.1 \text{ cm}^2/\text{gram}$

$$F = \frac{1}{2} C_d \left(\frac{A}{M} \right) \rho v^2$$

$$\rho = \rho(t, 10.7, [10.7], k_p) + 3.43 \times 10^{-19} e^{\frac{(h-h_0)}{H}} \text{ (grams/cm}^3\text{)}$$

ROTATING WITH EARTH

FIXED IN INERTIAL SPACE



114

PERIGEE HEIGHT q (km)	COS CAL SPH	SATELLITE
300	11796	
800	5398	
2800	1361	
5800	8820	
20000	14264	
42000	3431	
42000	ATS 5	

DAYS REV	$C_d = 2.2$	0.92 13.6
DAYS REV	$C_d = 2.2$	22.8 323
DAYS REV	$C_d = 2.2$	35.9 356
DAYS REVS	$C_d = 1.0$	94 (390) (2574) 600
DAYS REV	$C_d = 1.13$	320 640
DAYS REV	$C_d = 0.803$	774 774
DAYS REV	$C_d = 6.28$	90 99



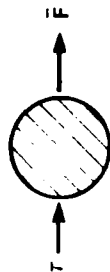
79262 8

MATHEMATICAL FORMALISM NONGRAVITATIONAL FORCES

SURFACE ELEMENT



SPHERE



RADIATION PRESSURE

$$q = \frac{S}{c} A \cos \theta [(1 - k_1) \tau + (2k_1 \cos \theta + \frac{2}{3} k_2) n]$$

$k_1 = k_2 = 1$ IF ELEMENT RERADIATES ALL ENERGY

$$S = S_0 \left(\frac{a}{r} \right)^2 \quad S_0 = 1.35 \cdot 10^6 \text{ erg (cm}^2\text{s)}$$

$$q_0 = \frac{S_0}{c} = 4.65 \cdot 10^5 \text{ dynes cm}^2$$

$$F = \frac{1}{2} C_d \frac{A}{M} \cos \theta \rho v^2$$

$$F = \frac{1}{2} C_d \frac{A}{M} \rho v^2$$

$$C_d = \left\{ \frac{\hat{\alpha} [2 - \frac{4}{3} \left(\frac{V_T}{V_S} \right)^2 - \frac{2}{15} \left(\frac{V_T}{V_S} \right)^4]}{\hat{\alpha} [1 - \frac{8}{3} \left(\frac{V_T}{V_S} \right) - \frac{8}{15} \left(\frac{V_S}{V_T} \right)]} \right\} \quad v_S \quad v_T$$

$$\alpha_1 = 2 \left(1 - \frac{1}{3} \frac{C\mu}{(1-\mu)^2} \sin 2\theta \right)$$

$$\alpha_2 = 1 - \frac{2}{3} \frac{1}{(1-\mu)^2} \frac{C\mu}{\cos \theta}$$

$$\hat{\alpha}_1 = 1$$

$$\hat{\alpha}_2 = 1 - \frac{4}{9} \sqrt{1 - \frac{C\mu}{(1-\mu)^2}}$$

$$2 \quad C \quad 4 \quad \mu \quad M_T \quad M_S$$

CHARGE DRAG

$$\left(\frac{b}{R} \right)^2 \left[\begin{array}{c} 1 \\ eU(R) \\ E(kT) \end{array} \right] \left[\begin{array}{c} R \rightarrow 0 \\ D \end{array} \right]$$

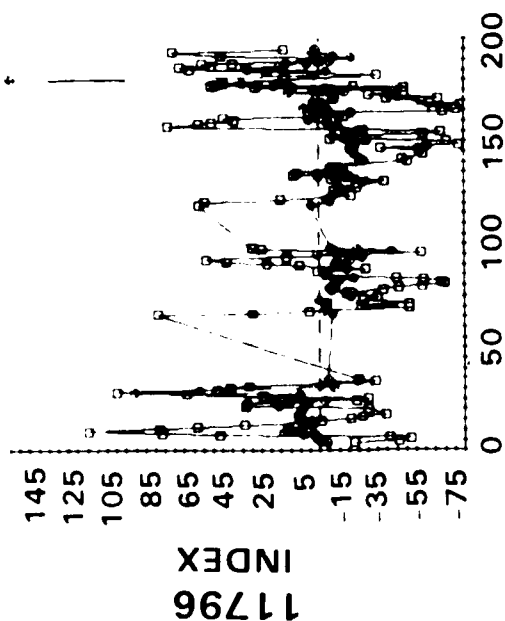
$$D = \left(\frac{\epsilon_0 kT}{e^2 n_0} \right) \text{ DEBYE LENGTH}$$



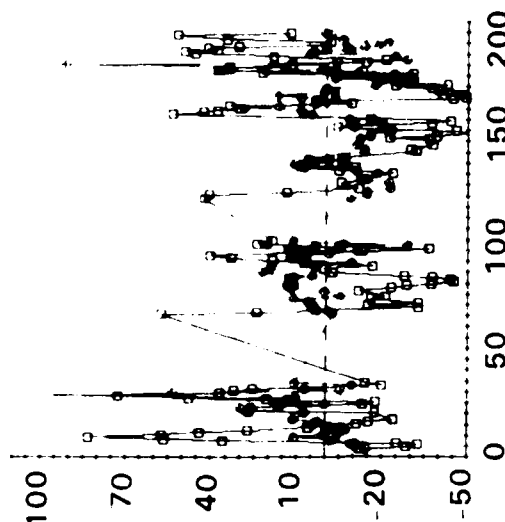
79262 9

CORRELATION OF K_p INDEX WITH SCALE FACTORS

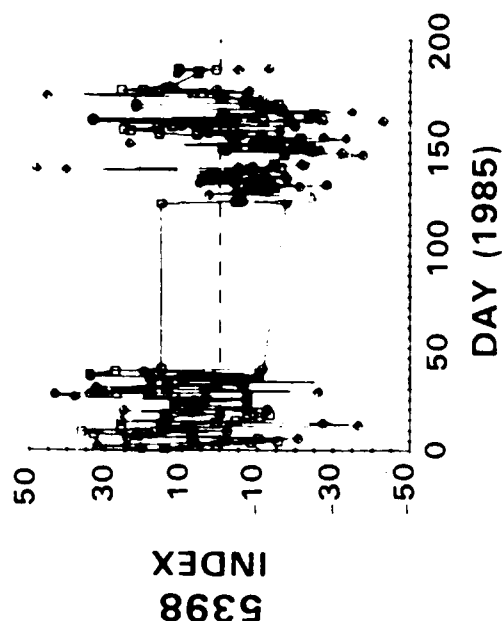
JACCHIA 1977S
CORRELATION = 0.40



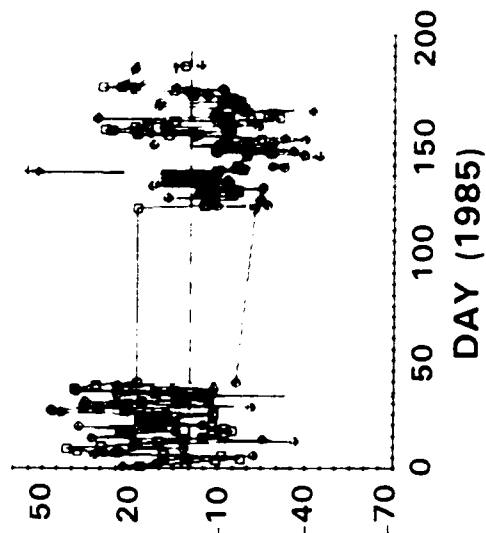
MSIS 1983S
CORRELATION = 0.28



CORRELATION = 0.27

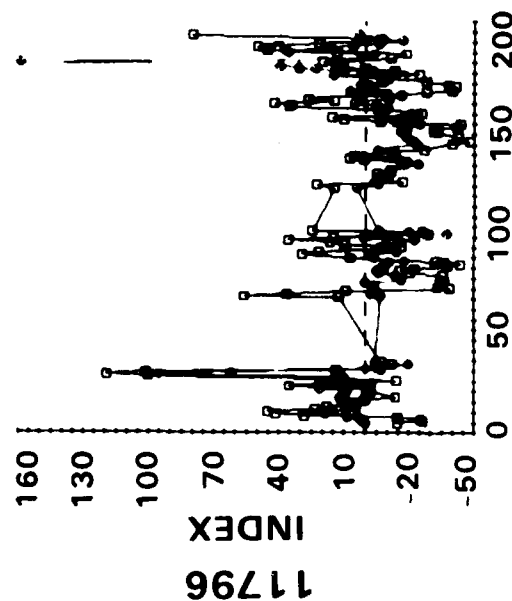


CORRELATION = 0.35

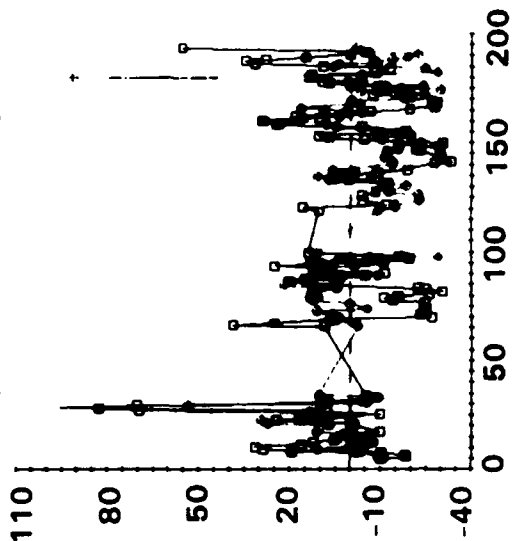


CORRELATION OF PRECIPITATION INDEX WITH SCALE FACTORS

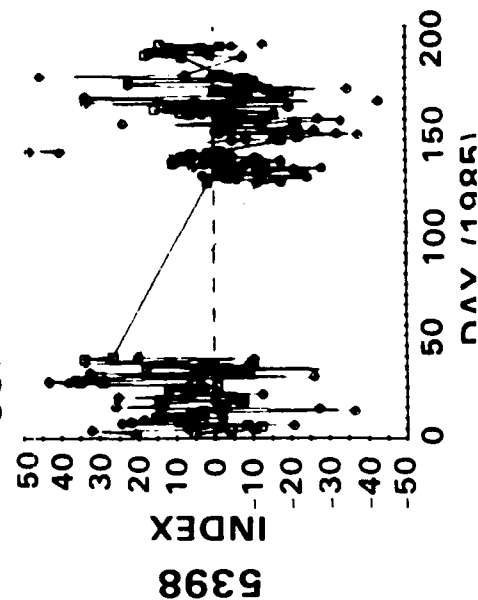
JACCHIA 1977S
CORRELATION = 0.48



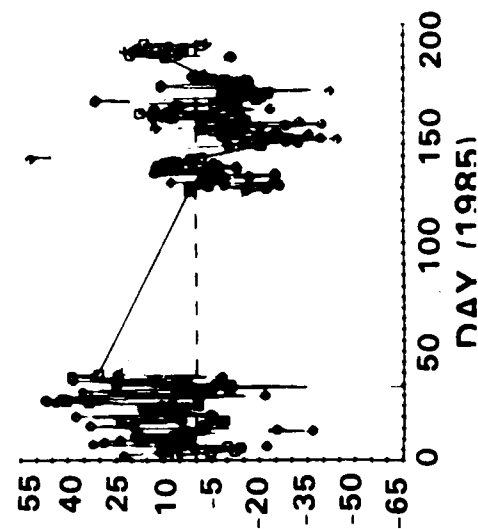
MSIS 1983S
CORRELATION = 0.42



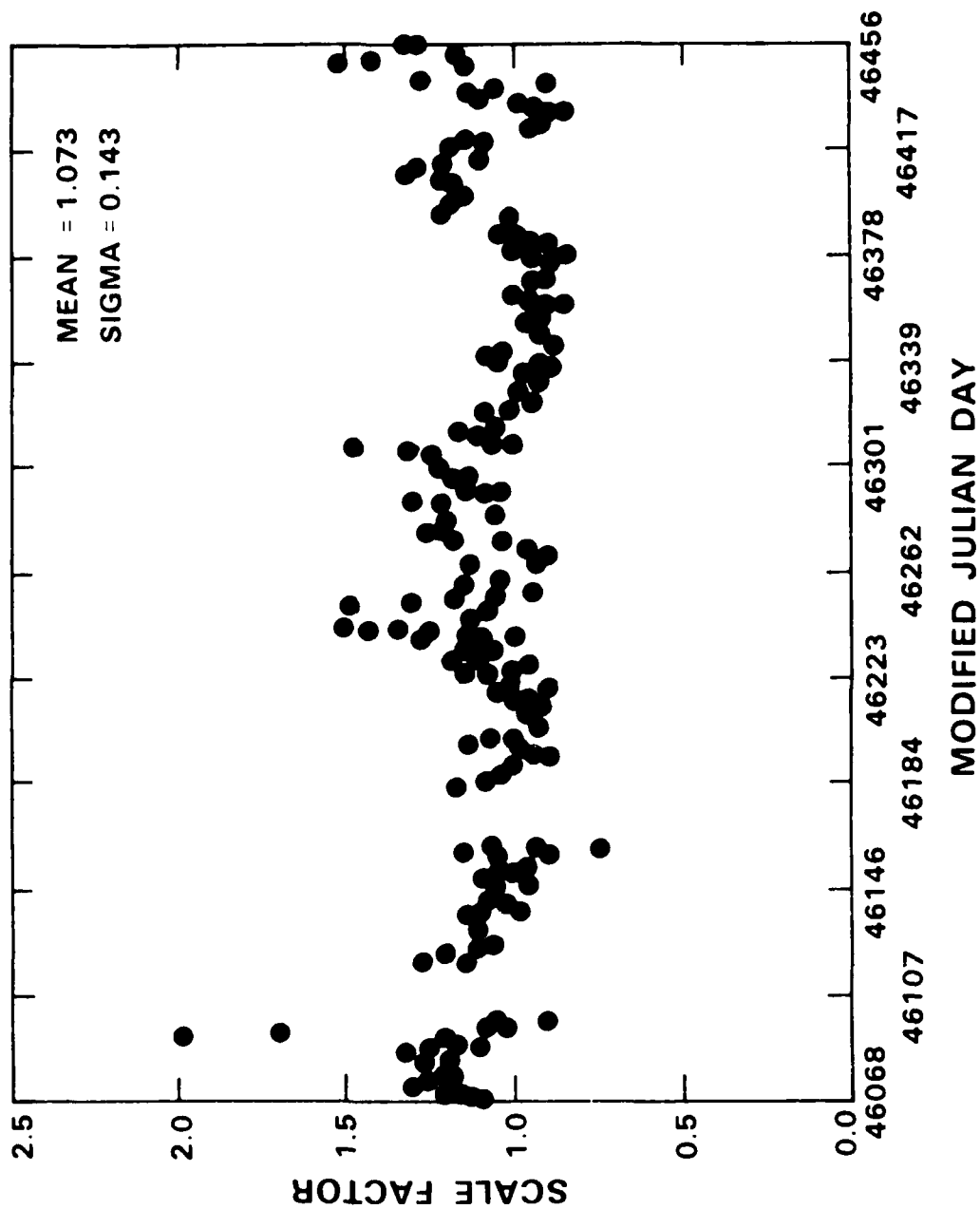
CORRELATION = 0.36



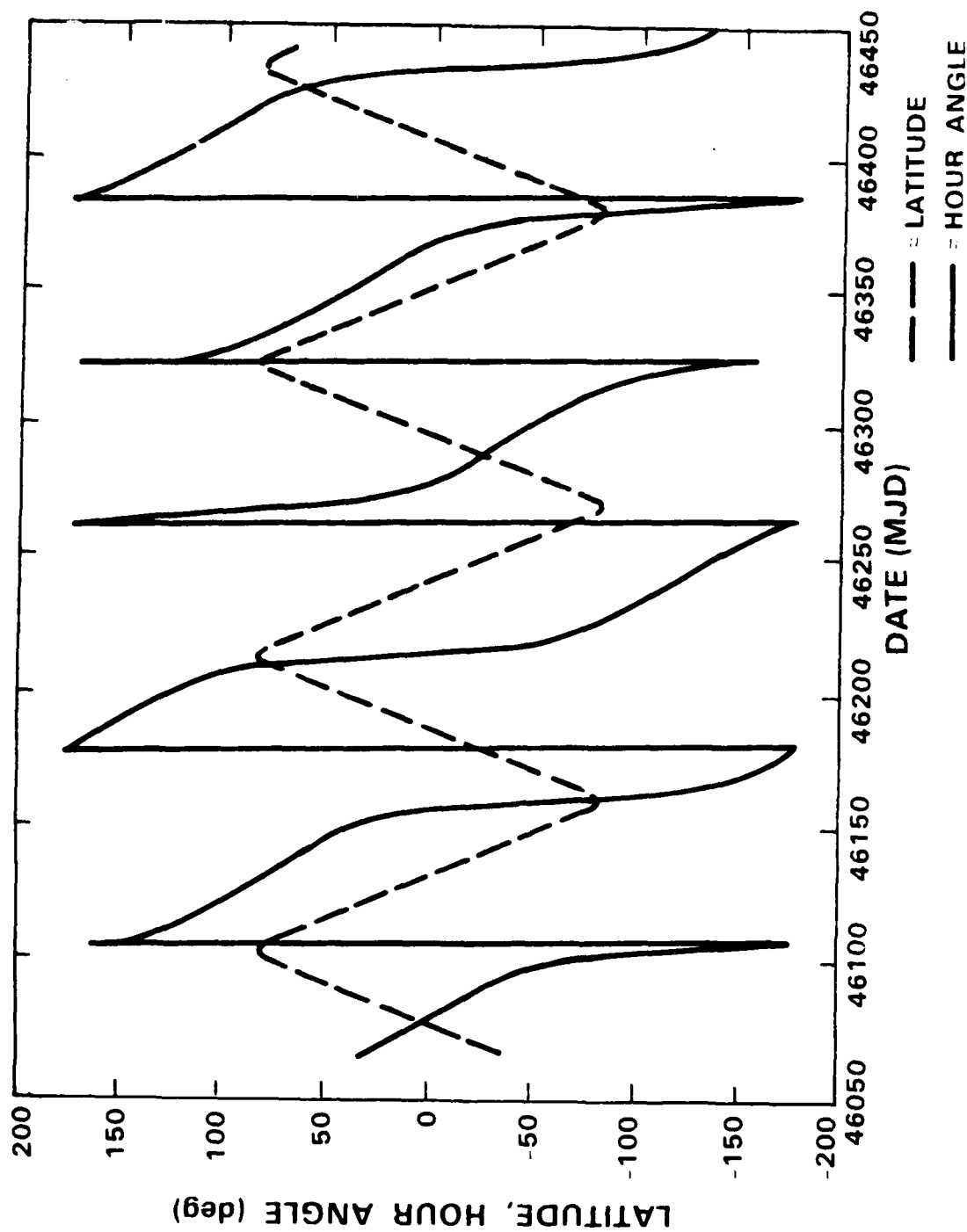
CORRELATION = 0.45



JACCHIA 77" DIFFUSE SCALE FOR 11796



LATITUDE AND HOUR ANGLE FOR 11796



SESSION 3

STATE-OF-THE-ART
MODELS
AND PROSPECTS

DR E. M. GAPOSCHKIN
CHAIRMAN

ACCURACY OF SATELLITE DRAG MODELS[†]

Frank A. Marcos*

Accelerometers flown on low-altitude satellites have provided our most extensive density data base in the 150-250 km region. These data have been obtained over a wide region of solar and geomagnetic conditions. A comprehensive comparison of our measurements, obtained 1974-1982, with several empirical models, has resulted in assessment of the current status and improvement prospects of our capability to specify and forecast density (drag). The model accuracies are compared by their mean values and standard deviations relative to the accelerometer data. Results indicate a lack of significant model accuracy improvements during the past two decades. Mean values are estimated to be given typically within $\pm 10\%$ and standard deviations are approximately $\pm 15\%$. Improved representation of atmospheric variability requires a program including coordinated measurements of atmospheric structure and dynamics, development of more accurate indicators of solar and geomagnetic activity and theoretical investigations using self-consistent numerical models.

INTRODUCTION

Empirical atmospheric density models based on large data sets have been developed to describe variations of the upper atmosphere. In atmospheric research these models serve as a reference and permit analysis of discrepancies with respect to new measurements. For practical applications models are also required for problems concerned with the effects of aerodynamic drag on satellites. Satellite lifetime, design, control, tracking, on-board fuel requirements and reentry are all affected by atmospheric drag and its variability. Two versions of models are currently used. Those of Jacchia [1-4] are based mainly on total density data derived from satellite orbital decay observations. Models based on in situ composition data and temperatures inferred from ground-based incoherent scatter radar have been formulated by Hedin et al [5-6] and Hedin [7-8]. A common feature of all the models is the use of relatively simplified physical concepts. Variations are described as a function of altitude, solar and geomagnetic activity, latitude, longitude [4, 6-8], local time and day of year.

[†]This paper also presented as AAS paper No. 87-552, AAS/AIAA Astrodynamics Specialist Conference, Kalispell, Montana, Aug 10-13, 1987

*Physicist, Ionospheric Physics Division, Air Force Geophysics Laboratory, Hanscom AFB, MA

Several limitations of present models with regard to solar and geomagnetic variations are recognized. Heating due to solar EUV radiation activity is taken into account by relations involving ground-based measurements of the 10.7 cm solar flux, $F_{10.7}$, and some mean value, \bar{F} , measured over several solar rotations. This index does not necessarily represent the complex mechanisms of interactions between the solar extreme ultraviolet (EUV) flux and the thermosphere. Since it has been found to generally reflect variations in the thermospheric energy input, it is routinely used as a readily available, but imperfect, indicator of solar activity. Studies to determine the relationship between $F_{10.7}$ and satellite measurements of EUV [9] reveal correlations that are non-linear and both wavelength and solar cycle dependent. Similarly, the planetary 3-hr Kp or daily Ap index used as a geomagnetic activity indicator does not necessarily represent the physical mechanisms responsible for density variations. The indices are derived from ground-based magnetic field fluctuations. They are used as indicators of heating at high latitudes caused by the interaction of solar plasma with the upper atmosphere. However, it is the only routinely available index for geomagnetic activity. Based on a network of midlatitude stations, it is particularly limited when describing data at high latitudes. The need for improved geomagnetic indicators is particularly borne out by the data presented in this study.

Lack of comprehensive experimental data over the range of variables described in models also contributes to their limitations: (a) The dominance of the semidiurnal tide below 200 km has recently been revealed by low altitude satellite measurements. [10-11] This feature is incorporated in the MSIS models but not in those of Jacchia. However, the considerable phase and amplitude structure of the semidiurnal tide as a function of altitude and latitude is beyond the scope of these models. (b) Density variations with annual and sub-annual periodicities are characterized as a "semiannual variation" with maxima near equinox and minima near solstice. The cause of this variation has not been unambiguously resolved. Measured data show irregular variations from year to year in maxima and minima. (c) Satellite composition measurements have provided evidence of longitudinal variations. Density maxima for heavy constituents occur at the longitude of the north and south magnetic poles while the behavior of the lighter constituents is negatively correlated. This behavior is related to ionospheric plasma density and motion influenced by earth's magnetic field. The MSIS models rely on geographic coordinates and relatively few terms to describe the broad features of this variation. (d) Large scale gravity wave structures also occur. These have periods different from those of tidal waves and are not directly related to the earth-moon-sun geometry. They may be generated either locally in the thermosphere or at lower altitudes. Gravity waves with the largest amplitudes (~ 70% peak-to-peak) observed at high altitudes detected by accelerometers on the OV1-15 satellite, [12] were related to high-latitude heating as indicated by the auroral electrojet index. [13] Wave struc-

tures are not incorporated into present models. (e) Latitude dependences, associated with all of the atmospheric variations, are not well understood. A particular problem for the geomagnetic activity effect is that the time delay between storm onset and density variation is latitude-dependent.

In the lower thermosphere, below about 250 km, model deficiencies are particularly acute since they are based primarily on data at higher altitudes. Physical and mathematical difficulties limit extrapolation of these data to lower altitudes: the assumption of diffusive equilibrium is not always valid, and the lower thermosphere boundary conditions are poorly known and variable. AFGL is accumulating an extensive atmospheric density data base, from satellite accelerometer measurements, for the 150-240 km region [14]. The present study uses these data to determine the validity of empirical models and establishes phenomena not contained in them. Definitive low-altitude satellite measurement programs, to guide development of computationally efficient dynamic models utilizing realistic indicators of atmospheric energy sources, are recommended. The effects of high latitude processes on lower thermosphere dynamics are emphasized.

DATA DESCRIPTION

Extensive measurements of the lower thermosphere neutral density have been derived using the satellite accelerometer experiment. Instrument operating principles have been described by Marcos and Swift [15]. Density is derived from direct measurements of aerodynamic drag together with knowledge of the satellite's mass, area, velocity and drag coefficient. Figure 1 shows the flight history of the accelerometer from 1974 to the present. All spacecraft had near-polar orbits except for AE-C (68°) and AE-E (19°). This extensive lower thermosphere data set has been obtained over a wide range of latitudes and solar and geomagnetic conditions. Data from the first seven flights have been used in the present analysis of empirical models. The satellites used and the dates of data acquisition are given in Table 1. The altitude range of the data is generally 150-240 km for AE-C, -D, and -E and S3-1 and 170-240 km for S3-4 and SETA-1 and -2.

Data reduction techniques implemented for the SETA flight data are described in Reference 15. Because of the high length-to-diameter ratio of the host vehicle, the equations used for determination of atmospheric density (ρ) and cross-track winds [16] are:

$$a_D = \frac{A_{ref}}{2M} C_i \rho V^2 \quad (2)$$

where $i = x, y, z$

M = satellite mass

A_{ref} = satellite frontal area

$$\vec{V} = -\vec{V}_G + \vec{V}_A + \vec{V}_W$$

with \vec{V}_G , \vec{V}_A and \vec{V}_W representing respectively inertial satellite velocity, the atmospheric rotation velocity (assumed equal to earth's rotation velocity) and the neutral wind velocity.

C_i = drag coefficients; $C_i = C_i(V_x, V_y, V_z)$.

The equation for the component, in a particular direction, of the total force on an element of area is given by:

$$dC = \frac{1}{A_{ref}} \cdot \{ (\epsilon k + \gamma \ell + \eta t) [\gamma \cdot (1 + \operatorname{erf} \gamma S) + \frac{1}{S\sqrt{\pi}} e^{-\gamma^2 S^2}] + \frac{\ell}{2S^2} (1 + \operatorname{erf} \gamma S) + \frac{\ell}{2} \sqrt{\frac{T_r}{T_i}} \left[\frac{\gamma\sqrt{\pi}}{S} (1 + \operatorname{erf} \gamma S) + \frac{1}{S^2} e^{-\gamma^2 S^2} \right] \} dA ,$$

where

$$dC = \frac{2 dF}{A_{ref} \rho V^2}$$

F = aerodynamic force

ϵ, γ, η = direction cosines between mass velocity vector and axes of element of area, respectively

k, ℓ, t = direction cosines between the axes of element of area, and the direction in which force is desired (accelerometer axis)

$\operatorname{erf} \gamma S$ = error function of γS

S = molecular speed ratio = (mass velocity of gas)/(most probable random speed of molecules)

T_i = temperature of incident molecules

T_r = temperature of reflected molecules (assumed = 300°K)

This equation is integrated over the entire satellite surface area to obtain the drag coefficient for a particular axis. Values appropriate to this satellite were used with the MSIS model and the above equation to derive drag coefficients. For AE-C, -D and -E and S3-1, which had length-to-diameter ratios near unity, a constant value of $C_D=2.2$ was used.

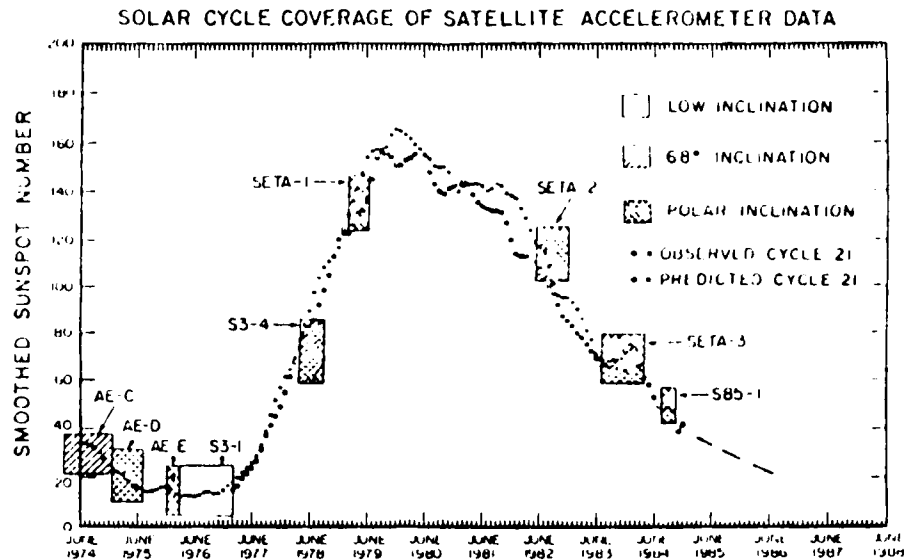


Fig. 1. Satellite accelerometer flight history and solar activity vs. time.

TABLE 1. SATELLITE ACCELEROMETER DATA SOURCES

Satellite	Data Acquisition Period
AE-C	Jan - Dec 74
S3-1	Oct 74 - May 75
AE-D	Oct 75 - Jan 76
AE-E	Nov 75 - Nov 76
S3-4	May - Aug 78
SETA-1	Mar - Apr 79
SETA-2	May - Nov 82

MODEL EVALUATIONS USING ACCELEROMETER DATA

The models considered were those of Jacchia, designated J65 [1], J70, [2] J71, [3] J73 (unpublished, see Ref 17) and J77, [4] Jacchia-Walker-Bruce, [17] Densel, [17] Lockheed-NASA, [18] U.S. Standard Atmosphere, 1962, [19] U.S. Standard Atmosphere Supplements, 1966 [20] and the Mass Spectrometer Incoherent Scatter models designated MSIS77, [5] MSIS79 [6], MSIS83 [7] and MSIS86 [8]. Two versions of the 1983 MSIS model were tested: MSIS83A used a daily averaged Ap index for the geomagnetic activity effect and MSIS83B used a weighted average of the 3-hr index over a 59 hour interval. The latter version of MSIS86 was used in this study.

Comparisons of model predictions with measurements not used in the model construction are valuable for testing the model reliability. While some AE mass spectrometer data were used in developing the MSIS models the density data were not. Also the S3-1 and -4 and the SETA-1 and -2 data were not used in construction of any of the models. The quantity statistically analyzed is the ratio (R) between measured density and model density. Results are given for mean ratios (R) and standard deviations (σ_R) in Table 2. Models are listed in chronological order. This Table indicates the lack of significant improvement in model accuracies during the past two decades.

The results of Table 2 indicate some of the difficulties in improving the accuracy of empirical models. The MSIS79 model added longitude variations, based on direct satellite composition measurements, to the MSIS77 model. This was done without changing the zonally averaged values. Incorporation of an observed phenomenon resulted in a less accurate model (by 0.1 to 0.5% in σ) for every data set. The MSIS83 models are based on a data set much more extensive than that used for MSIS77. While a small accuracy improvement results in MSIS83B from a weighted average vs a daily average for MSIS83A, neither model is generally more accurate than MSIS77. As part of a revised and updated J71 model, a more complex geomagnetic variation was incorporated into the J77 model. For all data sets, the standard deviations of J77 are 0.4 to 2.8% higher than those of J71. Revisions made to the J71 coefficients and formulas to produce the J73 model resulted in the most accurate of the Jacchia models; yet, this model was never published. MSIS86 is very similar to MSIS83 but with additional terms to represent seasonal differences in polar composition variations. The modifications are based mainly on Dynamics Explorer satellite composition data obtained above 300 km. The model provides typically a 1% reduction in standard deviations over MSIS83 in the 150-240 km region. However, the MSIS86 errors remain comparable to those in J71 and J73.

TABLE 2. ACCELEROMETER, TOTAL MASS DENSITY RATIOS TO MODELS
(ALTITUDE 150-240 KM)

	AE-C		AE-D		AE-E		S3-1	
	\bar{R}	σ_R	\bar{R}	σ_R	\bar{R}	σ_R	\bar{R}	σ_R
MSIS86B	1.10	14.5	0.95	15.1	1.02	13.0	1.03	14.4
MSIS83B	1.11	15.0	0.98	15.6	1.02	13.0	1.07	14.6
MSIS83A	1.12	15.2	0.99	16.2	1.03	13.6	1.08	14.8
MSIS79	1.05	14.2	0.98	16.5	1.01	13.6	1.00	14.7
MSIS77	1.05	14.0	0.98	16.3	1.01	13.5	1.00	14.2
J77	1.05	15.9	1.01	15.3	1.02	15.3	1.04	14.3
J73	1.07	14.0	1.02	14.7	1.07	13.7	1.06	13.5
J71	1.10	14.7	1.05	14.8	1.08	15.0	1.08	13.7
J70	1.05	17.1	0.98	15.4	1.00	15.8	1.04	14.6
J64	0.94	17.0	0.89	17.4	0.92	15.5	0.92	17.8
L-N	0.94	17.7	0.86	16.5	0.86	15.8	0.94	14.9
JWB	0.99	19.5	0.99	18.8	1.01	19.4	0.99	19.6
US66	0.95	16.5	0.89	15.6	0.92	15.5	0.95	14.4
US62	0.84	30.0	0.70	32.4	0.72	30.3	0.73	32.7
DENS	1.45	21.3	1.00	21.0	0.94	23.0	1.31	19.5

Number of Points	56908	28273	33835	25825
------------------	-------	-------	-------	-------

	S3-4		SETA-1		SETA-2	
	\bar{R}	σ_R	\bar{R}	σ_R	\bar{R}	σ_R
MSIS86B	1.04	11.1	1.01	9.8	0.94	11.0
MSIS83B	0.98	11.8	0.92	9.7	0.87	11.6
MSIS83A	0.99	12.1	0.93	10.1	0.88	11.8
MSIS79	0.98	11.5	0.96	11.7	0.92	11.7
MSIS77	0.98	11.2	0.96	11.5	0.92	11.2
J77	0.94	13.7	0.88	12.6	0.89	13.9
J73	0.96	11.6	0.92	9.8	0.92	10.2
J71	0.99	12.1	0.94	9.9	0.95	10.1
J70	0.97	12.0	0.99	9.3	0.93	10.4
J64	0.90	11.6	0.99	11.1	0.88	11.3
L-N	0.93	14.6	0.99	9.9	0.91	11.4
JWB	0.86	11.0	0.90	10.4	0.82	10.9
US66	0.90	11.5	0.99	11.0	0.88	11.2
US62	0.93	17.6	1.13	12.0	0.96	15.0
DENS	0.79	19.9	0.87	14.9	0.99	15.2

Number of Points	38215	56530	277442
------------------	-------	-------	--------

More detailed analyses of the statistical properties of the SETA accelerometer data have been made by partitioning data (to 240 km) into 5° geographic latitude bins and day/night local time bins as well as four K_p four bins. Local time bins of 08-16 hr and 16-24 hr were used to separate SETA dayside and nightside northern hemisphere data occurring at the same latitude.

Mean values relative to the J71 MSIS83B and MSIS86 models for SETA-1 data (Mar-Apr 79) are shown in Figs. 2-4 respectively as a function of geographic latitude. Part a of each Figure consists of daytime measurements (~ 1000 hours local time) and part b consists of nighttime measurements (~ 2200 hours local time). The horizontal axis from right to left, follows the satellite trajectory. The satellite altitude as a function of latitude typically decreases from 240 km at low northern hemisphere latitudes on the nightside to 200 km near the pole down to about 170 km near 30°N on the dayside. It then increases to about 180 km at the equator. Since the orbit is not quite polar, no data are available for the 85-90° bins. Model ratios indicate dayside relative density enhancements near 20°N and 65°N. Nighttime densities are underestimated, particularly near 30°N, by 10-15%. J71 tends to overestimate the geomagnetic activity response at all latitudes and particularly at night. The high K_p bin data are about 8% (dayside) and 15% (nightside) lower than those of the low K_p bin. The MSIS models show good agreement of the low and high K_p bins on the dayside and about a 7% overestimation on the nightside.

Mean values of SETA-2 data (Jul-Nov 82) are compared to J71, MS83B and MSS86B in Figs. 5-7 respectively. Peaks in ratios near 65°N on the dayside and increasing ratios with decreasing latitude on the nightside are again prominent features of all data sets. The geomagnetic activity representation of MSIS is less accurate than for SETA-1 data. Maximum density response overestimations occur for the highest K_p bin at high latitudes on the nightside. J71 provides a better estimation of the nightside density response than it did for SETA-1 data and than MSIS83B for the SETA-2 data.

Figs. 8 and 9 show the standard deviations for J71 and MSIS83 respectively. These Figures show a striking latitude dependence. The major errors occur at auroral and polar latitudes, even during geomagnetically quiet conditions. The maximum error of about 15% occurs for the highest K_p bin in both cases. Similar results were shown by Marcos [13] for the SETA-2 and S3-4 data relative to the J71 model. The MSIS86 data (not shown) give a similar result.

The previous analyses show that lower mean values and standard deviations are obtained with the SETA-1, -2 and -3 and S3-4 satellite data set. However, systematic differences between the data from these satellites and the data from the AE/S3-1 satellites are to be expected [14].

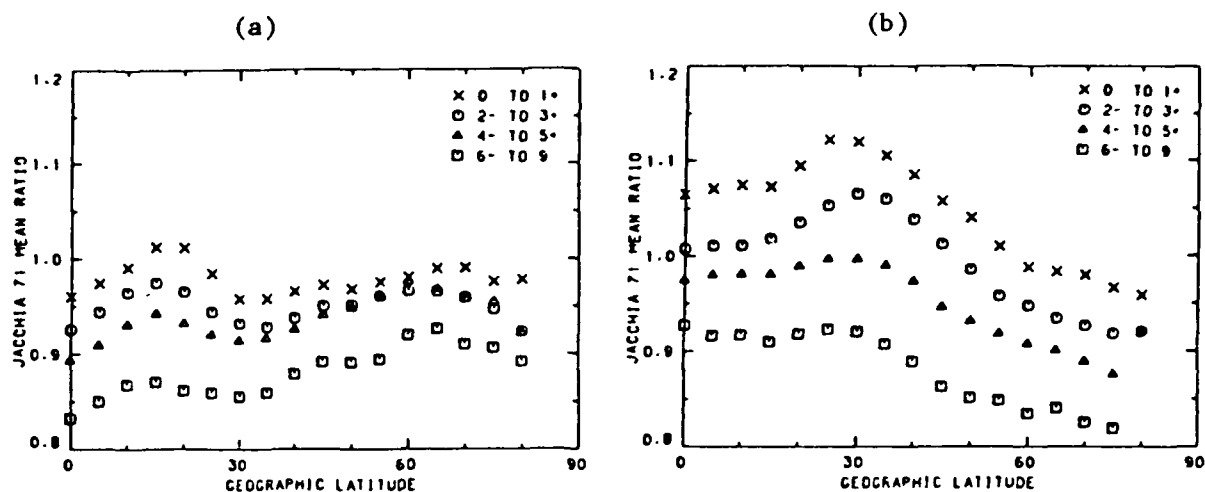


Fig. 2 Mean values of SETA-1 data to J71 model plotted as a function of geographic latitude (four Kp bins).

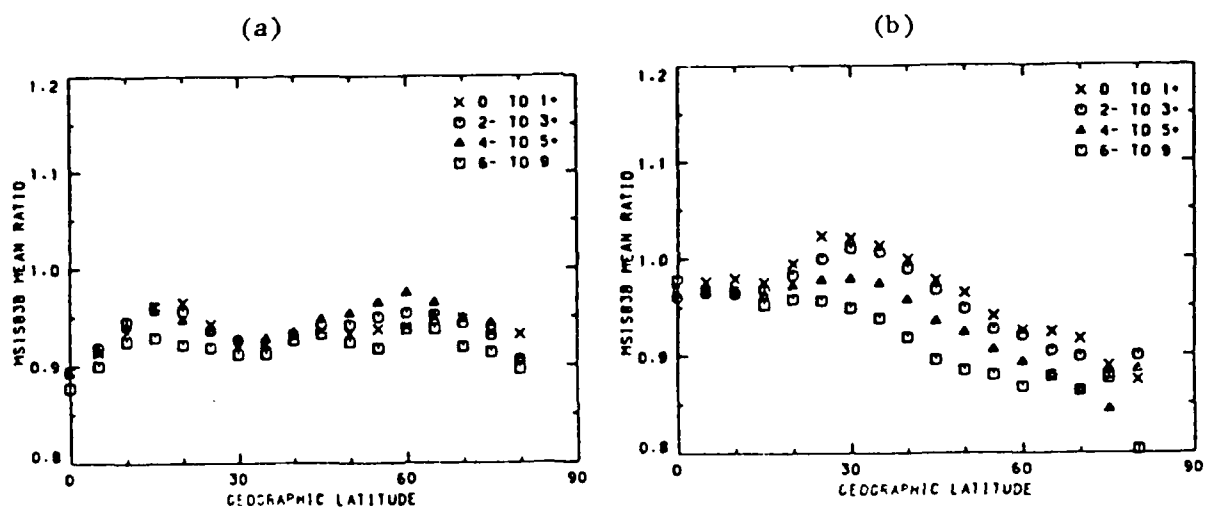


Fig. 3 Mean values of SETA-1 data to MSIS 83 model plotted as a function of geographic latitude (four Kp bins).

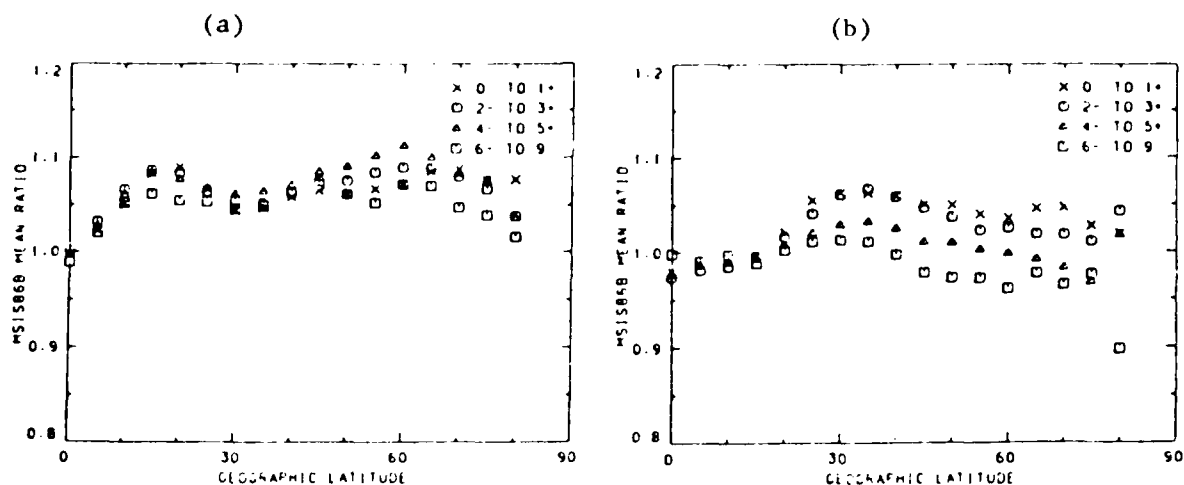


Fig. 4 Mean values of SETA 1 data to MSIS 86 model plotted as a function of geographic latitude (four Kp bins).

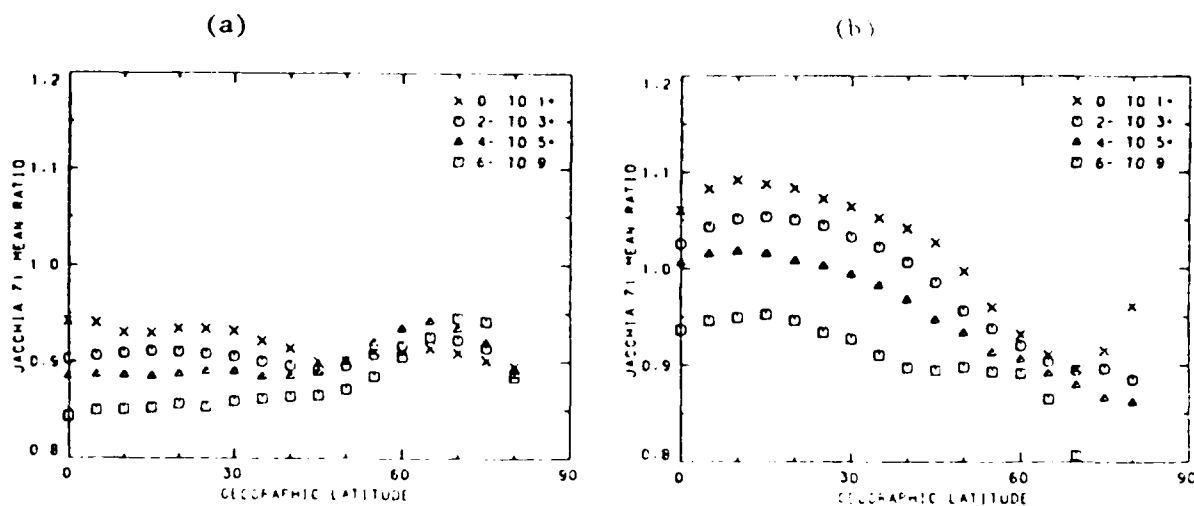


Fig. 5 Mean values of SETA-2 data to J71 model plotted as a function of geographic latitude (four Kp bins).

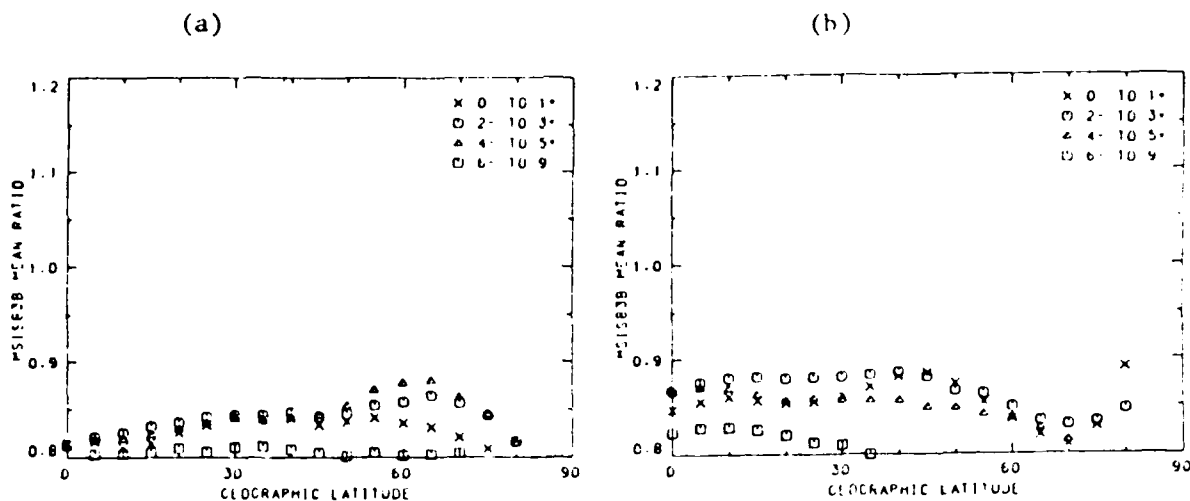


Fig. 6 Mean values of Seta-2 data to MSIS 83 model plotted as a function of geographic latitude (four Kp bins).

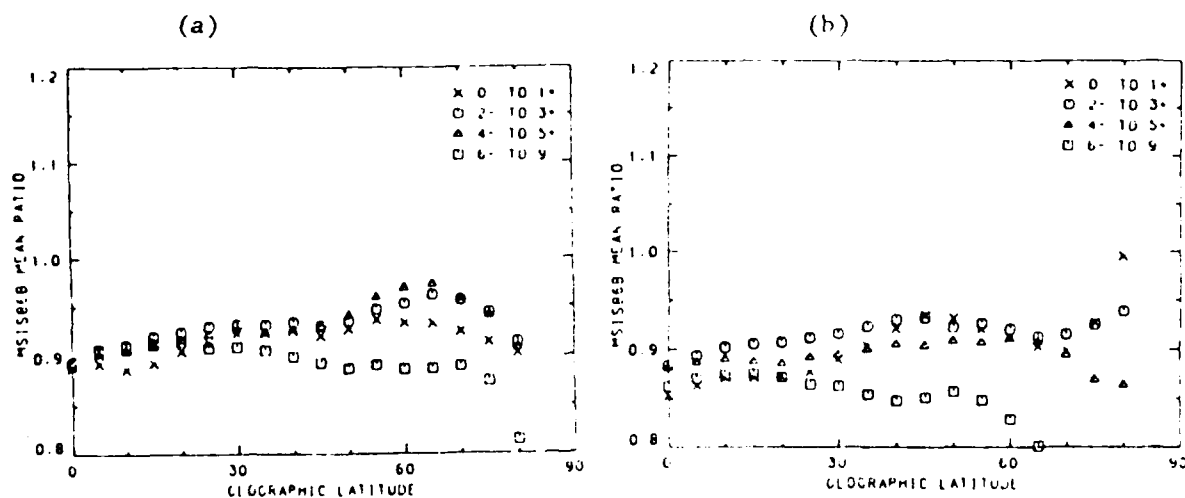


Fig. 7 Mean values of Seta-2 data to MSIS 86 model plotted as a function of geographic latitude (four Kp bins).

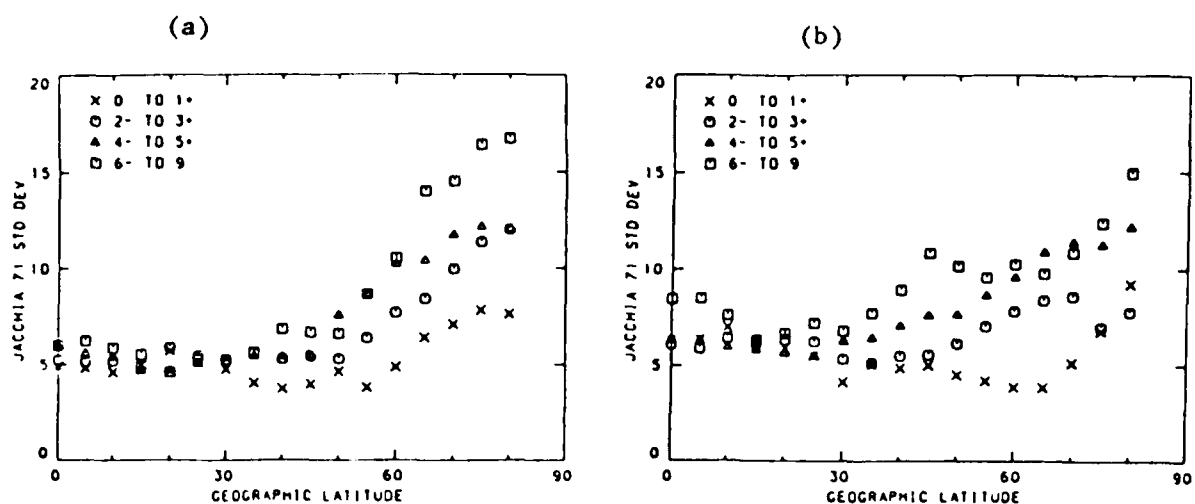


Fig. 8 Standard deviations of ratios of SETA-1 data to J71 model plotted as a function of geographic latitude (four Kp bins).

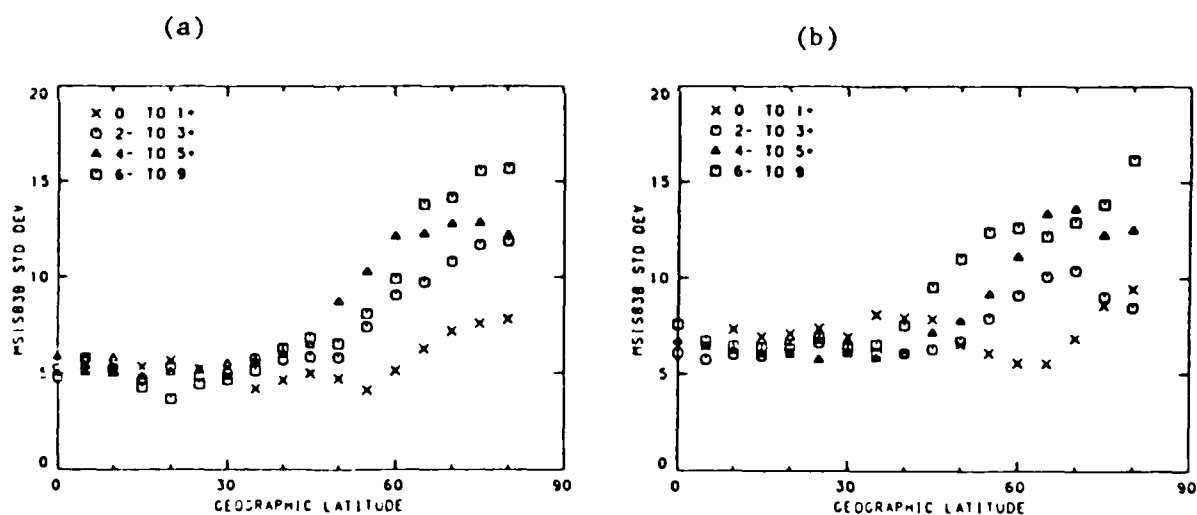


Fig. 9 Standard deviations of ratios of SETA-1 data to MSIS 83 model plotted as a function of geographic latitude (four Kp bins).

The Table 2 AE/S3-1 ratios imply densities generally above model values while the SETA ratios imply densities below model values. This difference between the two satellite data sets is believed due mainly to uncertainties in the ballistic coefficients used to convert orbital drag measurements to atmospheric density values. Drag coefficient (C_D) estimates contribute the major uncertainty to ballistic coefficient errors. Our estimated errors in C_D are $\pm 10\%$. It is possible that the SETA C_D errors exceed $\pm 15\%$ due to the spacecraft shape [21]. Therefore, systematic errors in drag coefficient may completely account for the absolute value differences between AE/S3-1 and SETA total mass densities. We conclude that, on average, recent models reflect density to within the $\pm 10\%$ accuracy of the Atmosphere Explorer accelerometer measurements.

The standard deviation difference has been attributed to be the manner in which altitude, latitude and local time variations were sampled for each data set. The AE/S3-1 data were sampled over a mix of altitudes, latitudes and local times. For SETA data, these parameters were highly correlated; e.g., mid-latitudes were sampled near 170 km and 1030 hrs LT on the dayside. AE-E and S3-1 data have been further analyzed at low latitudes to show quantitatively that reducing the range of variables over which a model must predict density leads to a reduced standard deviation in agreement with the SETA values.

The AE-E satellite acquired data between $\pm 20^\circ$ latitude over a period of about one year. During this time data were sampled over four local time cycles. Data obtained in the spinning mode were analyzed in altitude, latitude, K_p , local time and seasonal bins. Results presented in Table 3, show reductions in σ associated with these bin limitations. The AE-E 170 - 175 km data, grouped by season show values of σ between 5% and 7% in good agreement with SETA low latitude values. A similar analysis was performed with the S3-1 data. Results of binning are given in Table 4 for 170 - 175 km 0-20°N and for 170 - 200 km for 0-80°N. Local time was near 0730 hours for this data set. Note that for 0-10°N, 170 - 200 km, σ is 6.5% in excellent agreement with the Table 4 AE-E data. Therefore the typically 15% standard deviations obtained from the AE/S3-1 data, not the lower values obtained with the S3-4/SETA flights, are representative of model errors over "all" conditions.

DISCUSSION

Accelerometer data have revealed unmodeled features of lower thermospheric structure. Particularly significant are observed variations at high latitudes as a function of latitude, local time and level of geomagnetic activity. The importance of new knowledge at auroral and polar latitudes is borne out by the maximum standard deviations of models in those regions. However, additional density data alone

Table 3. Atmosphere Explorer - E Statistical Results with Local Time, Latitude, Season, Altitude and Kp Bins Spinning Orbit Data

Altitude	Lat	Kp	LT	Mo	N.	J71		MSIS 83	
						\bar{R}	σ	\bar{R}	σ
170-175	± 20	All	All	All	1929	0.088	0.136	0.028	0.108
↓	0-10	0-3+	All	All	280	0.104	0.142	0.025	0.100
	± 20	0-3+	10-11	DJF	47	0.058	0.078	-0.041	0.071

Table 4. S3-1 Statistical Results vs. Latitude; Kp 0 to 3+

Altitude	Lat	Mean LT	N.	J71		MSIS 83	
				\bar{R}	σ	\bar{R}	σ
170-175	0-10	0736	51	0.214	0.066	0.058	0.068
170-175	10-20	0737	66	0.206	0.059	0.076	0.066
170-200	0-10	0736	136	0.194	0.065	0.016	0.073
↓	10-20	0737	244	0.180	0.061	0.025	0.073
	20-30	0736	188	0.138	0.075	0.026	0.068
	30-40	0733	134	0.132	0.084	0.068	0.086
	40-50	0734	101	0.153	0.104	0.122	0.088
	50-60	0748	226	0.095	0.117	0.106	0.098
	60-70	0805	306	0.038	0.081	0.090	0.076
	70-80	0846	232	0.131	0.124	0.172	0.109

will not be sufficient to improve models. More recent models, utilizing extensive satellite measurements of atmospheric composition have been shown to specify total density with about the same accuracy as older models based on satellite orbital decay measurements.

Problems in accurately describing the spatial/temporal characteristics of density variability are indicated by the diagram of Fig. 10. The complex phenomena contributing to atmospheric heating and dynamics are dominated by two sources of solar energy: electromagnetic radiation and particles. Solar EUV, the most important thermospheric heat source, is deposited mainly at low latitudes and in the summer hemisphere. The circulation and structure of the thermosphere are controlled primarily by this heating. The processes involved are reasonably well understood. At auroral latitudes, the situation is different. The thermosphere is driven by electrodynamic coupling between the solar wind, magnetosphere, ionosphere and neutral atmosphere. Energetic charged-particle precipitation from the magnetosphere and Joule (resistance) heating due to electric current systems within the ionosphere are the major energy sources. Also, ionospheric plasma, driven by the magnetospheric convection electric field, transfers momentum to the neutral particles and can produce winds of about one km sec^{-1} . Both the magnitude and spatial extent of the auroral processes are extremely variable and related to the level of geomagnetic activity. During large storms, the energy dumped into the relatively narrow auroral region can exceed the global EUV input. These localized heat sources can cause large and sudden density variations, perturb circulation patterns and launch gravity waves. High latitude processes can therefore significantly alter thermospheric density, composition and temperature on a global scale as a result of large geomagnetic disturbances. Hence, density observed at a given location can depend on both the past history of density at that location and on events that occurred at varying distances and times.

Dynamic models are now being developed [22 and 23]. These are theoretical three-dimensional and time-dependent models that numerically solve the primitive energy and momentum equations. They attempt to understand the physics, chemistry and dynamics responsible for thermospheric structure. Parameterizations of various input fields are necessary for the specification of the physical processes described in these models. These inputs include solar UV and EUV energy and their heating efficiencies and energy and momentum sources resulting from the solar wind-magnetosphere interaction. The output is a global simulation of the structure and dynamics of the thermosphere. In their present form, the models would not be feasible for operational use since they require a CRAY computer. However, these numerical models provide the means for guiding development of a new generation of operational models utilizing realistic physical concepts.

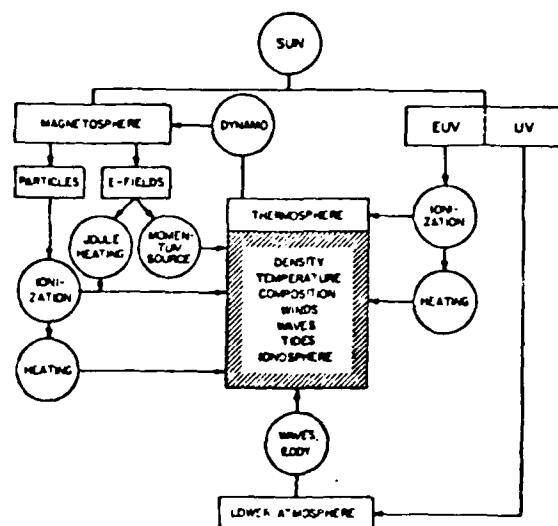


Fig. 10. Schematic block diagram illustrating interactions between the lower atmosphere, thermosphere and magnetosphere.

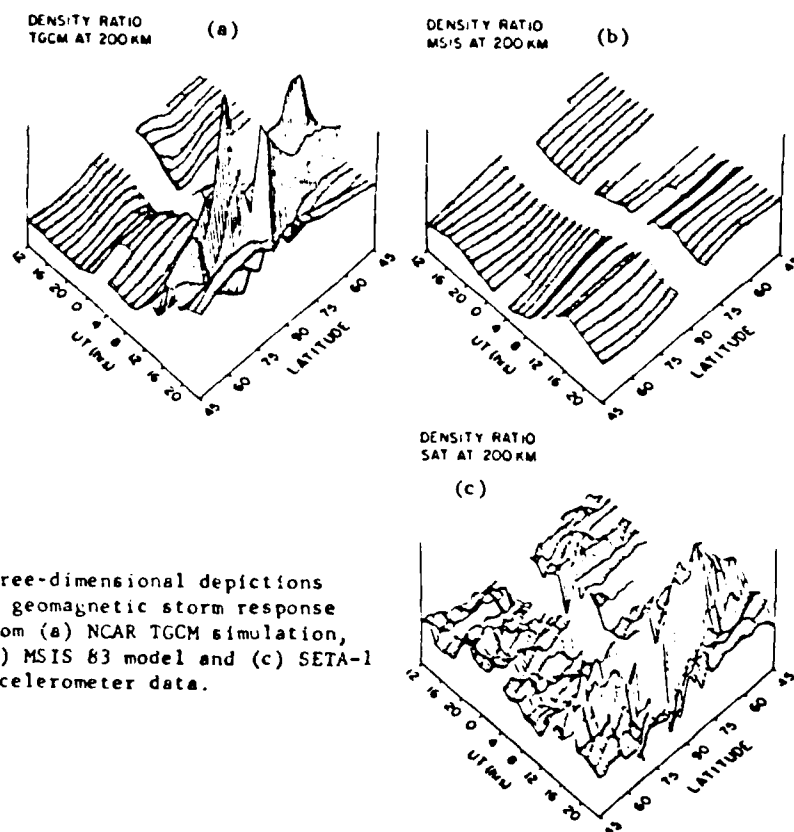


Fig. 11 Three-dimensional depictions of geomagnetic storm response from (a) NCAR TGCM simulation, (b) MSIS 83 model and (c) SETA-1 accelerometer data.

SETA-1 density and winds obtained during the March 22, 1979 geomagnetic storm have provided a unique opportunity to test and evaluate our knowledge and modeling capability of the magnetosphere/ionosphere/thermosphere system. This period was one of intense solar-terrestrial observations and analysis. As a result, the time-dependent variations of auroral and magnetospheric convection model parameterizations incorporated within the National Center for Atmospheric Research thermospheric general circulation model (TGCM) were prescribed in detail as input to the storm simulation [24]. The TGCM predictions of density variability for this storm period are compared [25] with the satellite data and the MSIS83 model in Fig 11. Three-dimensional depictions are given for latitudes above 45° in the northern hemisphere for local times ~ 2200 hrs (left side) and ~ 1100 hrs (right side). In the day sector, the SETA measurements clearly confirm the TGCM predictions of a high-latitude (60° - 85°) localized region of intense heating and density enhancement ($\sim 60\%$) between 1400 and 1500 UT (Universal Time), the period of maximum magnetic disturbance. The night sector is characterized by more wavelike structures and density perturbations of 20-40% in both the SETA and TGCM data. The extension of the TGCM "hot spot" farther into the nighttime sector than is consistent with SETA data is believed due to inaccuracies in the TGCM convection model position, orientation or latitudinal extent. Over the complete range of latitudes, Ref. 25 shows that the TGCM and SETA data are characterized by generally elevated densities (10-20%) after the storm (2200 UT) as compared with pre-storm conditions (0800 hrs GMT). The MSIS model predicts density enhancements of only 10-20% between 1100 UT and 1800 UT, without the pronounced latitudinal and temporal structure indicated by the TGCM and the SETA data. It is evident that the TGCM accounts for time-dependent localized processes with a much higher time resolution than the MSIS83 model.

CONCLUSIONS

Satellite accelerometer measurements have provided the first extensive description of density variability at low satellite altitudes and high latitudes. The data have been obtained over a wide range of solar and geomagnetic conditions. Statistical evaluations of density results from seven satellites demonstrate that model accuracies have not progressed significantly in the past 20 years. Mean values are given within $\pm 10\%$ with standard deviations of $\pm 15\%$. Errors encountered for specific applications have been shown to be sensitive to geographic location, local time and level of geomagnetic activity as well as to the model used. Development of better models will result from improvements in our knowledge of the magnitude, distribution and transport of thermospheric heating. This requires coordinated theoretical/observational programs. Specific recommendations for the lower thermosphere include:

Extensive interpretation and analyses of the accelerometer data base. Emphasis should be placed on case studies of spatial/temporal variations related to geomagnetic activity as a function of solar flux, season, latitude, longitude and local time.

Continued development of dynamic global circulation models. Accelerometer density and winds data as well as Dynamics Explorer satellite data are needed to validate and improve input assumptions.

More realistic indices to describe energy inputs related to auroral processes and their interaction with the magnetosphere/ionosphere system. Auroral electrojet parameters and new high latitude indices derived from ground-based magnetometers can be evaluated with accelerometer density data for the same periods.

An extensive lower thermosphere measurements program that provides a basis for developing accurate relationships between energy inputs and global density variability. An initial payload measuring density, composition, winds, temperature and ionospheric properties is required. A low eccentricity sun-synchronous orbit (1400/0200 LT) would provide data in local time-latitude regions not covered by the present data set. Coordination with ground-based thermosphere dynamics measurements programs (such as the Coupled Energetics and Dynamics of Atmospheric Regions program) will greatly enhance data interpretation.

The above recommendations have focussed on applications of accelerometer data to improve density models. Since these data measure the parameter to be modeled, atmospheric density, they must be an integral part of future programs that attempt to improve density models. Continued progress in numerical modeling and in geomagnetic index development together with interpretations of present data and a critical new measurements program can provide important advances in thermospheric models.

ACKNOWLEDGEMENTS

Critical data support was provided by: E. Robinson, AFGL/LCY; and K. Bhavnani, J. Bass, C. Bryant and N. Bonito of RADEX Corp. Critical typing support was provided by Ms. Nancy Fleming and Mrs. Nadine Mayo of the Ionospheric Physics Division.

REFERENCES

1. L.G. Jacchia, Static Diffusion Models of the Upper Atmosphere with Empirical Temperature Profiles, SAO Special Report No. 170, 1965.
2. L.G. Jacchia, New Static Models of the Thermosphere and Exosphere with Empirical Temperature Profiles, SAO Special Report No. 313, 1970.
3. L.G. Jacchia, Revised Static Models of the Thermosphere and Exosphere with Empirical Temperature Profiles, SAO Special Report No. 332, 1971.
4. L.G. Jacchia, Thermospheric Temperature Density and Composition: New Models, SAO Special Report No. 375, 1977.
5. A.E. Hedin, J.E. Salah, J.V. Evans, C.A. Reber, G.P. Newton, N.W. Spencer, D.C. Kayser, D. Alcayde, P. Bauer, L. Coyger, and J.P. McClure, "A global thermospheric model based on mass spectrometer and incoherent scatter data, MSIS 1, N₂ density and temperature," J. Geophys. Res. Vol. 82, 1977, p. 2139.
6. A.E. Hedin, C.A. Reber, N.W. Spencer, and H.C. Brinton, "Global model of longitude/UT variations in thermospheric composition and temperature based on mass spectrometer data," J. Geophys. Res., Vol. 84, 1979, p. 1.
7. A.E. Hedin, "A revised thermospheric model based on mass spectrometer and incoherent scatter data; MSIS-83," J. Geophys. Res., Vol. 88, 1983, p. 10, 170.
8. A.E. Hedin, MSIS-86, to be published.
9. H.E. Hinteregger, "Development of Solar Cycle 21 Observed in EUV Spectrum and Atmospheric Absorption," J. Geophys. Res., Vol. 84, 1979, p. 1933.
10. J.M. Forbes and F.A. Marcos, "Tidal variations in total mass density as derived from the AE-E MESA experiment," J. Geophys. Res., Vol. 84, 1979, p. 31.
11. A.E. Hedin, N.W. Spencer and H.G. Mayr, "The semidiurnal and ter-diurnal tides in the equatorial thermosphere from AE-E measurements," J. Geophys. Res., Vol. 85, 1980, p. 1781.
12. F.A. Marcos, and K.S.W. Champion, "Gravity waves observed in high latitude neutral density profiles," Space. Res. Vol. 12, 1972, p. 791.

13. J.M. Forbes, and F.A. Marcos, "Thermospheric density variations associated with auroral electrojet activity," J. Geophys. Res. Vol. 78, 1973, p. 3841.
14. F.A. Marcos, Application of Satellite Accelerometer Data to Improve Density Models, AFGL-TR-84-0211, 1984.
15. F.A. Marcos and E.R. Swift Application of the Satellite Triaxial Accelerometer to Atmospheric Density and Wind Studies, AFGL-TR-82-0091, 1982.
16. F.A. Marcos, and J.M. Forbes, (1985) "Thermospheric Winds From The Satellite Electrostatic Triaxial Accelerometer System", J. Geophysical Res., Vol 90, 1985, p. 6543.
17. A.S. Bramson and J.W. Slowey, Some Recent Innovations in Atmospheric Density Programs, AFCRL-TR-74-0370, 1974.
18. J.H. Butler, A Preliminary Upper Atmosphere Density Model Derived from Satellite Drag Density, Lockheed Missiles and Space Co., NASA Contractor Report No. 61298, Aug. 1969.
19. COESA, U.S. Standard Atmosphere, 1962, U.S. Government Printing Office, Washington, D.C., 1962.
20. COESA, U.S. Standard Atmosphere Supplements, 1966, U.S. Government Printing Office, Washington, D.C., 1966.
21. J.M. Forbes, and F.A. Marcos, "Thermospheric Winds, Densities and Temperatures During an Isolated Magnetic Substorm", submitted to J. Geophysical Res., 1985.
21. F.A. Herrero, "The Drag Coefficient of a Cylindrical Spacecraft in Orbit at Altitudes Greater than 150 km," NASA-TM-85043, 1983.
22. R.G. Roble, R.E. Dickinson, and E.C. Ridley, (1982) "Global circulation and temperature structure of thermosphere with high-latitude plasma convection", J. Geophys. Res., Vol 87, 1982, p. 1599.
23. D. Rees, T.J. Fuller-Rowell, and R.W. Smith, "Measurements of high latitude thermospheric winds by rocket and ground-based techniques and their interpretation using a three-dimensional time-dependent dynamical model", Planet Space Sci., Vol 28, 1980, p. 919.
24. R.G. Roble, J.M. Forbes and F.A. Marcos, "Thermosphere Dynamics During the March 22, 1979 Magnetic Storm, 1, Model Simulations," J. Geophys. Res., Vol. 92, 1987, P. 6045.
25. J.M. Forbes, R.G. Roble and F.A. Marcos, "Thermosphere Dynamics During the March 22, 1979 Magnetic Storm, 2, Comparisons of Model Predictions with Observations," J. Geophys. Res., Vol. 92, 1987, P. 6069.

MSIS Empirical Model Status and Directions for Improvement

by A. E. Hedin (NASA/GSFC)

for AFSPACOM Atmospheric Neutral Density Specialist Conference
Colorado Springs, CO March 22-23, 1988

I. Introduction

With the detection of atmospheric drag effects in early artificial satellites, data became available which led to the well known series of Jacchia models. The J65 (also called J64) model was the earliest comprehensive global model based on satellite drag (orbital decay). This model was the first to include the principal types of thermospheric density variations and, unlike the standard atmospheres, provides an approximation to the true spatial and temporal variations of the thermosphere. While drag based models use temperature and composition as intermediate parameters for the calculation of total density, these intermediate parameters may be in error since drag data provide no direct information on composition and temperature. The J77 model introduced separate pseudo-temperatures for each constituent, but this significant artificial complication was only partially successful in reproducing composition variations.

The OGO-6 satellite mass spectrometer launched in 1969 provided the first extensive measurements of the densities of molecular nitrogen, atomic oxygen, and helium in the thermosphere. Their sum provides an independent determination of total density. The observed variations in composition could be quite different from the Jacchia model predictions and led to a new approach to represent the observed variability. The ground based incoherent scatter measurements of temperature were subsequently combined with the in situ composition measurements in the MSIS (Mass Spectrometer and Incoherent Scatter) models to provide composition and temperature as well as total density predictions of equivalent accuracy for various geographical, temporal, and solar conditions. The latest model, MSIS-86, was chosen for CIRA 1986, but publication of CIRA 1986 has been delayed.

II. Present accuracy

Comparisons of measured total densities with various models (Tables 1 & 2 show mean absolute differences and standard deviations for magnetically quiet conditions, and Table 3 shows standard deviations for magnetically active conditions, all in terms of log to base e) indicate a general accuracy of 15% to 20% in the 200 to 400 km range and 25 to 30% at higher altitudes. Data is scarce at lower altitudes, but what is available suggests model accuracies in the 15 to 20% range. Ranking the models from 1 to 5 (1 best) for each data set in selected altitude ranges and plotting (Figs. 1 to 3) for each model how many data sets (counting each altitude range separately) are best (or second best, etc.) represented by that model shows that there is little difference between models with respect to absolute differences between data and model. With respect to standard deviations between data and model, the later (MSIS) models have a better ranking with more data sets than the earlier Jacchia models. However, the difference between the worst and

best model is often only a few percentage points.

The data set labeled Jacchia drag, for instance, consists of densities determined from orbital decay by the Smithsonian group and were used in generating the Jacchia models but not the MSIS models. The comparison results point to both consistency (within 15%) between two quite different techniques (mass spectrometer and drag) and between two different time periods, since the drag data generally come from an older time period than the mass spectrometer measurements.

While total density predictions have improved relatively little, the predictions of composition and temperature have improved considerably (Table 4 and Fig. 4). The most dramatic improvements are for the minor constituents in each altitude range, but there are improvements at altitudes where a species is not minor also. For example, in the 200 to 400 km range predictions by J70 for both N₂ and O density are worse than predictions by MSIS-86, yet the differences in total density are small because the errors in J70 model predictions for these two major gases approximately compensate. The J70 model helium densities are not as good as MSIS-86 above 800 km (where He is a major constituent), while J70 compares better to drag densities than MSIS. Solving this puzzle, which may be due to errors in the drag coefficient which would appear as errors in the Jacchia densities or the possible existence of a hot oxygen population which has not been taken into account, would certainly improve calculation of drag force at the higher altitudes. Since the drag coefficient depends on atmospheric composition and temperature it is important to predict these quantities correctly in order to calculate drag force or infer density. The accuracy of the composition at one altitude also determines the accuracy of extrapolated densities using diffusive equilibrium.

Winds at high latitudes can change drag force by 10 to 20% but this effect has not been included in deductions of density nor in tracking errors because no suitable wind model existed. The Dynamics Explorer satellite measured winds over the whole globe and these together with Atmosphere Explorer wind measurements have been used to create the first empirical model of global winds. An example for solstice conditions is shown in Fig. 5 where the solid contours show temperature and the dashed contours pressure. The winds blow approximately from high to low pressure areas but are higher in the polar region due to magnetospheric forcing. Note that temperature and pressure (as well as density) do not maximize at the same location and this is contrary to a basic assumption of the early Jacchia models. The winds shown are in addition to the rigid body rotation of the atmosphere with the earth. Super-rotation effects (a net or zonally averaged flow beyond the rigid body rotation speed) are not of great practical importance for drag. Because the effect on drag force depends on the direction the satellite is moving with respect to the wind, the wind effects may not have seriously corrupted a density model if there were a sufficient variety of orbits involved in the model database.

Waves provide a basic floor to achievable prediction accuracy which available measurements indicate is in the 2 to 10% range depending on latitude (larger at high latitudes). A model predicting the likelihood of waves of a certain amplitude in the upper thermosphere is

currently feasible. Unless the lower thermosphere boundary can be described in some detail with observations, the lower atmosphere weather will also provide some noise level in the thermosphere (particularly the lower thermosphere) which is not well established.

III. Calculation efficiency

The following times were found for total density calculation on a MicroVax computer:

MSIS-86	47 millisecc
J70	40 millisecc
J77	123 millisecc

These calculations did not use any optimizing algorithms. Order of magnitude timing improvements are possible for the Jacchia models because of the unique density-temperature relationship which is assumed in their formulation. However, it is this very assumption which is a basic cause of errors in composition and temperature in these models. The MSIS timing can be improved by about a factor of 2 for total density by skipping the calculation of constituents which are of minor importance for the particular altitude.

It is likely that the timing of any of the models can be improved for particular applications where certain types of variations can be disregarded.

IV. Directions for accuracy improvement

IVa. General

Although engineering and operational interests frequently focus on total density, an effort to improve predictions of total density without regard to composition, temperature, and wind is not particularly interesting to the wider scientific community because it is not likely to improve our understanding of the atmosphere and its processes. In any case, more accurate density by itself may not lead to higher accuracy drag force determinations since the drag coefficient depends on composition of the atmosphere and drag depends on wind as well. Spacecraft design also depends more and more on accurate composition for problems like material degradation and surface glow.

Improvements are likely to come in small steps rather than dramatic breakthroughs since the current accuracy limit seems to have a number of diverse causes such as measurement accuracy of historical data, differences between techniques, undiscovered systematic variations, unpredictable natural variability, and difficult to predict (with limited ancillary data) effects of magnetic storms. It should also not be forgotten that current models already account for a large proportion of the observed density variance. Improved models of total density and other atmospheric parameters will require a sustained program involving a wide range of experimental and theoretical approaches and must include new measurements.

IVb. Existing Data

Existing data (from previous scientific satellites, ground based techniques, and possibly unexploited satellite tracking data) should be analyzed for a better understanding of:

- magnetic storm effects;
- semiannual variations;
- EUV (F10.7) variations;
- interactions between known effects;
- differences between solar cycles;
- differences between techniques.

This is the easiest approach and shows promise of making some improvement in the near term. These studies will also benefit from ongoing scientific programs involving ground based measurements of parameters other than density.

IVc. New Measurements

A model can only be as good as the available data. No theory is good enough to calculate atmospheric parameters without reference to measurements. Furthermore, we have no certainty that the relations we derive (such as between density and the 10.7 cm solar flux) hold for the indefinite future.

New density and other measurements must be designed to surpass the required accuracy. Densities must be corrected for wind and be cross-checked by different techniques to check basic assumptions. If global predictions are required then measurements must be global in scope. Since we know the semiannual variation is different from year to year, we assume the lower boundary will be different from year to year (if not day to day), and we are not sure what happens in each new solar cycle, measurements must be taken reasonably near the required time.

IVd. Theoretical Support

Theoretical analysis and Global Circulation Models (GCM): provide guidance for organizing and interpreting measurements and fill in where measurements are missing (such as the lower thermosphere). Current models should be evaluated for their current ability to predict data, just as empirical models. Theoretical models may be particularly valuable for highly dynamic effects and may possibly be combined with empirical models. An important question is how accurate and detailed our knowledge must be of the auroral energy inputs in order that the additional detail predicted by theoretical models is sufficiently correct in phase and amplitude as to be more useful than a smoothed representation.

IVe. Ancillary Measurements

To provide energy input for theoretical models and correlation parameters for empirical models we must continue or improve measurements such as:

- solar radio flux;
- solar EUV flux;
- IMF;
- magnetic indices;
- auroral morphology;
- particle precipitation.

The present plans to measure an EUV band on a long term basis from the GOES satellite is an encouraging step. While there may be some prediction improvement possible by correlating this new measurement with the 10.7 cm flux and thus introducing it into the existing models, it will only be through direct correlation with new measurements of density and temperature that the full usefulness of this measurement can be realized and validated.

To both interpret drag data in terms of density and make better predictions of drag from density models there is a need for improved knowledge of the drag coefficient under a wide variety of conditions through laboratory and space experiments.

Overall mean (magnetically quiet)

(preliminary)

	Alt	Pts	MSIS-86	MSIS-83	MSIS-77	J77	J70
Jacchia drag	200-400	3197	-.05 (3)	-.05 (3)	-.21 (4)	-.03 (1)	-.04 (2)
	400-800	6516	-.05 (1)	-.06 (2)	-.23 (3)	-.05 (1)	-.06 (2)
	800-1200	3386	.04 (2)	.04 (2)	-.04 (2)	-.03 (1)	-.05 (3)
Barlier drag	120-200	1050	.02 (1)	-.03 (2)	-.02 (1)	-.04 (3)	-.07 (4)
	200-400	4761	.04 (3)	.02 (1)	-.06 (4)	-.04 (3)	.03 (2)
	400-800	1447	.10 (2)	.10 (2)	-.04 (1)	.10 (2)	.15 (3)
AE-C MESA accel	120-200	5746(.25)	.11 (3)	.11 (3)	.05 (2)	.05 (2)	.00 (1)
	200-250	6101(.55)	.02 (1)	.04 (3)	-.08 (4)	.03 (2)	-.03 (2)
AE-C OSS ms	120-200	6447(.65)	-.01 (1)	-.01 (1)	-.05 (3)	-.02 (2)	-.07 (4)
	200-390	6279(.2)	.02 (2)	.06 (3)	-.08 (4)	.09 (5)	.01 (1)
AE-D MESA accel	120-200	11024(.7)	-.03 (3)	.00 (1)	.00 (1)	.02 (2)	-.02 (2)
	200-250	4399	-.08 (3)	-.04 (2)	-.11 (4)	.01 (1)	-.04 (2)
AE-D OSS ms	120-200	11787	-.01 (1)	.01 (1)	.01 (1)	.04 (2)	.01 (1)
	200-390	10923(.75)	-.06 (3)	-.02 (1)	-.20 (4)	.03 (2)	-.03 (2)
AE-E MESA accel	120-200	11455(.45)	.02 (2)	.02 (2)	-.01 (1)	-.01 (1)	-.03 (3)
	200-250	8363	-.01 (2)	.00 (1)	-.06 (4)	.05 (3)	-.01 (2)
AE-E OSS ms	120-200	11812(.62)	-.01 (2)	.00 (1)	-.07 (4)	-.05 (3)	-.07 (4)
	200-400	9741(.12)	-.03 (2)	-.03 (2)	-.15 (3)	-.01 (1)	-.03 (2)
AE-E NACE ms	120-200	7533	-.05 (1)	-.05 (1)	-.05 (1)	-.05 (1)	-.07 (2)
	200-400	10158(.14)	-.09 (3)	-.09 (3)	-.22 (4)	-.02 (2)	-.07 (1)
	400-600	10243(.20)	-.17 (4)	-.14 (3)	-.32 (5)	-.12 (2)	-.08 (1)
			1-6	1-8	1-6	1-7	1-5
			2-7	2-7	2-2	2-9	2-10
			3-7	3-6	3-3	3-4	3-3
			4-1	4-0	4-9	4-0	4-3
					5-1	5-1	

Overall Standard Deviation (magnetically quiet)

(preliminary)

	Alt	Pts	MSIS-86	MSIS-83	MSIS-77	J77	J70
Jacchia	200-400	3197	.15 (1)	.16 (2)	.18 (3)	.15 (1)	.16 (2)
drag	400-800	6516	.26 (2)	.26 (2)	.29 (3)	.25 (1)	.26 (2)
	800-1200	3386	.27 (3)	.26 (2)	.30 (4)	.29 (3)	.22 (1)
Barlier	120-200	1050	.22 (1)	.23 (2)	.22 (1)	.22 (1)	.23 (2)
drag	200-400	4761	.20 (1)	.20 (1)	.21 (2)	.21 (2)	.21 (2)
	400-800	1447	.31 (1)	.31 (1)	.33 (3)	.32 (2)	.31 (1)
AE-C MESA	120-200	5746(.25)	.16 (2)	.16 (2)	.15 (1)	.18 (3)	.18 (3)
accel	200-250	6101(.55)	.21 (1)	.21 (1)	.21 (1)	.21 (1)	.21 (1)
AE-C OSS	120-200	6435(.65)	.12 (2)	.12 (2)	.10 (1)	.13 (3)	.13 (3)
ms	200-390	6279(.2)	.14 (1)	.14 (1)	.14 (1)	.15 (2)	.16 (3)
AE-D MESA	120-200	11024(.7)	.15 (2)	.15 (2)	.14 (1)	.15 (2)	.14 (1)
accel	200-250	4399	.18 (1)	.19 (2)	.18 (1)	.18 (1)	.18 (1)
AE-D OSS	120-200	11787	.11 (1)	.11 (1)	.11 (1)	.13 (2)	.11 (1)
ms	200-390	10923(.75)	.17 (1)	.18 (2)	.18 (2)	.17 (1)	.17 (1)
AE-E MESA	120-200	11455(.45)	.12 (1)	.12 (1)	.12 (1)	.14 (2)	.14 (2)
accel	200-250	8363	.18 (1)	.18 (1)	.19 (2)	.20 (3)	.20 (3)
AE-E OSS	120-200	11812(.62)	.15 (3)	.14 (2)	.13 (1)	.16 (4)	.17 (5)
ms	200-400	9741(.12)	.19 (2)	.18 (1)	.21 (4)	.20 (3)	.21 (4)
AE-E NACE	120-200	7533	.11 (1)	.11 (1)	.15 (2)	.17 (4)	.16 (3)
ms	200-400	10158(.14)	.20 (2)	.19 (1)	.20 (3)	.20 (2)	.20 (2)
	400-600	10243(.20)	.19 (2)	.19 (2)	.22 (4)	.18 (1)	.20 (3)
			1-12	1-10	1-10	1-7	1-7
			2-7	2-11	2-4	2-7	2-6
			3-2	3-0	3-4	3-5	3-6
			4-0	4-0	4-3	4-2	4-1
							5-1

Overall Standard Deviation (magnetically active)

(preliminary)

	Alt	Pts	MSIS-86	MSIS-83	MSIS-77	J77	J70
Jacchia drag	200-400	2464	.18 (1)	.19 (2)	.20 (3)	.21 (4)	.18 (1)
	400-800	4007	.29 (2)	.30 (3)	.31 (4)	.29 (2)	.28 (1)
	800-1200	2549	.29 (2)	.30 (3)	.33 (5)	.32 (4)	.23 (1)
Barlier drag	120-200	1050	.22 (2)	.22 (2)	.22 (2)	.23 (3)	.21 (1)
	200-400	2767	.20 (1)	.21 (2)	.22 (3)	.23 (4)	.21 (2)
	400-800	824	.30 (2)	.29 (1)	.32 (4)	.31 (3)	.30 (2)
AE-C MESA accel	120-200	12359(.25)	.16 (2)	.16 (2)	.15 (1)	.21 (4)	.18 (3)
	200-250	11585(.55)	.21 (2)	.21 (2)	.20 (1)	.23 (3)	.21 (2)
AE-C OSS ms	120-200	12370(.65)	.13 (2)	.13 (2)	.11 (1)	.16 (4)	.14 (3)
	200-390	6279(.2)	.15 (1)	.16 (2)	.17 (3)	.19 (4)	.16 (2)
AE-D MESA accel	120-200	8907(.7)	.15 (1)	.15 (1)	.15 (1)	.17 (2)	.15 (1)
	200-250	3723	.19 (1)	.19 (1)	.19 (1)	.20 (2)	.19 (1)
AE-D OSS ms	120-200	7608	.13 (1)	.13 (1)	.13 (1)	.15 (3)	.14 (2)
	200-390	7476(.75)	.22 (2)	.21 (1)	.21 (1)	.23 (3)	.21 (1)
AE-E MESA accel	120-200	8289(.45)	.13 (1)	.13 (1)	.13 (1)	.16 (3)	.15 (2)
	200-250	5582	.17 (1)	.18 (2)	.18 (2)	.20 (4)	.19 (3)
AE-E OSS ms	120-200	7868(.62)	.16 (2)	.15 (1)	.15 (1)	.19 (4)	.18 (3)
	200-400	7854(.12)	.19 (1)	.20 (2)	.22 (4)	.23 (5)	.21 (3)
AE-E NACE ms	120-200	6766	.13 (1)	.13 (1)	.17 (3)	.19 (4)	.16 (2)
	200-400	9079(.14)	.23 (2)	.22 (1)	.24 (3)	.23 (2)	.23 (2)
	400-600	7987(.20)	.23 (1)	.23 (1)	.27 (2)	.23 (1)	.23 (1)
			1-11	1-10	1-9	1-1	1-8
			2-10	2-9	2-3	2-4	2-8
			3-0	3-2	3-5	3-6	3-5
			4-0	4-0	4-3	4-9	4-0
					5-1	5-1	

Overall Standard Deviation (magnetically quiet)
MSIS selected temperature and composition data

	Alt	Pts	MSIS-86	MSIS-83	MSIS-77	J77	J70
Temperature	200-400	7608	92 (1)	99 (3)	97 (2)	102 (4)	110 (5)
	400-800	1363	96 (2)	106 (4)	95 (1)	102 (3)	122 (5)
He Density	120-200	804	.28 (1)	.29 (2)	.32 (3)	.47 (4)	.85 (5)
	200-400	7906	.27 (1)	.28 (2)	.36 (3)	.42 (4)	.87 (5)
	400-800	5344	.26 (1)	.27 (2)	.34 (3)	.40 (4)	.62 (5)
	800-999	313	.17 (1)	.19 (2)	.39 (4)	.44 (5)	.37 (3)
O + O2 Density	120-200	854	.16 (1)	.17 (2)	.18 (3)	.23 (4)	.23 (4)
	200-400	8067	.21 (1)	.22 (2)	.25 (4)	.24 (3)	.27 (5)
	400-800	4864	.29 (1)	.29 (1)	.31 (3)	.30 (2)	.30 (2)
N2 Density	120-200	929	.16 (1)	.16 (1)	.19 (2)	.21 (4)	.20 (3)
	200-400	8247	.37 (1)	.40 (2)	.40 (2)	.47 (3)	.55 (4)
	400-800	3910	.43 (1)	.44 (2)	.50 (3)	.51 (4)	.76 (5)
Ar Density	120-200	867	.34 (1)	.36 (2)	.41 (4)	.39 (3)	.44 (5)
	200-400	3178	.47 (1)	.52 (2)	.62 (4)	.58 (4)	.80 (5)
			1-13	1-2	1-1	1-0	1-0
			2-1	2-10	2-3	2-1	2-1
			3-0	3-1	3-6	3-4	3-2
			4-0	4-1	4-4	4-8	4-2
						5-1	5-9

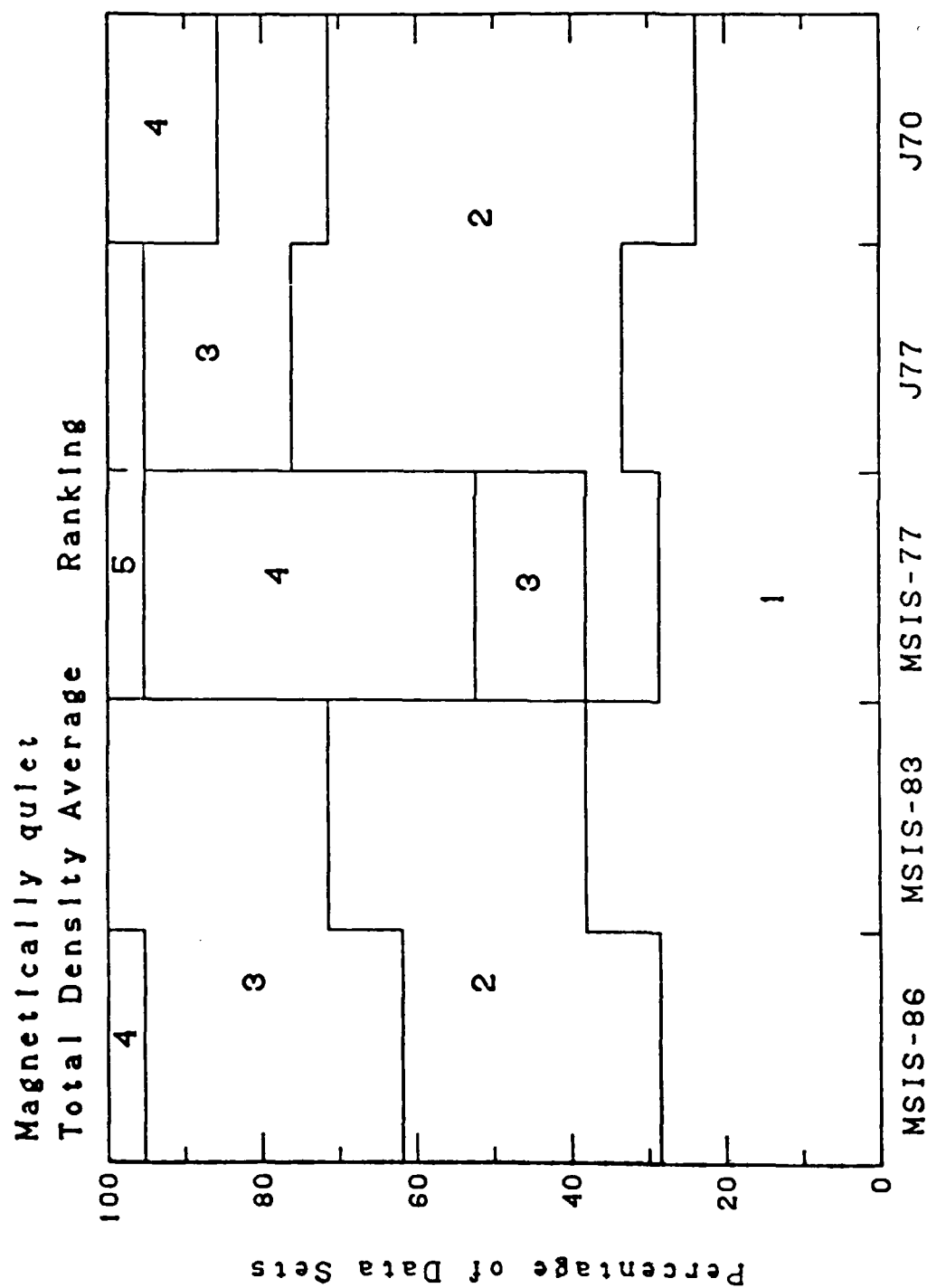
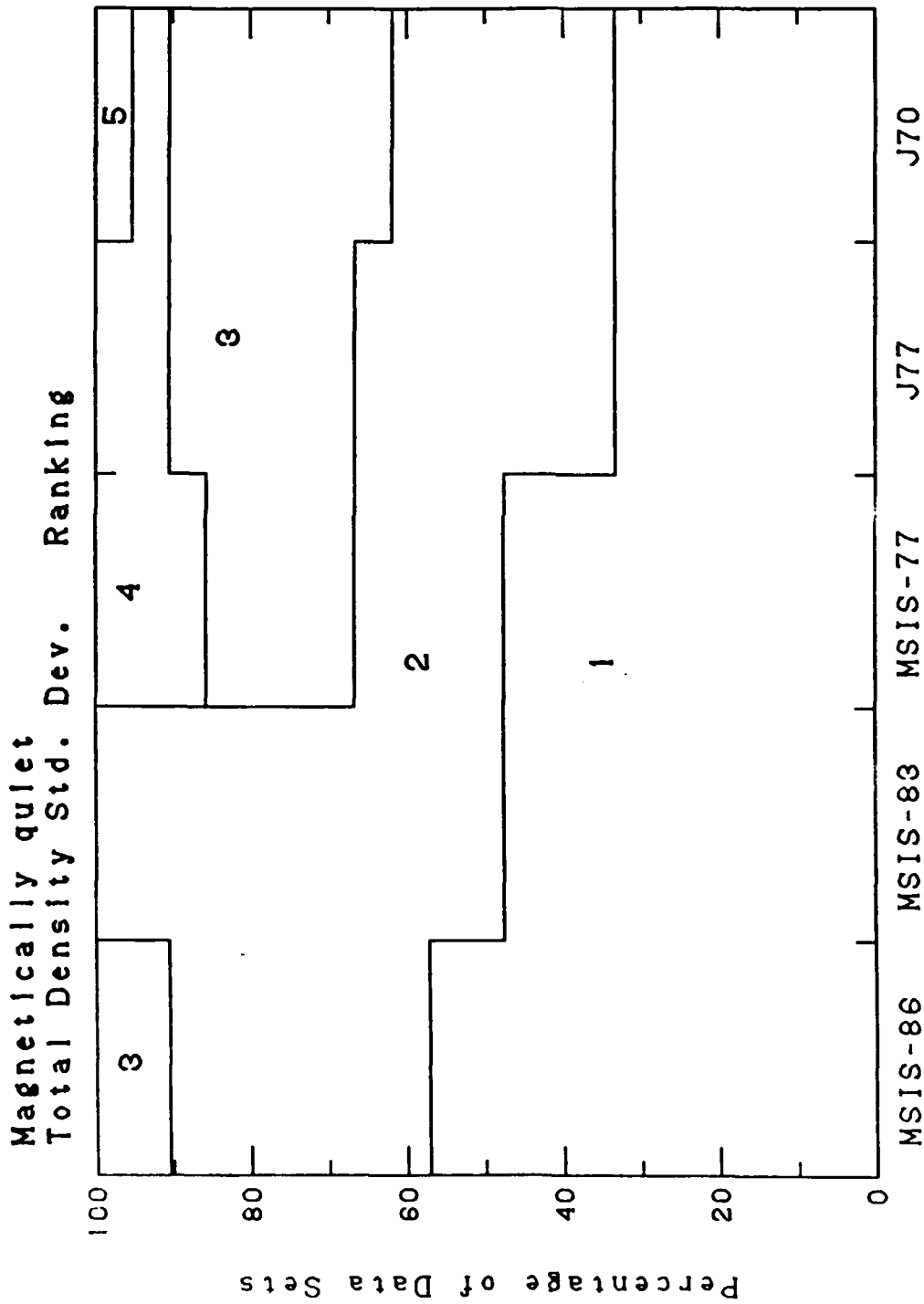
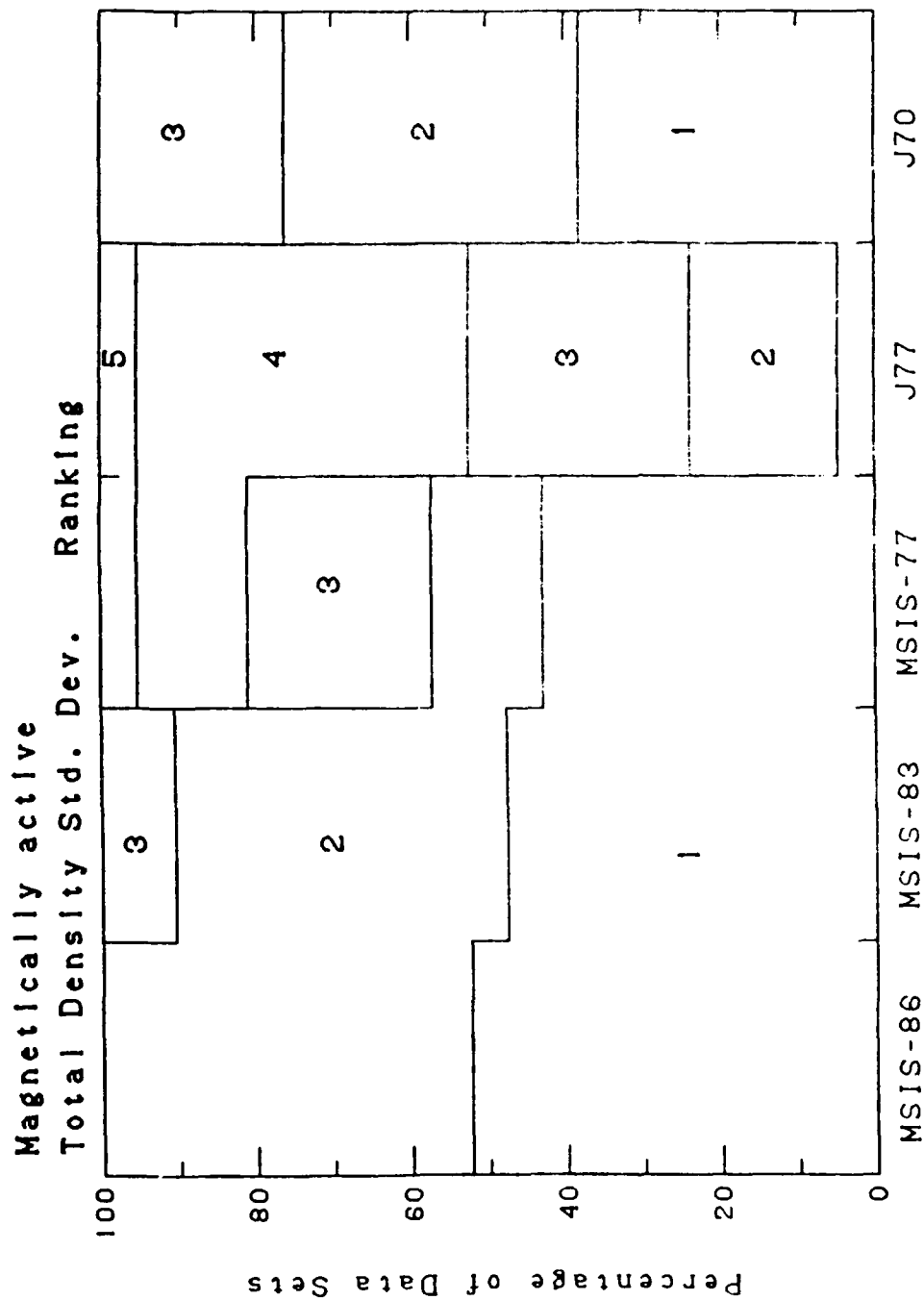


Fig. 1





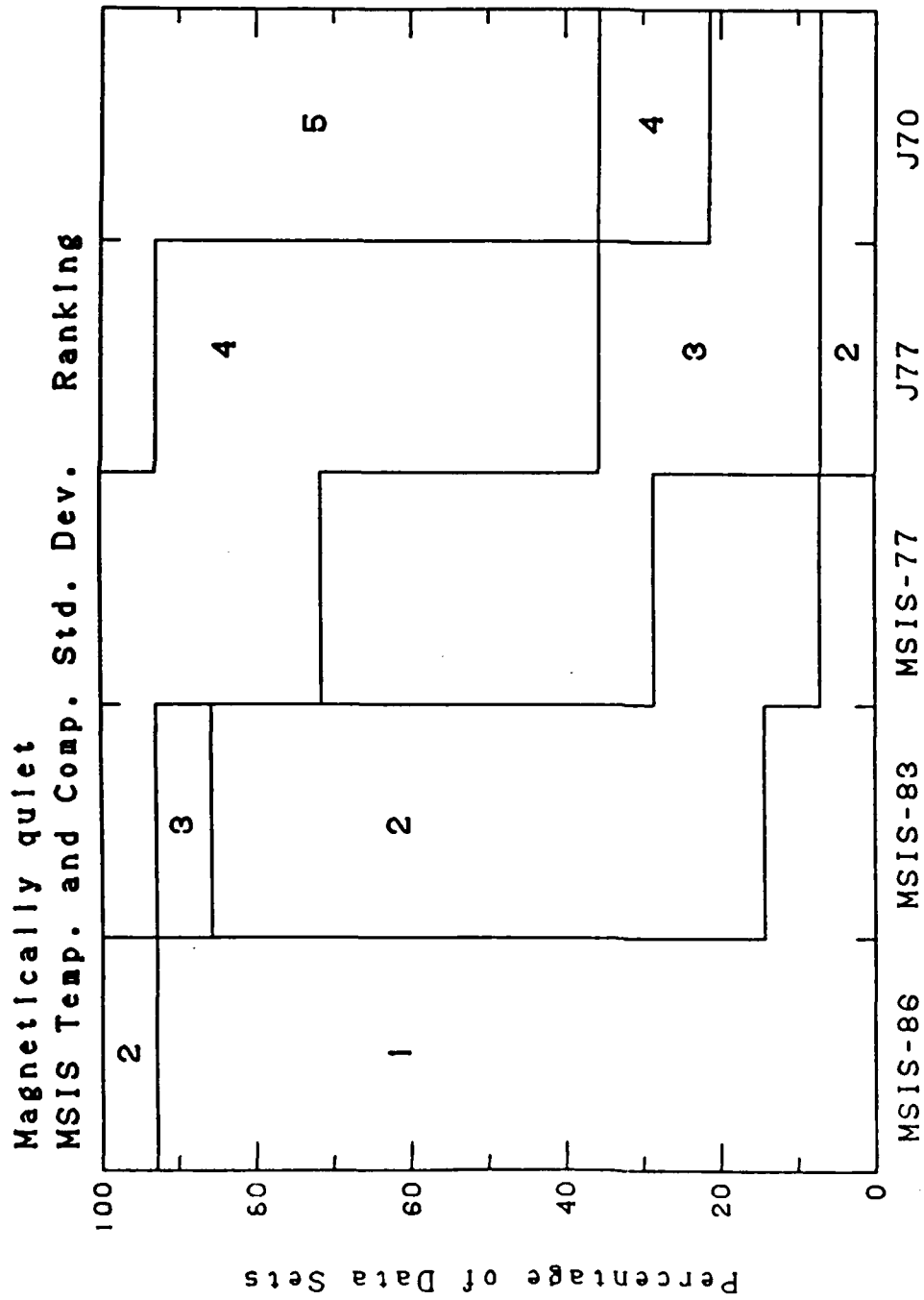
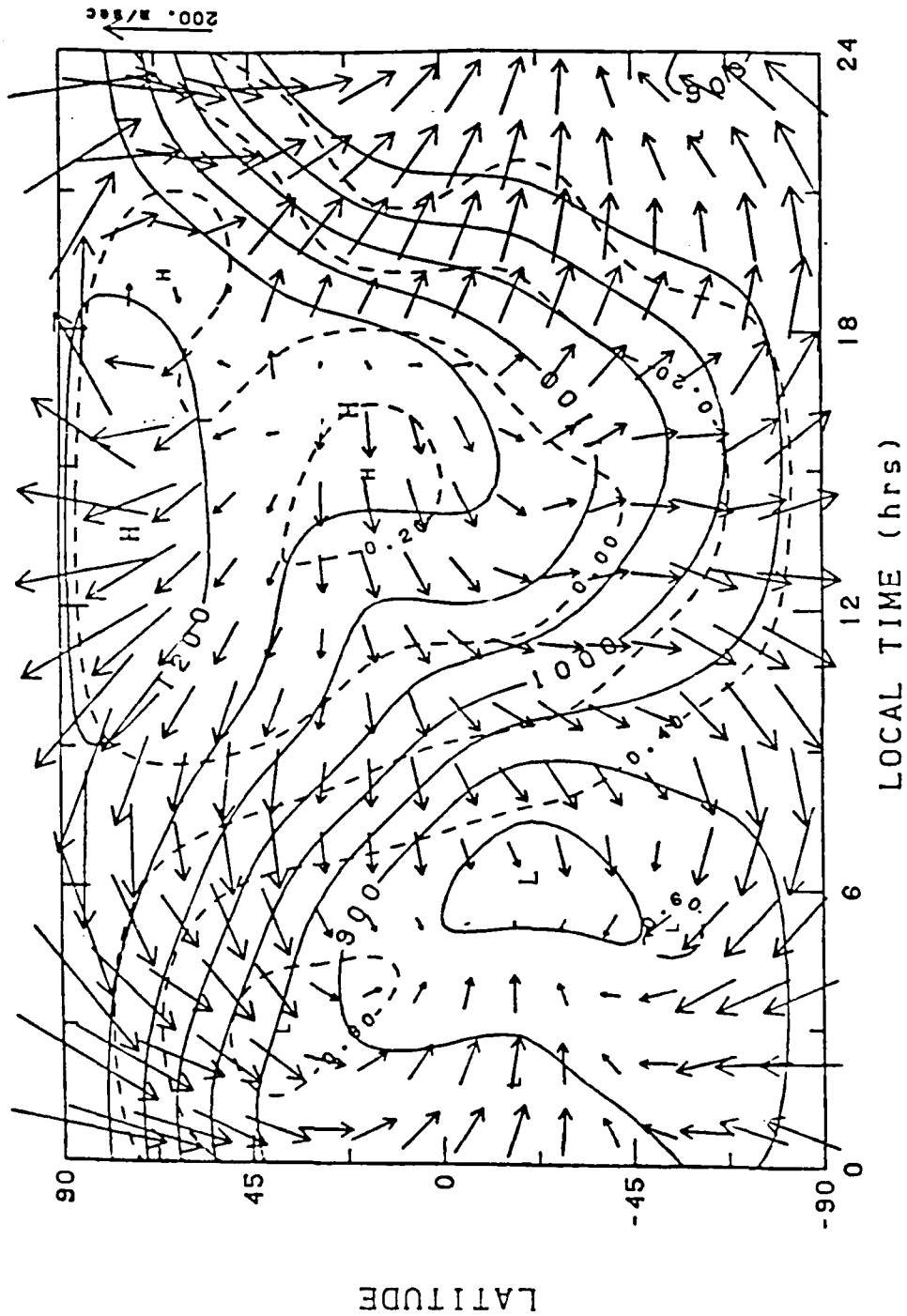


Fig. 4

MSIS-86 Temp. and Press. HWM87 Wind
 June Solstice Ap = 4 300 km



Measurements of Atmospheric Structure

by

Jeng-Hwa Yee

Paul B. Hays

V. J. Abreu

W. R. Skinner

C. R. Cornish

M. C. Luo

The University of Michigan
Space Physics Research Laboratory

Measurements of Atmospheric Structure (Density, Temperature or Pressure)

Prior To 1945 -- Ground-Based

Meteor Trails (as early as 1923)

*used a large number of visual observations of meteor trails from their appearance and disappearance, to determine densities at various heights ranging between 30 and 150 km.

*Lindemann and Dobson (1923)

"The density above 60 km appears to be much larger thanto an isothermal atmosphere at 200K, and the temperature appears to be at 300K. A tentative explanation is based on the radiative properties of ozone".

Between 1945 and 1965 - Rocket

*Rocket measurements began in 1947 when the first V2 rocket was launched.

*From the beginning of IGY, July 1957 thru March 1958, 41 rockets were launched and 27 of them were instrumented for the measurements of the atmospheric structure. All these 27 rockets were instrumented by either Naval Research Laboratory (NRL), or the University of Michigan in cooperation with the Air Force Cambridge Research Center (currently AFGL) and the U.S. Army Research and Development Laboratories.

- Three techniques were employed

- (1) Grenade Experiment
- (2) Falling Sphere Experiment
- (3) Pitot Technique

Rocket Grenade Experiment

- the experiment was first performed by scientists in in Meteorological Branch of the U.S. Army in 1945. Later it was re-designed and 16 of them were fired at White Sands between March 1950 and Sept. 1953. 12 of them were successful.
- used series of of grenade explosions at a constant altitude interval of 4-5 km and derive average wind and temperature in each layer from the speed of sound measured between two explosions.
- Altitude region: Mesosphere and upper Stratosphere.
- Parameter measured : Speed of sound
Parameters derived (primary) : Wind and Temperature
(secondary): Density and Pressure
- Density and pressure were derived from the hydrostatic equation with the aids of balloon radiosonde at the lower boundary.

Falling Sphere Experiment

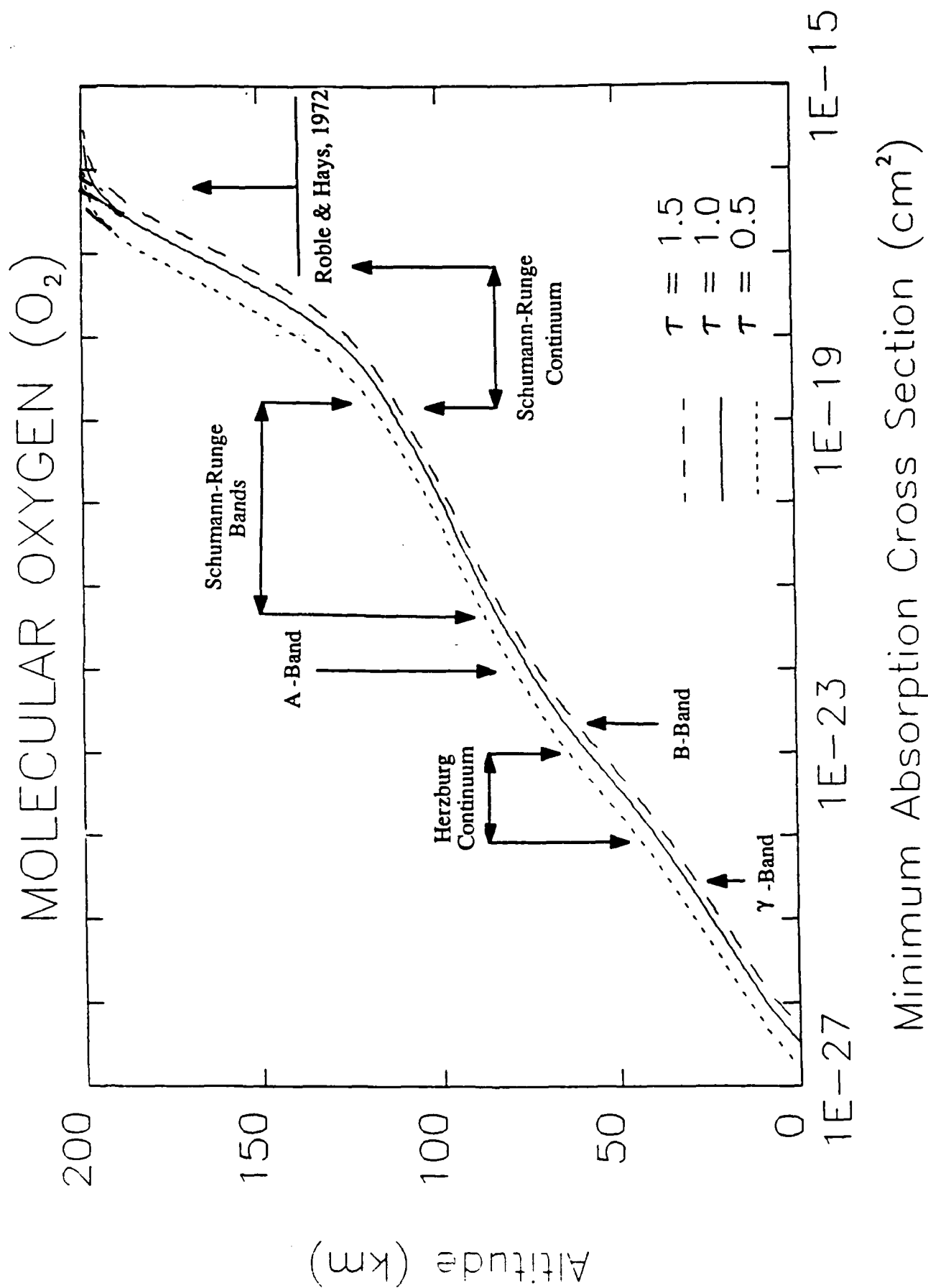
- the technique was developed at the University of Michigan and total of 12 successful measurements have been made.
- uses the drag acceleration of a falling sphere ejected from a rocket.
- Altitude region: Mesosphere and upper Stratosphere.
- Parameter measured : Sphere Drag
- Parameters derived (primary) : Density
(secondary): Pressure, Temperature

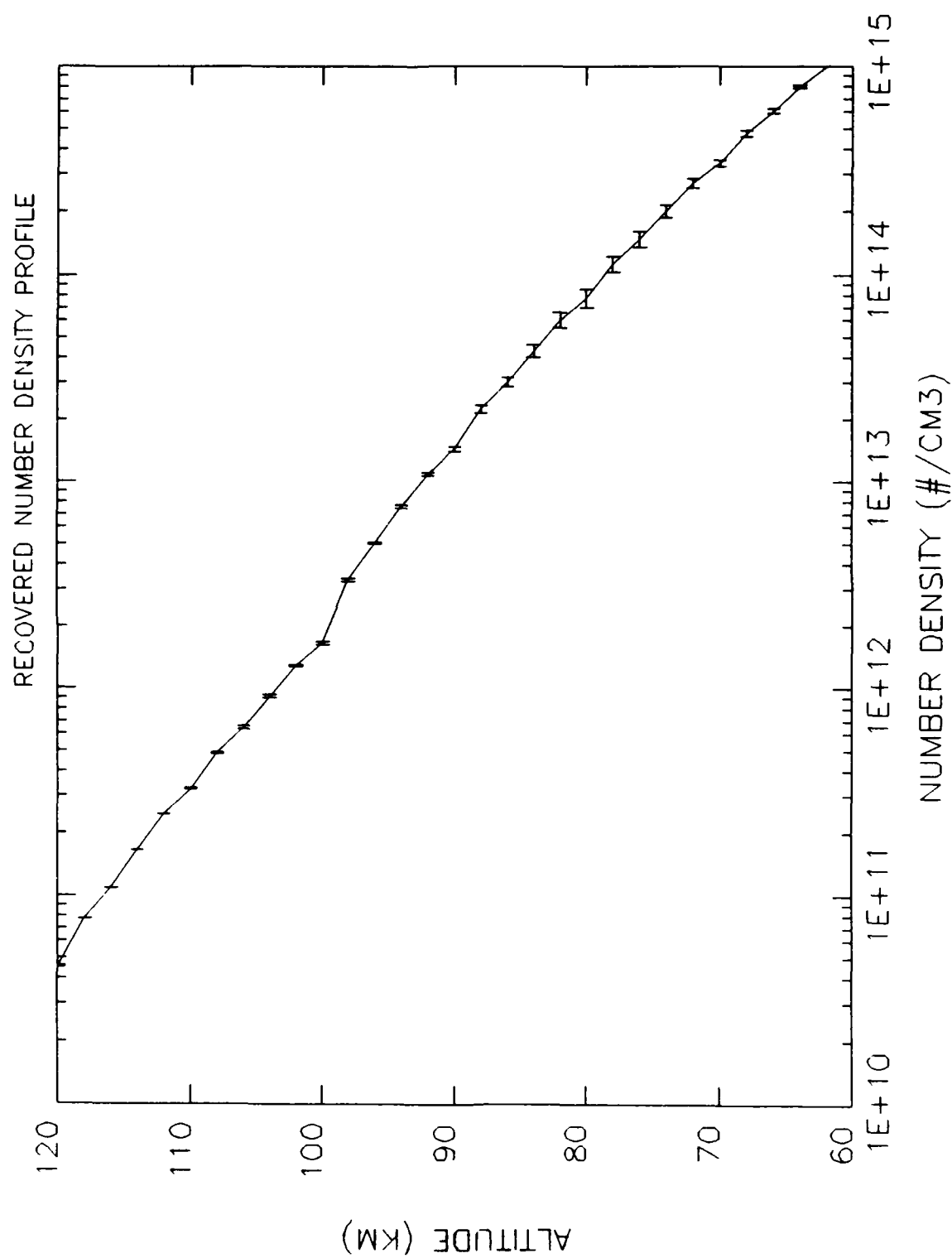
Pitot Technique

- Many of the data were obtained by the Naval Research Laboratory. In their experiments, pressure were measured at a special location on the rocket where wind-tunnel experiments have shown the pressure to be equal to the ambient pressure within a few percent.
- Later, firings by the University of Michigan under the support of the Air Force, measured pressures at the tip or several locations on the conical nose and derived ambient density and pressure from aerodynamic theory.
- Altitude region: Mesosphere and upper Stratosphere.
- Parameter measured : Impact pressure
Parameters derived (primary) : Density and Pressure
(secondary): Temperature

After 1965 to Present - Satellite

- Satellite Drag
- In-Situ Mass Spectrometer Measurements
 - * OGO
 - * AE-C,D and E
 - * DE
- Remote Sensing (currently being developed at the University of Michigan sponsored by the Air Force Geophysics Laboratory)
 - (1) Rayleigh Scattering
 - (2) Stellar Occultation
 - (3) Resonance Scattering of O₂

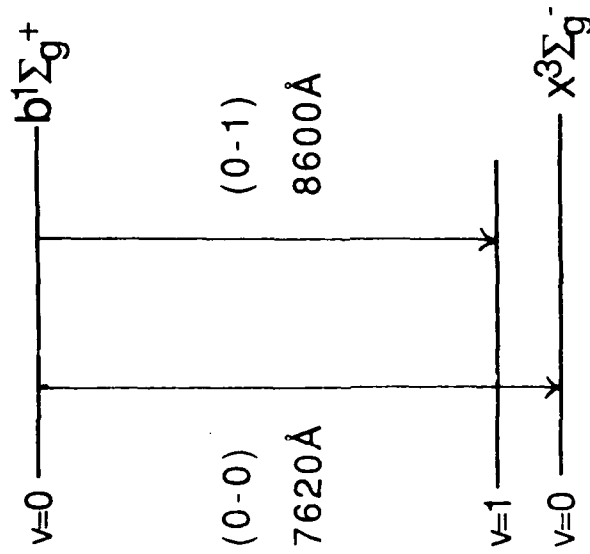




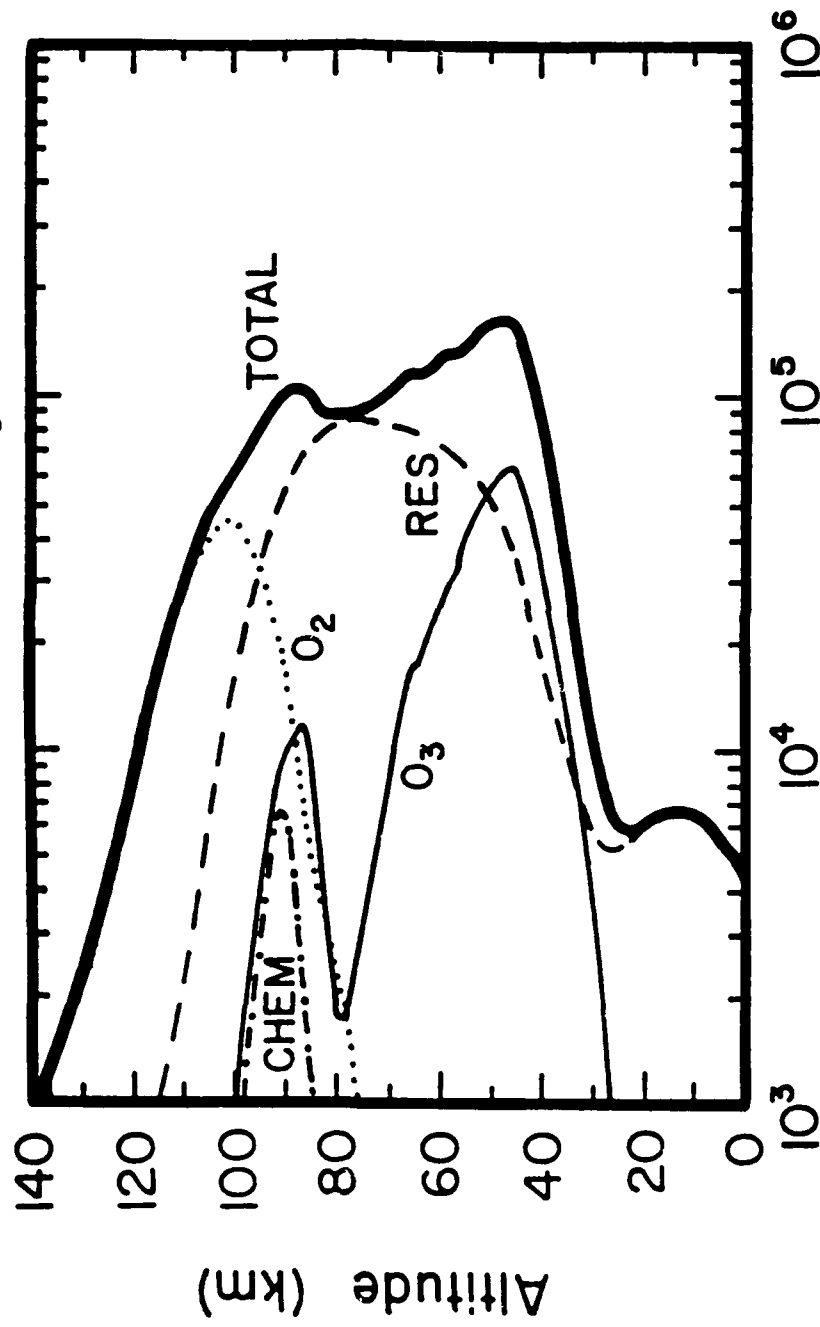
O₂ Atmospheric Band

Note:

1. The emission rates of (0-0) and (0-1) bands are related by the Frank-Condon Factor.
2. Due to frequent collisions and long lifetime, the O₂(b¹Σ_g⁺) are in rotational thermal equilibrium, i.e.
rotational Temp. = Ambient Temp.
3. (0-0) band emission can not be observed at the ground due to self-absorption. The degree of absorption, optical depth, is a function of O₂ column density and the atmospheric temperature.



VOLUME EMISSION RATES OF O_2 ($b^1\Sigma_g^+$)



Volume Emission Rate ($cm^{-3} sec^{-1}$)

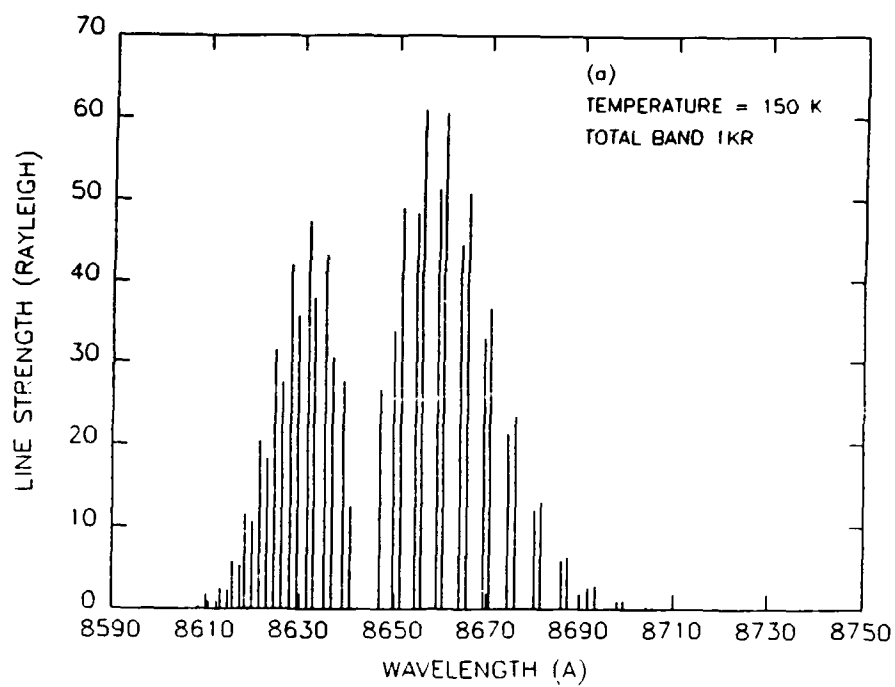


Fig.5 (a)

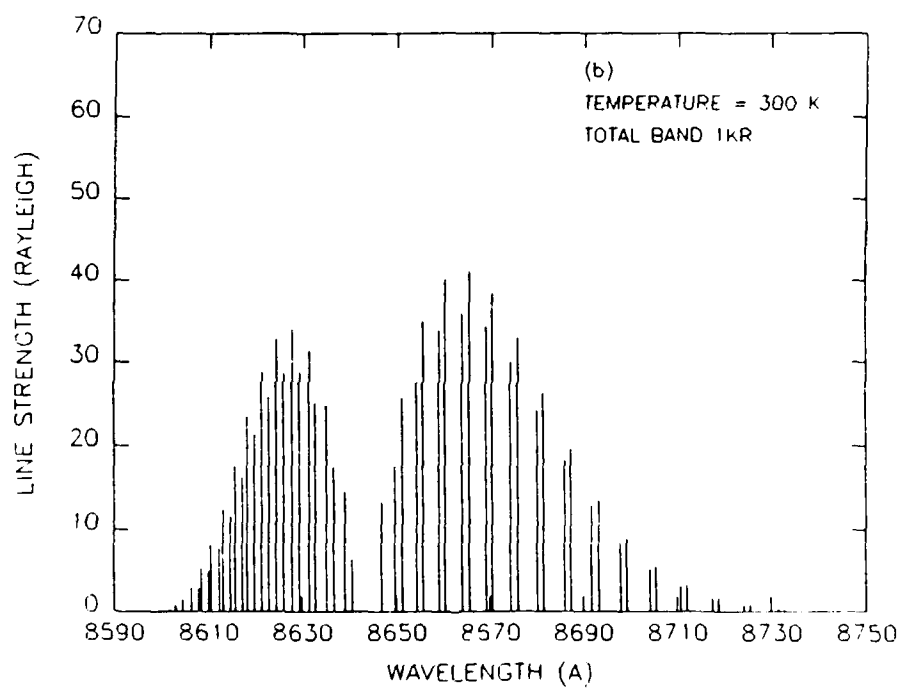
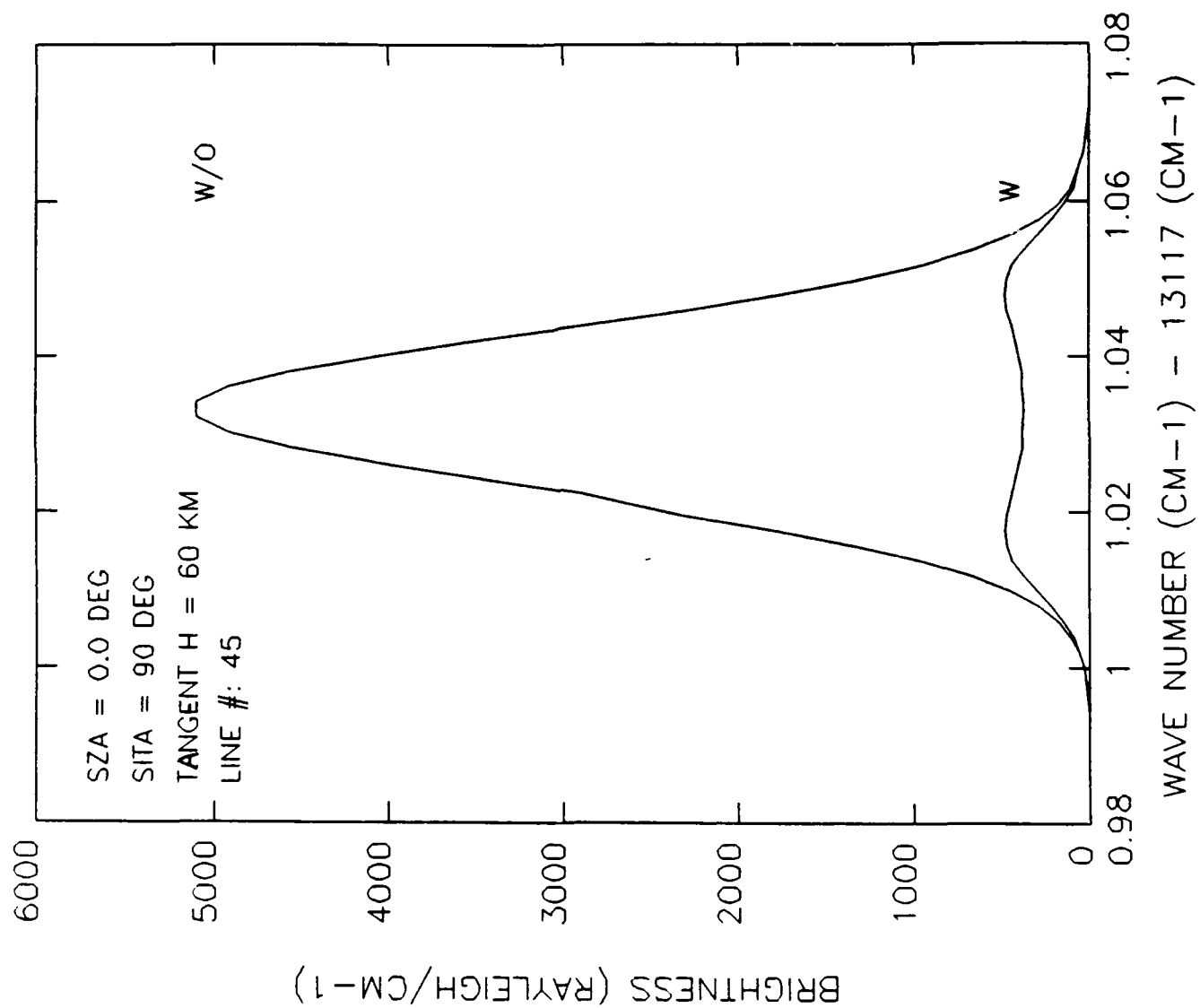
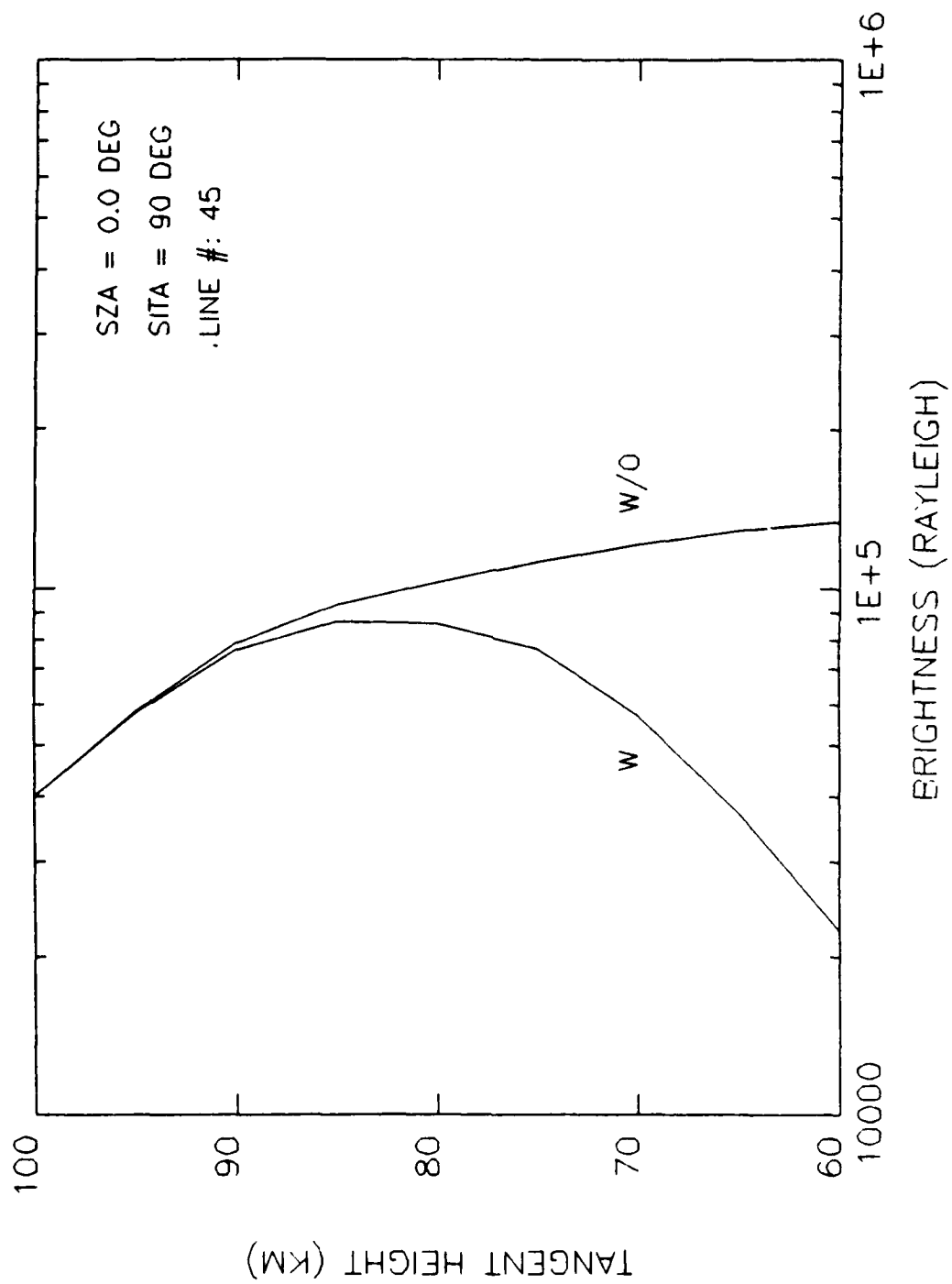
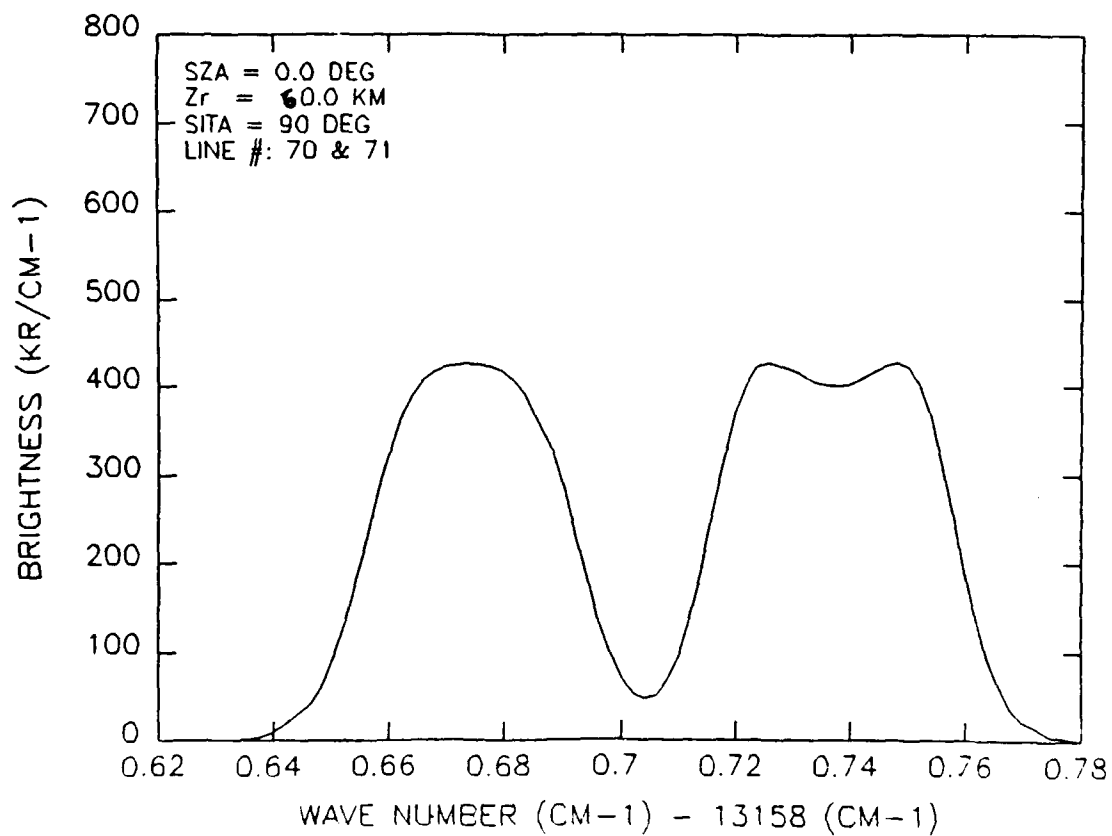
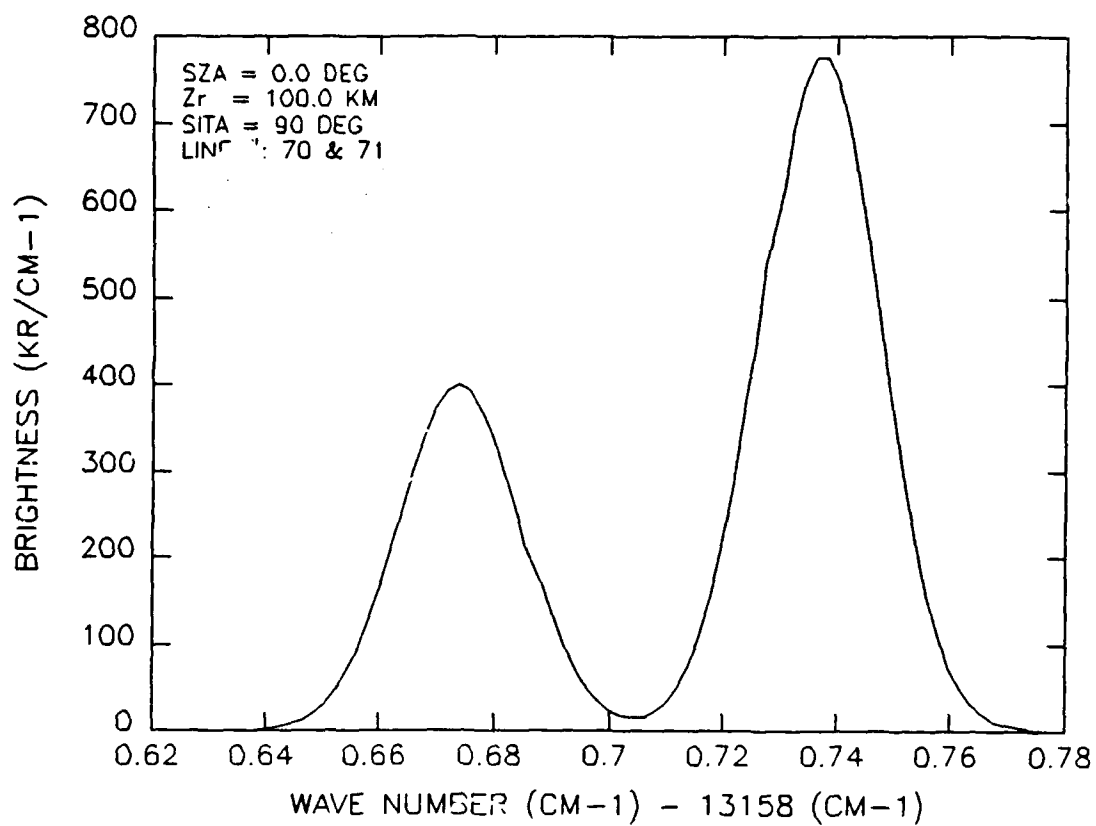
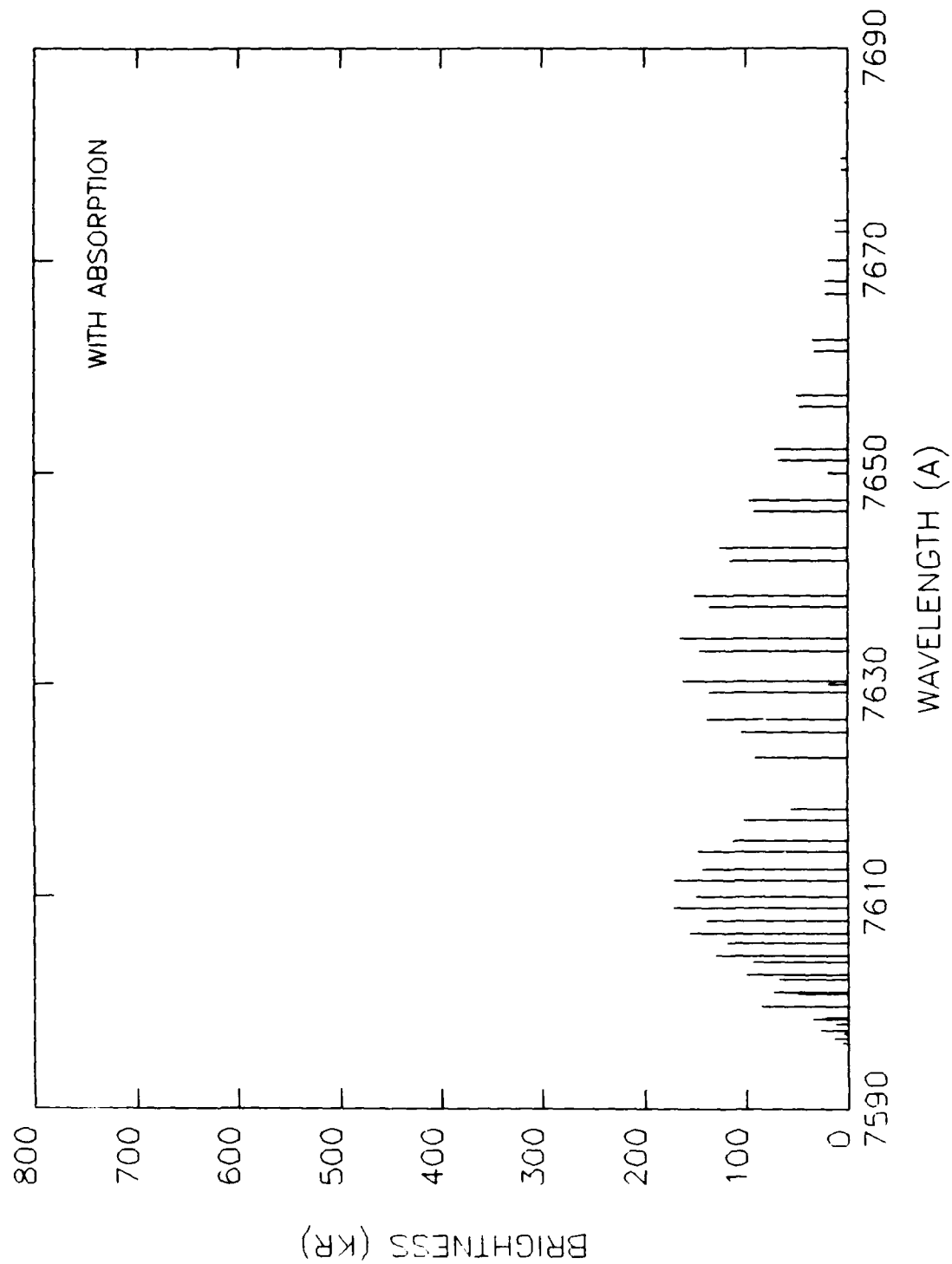


Fig.5 (b)









Measurements of Atmospheric Structure using O₂ Atmospheric Band

- Step 1: measure emission spectra of O₂(0-1) band
- Step 2: invert the measured spectra to obtain altitude profile of (0-1) band volume emission rate spectra
- Step 3: perform least-square-fit to the (0-1) band volume emission rate spectra to obtain the volume emission rate profile and emission temperature (=ambient temperature)
- Step 4: compute (0-0) volume emission rate profile by multiplying (0-1) profile by the Frank-Condon Factor
- Step 5: perform least-square-fit to the observed (0-0) spectra to obtain number density profile of O₂

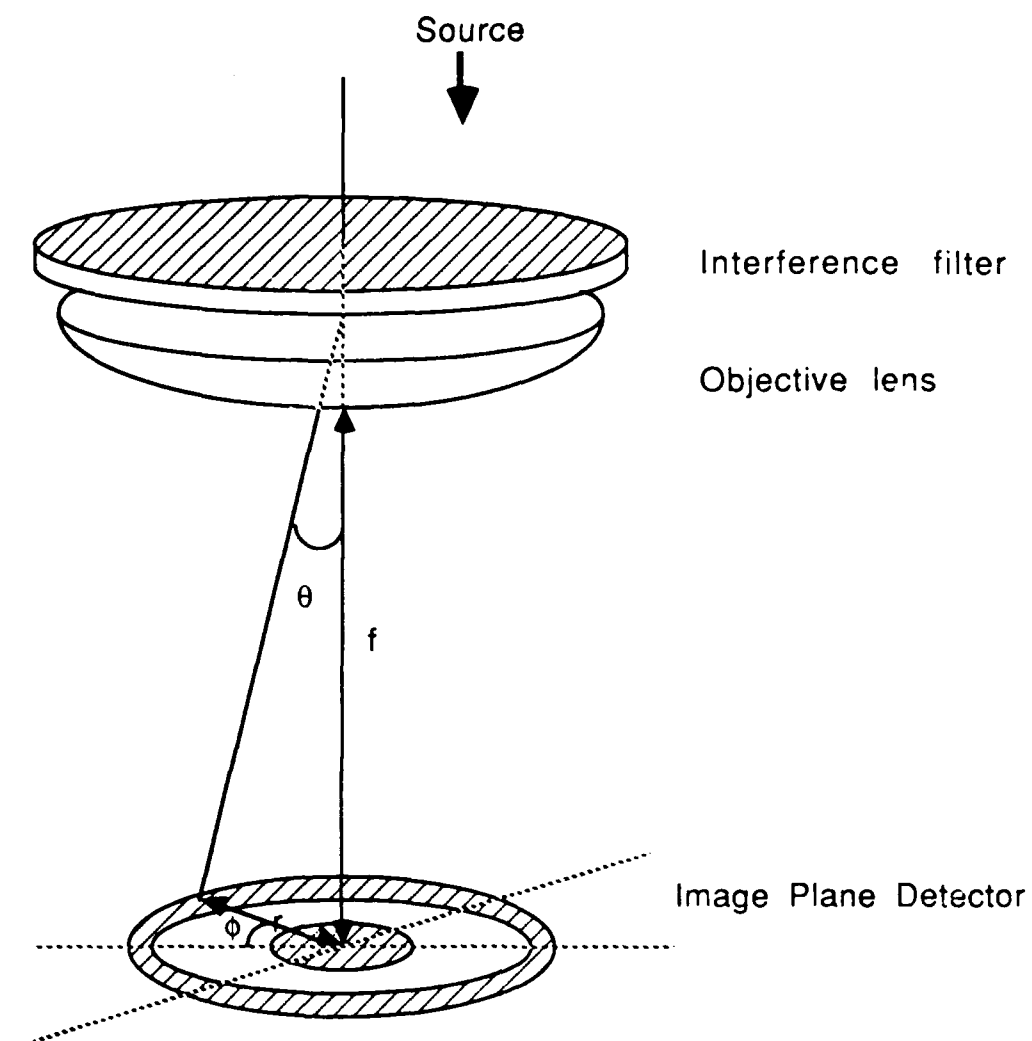
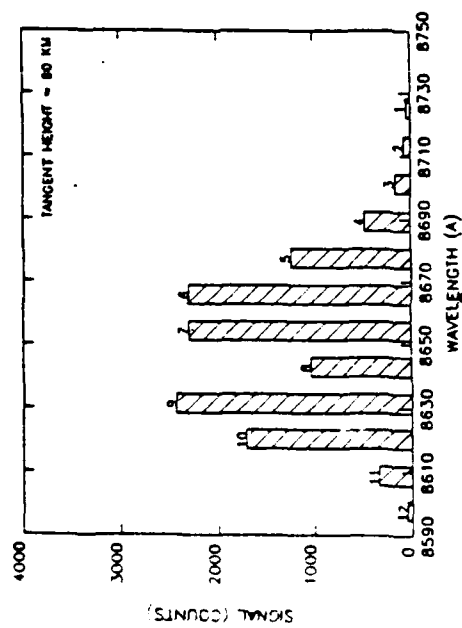
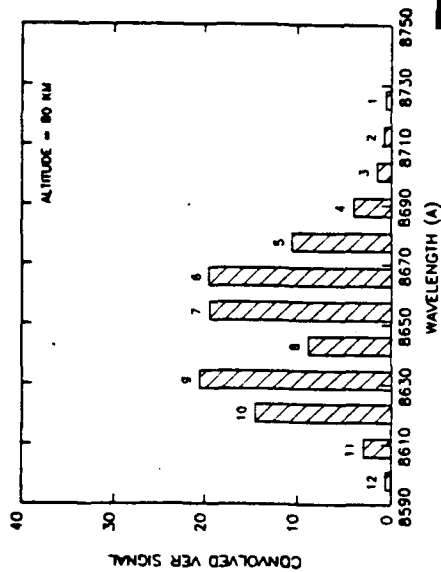


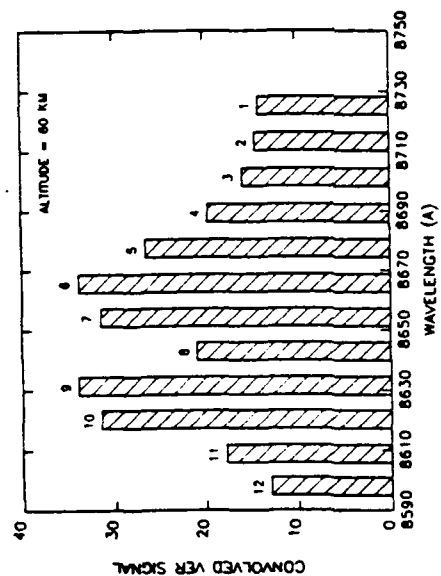
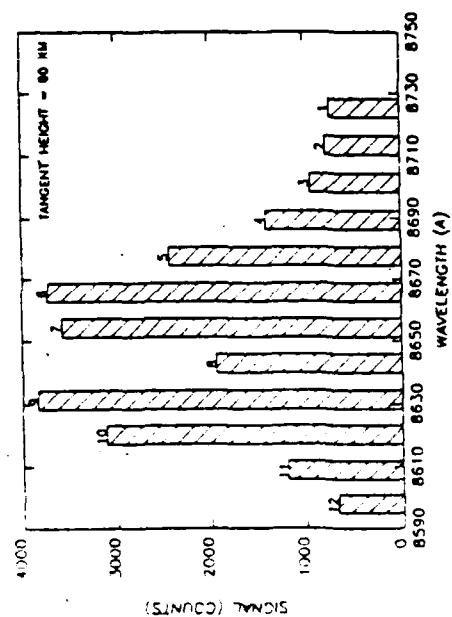
Fig. 1



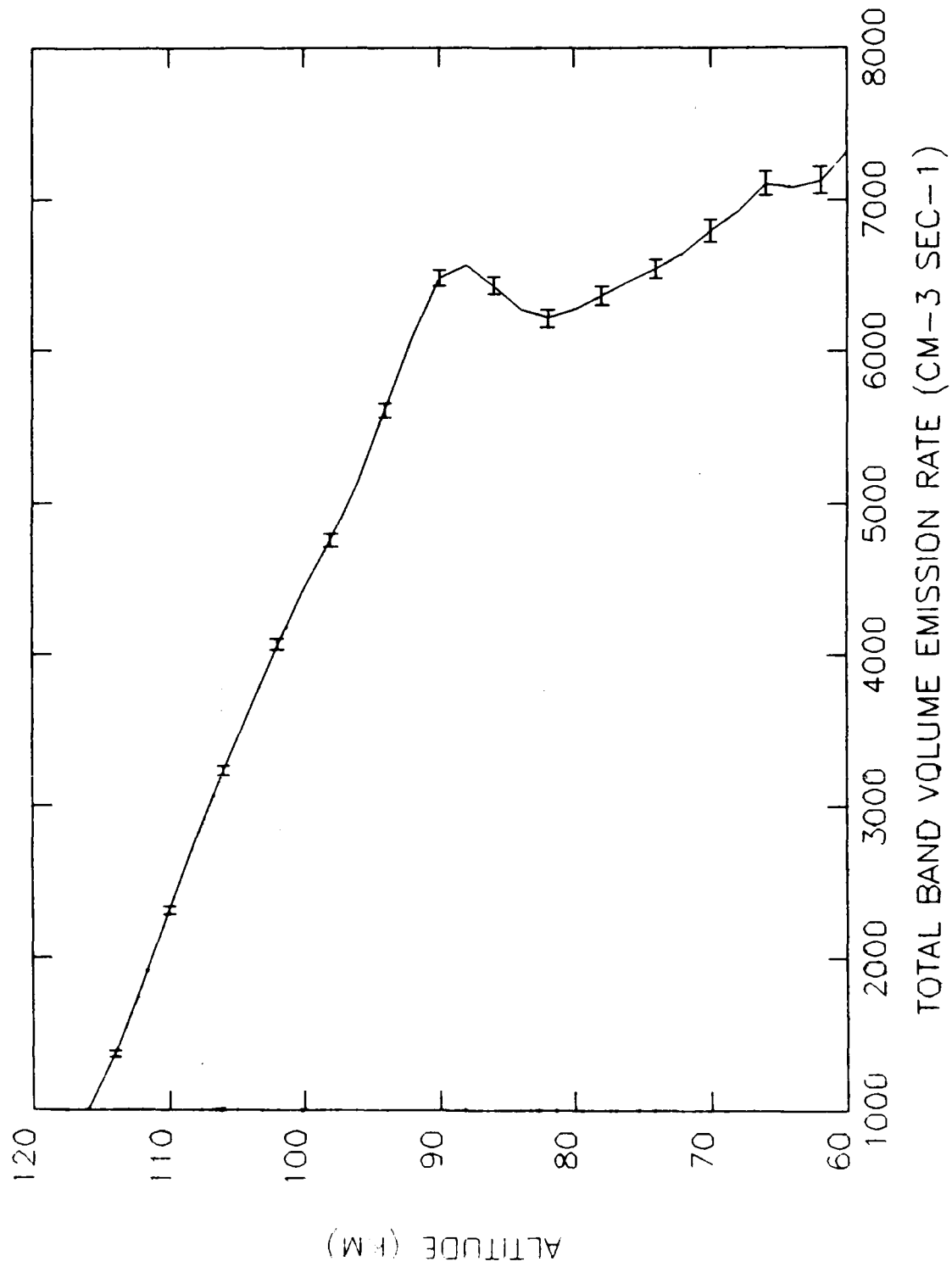
Inversion



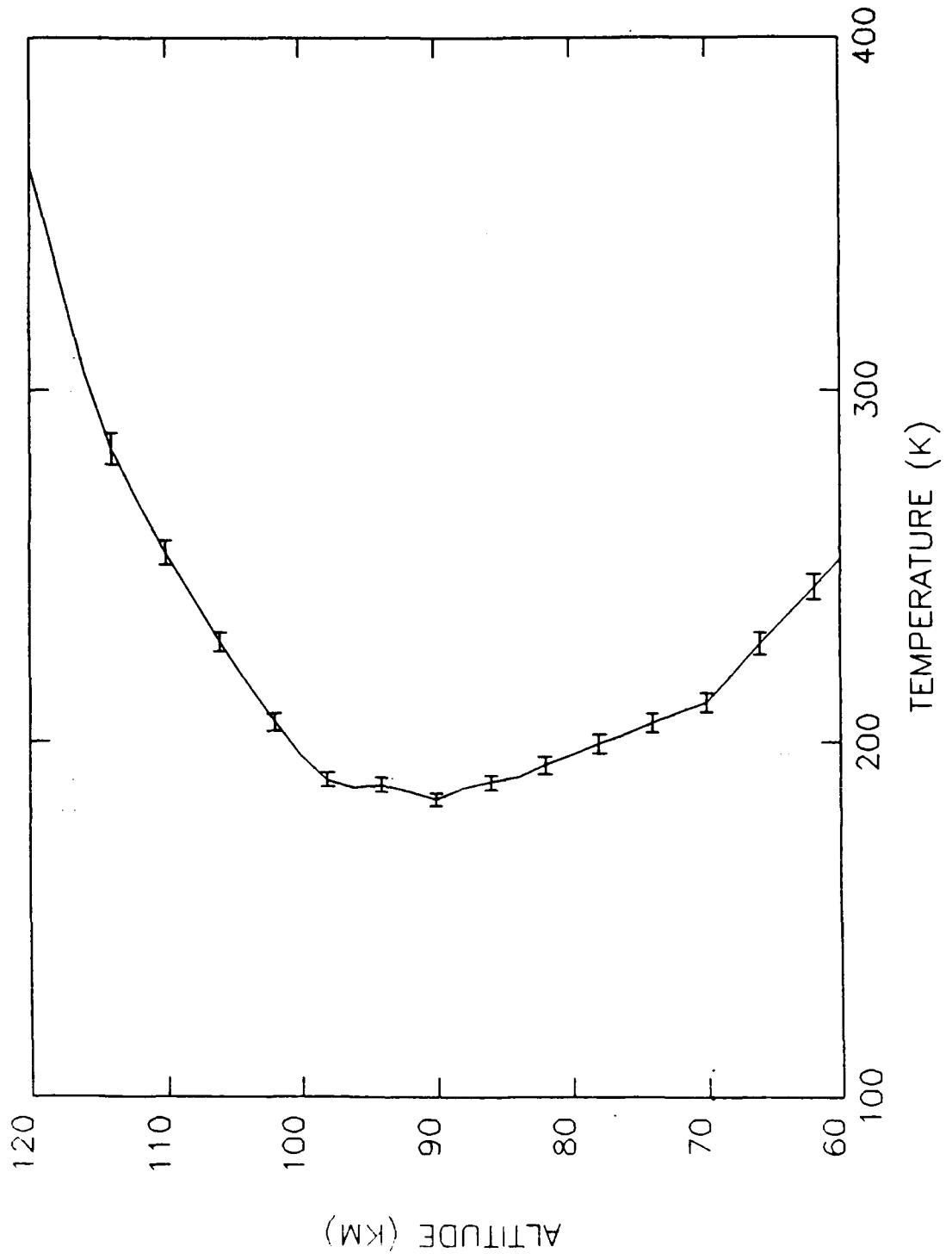
T, η

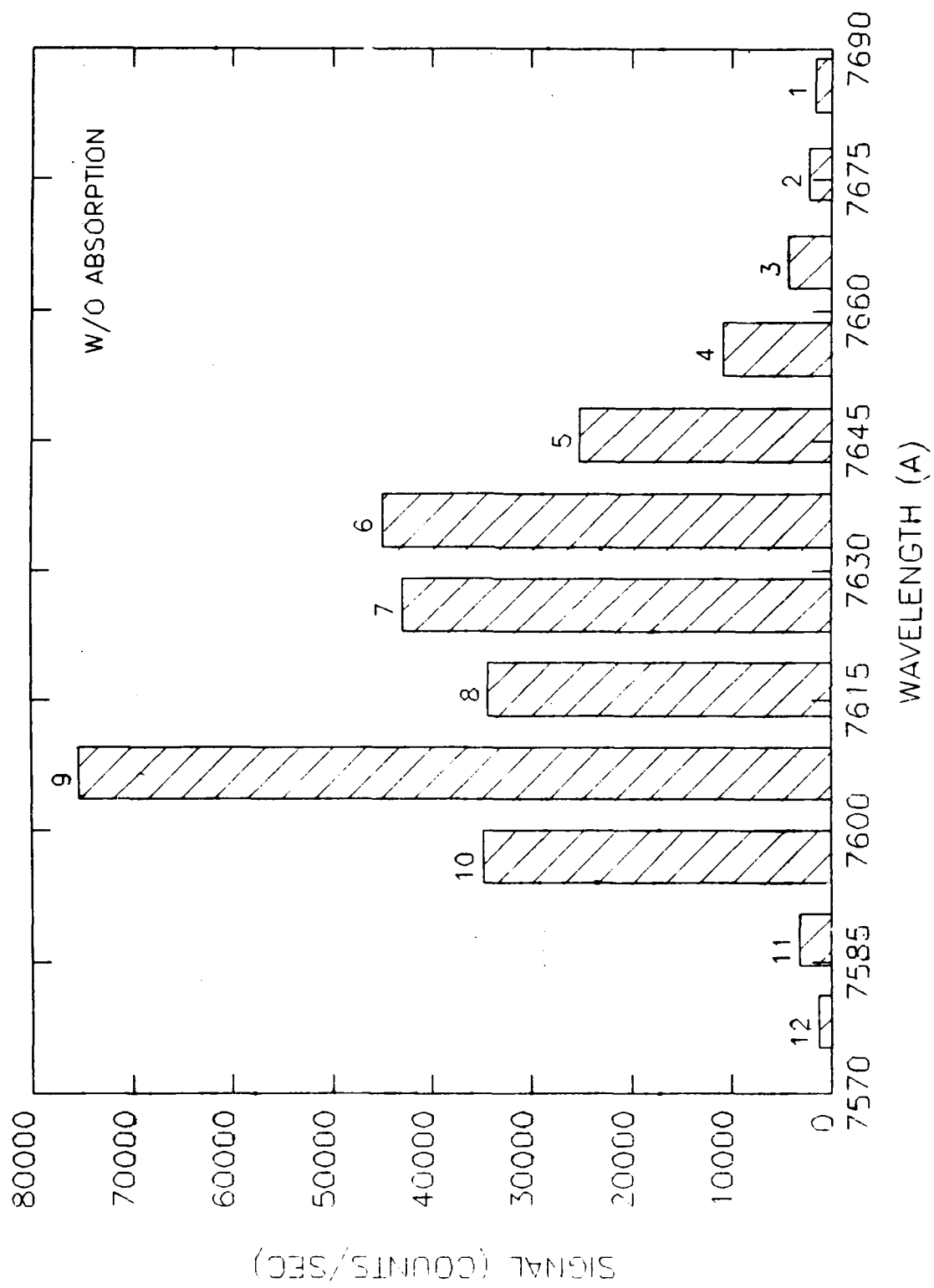


Recovered (0-1) Volume Emission Rate Profile



Recovered Temperature Profile





SUMMARY

1. Scientists have been probing the atmospheric structure for over 4 decades now. Our understanding to the regions between 60 and 120 km, however, has been mostly based upon measurements of several hundred limited rocket launches.
2. The feasibility of recovering the atmospheric structure has been demonstrated here by using one of several possible remote sensing techniques. The accuracy of the recovered atmospheric parameters depends on the design and the sensitivity of the instrument.
3. The ability to model the atmosphere in this region requires ample data which cover all geographic locations, local times, and variations in magnetic activity and solar condition. This global data set can only be provided by a space-borne instrument using remote sensing techniques.

A Coupled Thermosphere/Ionosphere General Circulation Model

R. G. Roble, E. C. Ridley, A. D. Richmond
High Altitude Observatory

and

R. E. Dickinson
Climate and Global Dynamics Division

National Center for Atmospheric Research*
P.O. Box 3000
Boulder, CO 80307

to be submitted to *Geophys. Res. Lett.*

April 1988

* The National Center for Atmospheric Research is sponsored by the National Science Foundation.

Abstract. The NCAR thermospheric general circulation model (TGCM) is extended to include a self-consistent aeronomic scheme of the thermosphere and ionosphere. The model now calculates total temperature, instead of perturbation temperature about some specified global mean, global distributions of $N(^2D)$, $N(^4S)$ and NO , and a global ionosphere with distributions of O^+ , NO^+ , O_2^+ , N_2^+ , N^+ electron density and ion temperature as well as the usual fields of winds, temperature and major composition. Mutual couplings between the thermospheric neutral gas and ionospheric plasma occur at each model time step. This is the first Eulerian model of the ionosphere and it is solved on the TGCM geographic grid. Steady state results for solar minimum equinox conditions are presented.

Introduction

The development of global numerical models of the thermosphere (Fuller-Rowell and Rees, 1980; Dickinson *et al.*, 1981) and global numerical models of the ionosphere (Sojka and Schunk, 1985) have proceeded generally independently of each other. Global empirical models of the ionosphere (e.g., Chiu, 1975) were used to specify ion drag in thermospheric general circulation models and global empirical atmospheric models, such as the mass spectrometer/incoherent scatter models (e.g., Hedin, 1987), were used to specify atmospheric properties for ionospheric models. Recently, Fuller-Rowell *et al.* (1987) constructed a coupled model of the polar ionosphere and the global thermosphere to study the dynamical and chemical interactions between the neutral and ionospheric constituents of the polar regions. They adapted the Lagrangian ionospheric model of Quegan *et al.* (1982) to the Eulerian thermospheric model of Fuller-Rowell and Rees (1980) using an interpolative scheme at each model time step. Their calculation was successful in reproducing a number of observed features in the high latitude thermosphere and

ionosphere.

In this paper, we present a self-consistent coupled Eulerian model of the thermosphere and ionosphere using an extension of the aeronomic scheme developed by Roble *et al.* (1987) and Roble and Ridley (1987). The ionosphere and thermosphere are both solved on the TGCM geographic grid and includes consideration of displaced geomagnetic and geographic poles. Ion drift for the ionospheric calculation is obtained from the empirical model of Richmond *et al.* (1980) for low- and mid-latitudes and the empirical model of Heelis *et al.* (1982) for high latitudes. Results for solar minimum equinox conditions are presented that show good agreement with MSIS-86 (Hedin, 1987). The self-consistent model requires only specifications of external sources as solar EUV and UV fluxes, aurora particle precipitation, ionospheric convection pattern, and the amplitudes and phases of semi-diurnal tides from the lower atmosphere.

TGCM Modifications

The NCAR-TGCM solves the primitive equations of dynamic meteorology adapted to the physics appropriate to thermospheric heights. The basic model and developments have been described in detail by Dickinson *et al.* (1981; 1984), Roble *et al.* (1982), Fesen *et al.* (1986) and Roble and Ridley (1987). The TGCM has been used for numerous studies involving ground-based and satellite measurements. All of these studies were performed with a TGCM that solved for perturbation temperatures about a global mean temperature profile that was obtained from an empirical model such as MSIS (Dickinson *et al.*, 1981). The previous procedure had been adopted because physical processes, such as non-local thermodynamic equilibrium (NLTE) cooling emissions from CO_2 and NO , and cooling by eddy transport, were not well known at the time of initial TGCM development. But recently, Roble *et al.* (1987) designed a self-consistent global mean

model of the basic structure of the thermosphere and ionosphere which were successful in calculating various thermospheric and ionospheric properties for both solar minimum and maximum conditions. The major heating and cooling processes that appear to be responsible for maintaining the global mean structure were identified and sufficient confidence in the aeronomic scheme and adapted rate coefficients was developed to warrant inclusion in a new version of the TGCM.

The thermodynamic equation in the original NCAR-TGCM (equation (1) of Dickinson *et al.*, 1981) is modified to calculate total temperature,

$$\begin{aligned} \frac{\partial T}{\partial t} = & \frac{g e^Z}{P_o C_p} \frac{\partial}{\partial Z} \left\{ \frac{K_T}{H} \frac{\partial T}{\partial Z} + K_E H^2 C_p \rho \left(\frac{g}{C_p} + \frac{1}{H} \frac{\partial T}{\partial Z} \right) \right\} \\ & - \underline{V} \cdot \nabla T - \omega \left(\frac{\partial T}{\partial Z} + \frac{RT}{C_p \bar{m}} \right) + (Q - L)/C_p \end{aligned} \quad (1)$$

where T is temperature, t is time, g gravitational acceleration, C_p is specific heat per unit mass, Z is our vertical coordinate defined as $Z = \ln P_o / P$, where P is pressure and P_o is a reference pressure ($5 \times 10^{-4} \mu b$), K_T is molecular thermal conductivity, H is the scale height, K_E is the eddy thermal conductivity, ρ is total density, \underline{V} is the horizontal velocity vector, ω is TGCM "vertical velocity," $\omega = dZ/dt$, R is the universal gas constant, \bar{m} is the mean mass and Q and L are heating and cooling rates, respectively. The eddy diffusion coefficient that is used for these calculations is (Dickinson *et al.*, 1984) $K_E(Z) = 5 \times 10^{-6} \exp(-7.1 Z) s^{-1}$. The eddy diffusion coefficient, multiplied by scale height squared to be in dimensional units, has a maximum value of $160 m^2 s^{-1}$ at the lower boundary (97 km). The various heating and cooling rates calculated by the TGCM are described by Roble *et al.* (1987).

The TGCM also has been modified to include minor species transport by solving addi-

tional composition equations of the form:

$$\begin{aligned} \frac{\partial \psi_n}{\partial t} = & -e^{-Z} \frac{\partial}{\partial Z} A_n \left[\frac{\partial}{\partial Z} - E_n \right] \psi_n + S_n - R_n \\ & - \left(\underline{V} \cdot \nabla \psi_n + \omega \frac{\partial \psi_n}{\partial Z} \right) + e^Z \frac{\partial}{\partial Z} e^{-Z} K_E(Z) \left(\frac{\partial}{\partial Z} + \frac{1}{\bar{m}} \frac{\partial \bar{m}}{\partial Z} \right) \psi_n \end{aligned} \quad (2)$$

$$\text{where } E_n = \left[1 - \frac{m_n}{\bar{m}} - \frac{1}{\bar{m}} \frac{\partial \bar{m}}{\partial Z} \right] - \alpha_n \frac{1}{T} \frac{\partial T}{\partial Z} + \underline{F} \Psi_n$$

The first three terms in E_n represent gravitational force, thermal diffusion and the frictional interaction with major species. Also ψ_n is the mass mixing ratio, A_n is the molecular diffusion coefficient and m_n is the mass of the minor species, n , \bar{m} is the average mass of the major species, α_n is a thermal diffusion coefficient, \underline{F} is a matrix operator that represents the frictional interaction of a minor species with the three major species O , O_2 and N_2 , and S_n and R_n represents the mass sources and sinks of minor species n respectively.

The upper boundary condition is diffusive equilibrium, $\left(\frac{\partial}{\partial Z} - E_n \right) \psi_n = 0$ and the lower boundary condition can be either photochemical equilibrium, a specified mass mixing ratio, or a specified mass flux. The odd nitrogen chemistry embedded in the TGCM is the same as that discussed by Roble *et al.* (1987). $N(^2D)$ is assumed to be in photochemical equilibrium throughout the thermosphere and transport equations are solved for $N(^4S)$ and NO . We consider $N(^4S)$ in photochemical equilibrium and specify a constant number density of 8×10^6 for NO at the lower boundary.

The ion-chemistry scheme, rate coefficients, and calculation procedure for the ionosphere have been discussed by Roble *et al.* (1987) and Roble and Ridley (1987). We con-

sider both magnetic field aligned diffusion and $\underline{E} \times \underline{B}$ transport in solving the O^+ transport equation,

$$\frac{\partial n}{\partial t} - Q + Ln = -\nabla \cdot n\underline{V} \quad (3)$$

where $\underline{V} = \underline{V}_\parallel + \underline{V}_\perp$ and,

$$\underline{V}_\parallel = (\underline{b} \cdot \frac{1}{\nu} (g - \frac{1}{\rho_i} \nabla P_i) + \underline{b} \cdot \underline{u}) \underline{b}$$

$$\underline{V}_\perp = \frac{1}{|B|} \underline{E} \times \underline{b}$$

n is O^+ number density, t is time, Q and Ln are production and loss rates of O^+ and \underline{V}_\parallel and \underline{V}_\perp are velocities parallel and perpendicular to the magnetic field line, \underline{b} is a unit vector along the magnetic field, ν is the O^+ ion-neutral collision frequency, g is gravity, ρ_i and P_i are the ion mass density and pressure respectively, \underline{u} is the neutral wind vector, $|B|$ is magnetic field strength and \underline{E} is the electric field vector. Equation (3) is solved on the TGCM geographic latitude and longitude grid using the mathematical framework for calculating neutral dynamics (Washington and Williamson, 1977). The ionosphere is thus solved using an Eulerian, as compared to the Lagrangian (Sojka and Schunk, 1985; Fuller-Rowell *et al.*, 1987) approach. The upper boundary condition is $n\underline{V}_\parallel = \Phi$, where Φ is a plasma flux from the magnetosphere and is assumed to be zero for these calculations. The lower boundary condition assumes photochemical equilibrium, $n = Q/L$. Once the O^+ density distribution is determined, the NO^+ , O_2^+ , N_2^+ and N^+ distributions are determined by assuming photochemical equilibrium and solving a quartic equation as discussed by Roble and Ridley (1987). TGCM temperature, dynamics, composition and the global ionosphere are calculated at each time step (~ 150 s) and the heating and cooling rates from chemical reactions and IR

emissions etc. are coupled into the thermodynamic equation at the next time step, as described by Roble *et al.* (1987). Likewise, neutral winds, temperature, composition, and ionization rates are updated at each time step for the ionospheric calculation. The electron energy equation is not solved at the present time and the electron temperature is arbitrarily set equal to the neutral temperature for these initial calculations.

Global Structure for Equinox Solar Minimum

The new TGCM is run to steady state, a diurnally reproducible solution, for equinox conditions during solar cycle minimum. The Hinteregger (1980) solar EUV and UV measurements for July 1976 are used to calculate photoionization and dissociation rates. The aurora particle precipitation model of Foster *et al.* (1986), assuming a power input of 11 GW, and a Heelis *et al.* (1982) ionospheric convection pattern, with a cross-polar cap potential drop of 60 kV, are used in the calculation. Tidal amplitudes are identical to those described by Fesen *et al.* (1986). The calculated global ionospheric structure at 1900 UT is shown in Figure 1. The F-region peak density structure is illustrated by contours of $f_o F_2$ plasma frequency (MHz) as shown in Figure 1a. The prominent feature is the density enhancement aligned along the magnetic equator on the dayside of the Earth with a long tail extending into the nightside. Aurora particle precipitation causes enhancements at high latitudes. Minimum $f_o F_2$ occur in mid latitudes at night. The very low values in that region are attributed to F-region decay and the lack of a specified plasma flow from the magnetosphere for this calculation.

Contours of electron density along the TGCM $Z = -4$ constant pressure surface near 120 km are shown in Figure 1b. Photochemical equilibrium prevails at this altitude with maximum values occurring at the subsolar point and in the auroral oval.

TGCM calculated contours of neutral gas temperature and wind vectors at 1900 UT

along the $Z = +2$ constant pressure surface near 280 km are shown in Figure 2a. Contours of the neutral gas temperature along the same constant pressure surface obtained from MSIS-86 are shown in Figure 2b for comparison. There is excellent agreement between the TGCM calculated temperature and MSIS-86 on the dayside of the Earth. At night, the midnight temperature bulge calculated in the TGCM appears too large, compared with MSIS-86, indicating that the tidal specification may be too large or the data averaging in MSIS-86 eliminates this variable feature. The neutral wind pattern is similar to that calculated in previous studies with a diurnal component at low- and mid-latitudes and strong enhancements at high latitudes caused by ion convection.

A latitudinal cross-section of the ionospheric density structure at 1900 UT along the 45° W longitude (16 solar local time) is shown in Figure 3. The prominent features are the equatorial structure in the F-region and auroral zone enhancements superimposed on a general dayside solar background. The low electron density values in the upper F-region at mid-latitudes are attributed to a zero flux plasma exchange between the ionosphere and magnetosphere and the low plasma temperature.

A longitudinal cross-section along the 17.5° N latitude circle is shown in Figure 4. In the lower ionosphere, photochemical equilibrium controls the density distribution. Above about 250 km, however, plasma motion caused by ionospheric $\underline{E} \times \underline{B}$ drifts and neutral winds forcing ionization up and down magnetic field lines control the general shape. In particular, the post-sunset elevation of the F-layer is clearly shown.

Finally, the TGCM calculated nitric oxide distribution at 1900 UT along the $Z = -4$ constant pressure surface is shown in Figure 5. The NO densities maximize at high latitudes with roughly a factor of 3 difference between high and low latitudes. There is also a diurnal NO density variation in the equatorial region with maximum values in the late afternoon. These features are similar to the Atmosphere Explorer-C measurements

described by Stewart and Cravens (1978) and Cravens and Stewart (1978). There is also a magnetic field control at high latitudes associated with aurora production similar to that described by Cravens and Killeen (1988).

The overall fields calculated by the TGCM include, T_n , u , v , w , h , and mass mixing ratios for O_2 , O , N_2 , $N(^2D)$, $N(^4S)$, NO , as well as O^+ , O_2^+ , NO^+ , N^+ , N_2^+ , n_e and T_e . These fields are obtained at each time step and only a few are presented in this paper to illustrate the basic TGCM calculated structure.

Summary and Conclusions

The self-consistent aeronomic scheme developed by Roble *et al.* (1987) has been incorporated into the NCAR-TGCM and used to calculate the global structure of the thermosphere and ionosphere for solar minimum equinox conditions. The Eulerian model gives a reasonable representation of the global ionospheric structure, and it is numerically efficient since thermospheric and ionospheric properties are calculated on the same grid. The TGCM time step is 2 1/2 minutes for both the thermosphere and ionosphere calculation and it takes approximately 1 hour of Cray XMP-48 CPU time to simulate 1 day. The numerical scheme is stable and has been tested for solar minimum and maximum with equinox and solstice conditions respectively and for aurora power inputs of 100 GW and a cross-polar cap potential drop of 150 kV for ionospheric convection. The results also indicate that a better specification of magnetosphere-ionosphere plasma transport including a calculation of electron temperature is needed to improve the overall structure of the topside ionosphere above the F-region peak.

Concluding Remarks

Considerable progress has been made in recent years in improving our understanding

of the main physical processes operating in the thermosphere and ionosphere. This progress was possible because of the availability of satellite data on the structure and dynamics of the thermosphere and ionosphere as well as in the development of new global dynamic models for use in interpreting measurements and for predictions of global phenomena. It appears that it may be possible, in the near future, to develop a sufficiently realistic TGCM for use in the prediction of thermospheric weather that can be used to improve forecasts of satellite drag and at the same time give a prediction of ionospheric phenomena for communication purposes.

Acknowledgements

This research effort was supported in part by the AFGL in-house laboratory independent research program.

References

- Chiu, Y. T., An improved phenomenological model of ionospheric density, J. Atmos. Terr. Phys., **37**, 1563-1570, 1975.
- Cravens, T. E., and T. L. Killeen, Longitudinal asymmetric transport of nitric oxide in the E-region, Planet. Space Sci., **36**, 11-20, 1988.
- Cravens, T. E., and A. I. Stewart, Global morphology of nitric oxide in the lower E-region, J. Geophys. Res., **83**, 2446-2452, 1978.
- Dickinson, R. E., E. C. Ridley, and R. G. Roble, A three-dimensional, time-dependent general circulation model of the thermosphere, J. Geophys. Res., **86**, 1499-1512, 1981.

- Dickinson, R. E., E. C. Ridley, and R. G. Roble, Thermospheric general circulation with coupled dynamics and composition, J. Atmos. Sci., **41**, 205-219, 1984.
- Fesen, C. G., R. E. Dickinson, and R. G. Roble, Simulation of thermospheric tides at equinox with the National Center for Atmospheric Research thermospheric general circulation model, J. Geophys. Res., **91**, 4471-4489, 1986.
- Foster, J. C., J. M. Holt, R. G. Musgrove, and D. S. Evans, Ionospheric convection associated with discrete levels of particle precipitation, Geophys. Res. Lett., **13**, 656-659, 1986.
- Fuller-Rowell, T. J., and D. Rees, A three-dimensional, time-dependent global model of the thermosphere, J. Atmos. Sci., **37**, 2545-2657, 1980.
- Fuller-Rowell, T. J., D. Rees, S. Quegan, R. J. Moffett, and G. J. Bailey, Interactions between neutral thermospheric composition and the polar ionosphere using a coupled ionosphere-thermosphere model, J. Geophys. Res., **92**, 7744-7748, 1987.
- Hedin, A. E., MSIS-86 thermospheric model, J. Geophys. Res., **92**, 4649-4662, 1987.
- Heelis, R. A., J. K. Lowell, and R. W. Spiro, A model of the high-latitude ionospheric convection pattern, J. Geophys. Res., **87**, 6339-6345, 1982.
- Hinteregger, H. E., Representations of solar EUV fluxes for aeronomical applications, Adv. Space Res., **1**, 39-42, 1981.
- Quegan, S., G. J. Bailey, R. J. Moffett, R. A. Heelis, T. J. Fuller-Rowell, D. Rees, and R. W. Spiro, A theoretical study of the distribution of ionization in the high-latitude ionosphere and the plasmasphere: First results on the mid-latitude trough and the light-ion trough, J. Atmos. Terr. Phys., **44**,

- Richmond, A. D., M. Blanc, B. A. Emery, R. H. Wand, B. G. Fejer, R. F. Woodman, S. Ganguly, P. Amayenc, R. A. Behnke, C. Calderon, and J. V. Evans, An empirical model of quiet-day ionospheric electric fields at middle and low latitudes, J. Geophys. Res., **85**, 4658-4664, 1980.
- Roble, R. G., and E. C. Ridley, An auroral model for the NCAR thermospheric general circulation model (TGCM), Annales. Geophysicae, **5A**, (6), 369-382, 1987.
- Roble, R. G., E. C. Ridley, and R. E. Dickinson, On the global mean structure of the thermosphere, J. Geophys. Res., **92**, 8745-8758, 1987.
- Sojka, J. J., and R. W. Schunk, A theoretical study of the global F-region for June solstice, solar maximum, and low magnetic activity, J. Geophys. Res., **90**, 5285-5298, 1985.
- 619-640, 1982.
- Stewart, A. I., and T. E. Cravens, Diurnal and seasonal effects in E-region low-latitude nitric oxide, J. Geophys. Res., **83**, 2453-2456, 1978.
- Washington, W. M., and D. L. Williamson, A description of the NCAR global circulation models, in Methods in Computational Physics, Vol. 17, General Circulation Models of the Atmosphere, edited by J. Chang, 111-172. Academic press, New York, 1977.

List of Illustrations

Fig. 1. (a) Contours of calculated $f_o F_2$ (Mz) and (b) contours of calculated electron density ($\log_{10}(n_e, \text{cm}^{-3})$) along the TGCM $Z = -4$ constant pressure surface near 120 km, both at 1900 UT for solar minimum equinox conditions.

Fig. 2. (a) Contours of TGCM calculated neutral gas temperature (K) and wind vectors, and (b) contours of MSIS-86 neutral gas temperature (K) both along the TGCM $Z = +2$ constant pressure surface near 280 km, at 1900 UT.

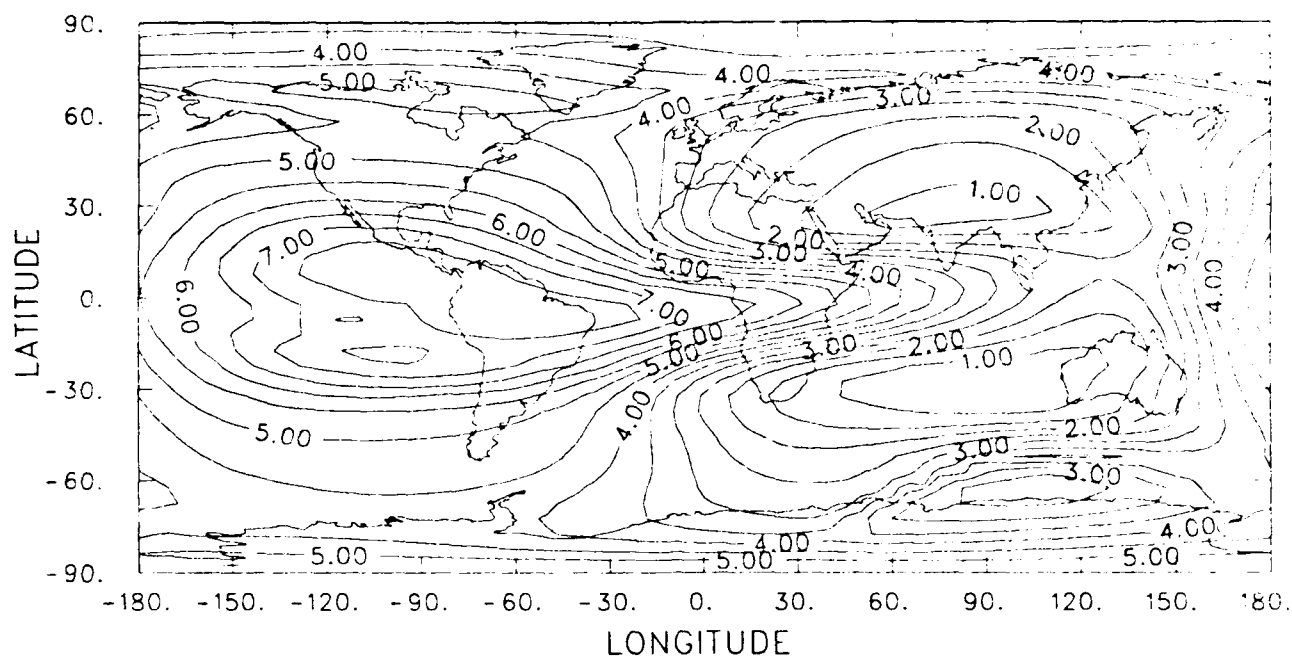
Fig. 3. Contours of TGCM calculated electron density ($\log_{10}(n_e, \text{cm}^{-3})$) along the 45° W longitude circle at 1900 UT (1600 SLT).

Fig. 4. Contours of TGCM calculated electron density ($\log_{10}(n_e, \text{cm}^{-3})$) along the 17.5° N latitude circle at 1200 UT.

Fig. 5. Contours of TGCM calculated NO density distribution ($\log_{10}(n(\text{NO}), \text{cm}^{-3})$) along the $Z = -4$ constant pressure surface near 120 km at 1900 UT.

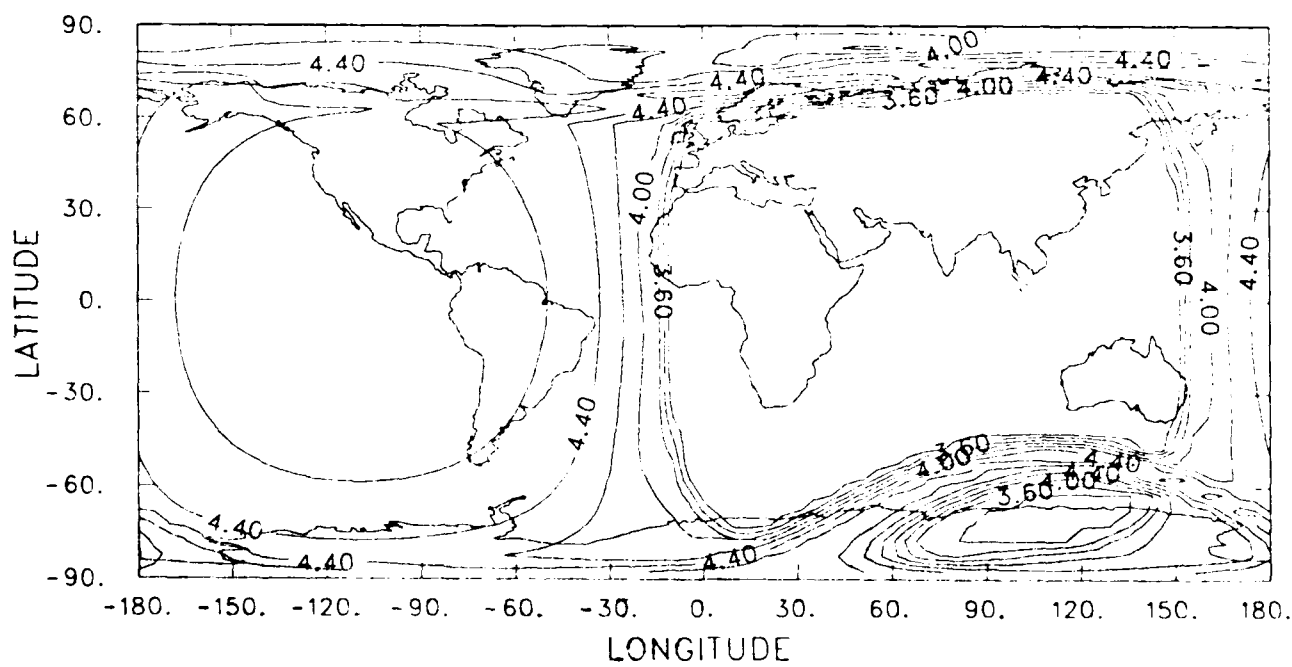
UT = 19.00

(a)



Z = -4.0

AVE HT = 123.0



(b)

Figure 1

Z = 2.0

AVE HT = 286.3

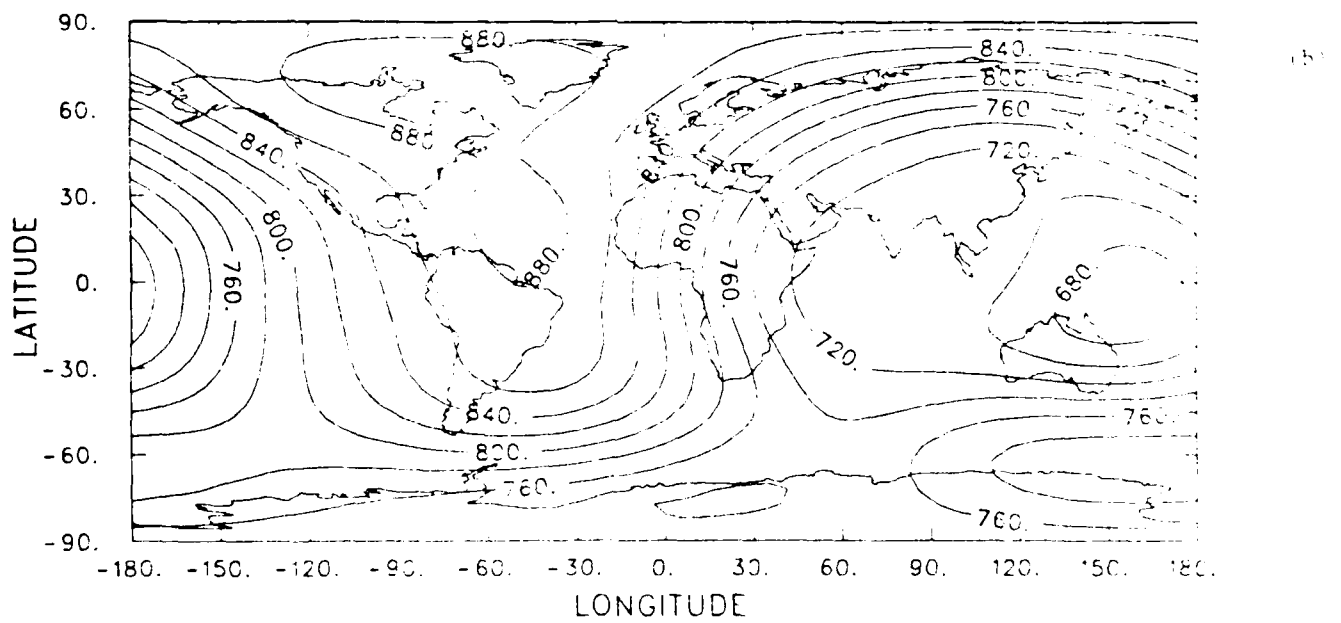
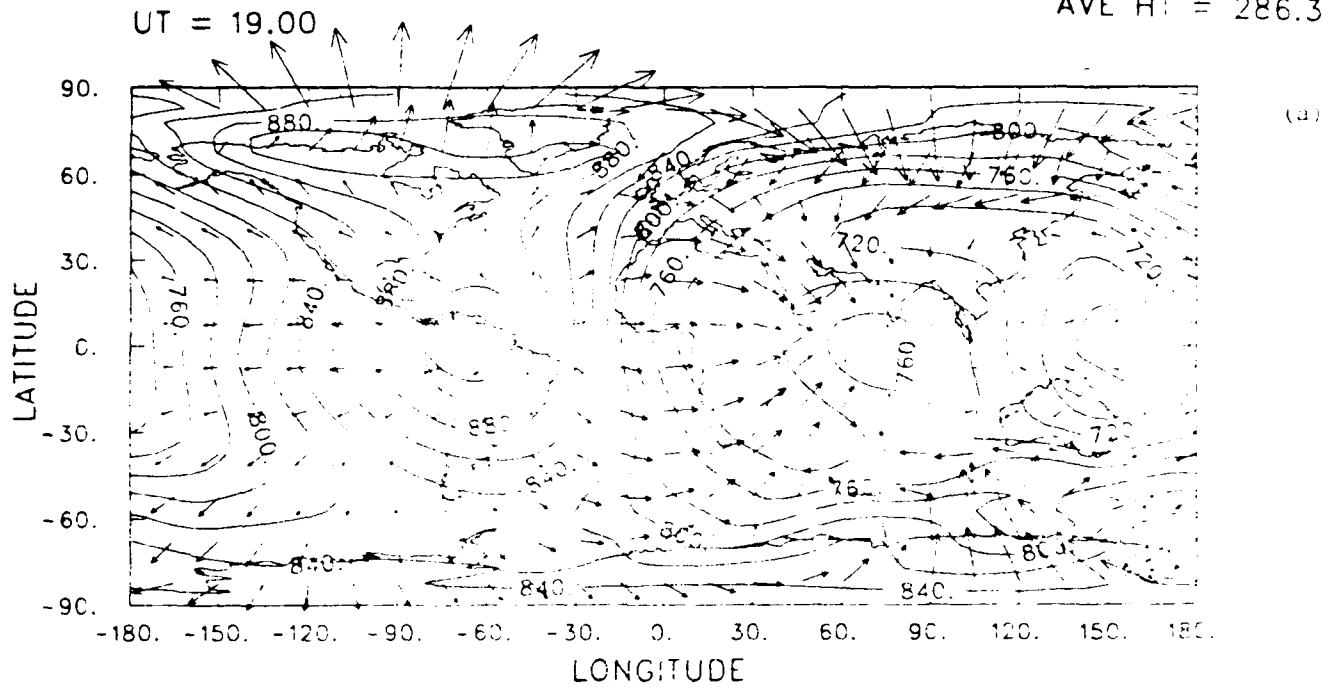


Figure 2

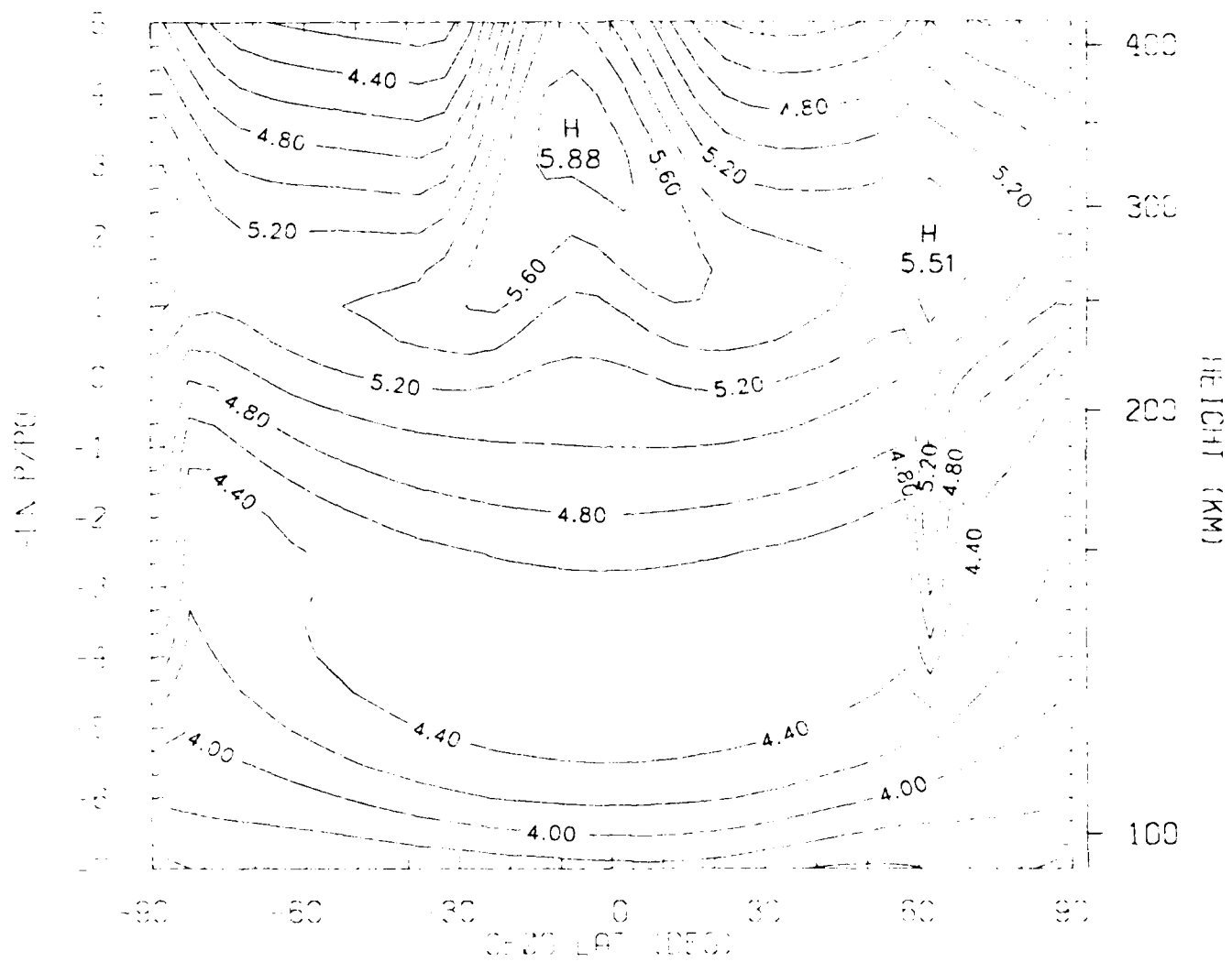


Figure 3

UT=12: 0

17.5N

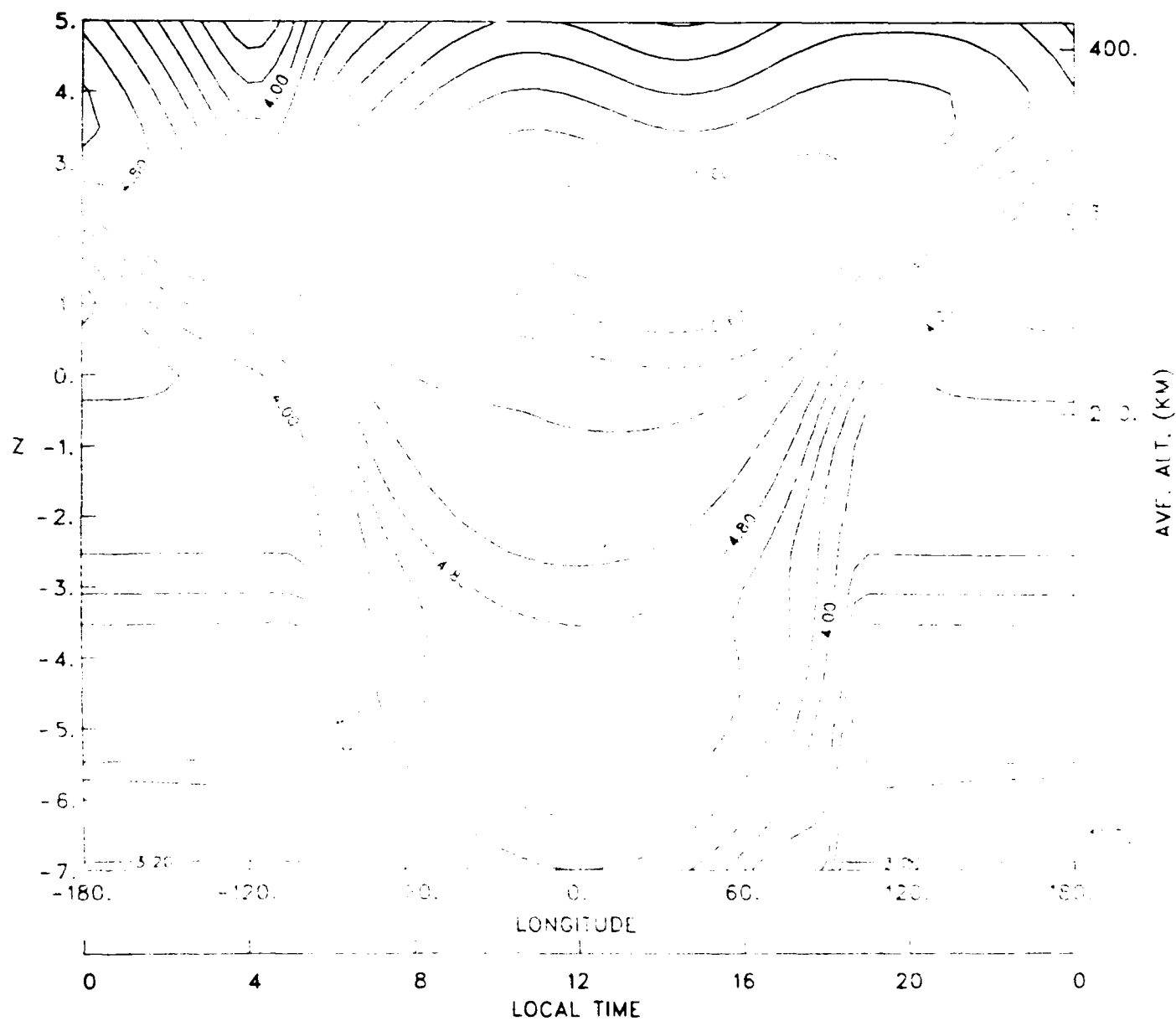


Figure 4

$Z = -4.0$

AVE HT = 123.0

UT = 19.00

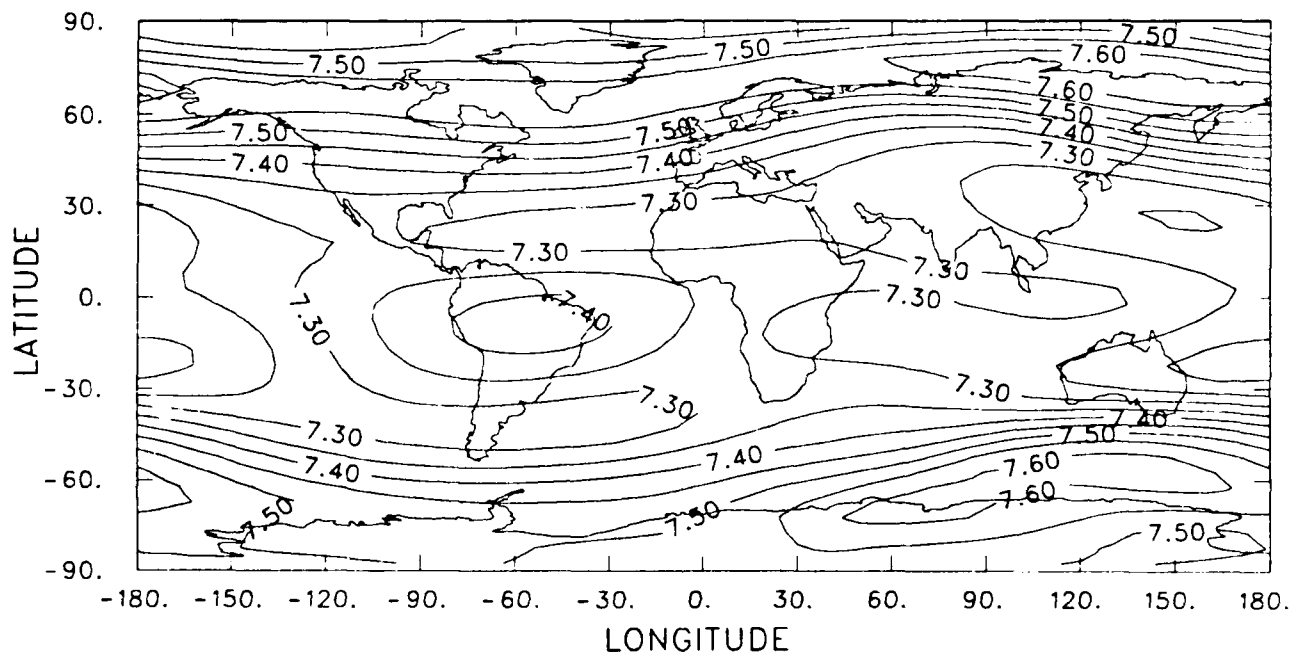


Figure 5

NCAR Thermospheric General Circulation Model (TGCM)

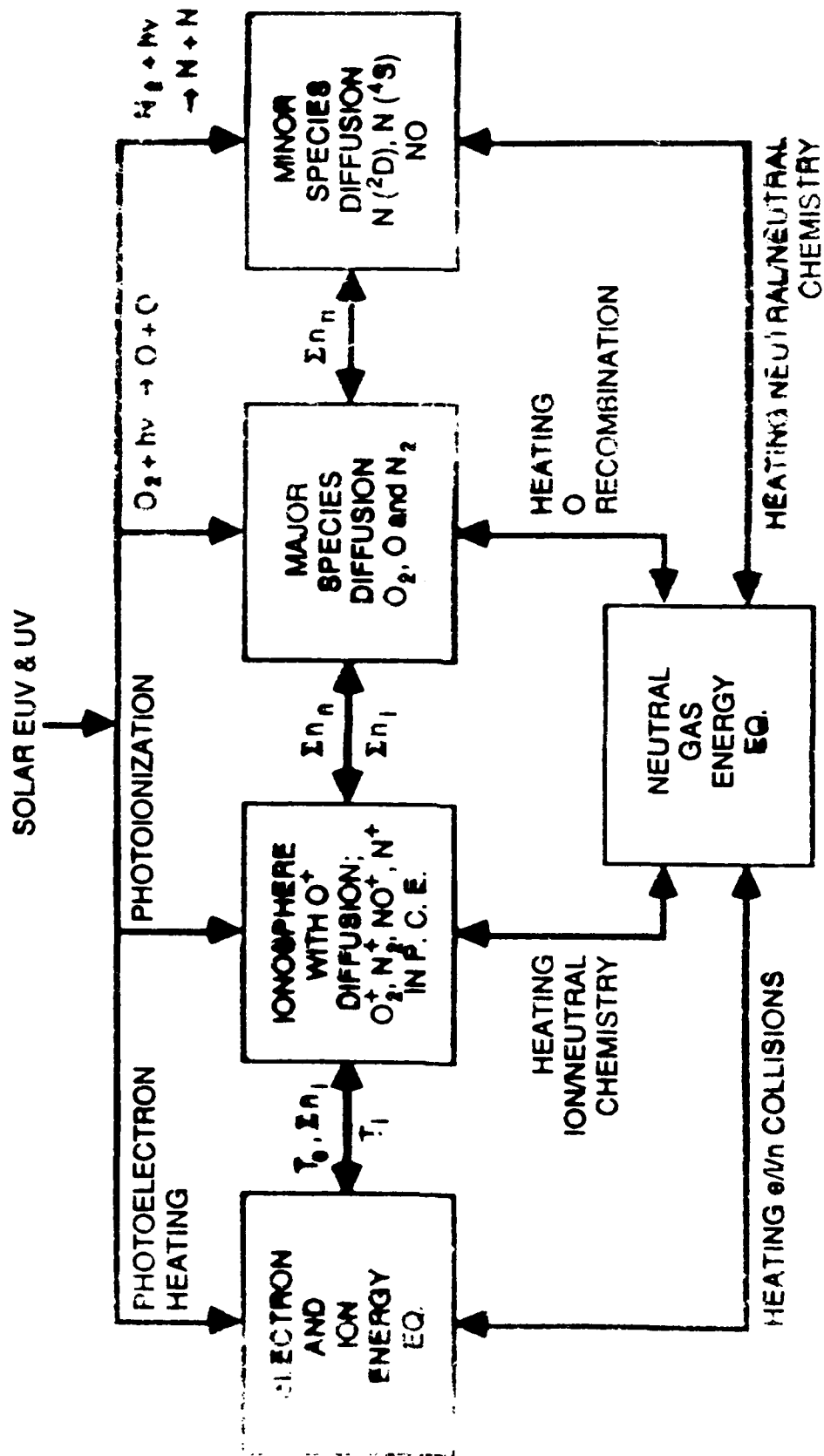
- **Primitive equations of dynamic meteorology adapted to thermospheric heights**
- **Horizontal grid 5° latitude × 5° longitude, geographic**
- **Vertical grid - 25 constant pressure surfaces, 2 grid points per scale height, 97 to 500 km**
- **Time step 150 or 300 S.**

Input

- **Solar EUV and UV radiation 5 to 250 nm**
- **Empirical magnetic field**
- **Empirical magnetospheric convection and auroral particle precipitation models**
- **Structure of upward propagating tides from middle atmosphere**
- **Plasma particle and heat fluxes from magnetosphere (SAR-arcs, O⁺ precipitation, neutral hydrogen)**

TGCM Output

- Neutral gas temperature, T_n
- Neutral winds, U , V , W
- Height of constant pressure surface, h
- Neutral composition and density
 - major - O , O_2 and N_2
 - minor - $N(^2D)$, $N(^4S)$, NO , He and Ar
- Ion composition,
 - O^+ , NO^+ , O_2^+ , N_2^+ , and N^+ , $\Sigma n_i = n_e$
 - Ion temperature, T_i
 - (electron temperature, T_e)
- Global dynamo

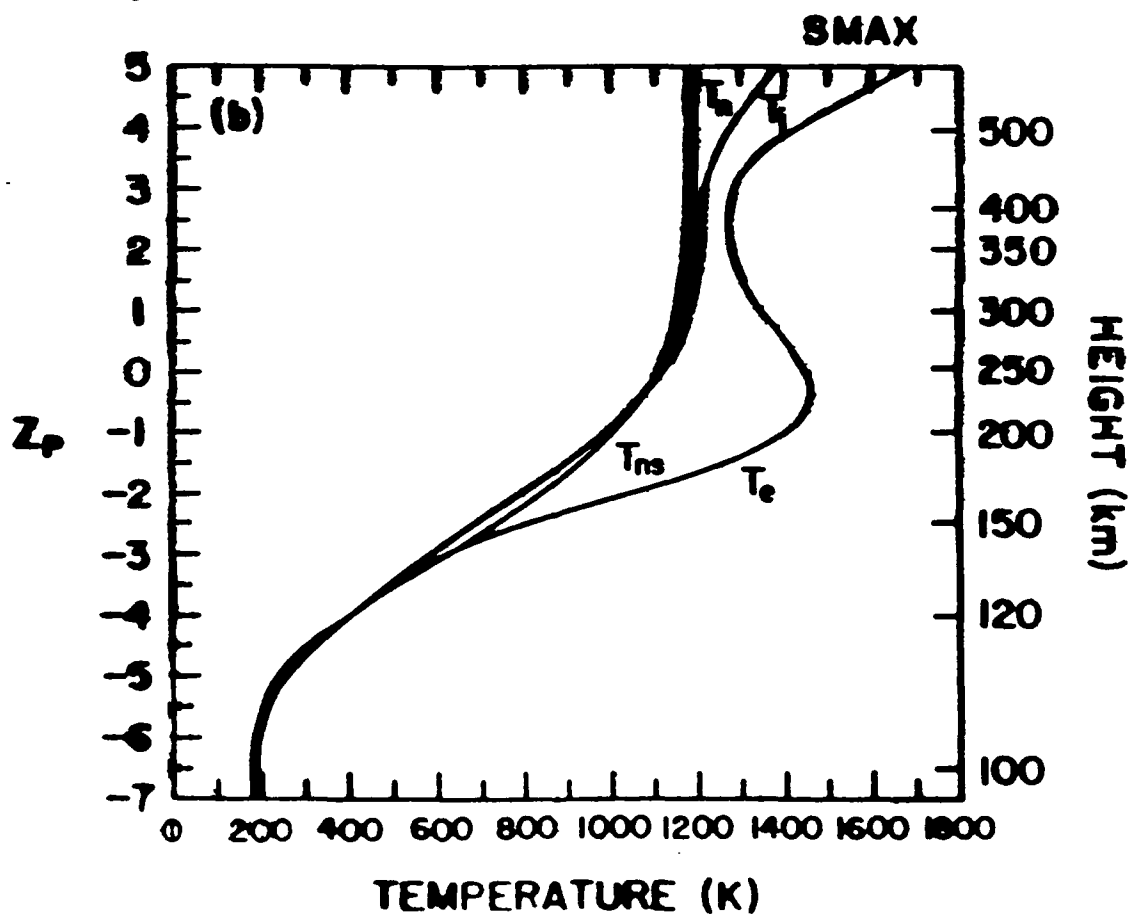
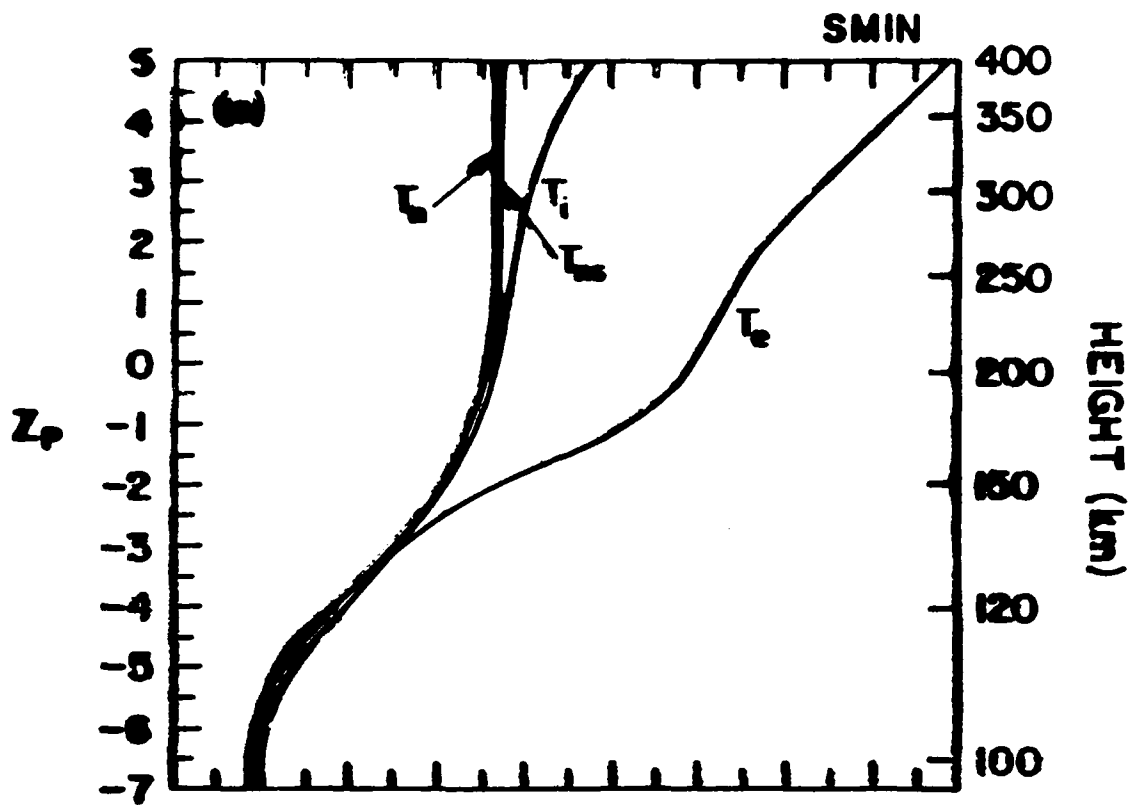


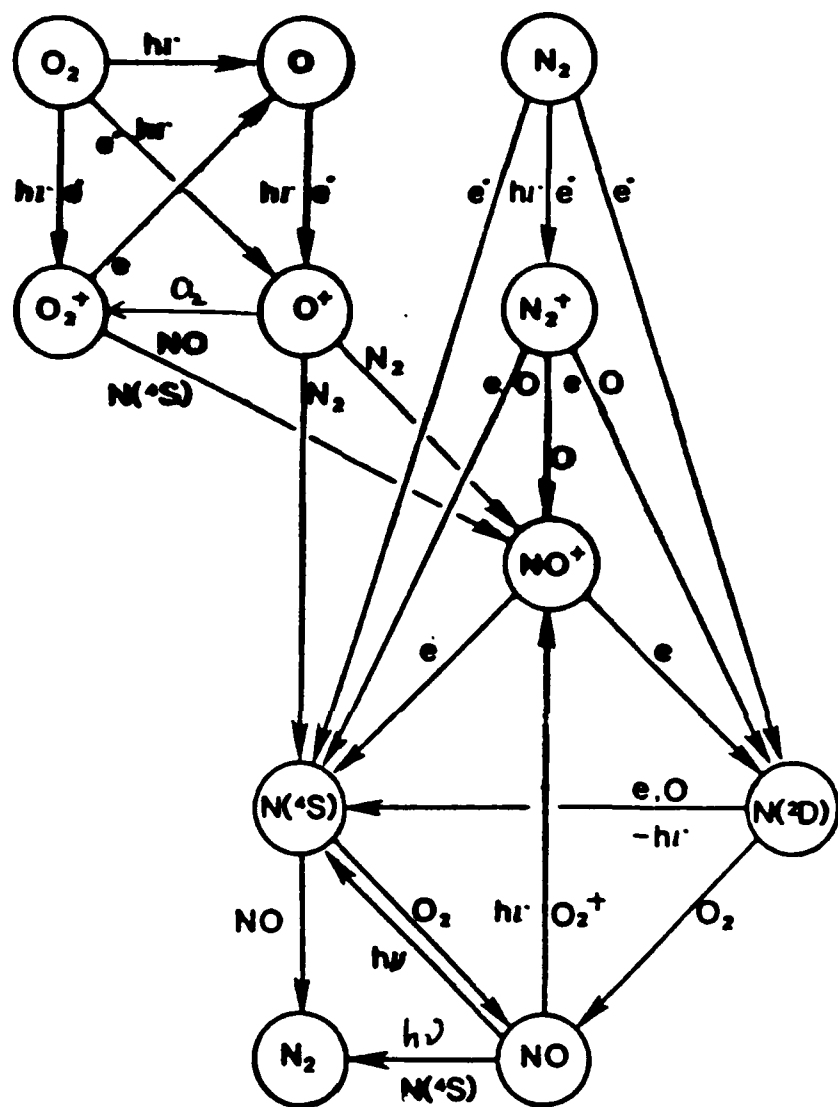
NEUTRAL HEAT SOURCES

1. SOLAR HEATING, SCHUMANN-RUNGE CONTINUUM
2. SOLAR HEATING, SCHUMANN-RUNGE BANDS
3. EXOTHERMIC MINOR NEUTRAL CHEMISTRY
4. EXOTHERMIC ION-NEUTRAL CHEMISTRY
5. QUENCHING OF $O(^1D)$
6. COLLISIONS BETWEEN THERMAL PARTICLES, n_e , n_i , n_n
ELASTIC AND INELASTIC
7. PHOTOELECTRON HEATING
8. ATOMIC OXYGEN RECOMBINATION
9. OZONE HEATING
10. AURORAL ELECTRON AND PROTON HEATING
11. JOULE HEATING

NEUTRAL COOLING

1. MOLECULAR HEAT CONDUCTION
2. EDDY HEAT CONDUCTION
3. NON-LTE CO_2 COOL-TO-SPACE
4. NON-LTE NO , $5.3\mu m$ COOL-TO-SPACE
5. $63\mu m$ COOLING FROM O FINE STRUCTURE





O^+ EQUATION WITH HORIZONTAL AND VERTICAL TRANSPORT

$$\frac{\partial n}{\partial t} - Q + Ln = -\nabla \cdot n \underline{V}$$

where $\underline{V} = \underline{V}_\beta + \underline{V}_\perp$

$$\underline{V}_\beta = \left[\underline{b} \cdot \frac{1}{\nu} \left(g - \frac{1}{\rho_i} \nabla p_i \right) + \underline{b} \cdot \underline{u} \right] \cdot \underline{b}$$

$$\underline{V}_\perp = \frac{1}{|B|} \underline{E} \times \underline{b}$$

now, $-\nabla \cdot n \underline{V}_\beta = b_z^2 \left(\frac{\partial}{\partial z} + \frac{\nabla \cdot \underline{b}}{b_z} \right) D \left(\frac{\partial}{\partial z} T_p + \frac{gm_i}{k} \right) n$

$$- (\underline{b} \cdot \underline{u}) n \nabla b - \underline{b} \cdot \nabla (\underline{b} \cdot \underline{u} n)$$

$$-\nabla \cdot \underline{v}_\perp = \underline{B} \times \underline{E} \cdot \nabla (n/B^2)$$

Upper Boundary Conditions

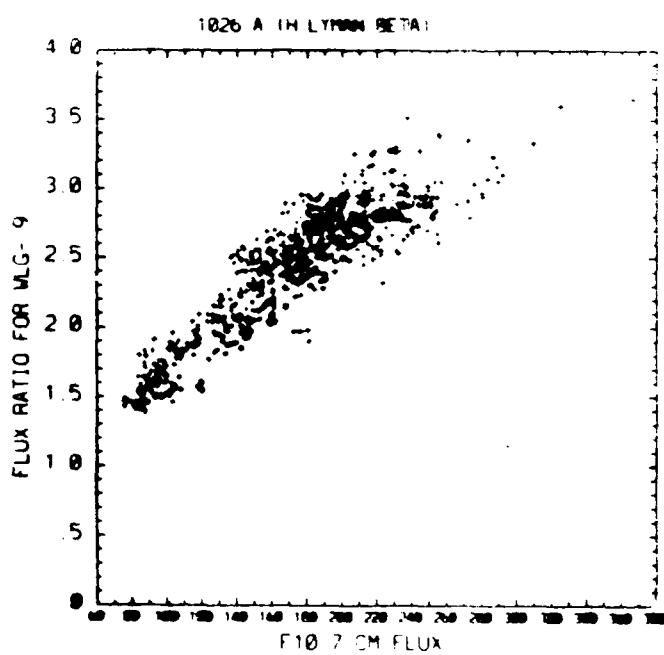
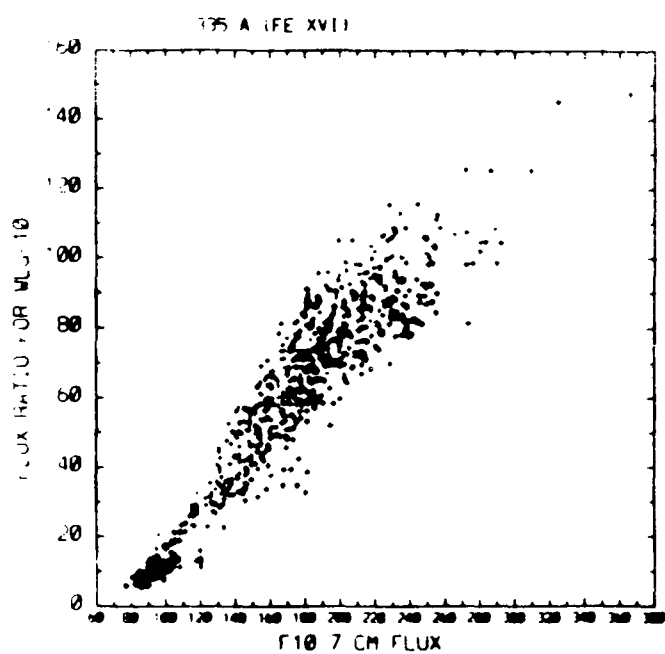
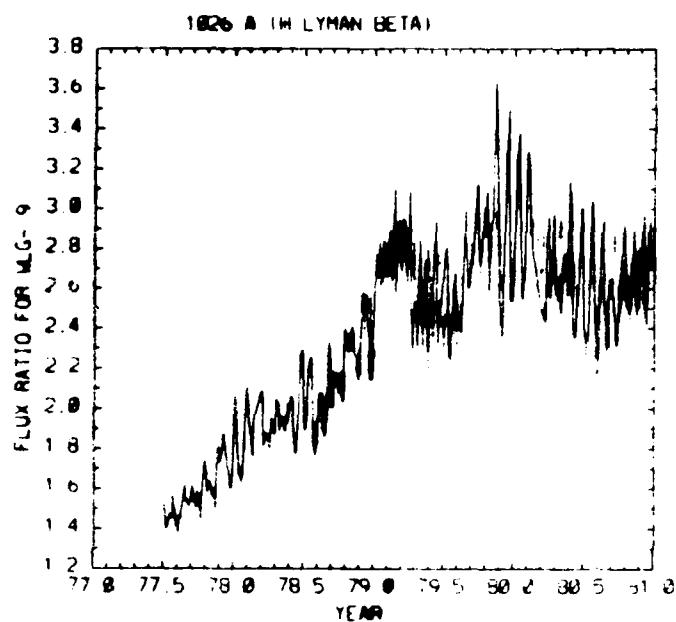
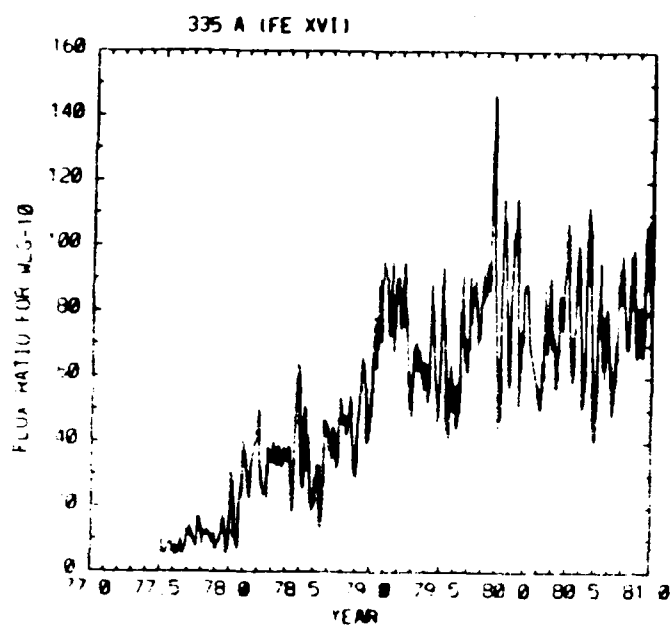
Mixed boundary condition

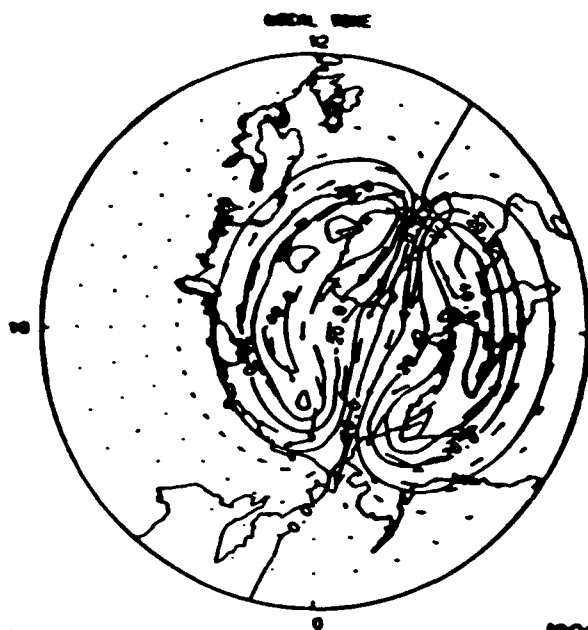
$$-b_z^2 D \left(\frac{\partial}{\partial z} T_p + \frac{gm_i}{k} \right) n + n (\underline{b} \cdot \underline{u}) b_z + \frac{n (\underline{E} \times \underline{B})_z}{B^2} = \Phi_z$$

Lower Boundary Conditions

Photochemical equilibrium

$$n = Q/L$$

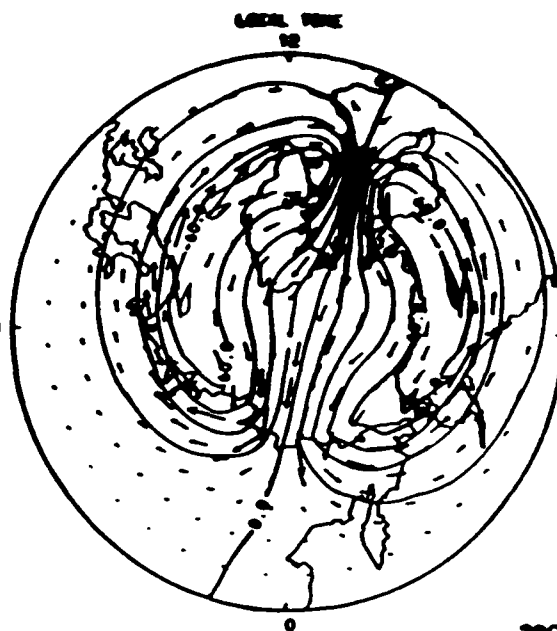




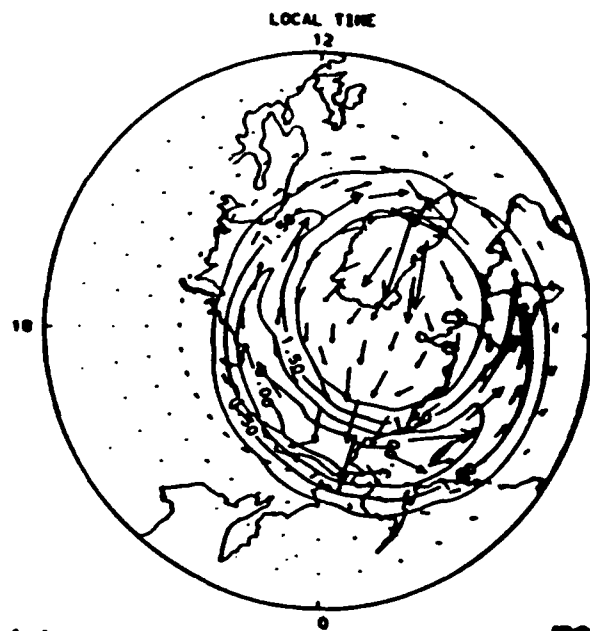
(a)

1900 M/S

(b)



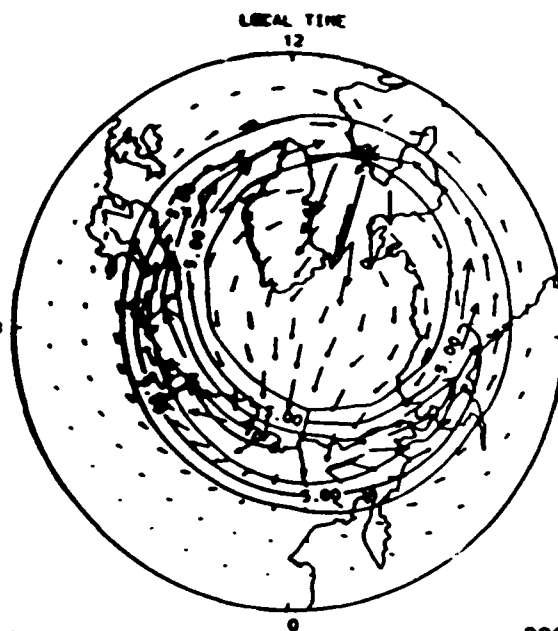
2900 M/S



(c)

1900 M/S

(d)



2900 M/S

LOG TGCM ELECTRON DENSITY (HIST) (CM-3)

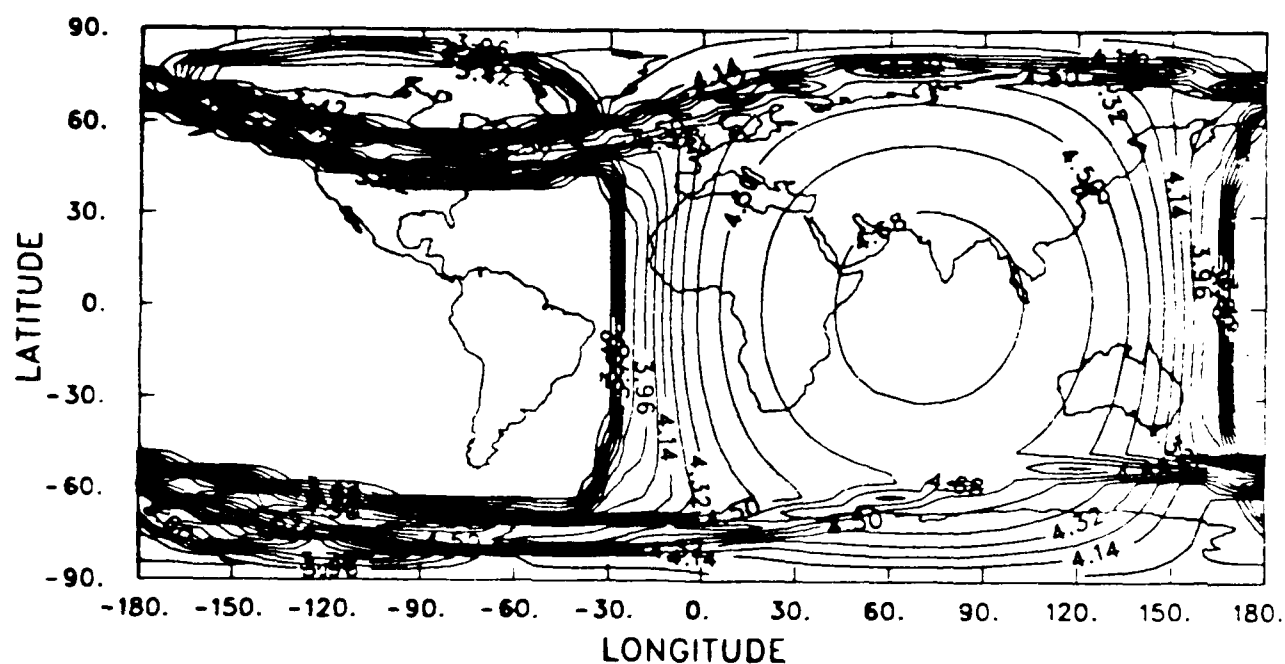
ECR245,246

Z = -4.0

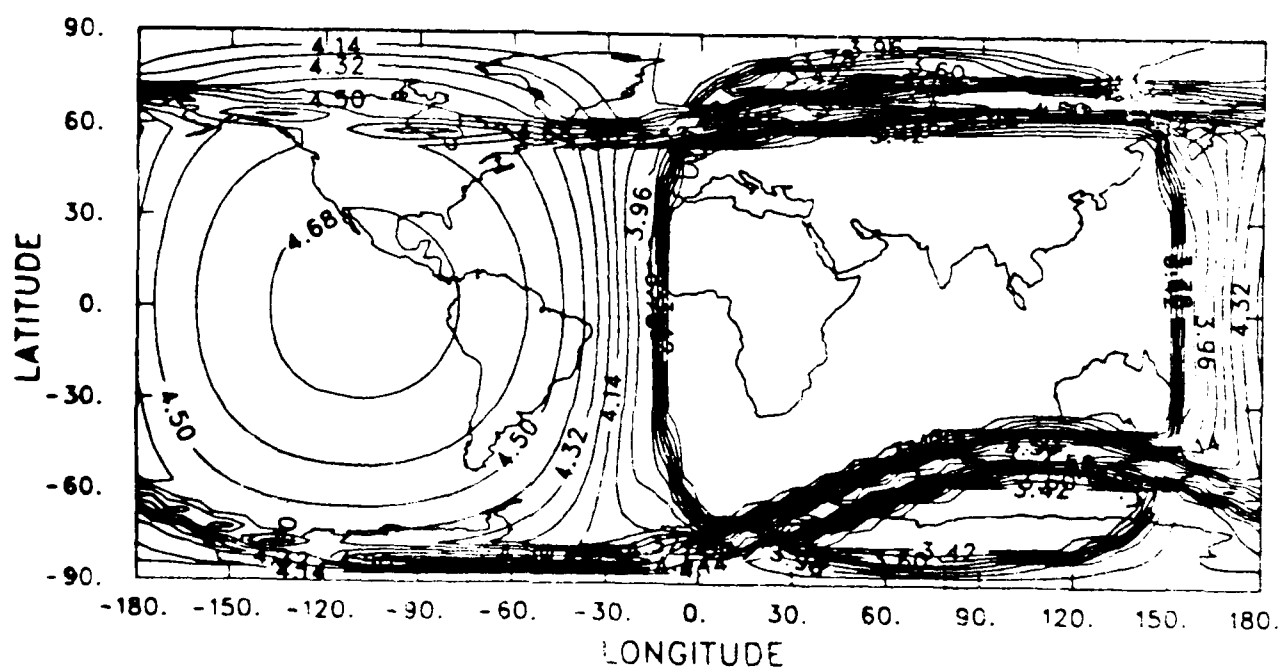
YD = 76081

AVE HT = 123.0

UT = 7.00



UT = 19.00



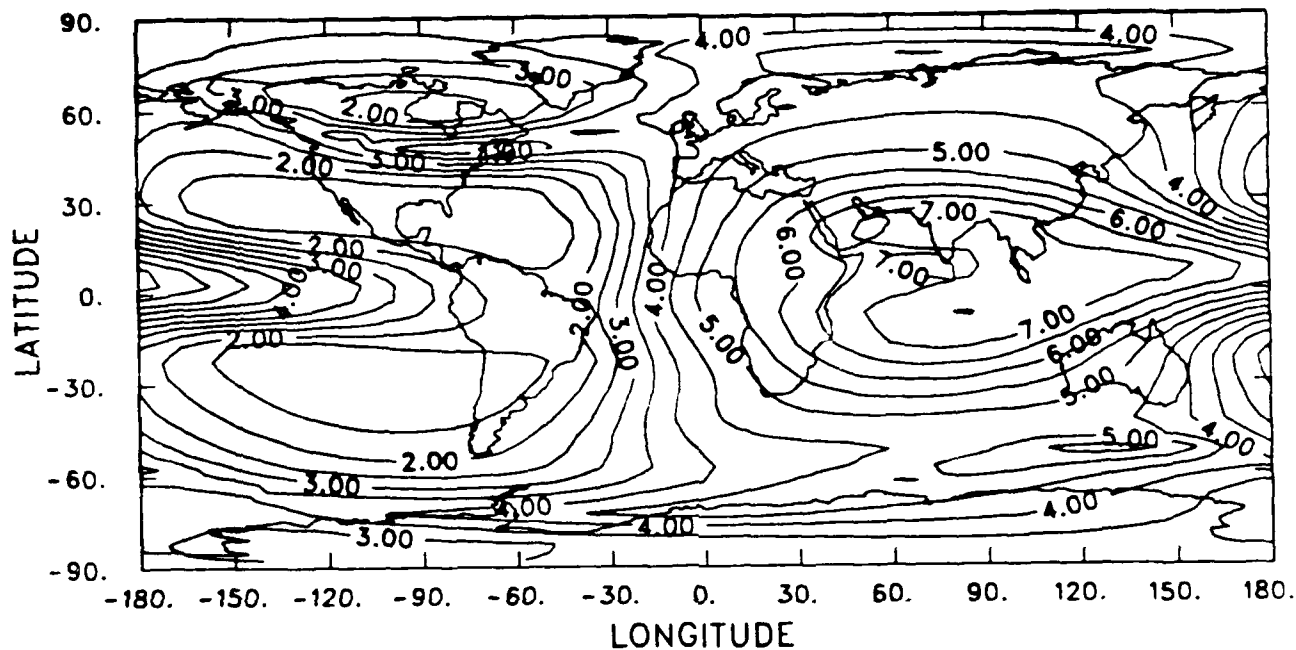
MAXIMUM foF2 (MHz) (FROM TGCM NE)

ECR245,246

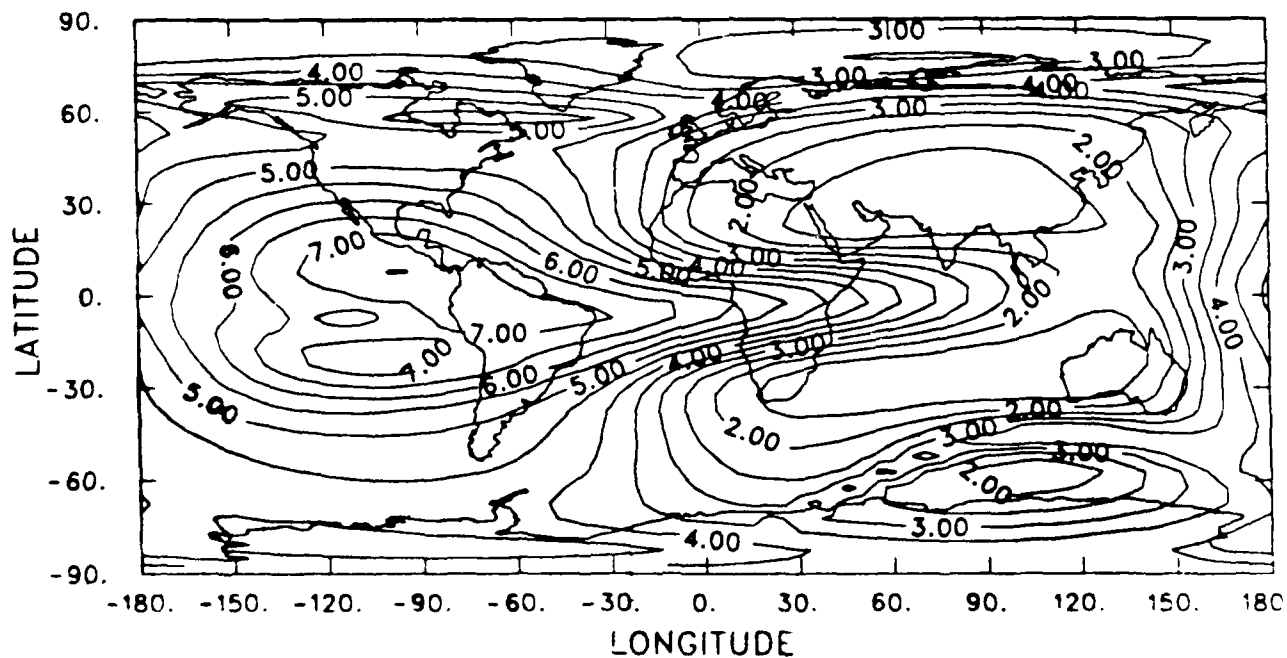
FOF2 GLBAV= 3.5

YD = 76081

UT = 7.00



UT = 19.00



LOG TGCM ELECTRON DENSITY (HIST) (CM-3)

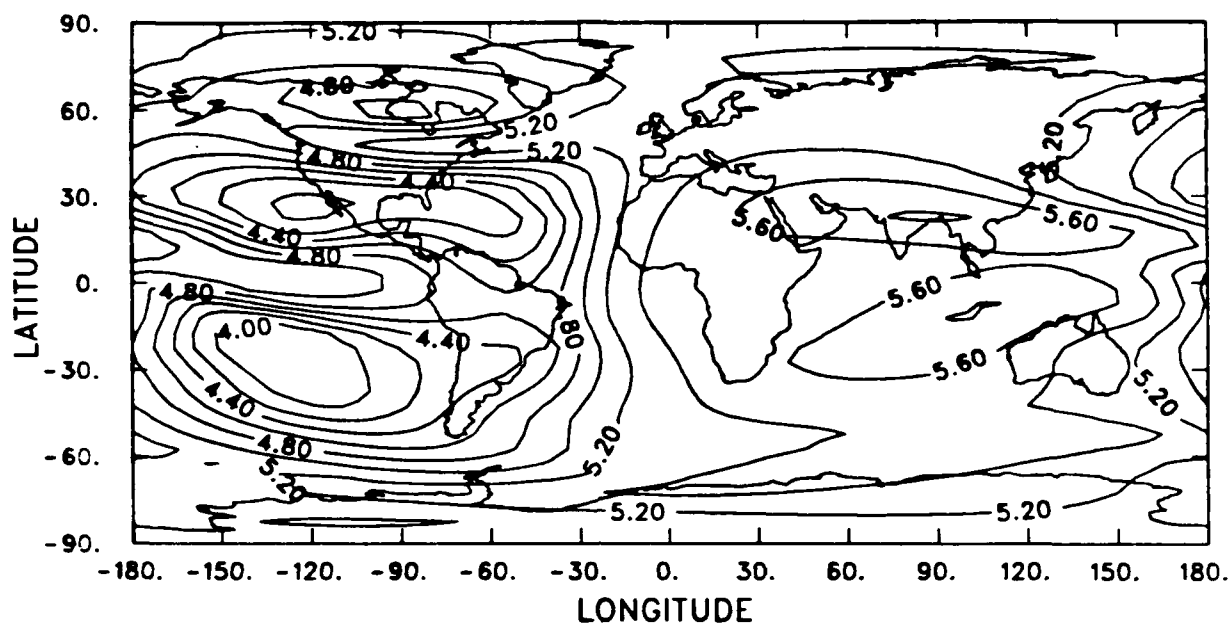
ECR245,246

Z = 2.0

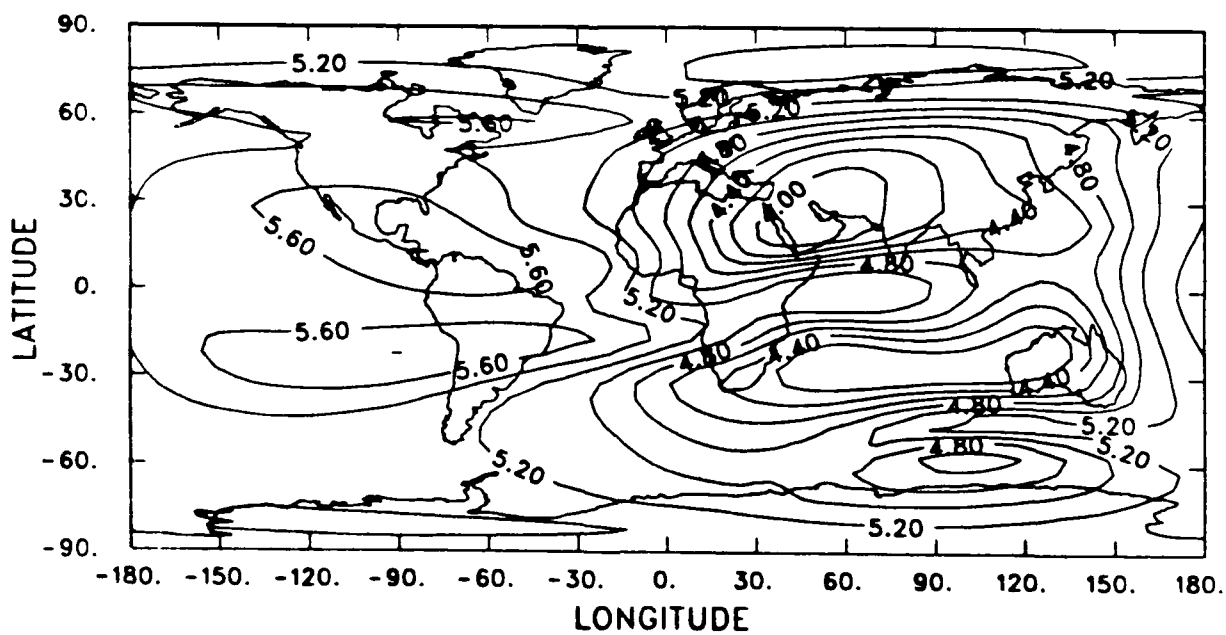
YD = 76081

AVE HT = 279.9

UT = 7.00



UT = 19.00



LOG IRI ELECTRON DENSITY + NE FROM OVAL (CM-3)

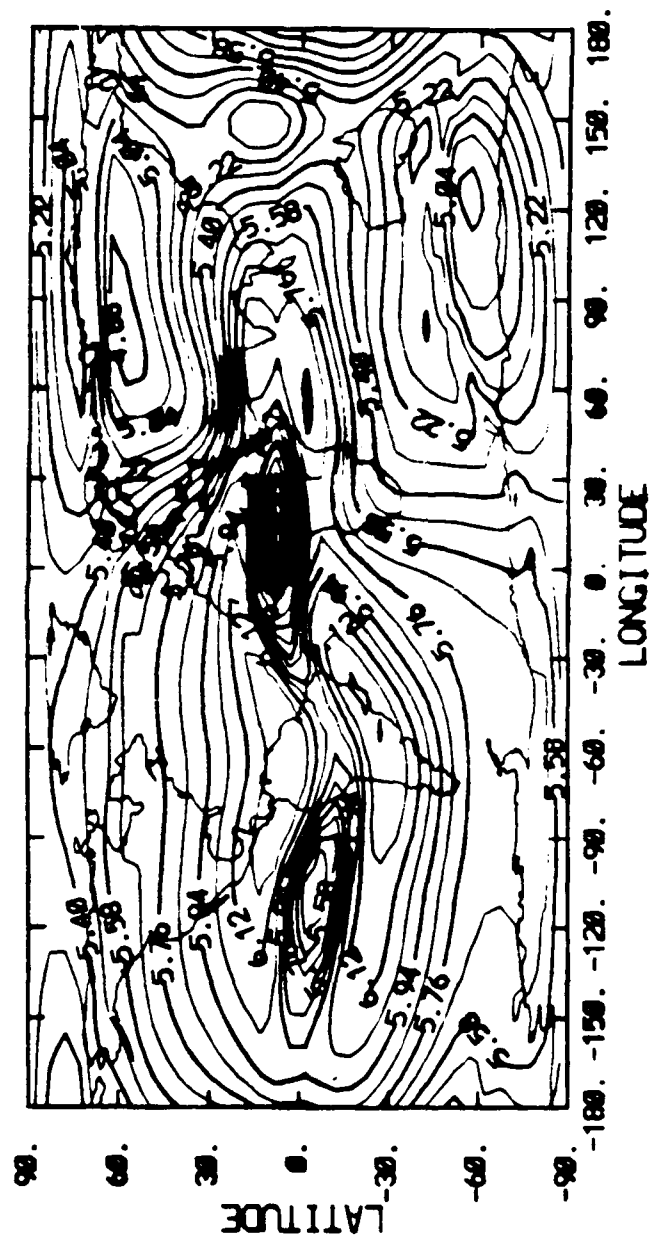
ECR245.246

Z = 2.0

YD = 76080

AVE HT = 279.5

UT = 19.00



FRAME 35

CONTINU FROM 4.1/88 TO 5.3000 CONTINUUM INTERVAL OF 0.000000-01 PTLJ 31- 5.5595

TGCM NEUTRAL TEMPERATURE (K) + (U,V) (M/S)

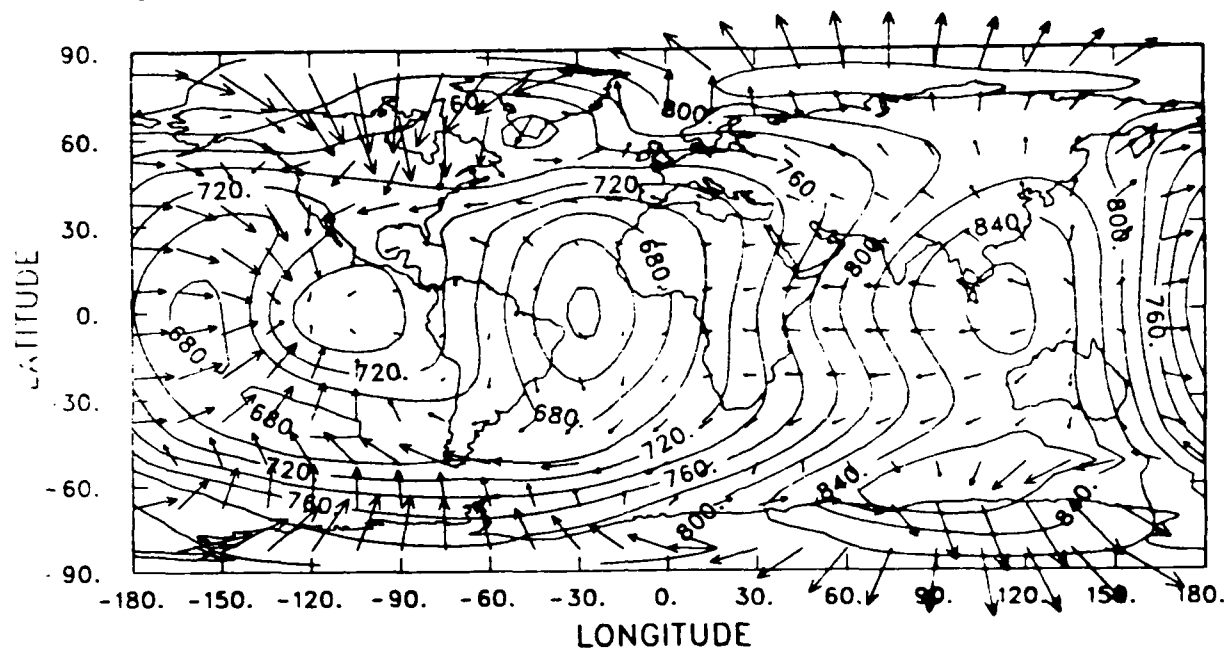
ECR245,246

Z = 2.0

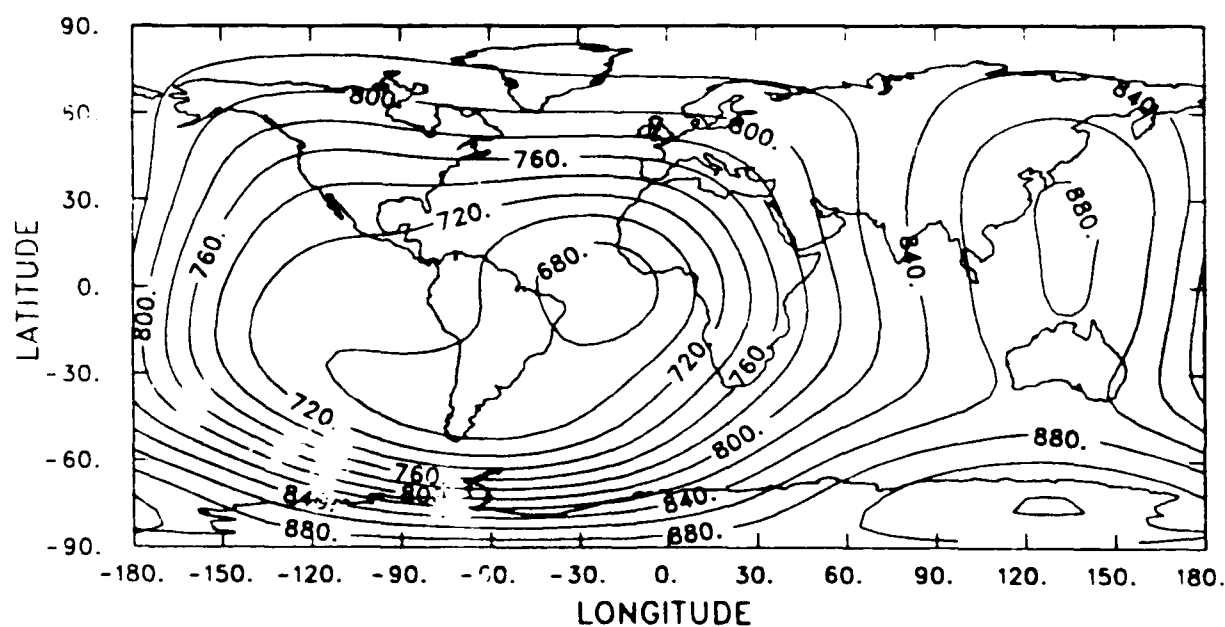
YD = 76081

AVE HT = 279.9

UT = 7.00



MSIS 86 NEUTRAL TEMPERATURE (K)



TGCM NEUTRAL TEMPERATURE (K) + (U,V) (M/S)

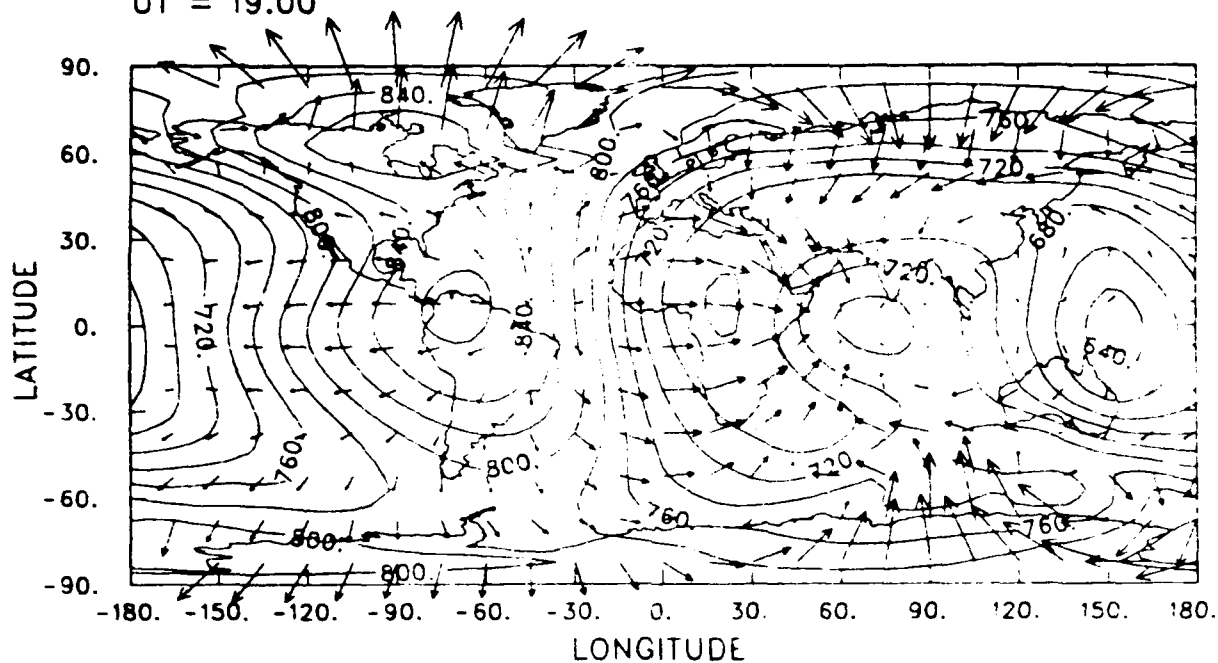
ECR245,246

Z = 2.0

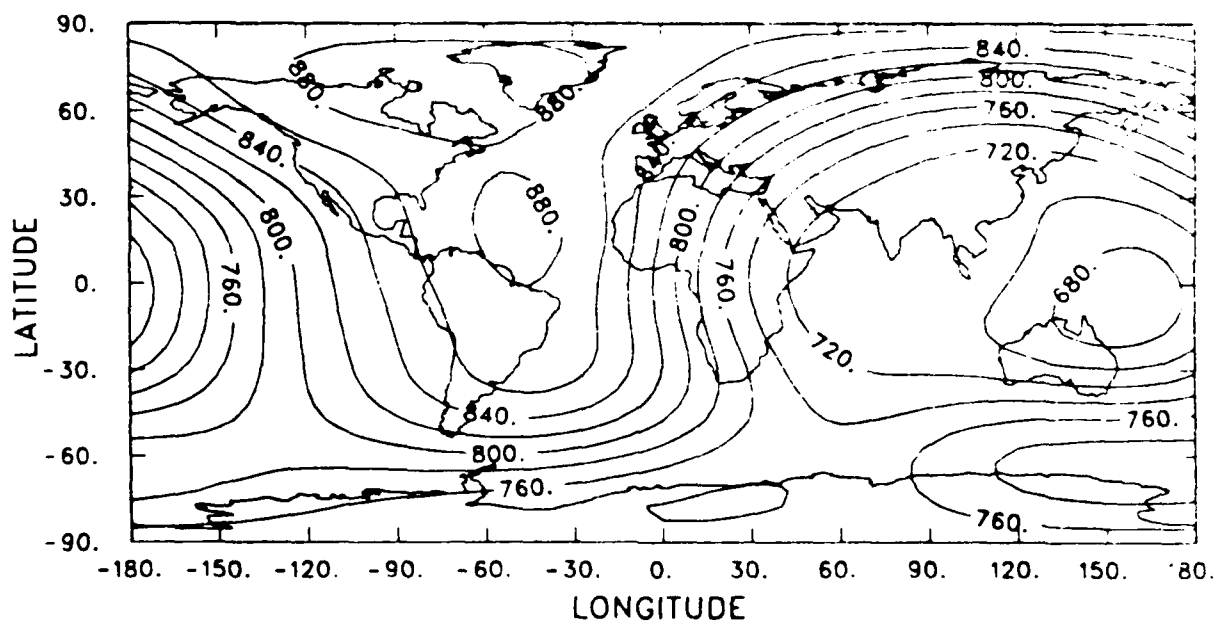
YD = 76080

AVE HT = 279.5

UT = 19.00



MSIS 86 NEUTRAL TEMPERATURE (K)



LOG TGCM O NUMBER DENSITY (CM-3)

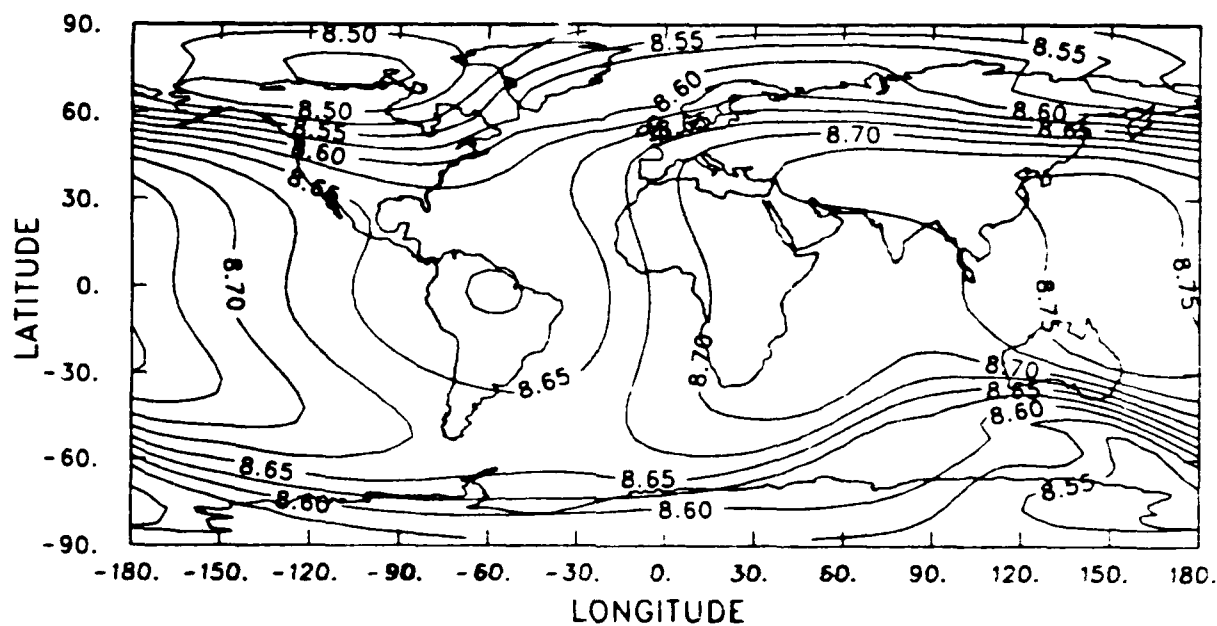
ECR245,246

Z = 2.0

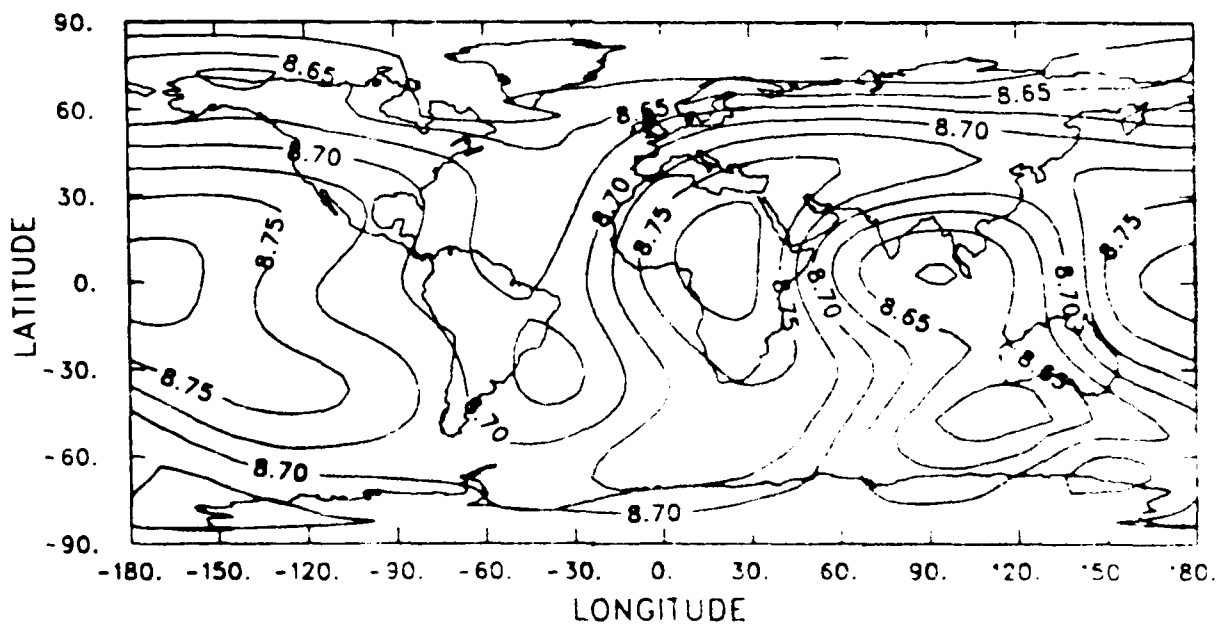
YD = 76080

AVE HT = 279.5

UT = 19.00



LOG MSIS 86 O NUMBER DENSITY (CM-3)



LOG TGCM O2 NUMBER DENSITY (CM-3)

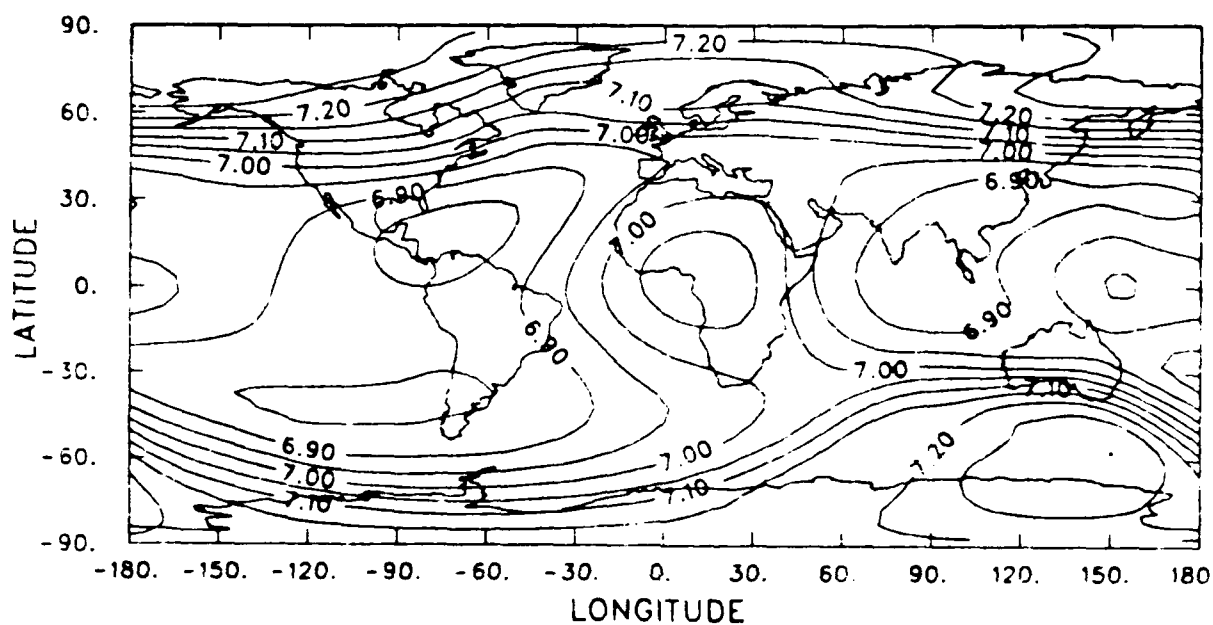
ECR245,246

Z = 2.0

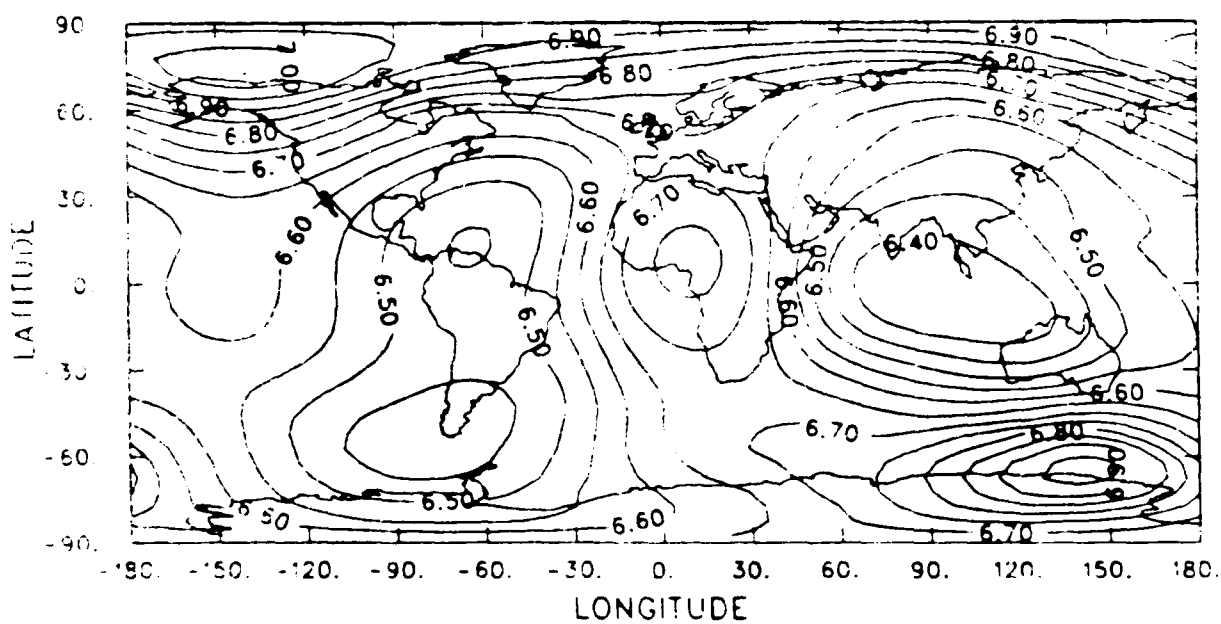
YD = 76080

AVE HT = 279.5

UT = 19.00



LOG MSIS 86 O2 NUMBER DENSITY (CM-3)



LOG TGCM N2 NUMBER DENSITY (CM-3)

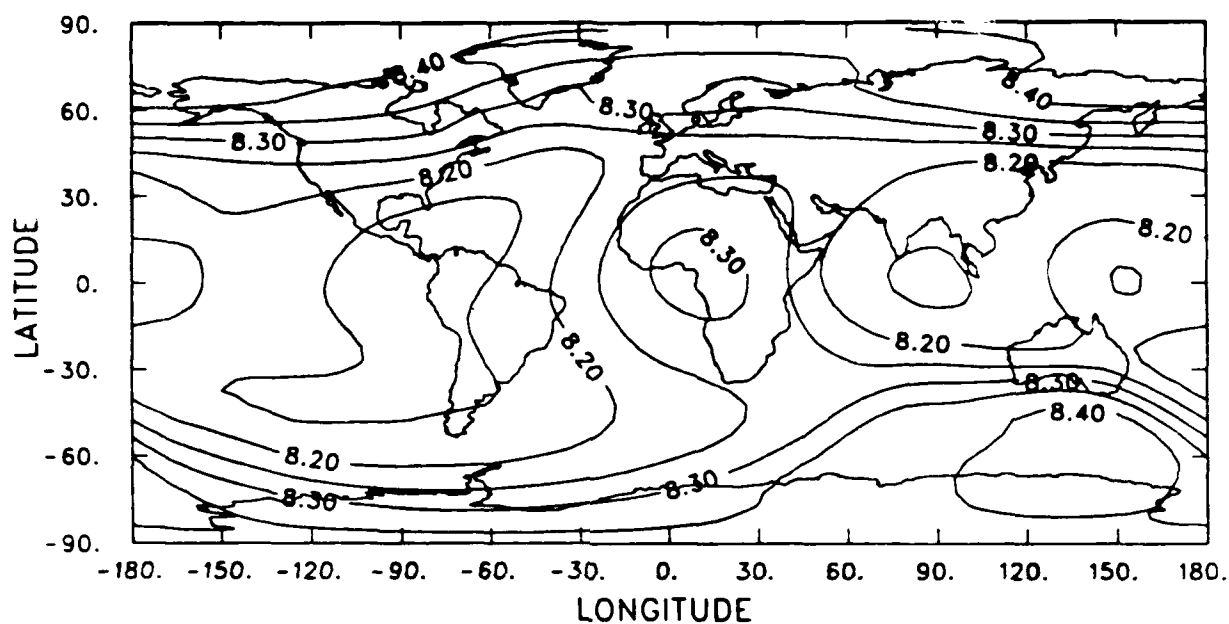
ECR245,246

Z = 2.0

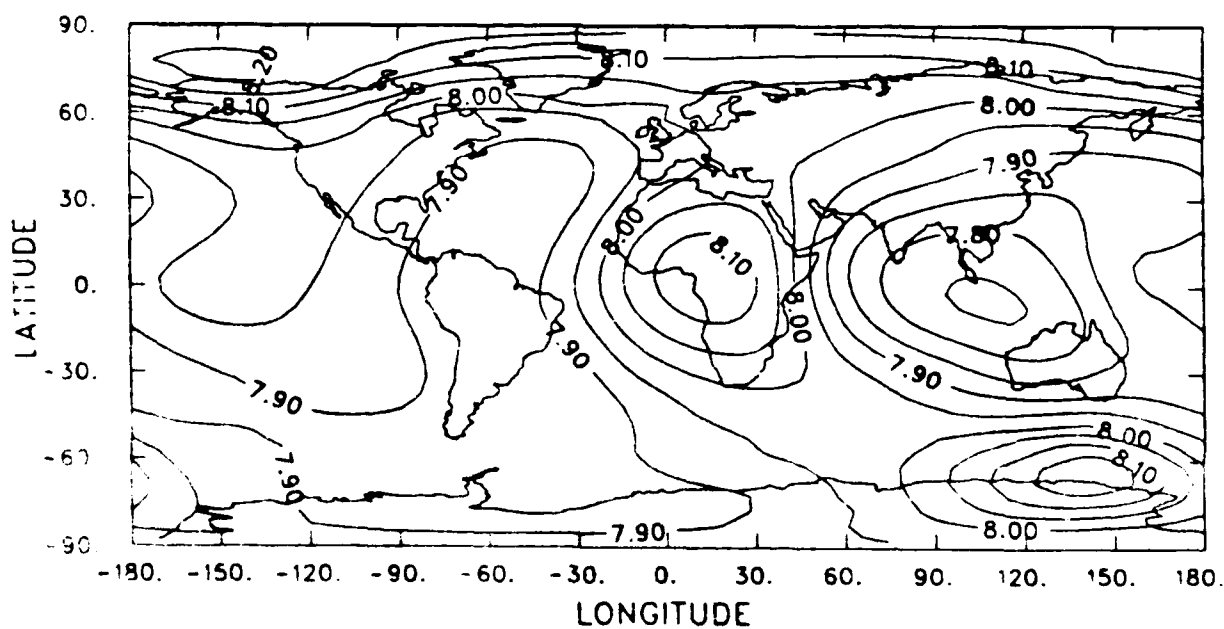
YD = 76080

AVE HT = 279.5

UT = 19.00



LOG MSIS 86 N2 NUMBER DENSITY (CM-3)



LOG TGCM N4S NUMBER DENSITY (CM-3)

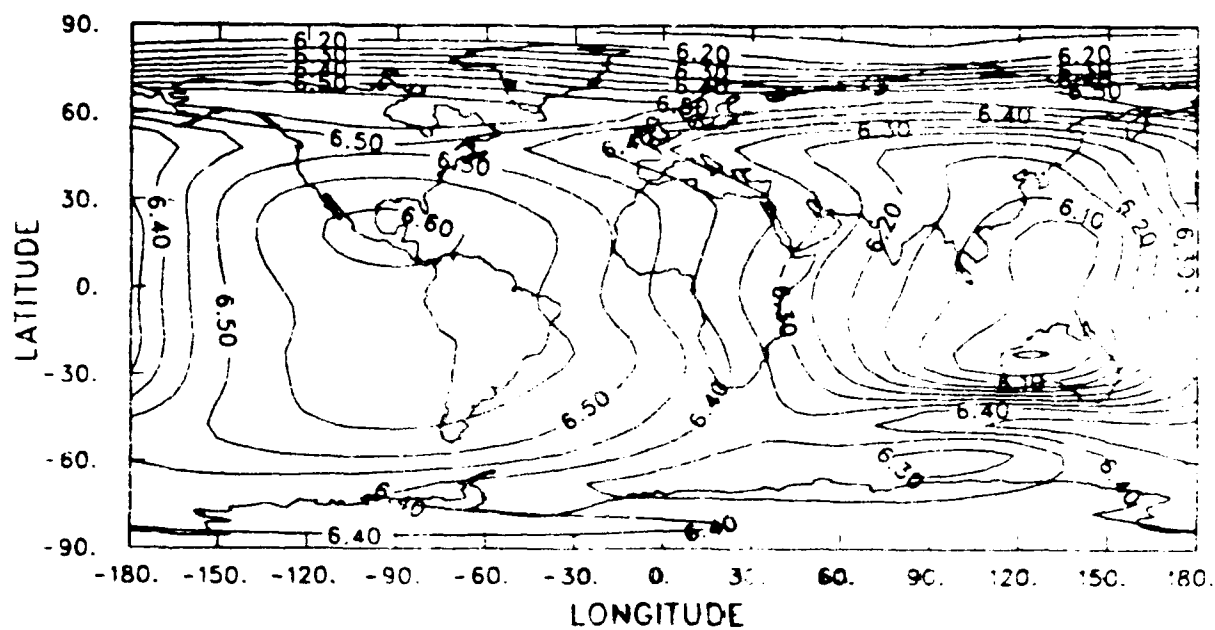
ECR245,246

Z = 2.0

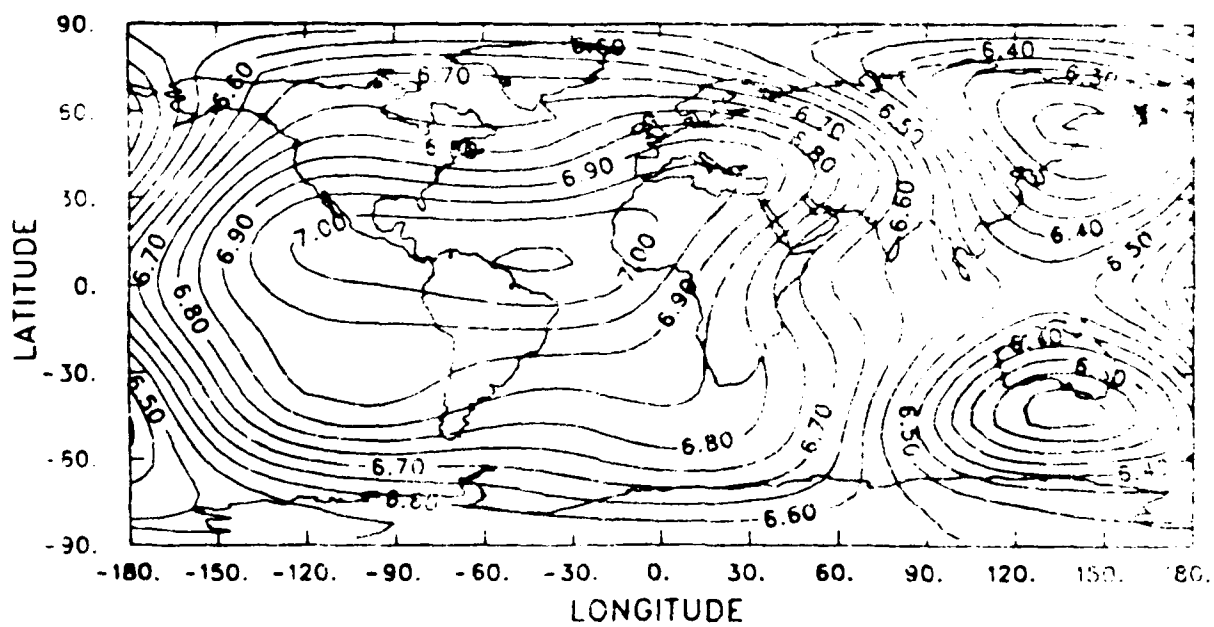
YD = 76080

AVE HT = 279.5

UT = 19.00



LOG MSIS 86 N NUMBER DENSITY (CM-3)



IGCM NEUTRAL TEMPERATURE (K) + (U,V) (M/S)

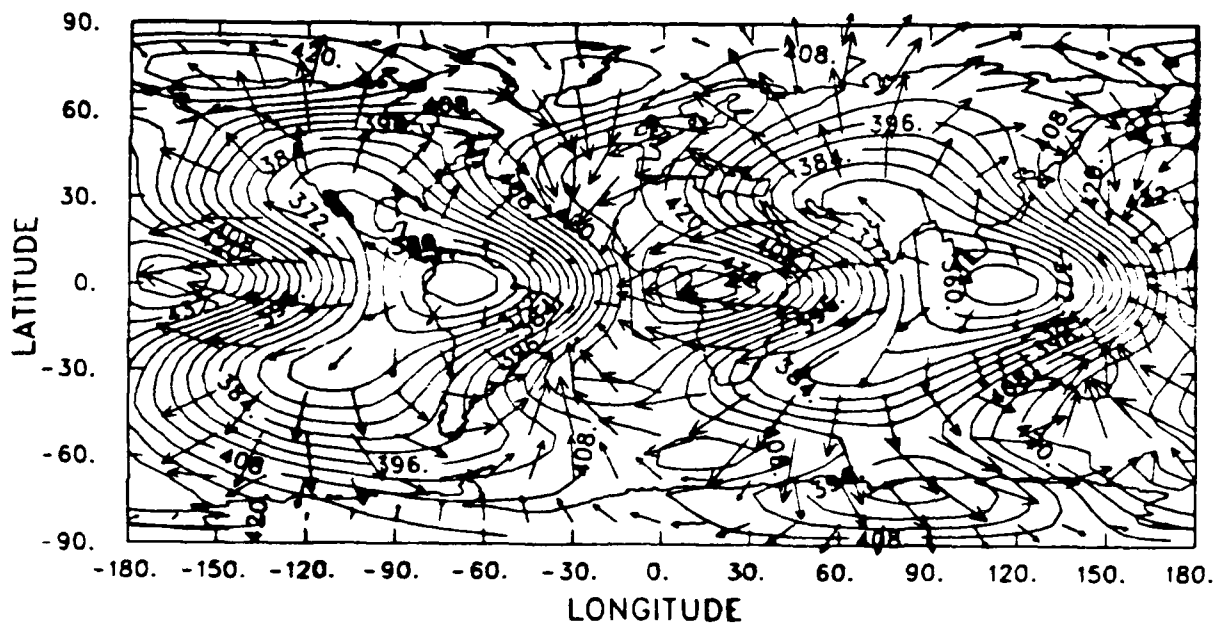
ECR245,246

Z = -4.0

YD = 76081

AVE HT = 123.0

UT = 7.00



LOG TGCM NO NUMBER DENSITY (CM-3)

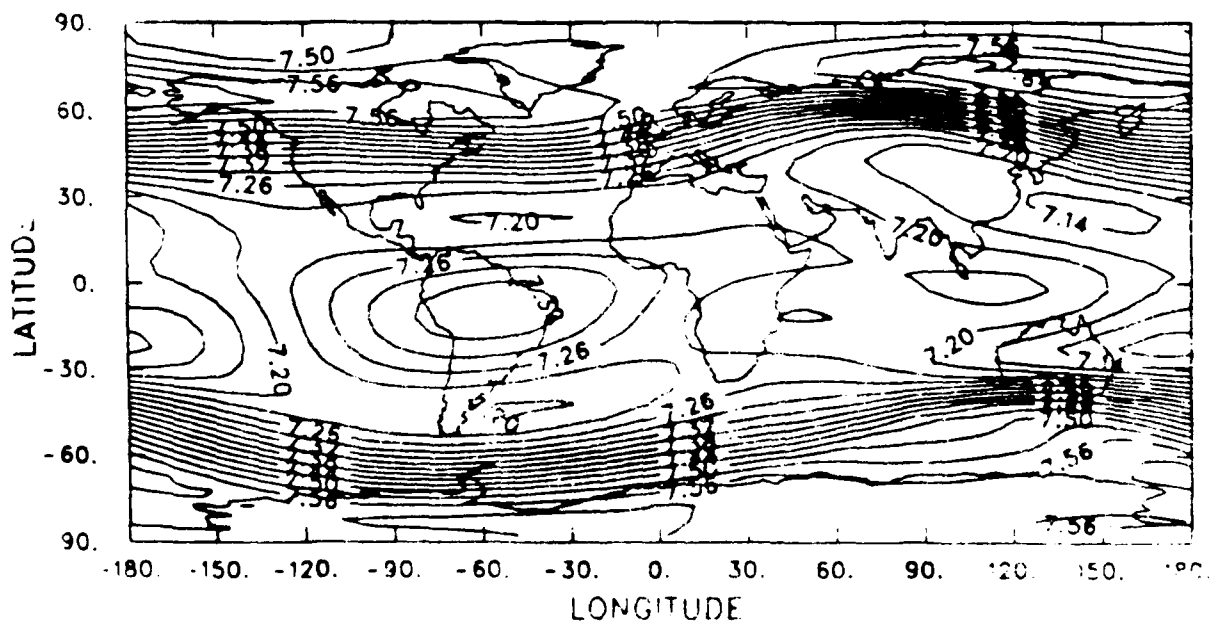
ECR245,246

Z = -4.0

YD = 76080

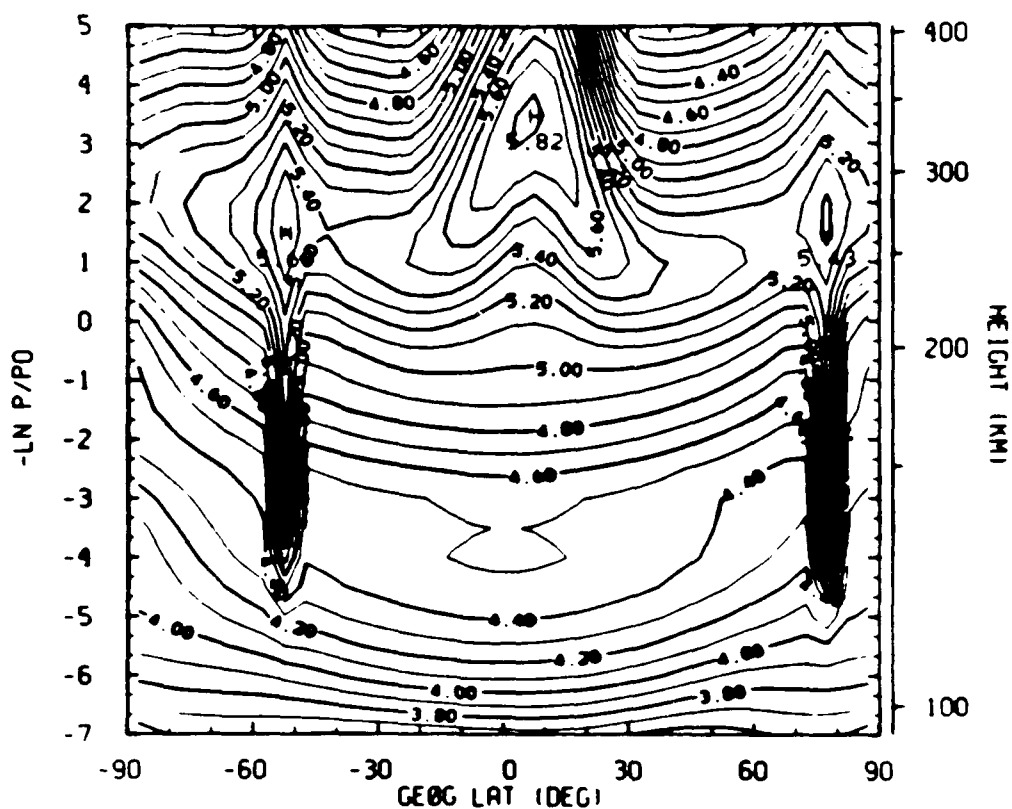
AVE HT = 123.1

UT = 19.00



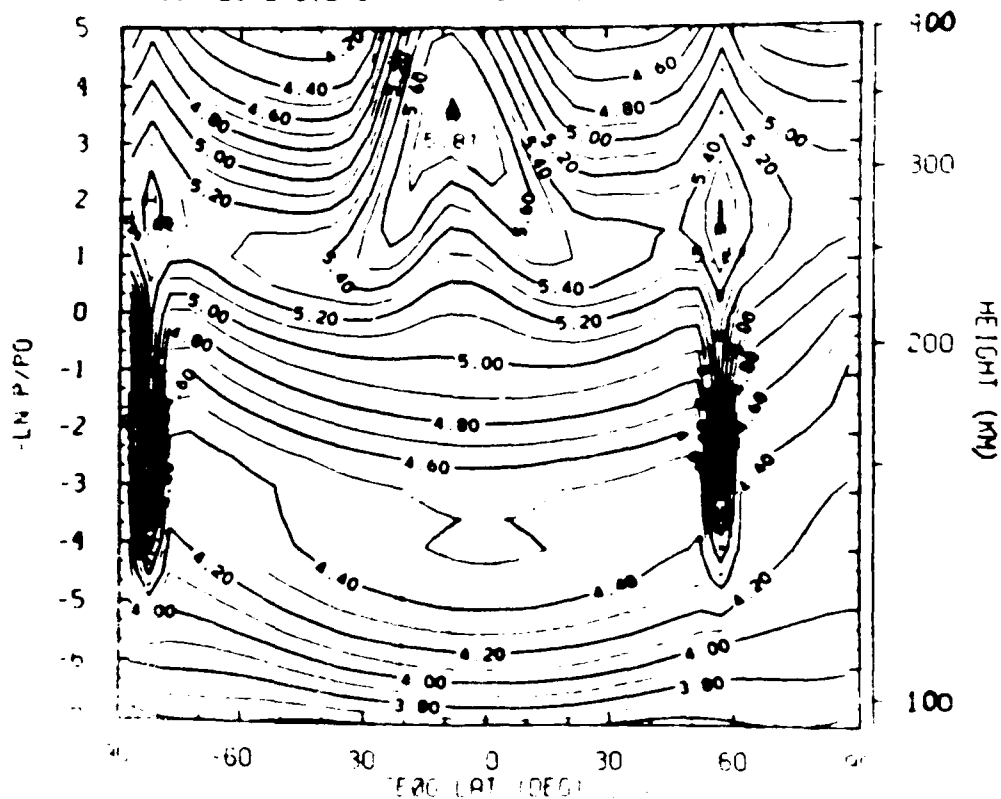
76081 ECR245.246

UT= 7.00 SLT=16.00 LON= 135.00



76080 ECR245.246

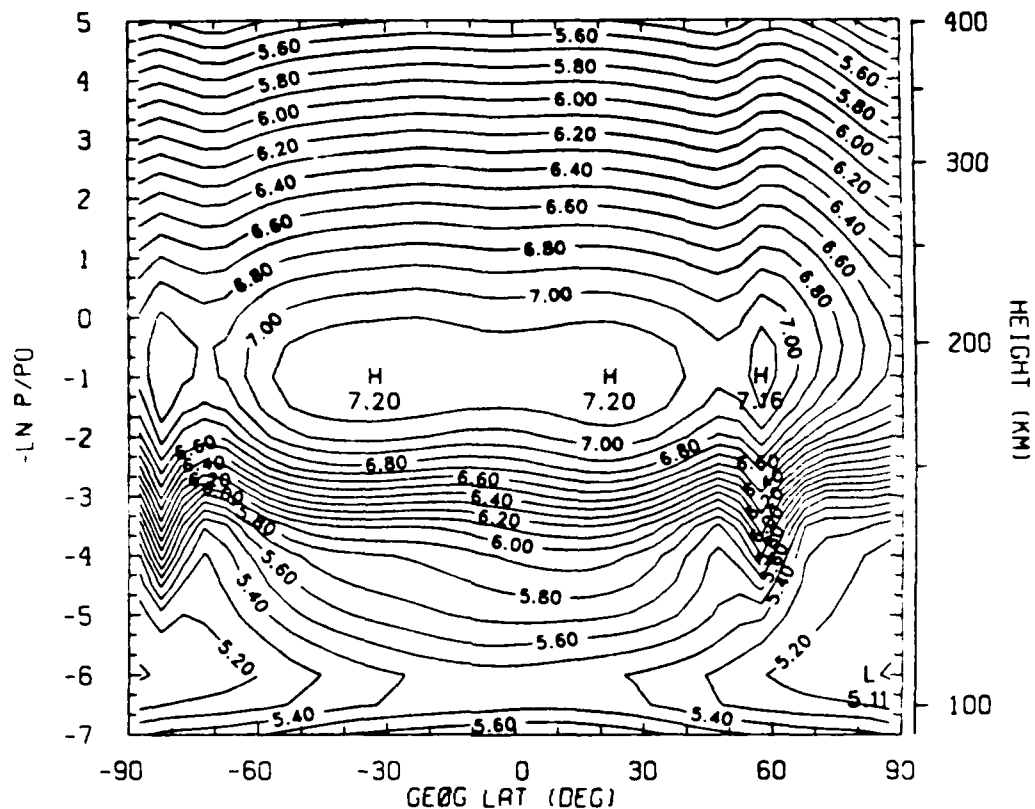
UT=19.00 SLT=16.00 LON 45.00



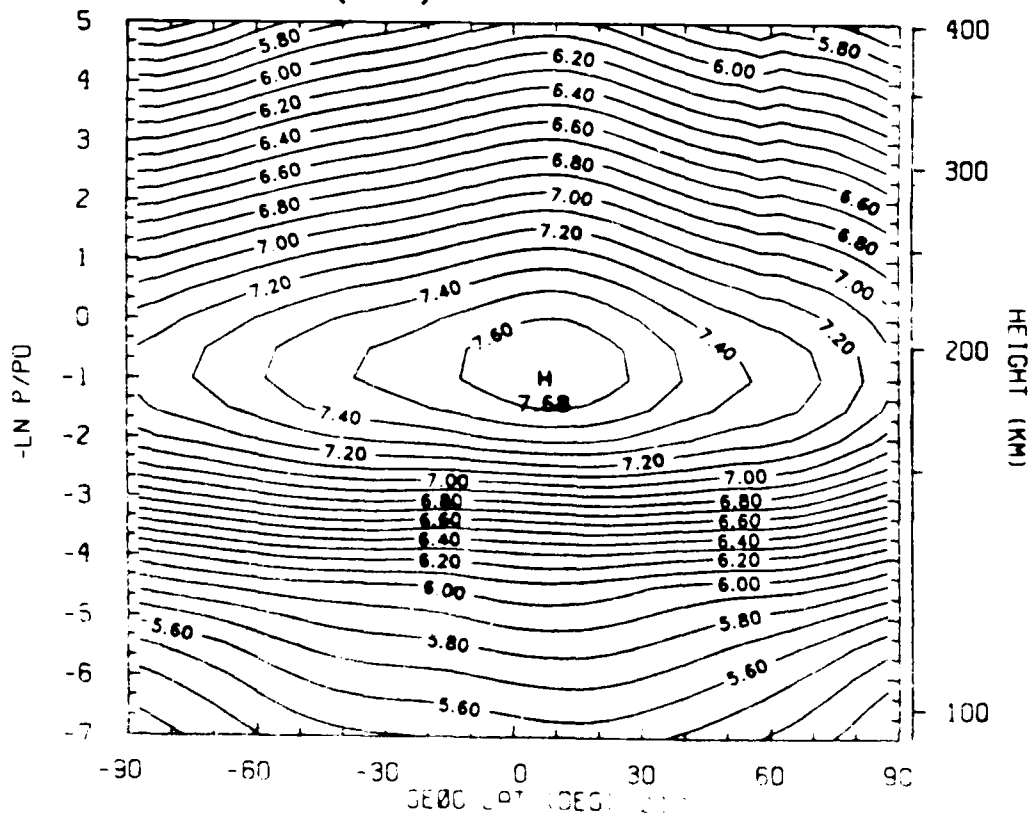
LOG TGCM N4S NUMBER DENSITY (CM-3)

76080 ECR245,246

UT=19.00 SLT=16.00 LON= -45.00



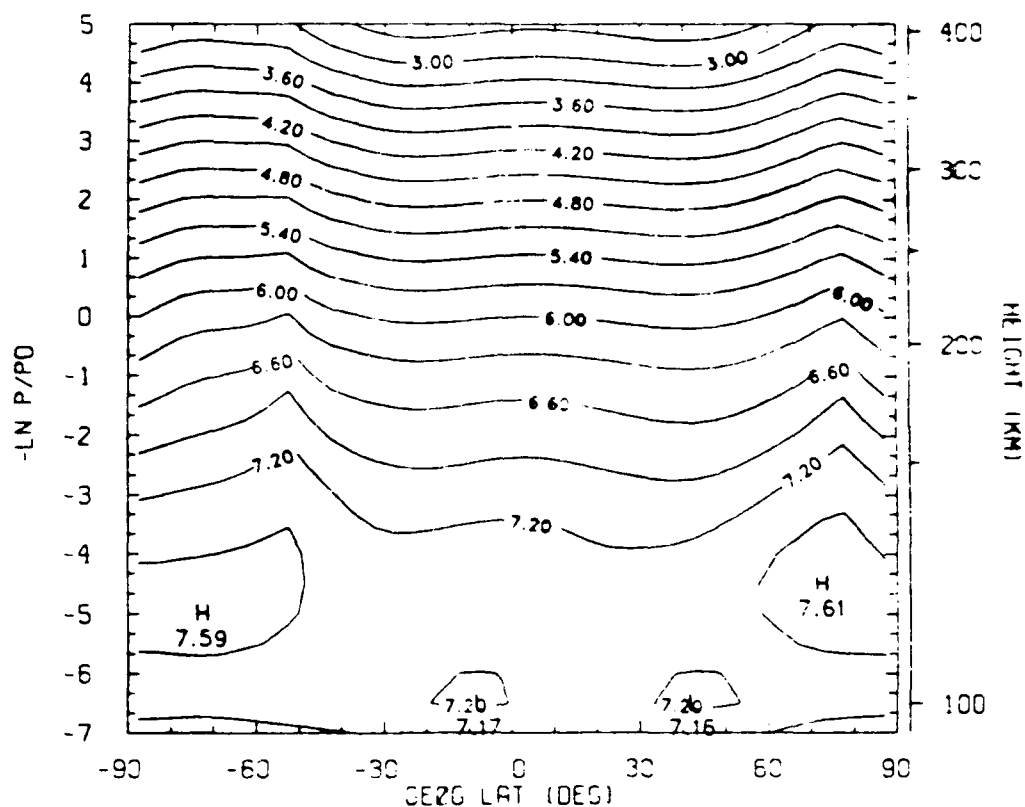
LOG MSIS 86 N (CM-3)



LOG TGCM NO NUMBER DENSITY (CM-3)

76081 ECR245,246

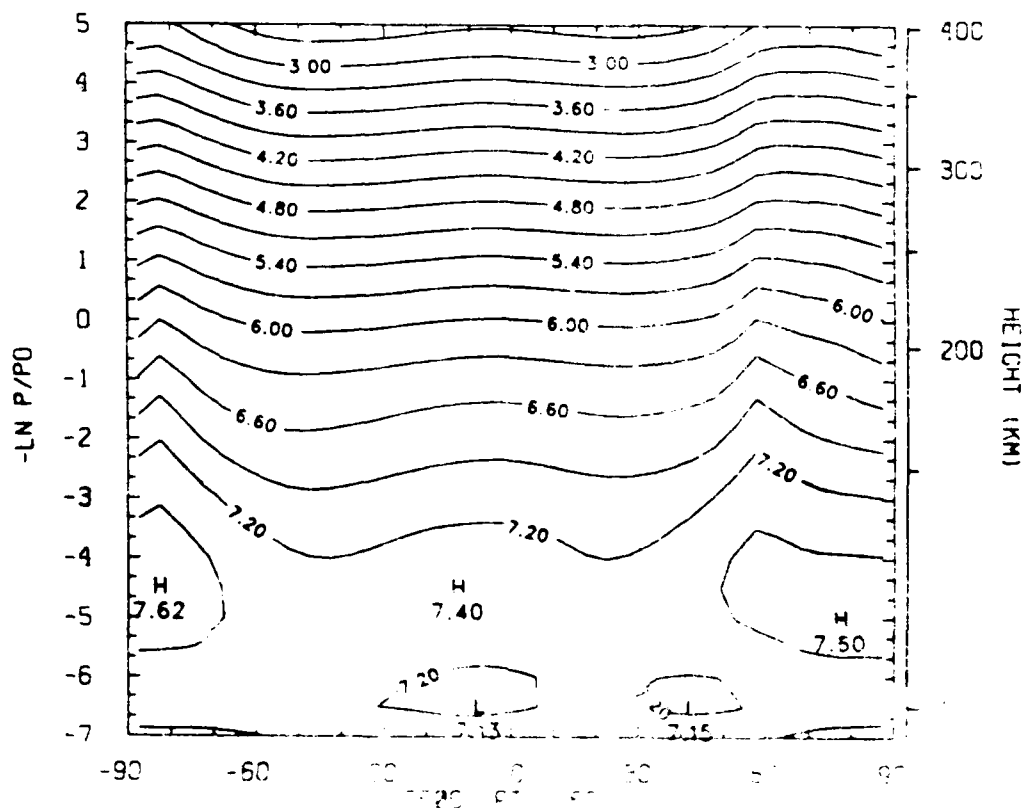
UT= 7.00 SLT=16.00 LON= 135.00



LOG TGCM NO NUMBER DENSITY (CM-3)

76080 ECR245,246

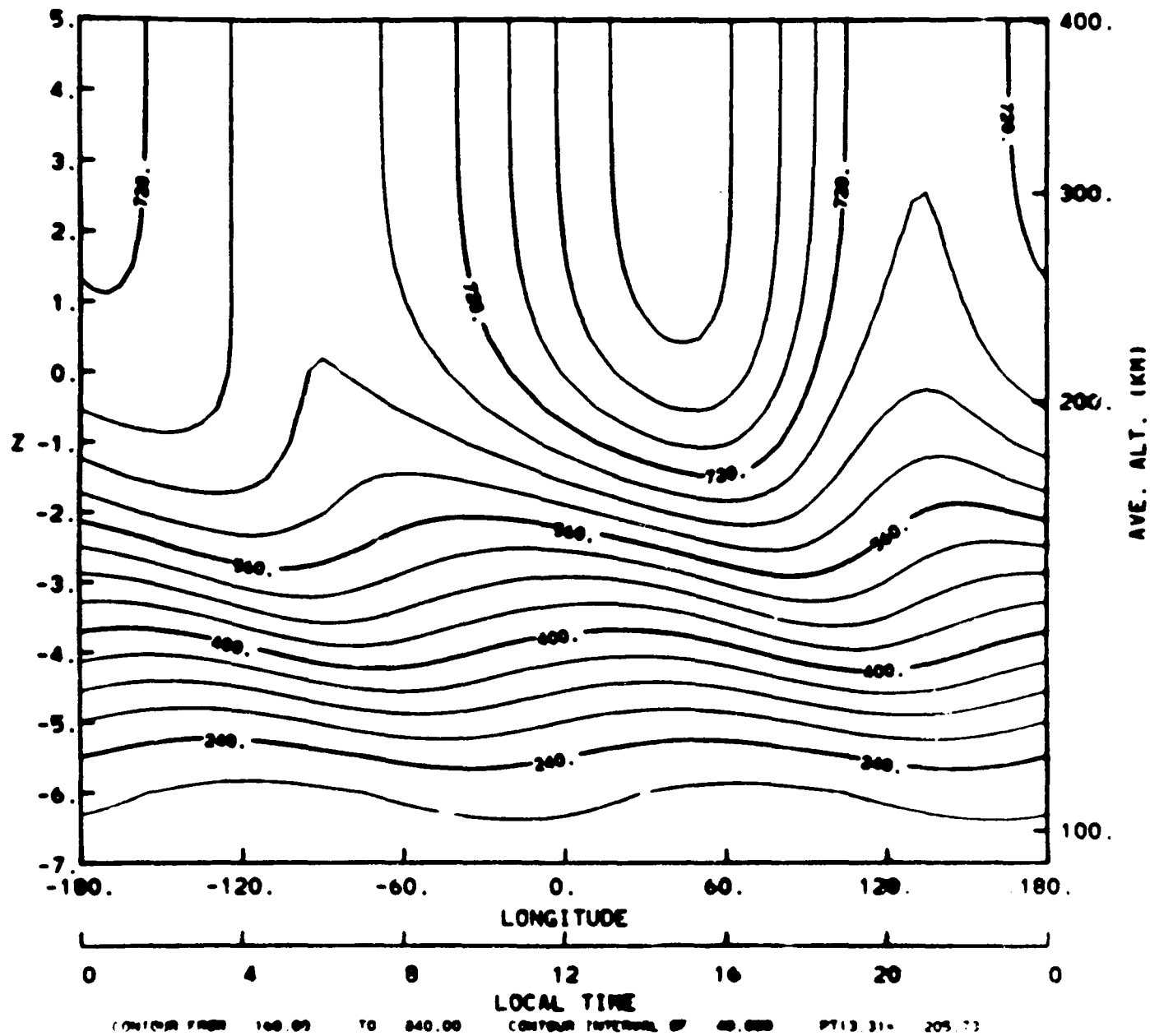
UT=19.00 SLT=16.00 LON= -45.00



UT=12. 0

FIELD=T

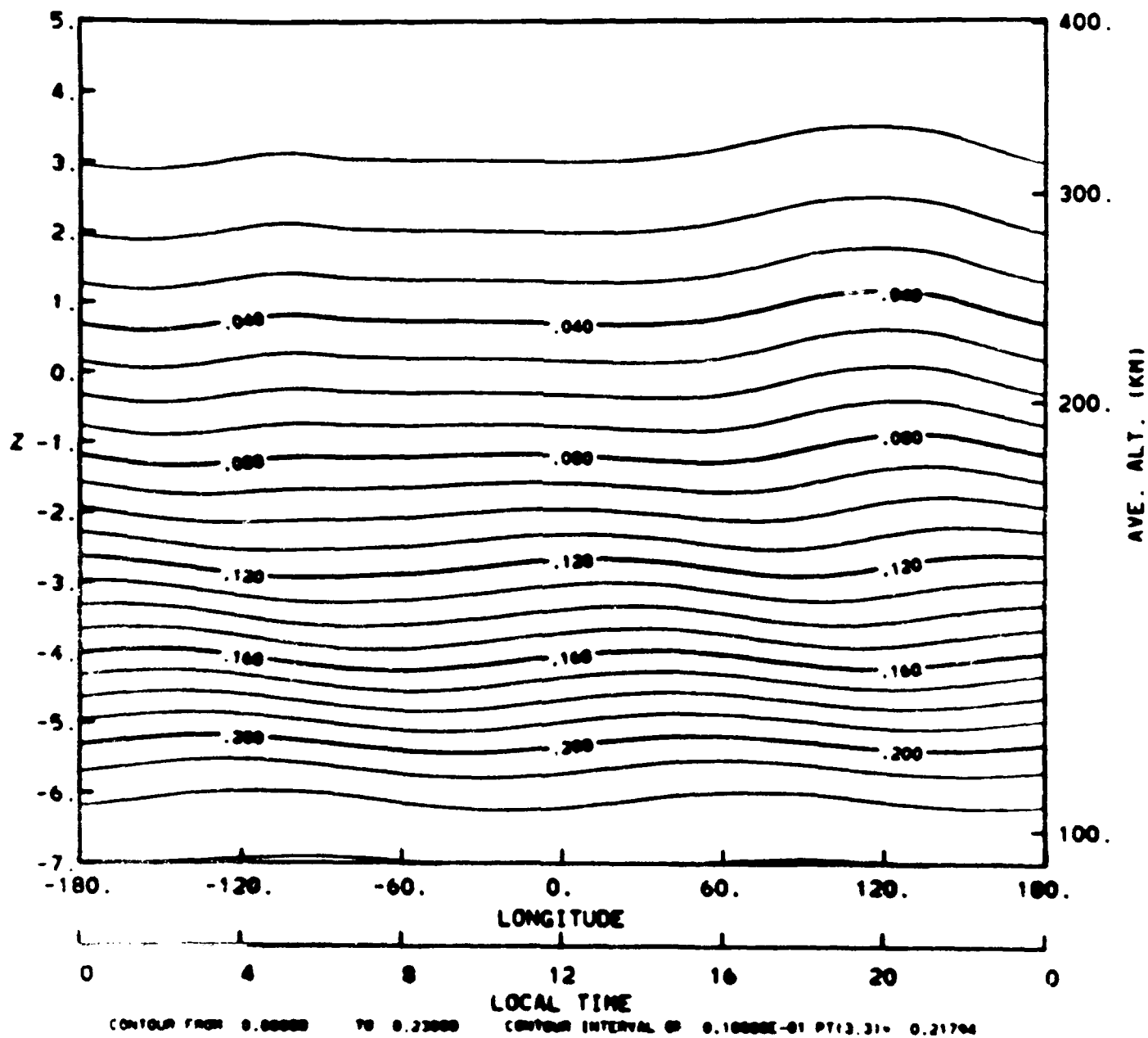
17.5N



UT=12. 0

PSI(02)

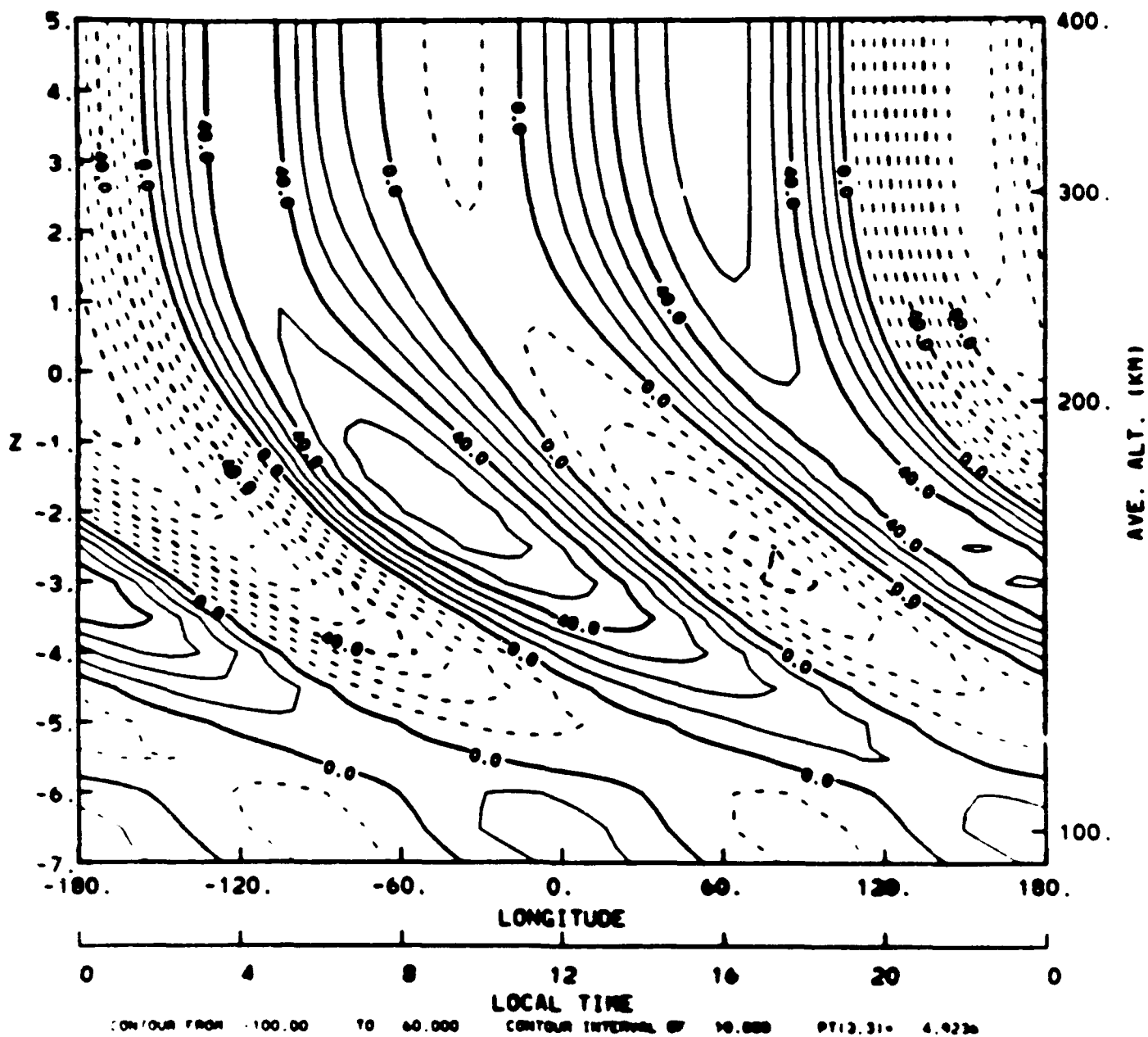
17.5N



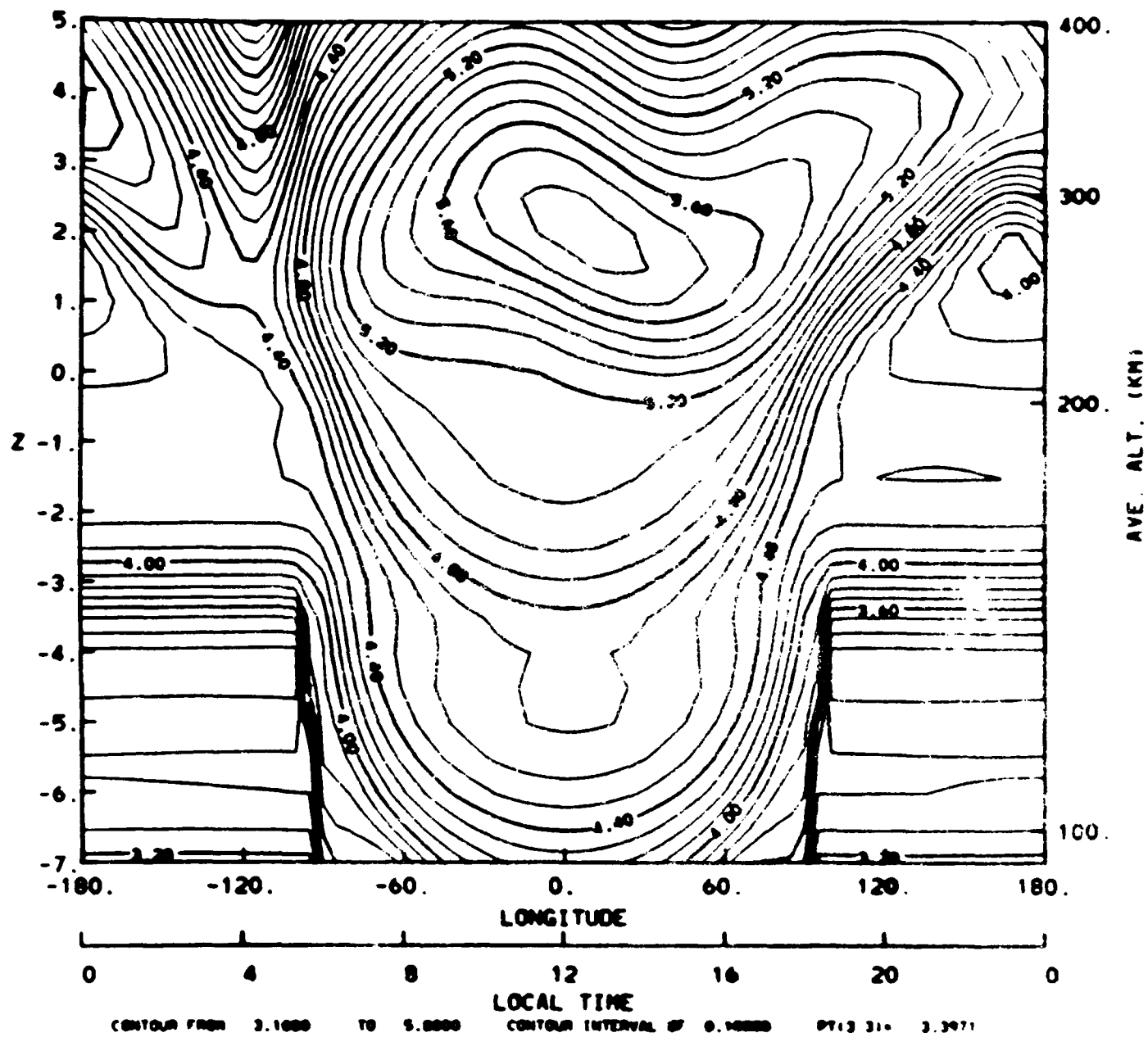
UT=12.0

FIELD=V

17.5N



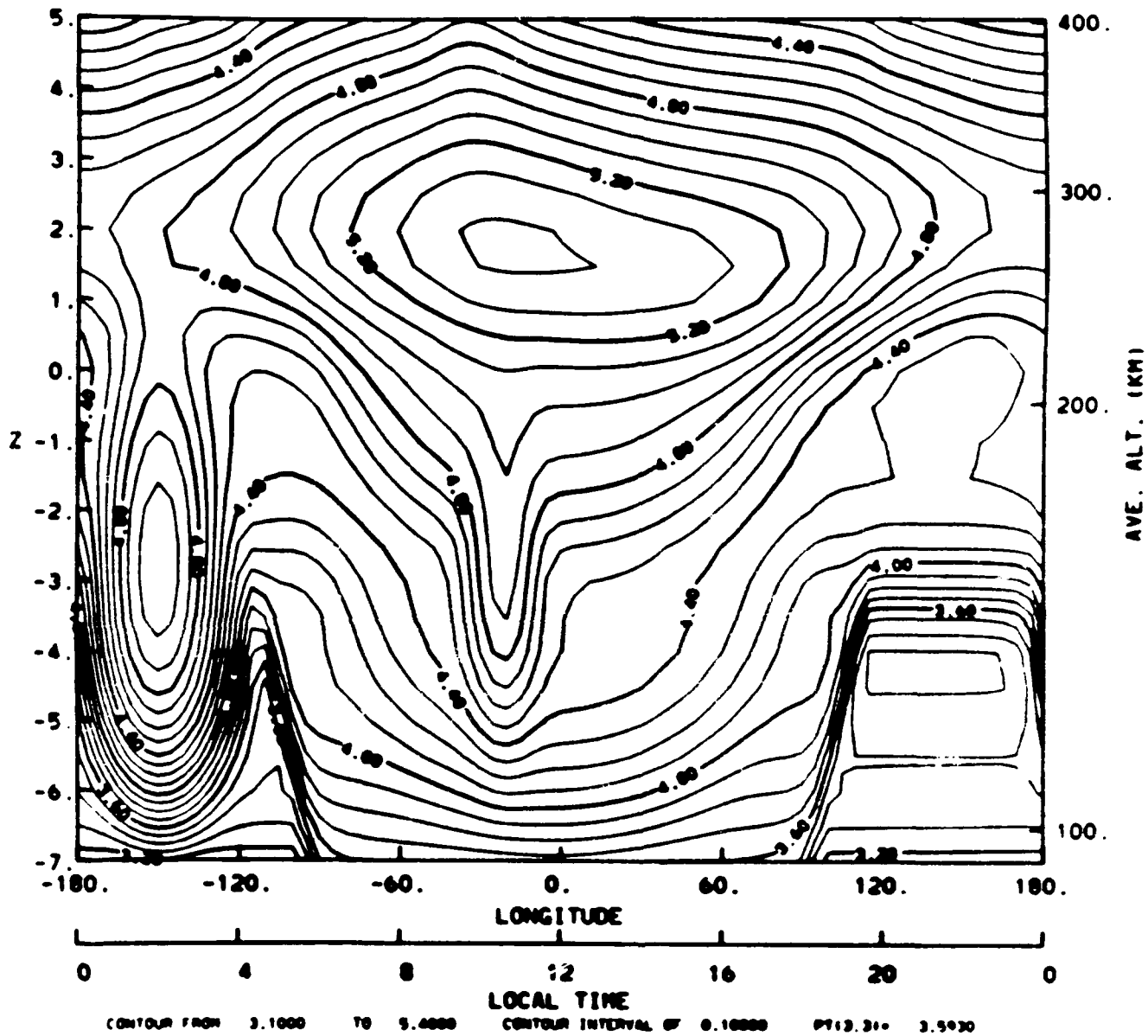
17.5M



UT=12.0

FLD=NE

67.5N



HEELIS VI (M/S) + POTENTIAL (KEV)

ECR245,246

YD = 76080

UT = 19.00

LOCAL TIME

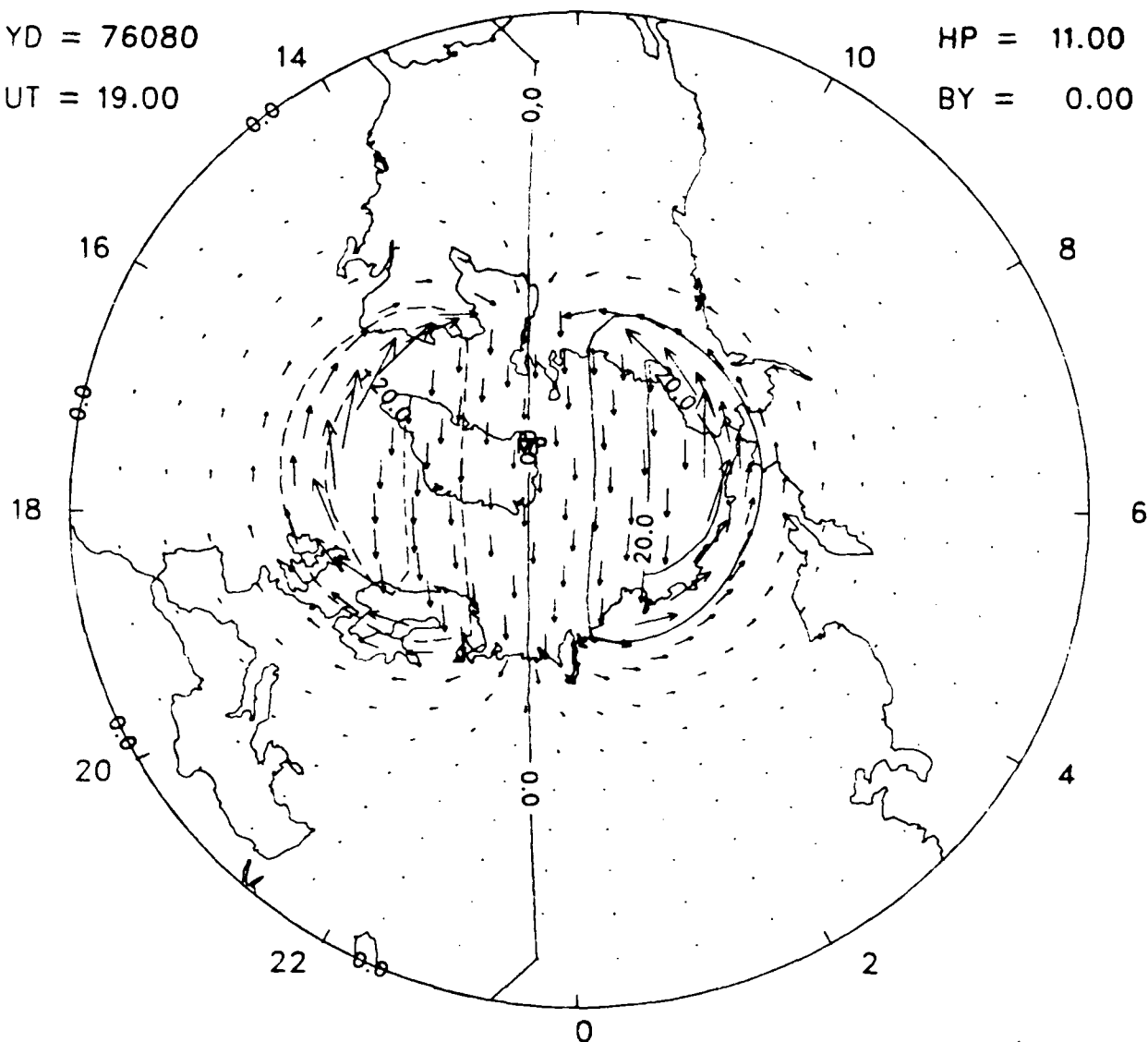
12

27.5 N

CP = 60.00

HP = 11.00

BY = 0.00



FRAME 301

800 M/S

CONTOUR FROM -20.000 TO 20.000 CONTOUR INTERVAL OF 10.000 PT(3,3)= 1.3047

TGCM NEUTRAL TEMPERATURE (K) + (U,V) (M/S)

27.5 N

ECR245,246

LOCAL TIME

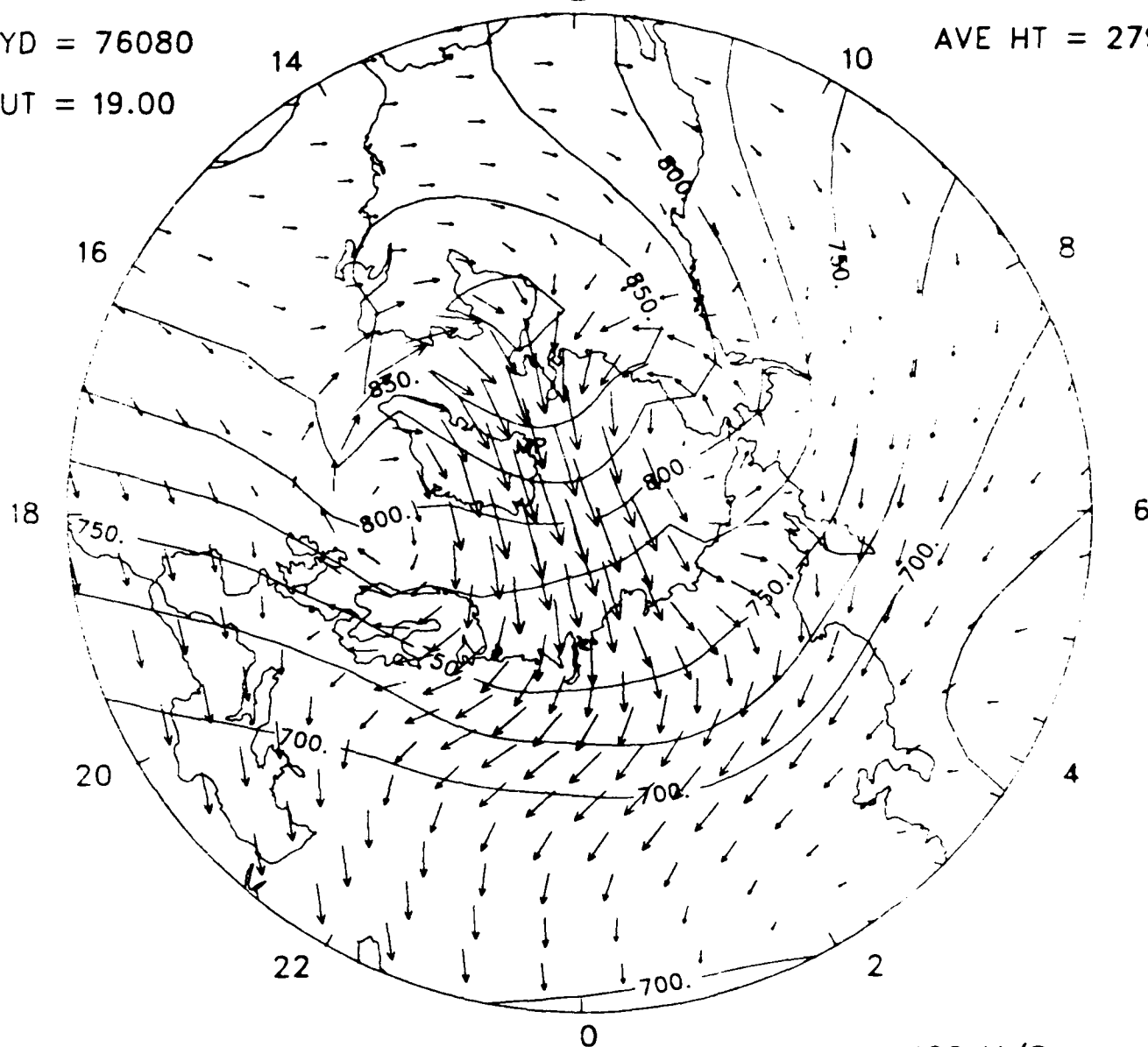
Z = 2.0

YD = 76080

12

AVE HT = 279.2

UT = 19.00



RAME 274

400 M/S

CONTOUR FROM 650.00 TO 875.00 CONTOUR INTERVAL OF 25.000 PT(3,3)= 715.13

LOG TGCM ELECTRON DENSITY (HIST) (CM-3)
LOCAL TIME

ECR245,246

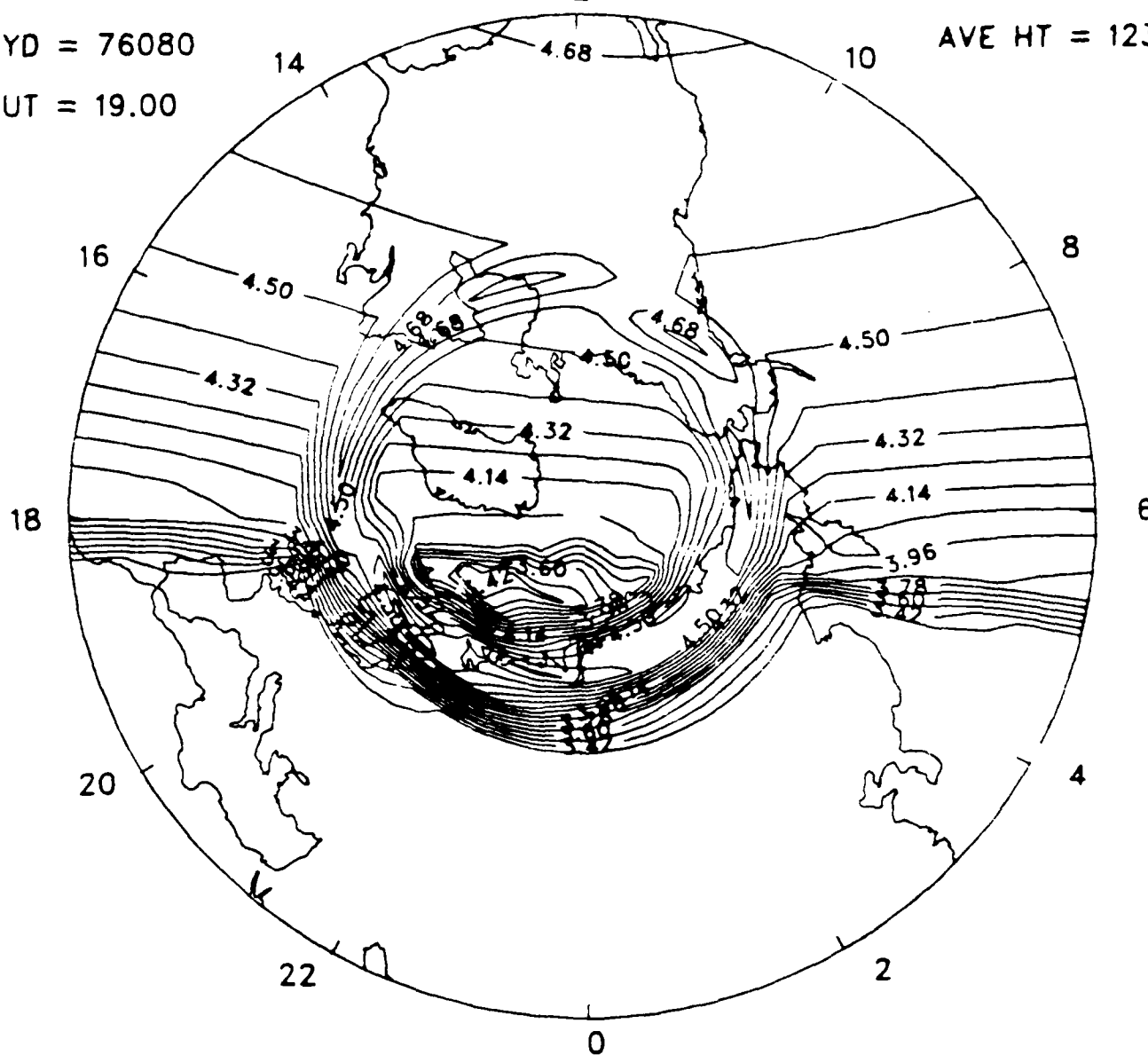
YD = 76080

UT = 19.00

27.5 N

Z = -4.0

AVE HT = 123.2



FRAME 228

CONTOUR FROM 3.2400 TO 4.7700 CONTOUR INTERVAL OF 0.90000E-01 PT(3,3)= 4.4848

LOG TGCM ELECTRON DENSITY (HIST) (CM-3)

ECR245,246

YD = 76080

UT = 19.00

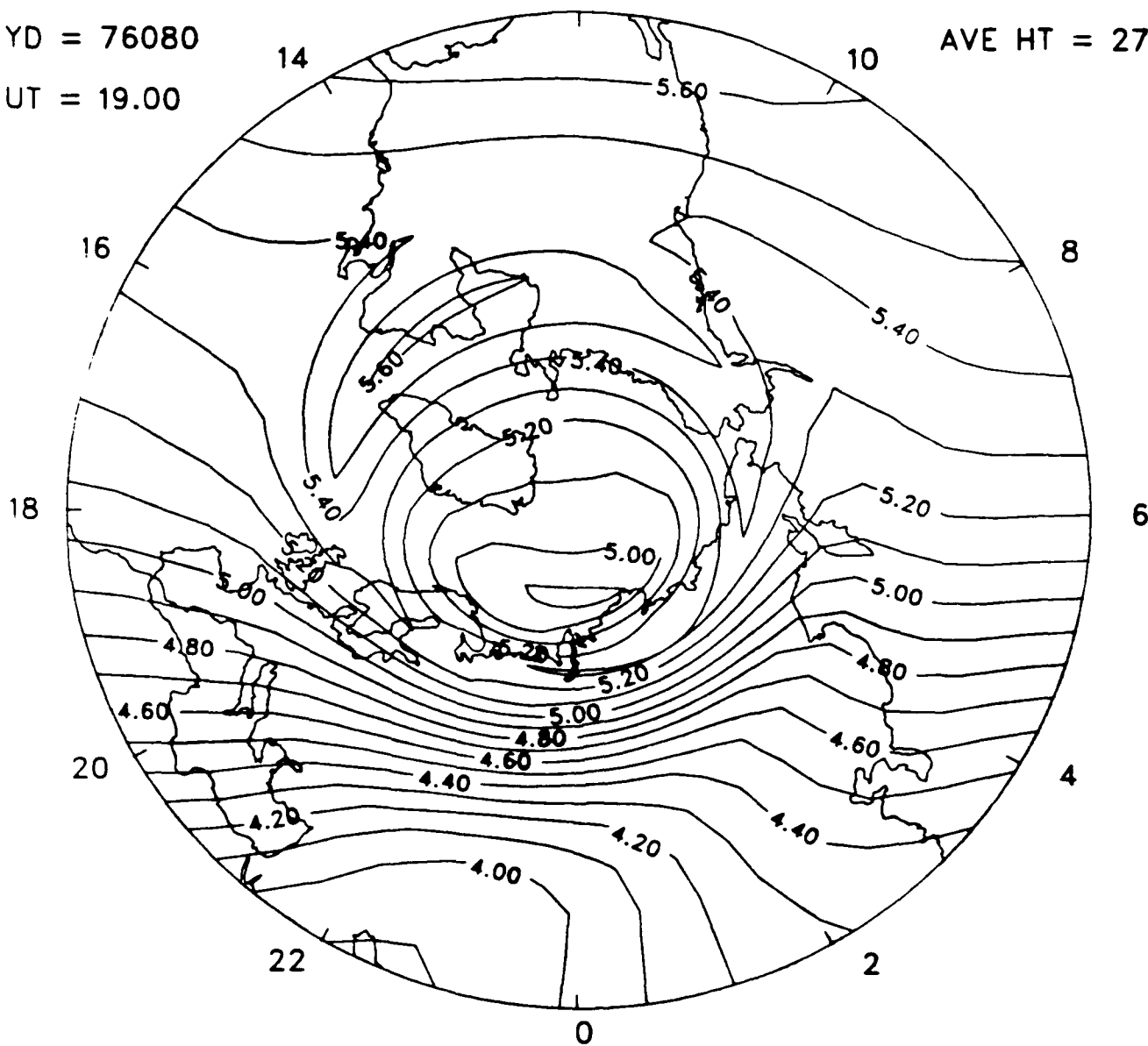
LOCAL TIME

12

27.5 N

Z = 2.0

AVE HT = 279.2



FRAME 282

CONTOUR FROM 3.8000 TO 5.6000 CONTOUR INTERVAL OF 0.10000 PT(3,3)= 5.4188

27.5 N

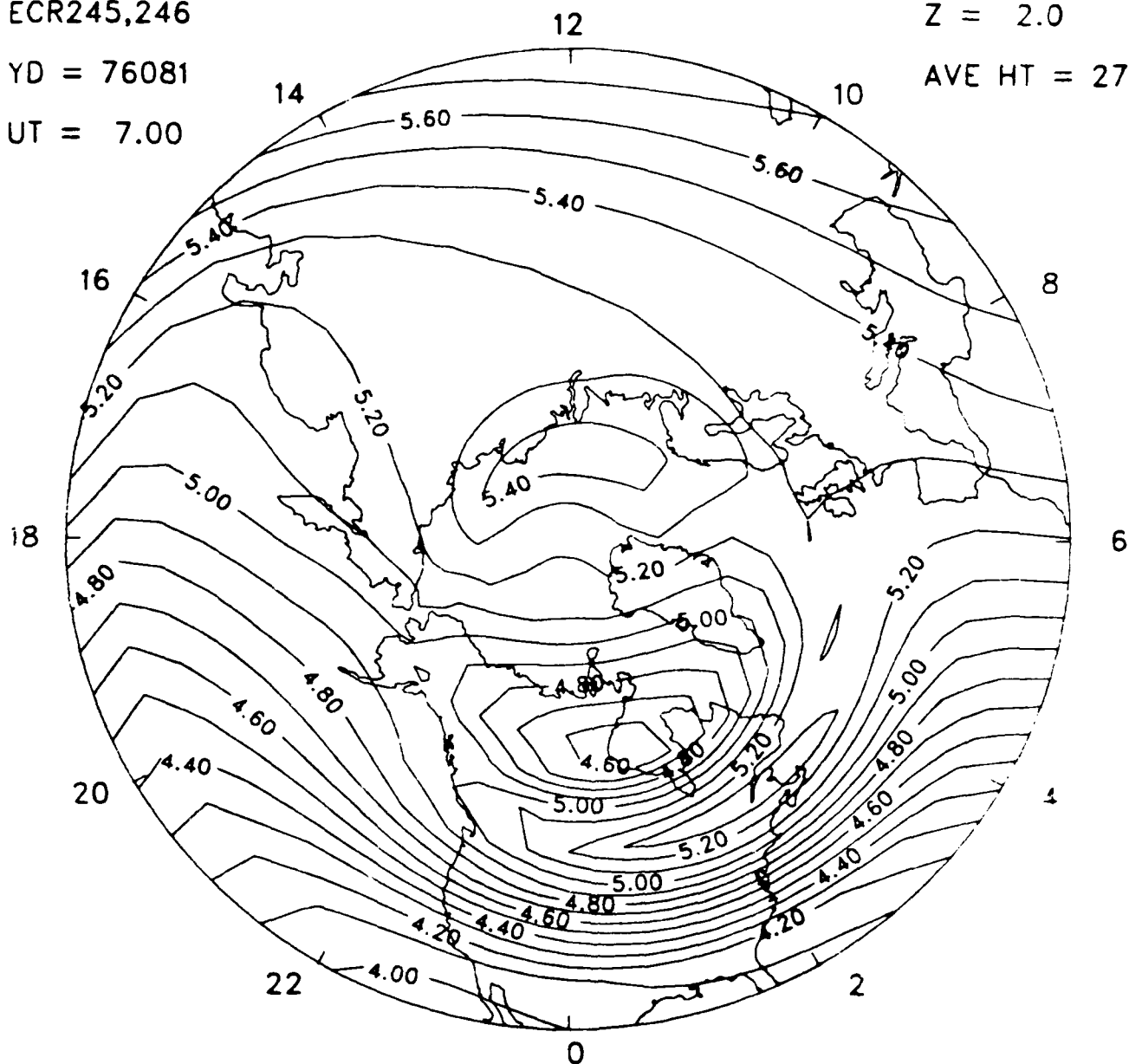
LOCAL TIME

$$Z = 2.0$$

YD = 76081

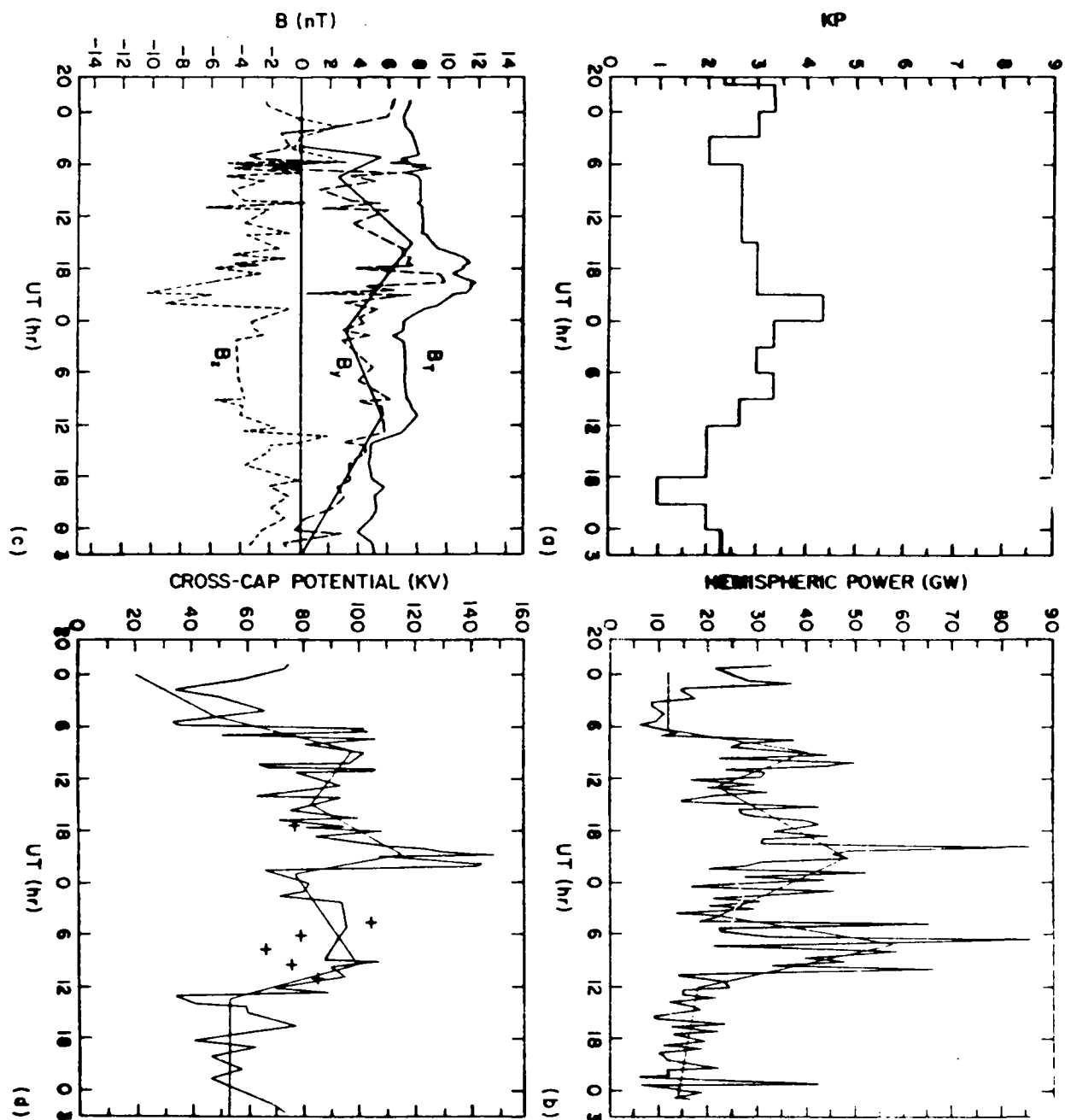
AVE HT = 279.9

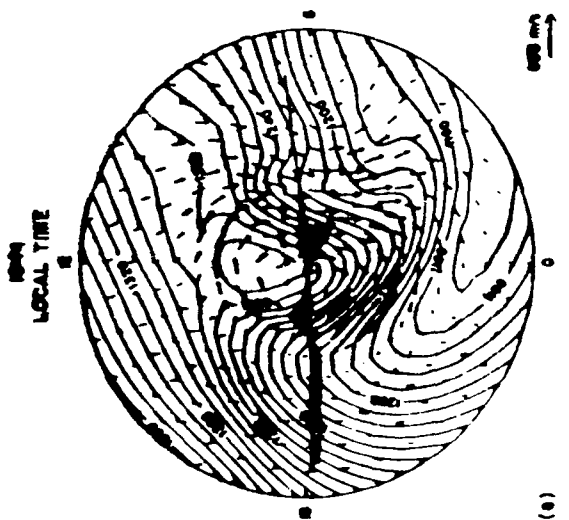
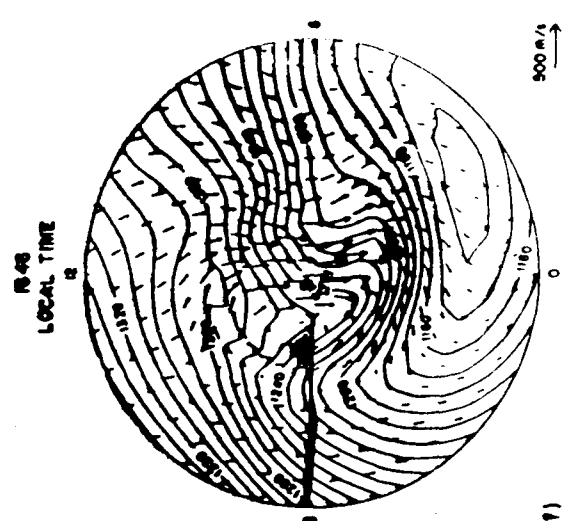
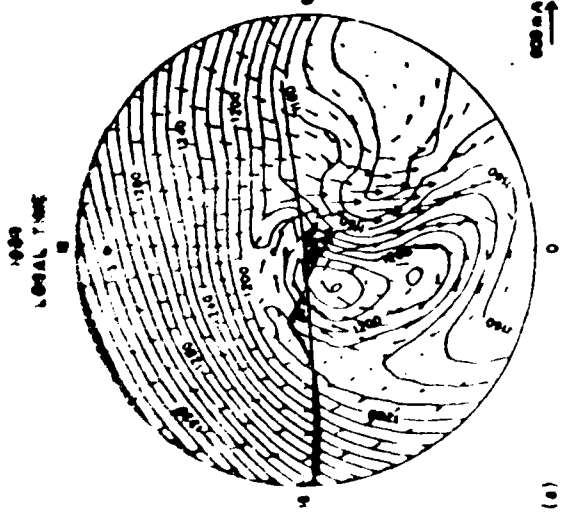
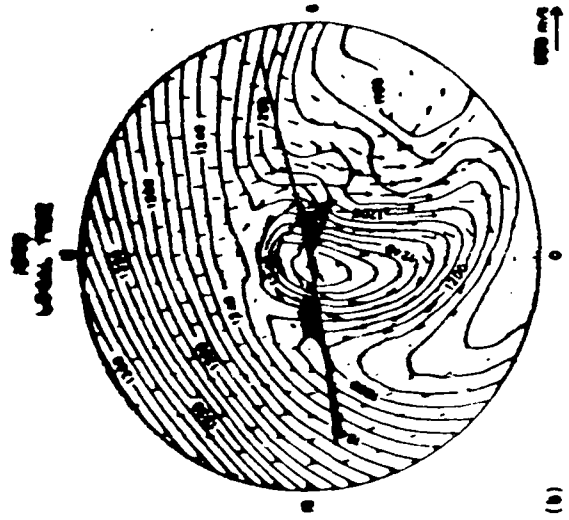
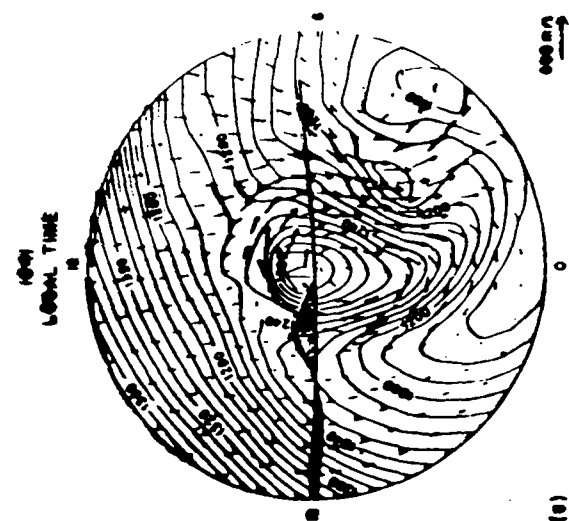
UT = 7.00

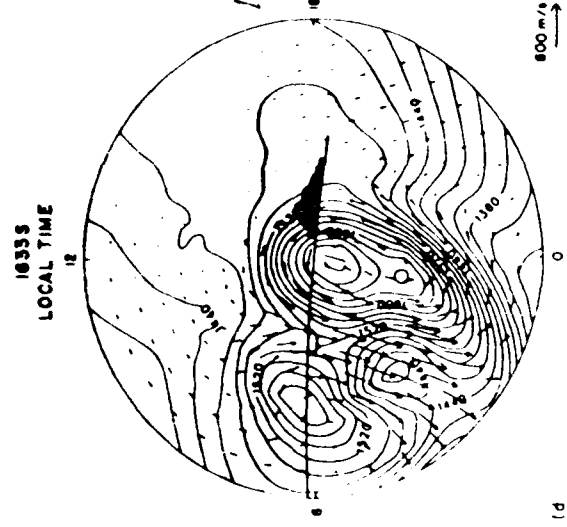
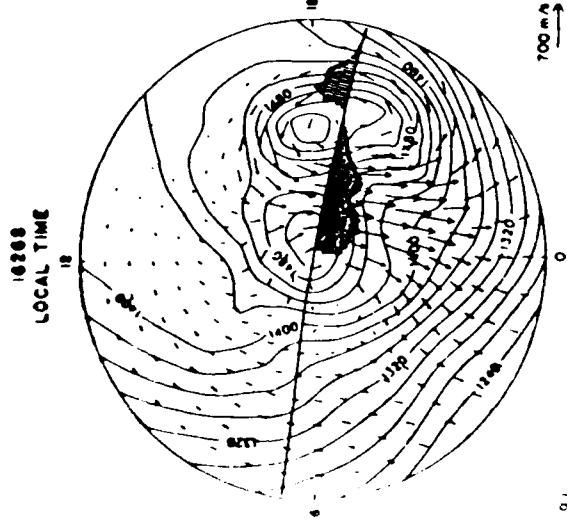
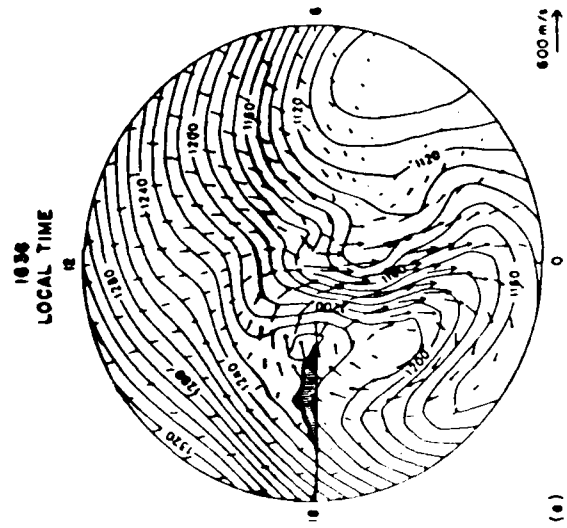
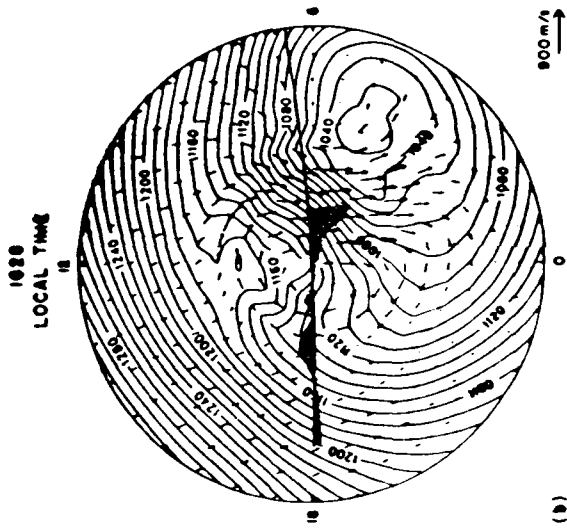
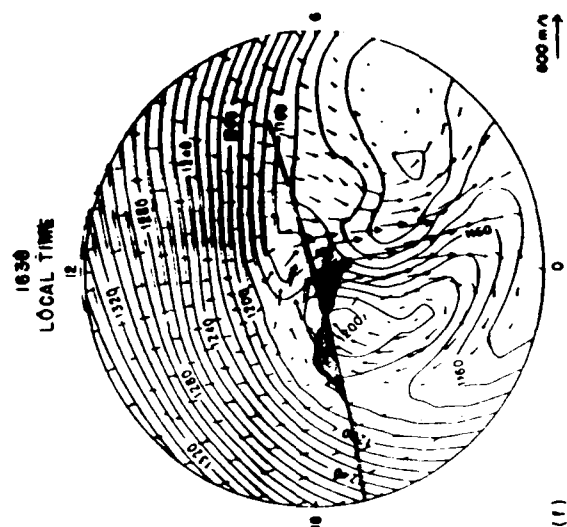
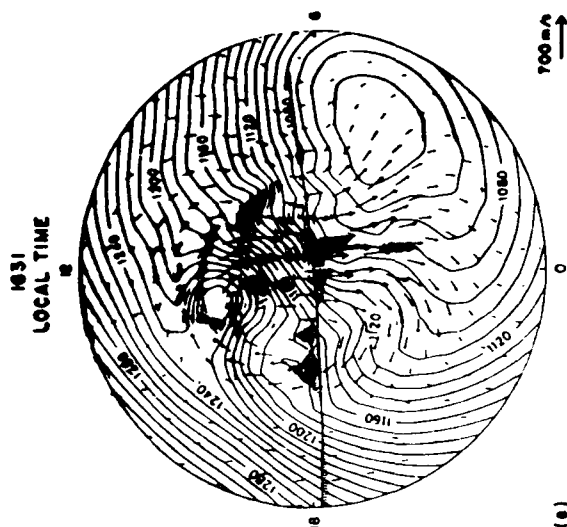


FRAME 582

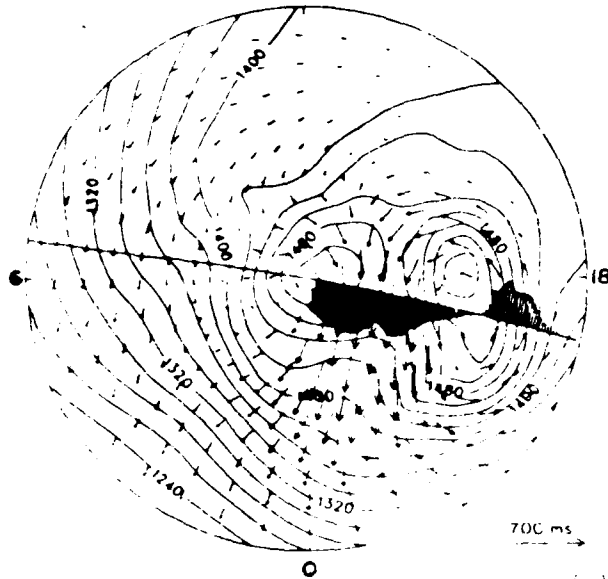
CONTOUR FROM 3.9000 TO 5.7000 CONTOUR INTERVAL OF 0.10000 PT(3,3)= 4.5245



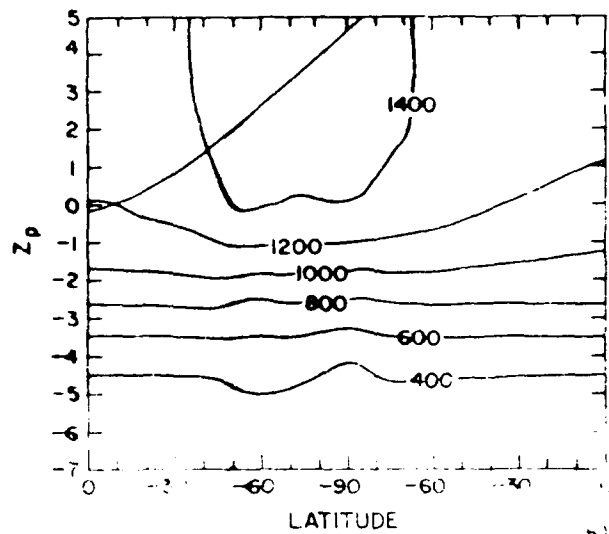




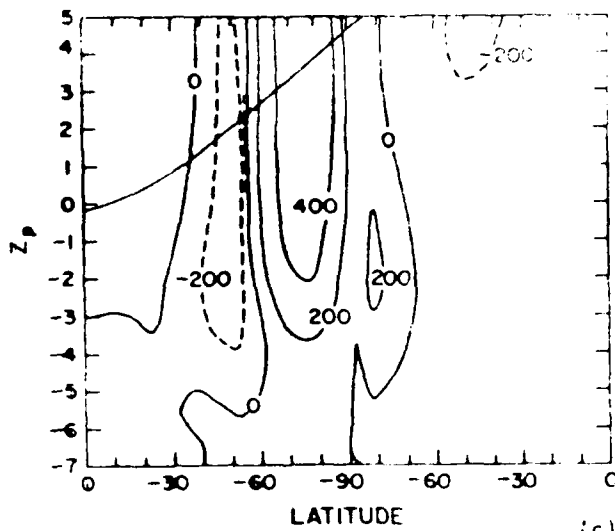
1626S
LOCAL TIME
12



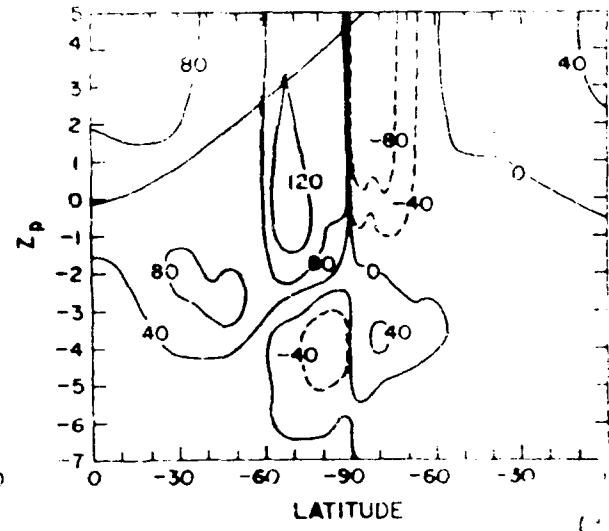
(a)



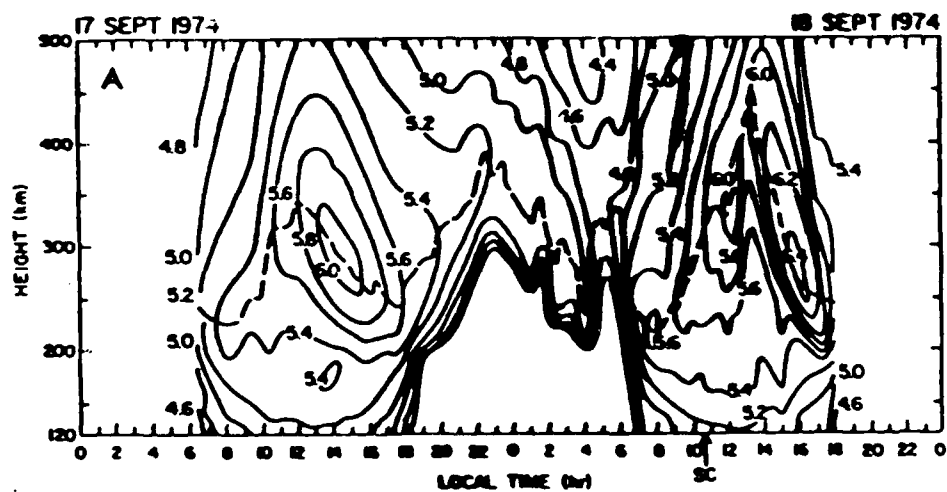
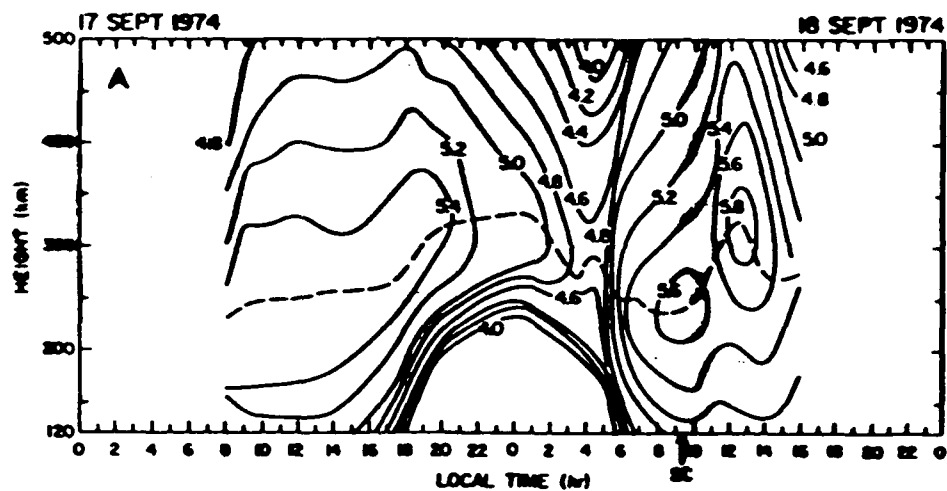
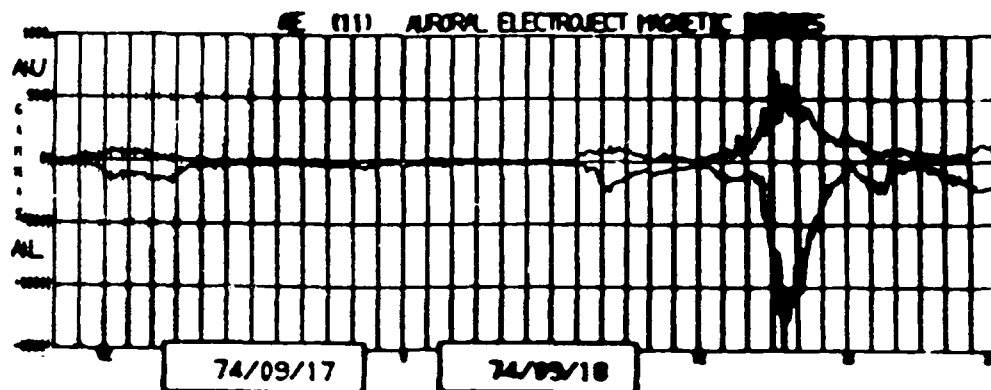
(b)



(c)

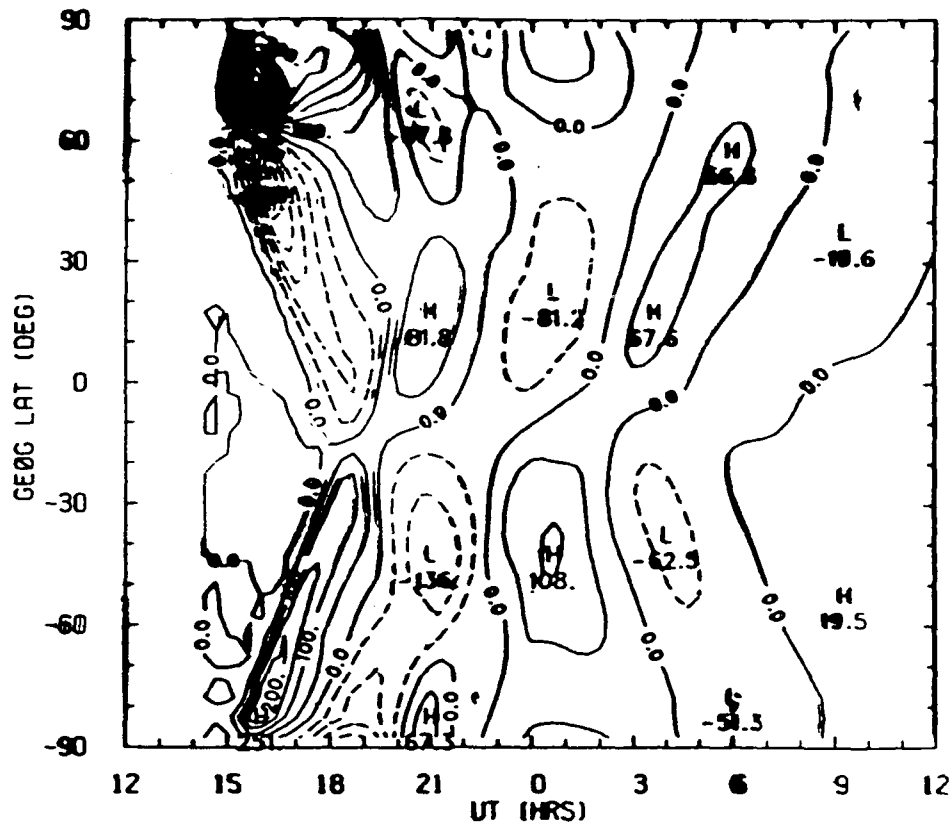


(d)



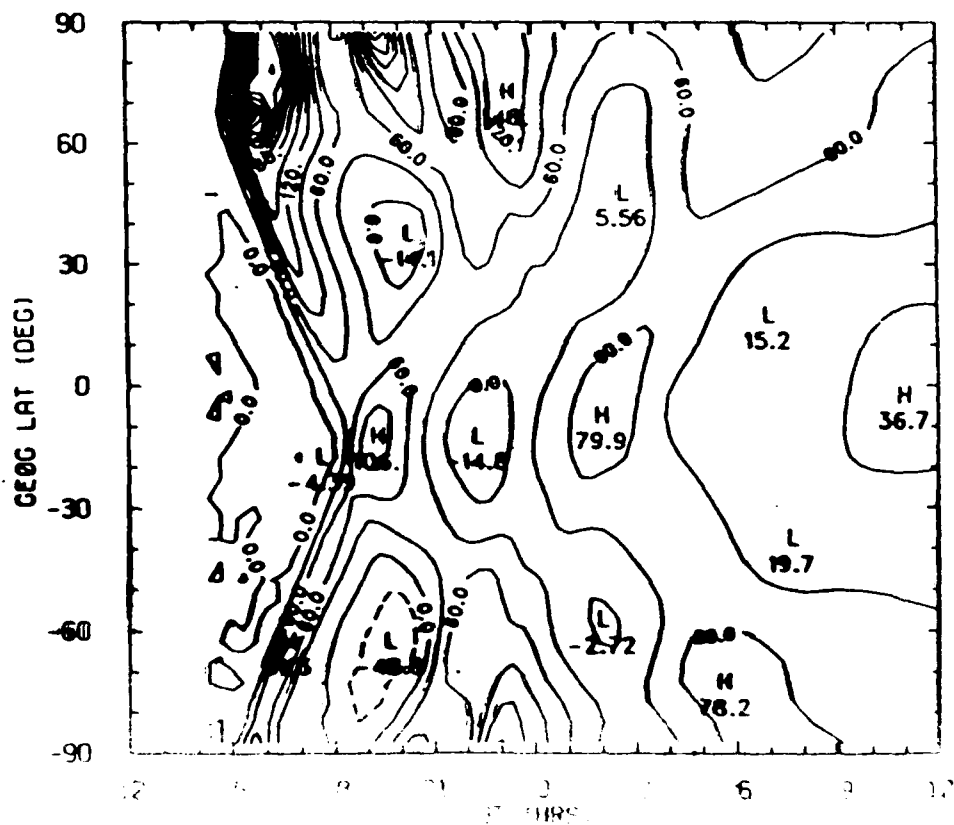
TGCM NEUTRAL MERIDIONAL WIND (M/S) (DIFF)

DIFF SEP18, 1974 Z = 2.0 AVE HT = 311.0 LON = -70.0



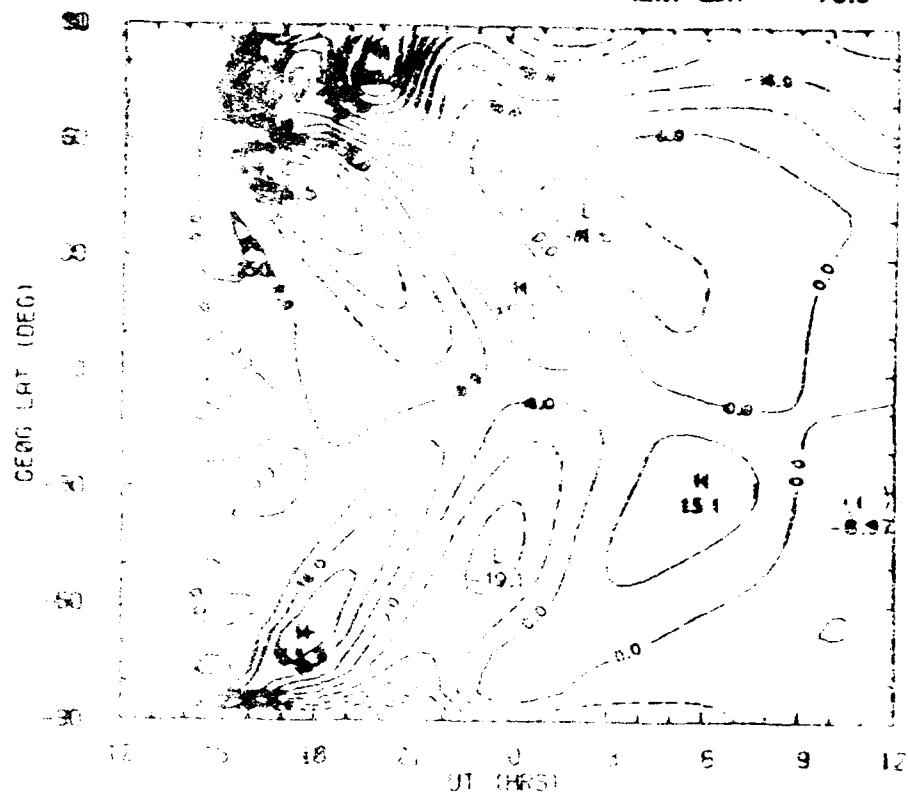
TGCM NEUTRAL TEMPERATURE (K) (DIFF)

DIFF SEP18, 1974 Z = 2.0 AVE HT = 311.0 LON = -70.0



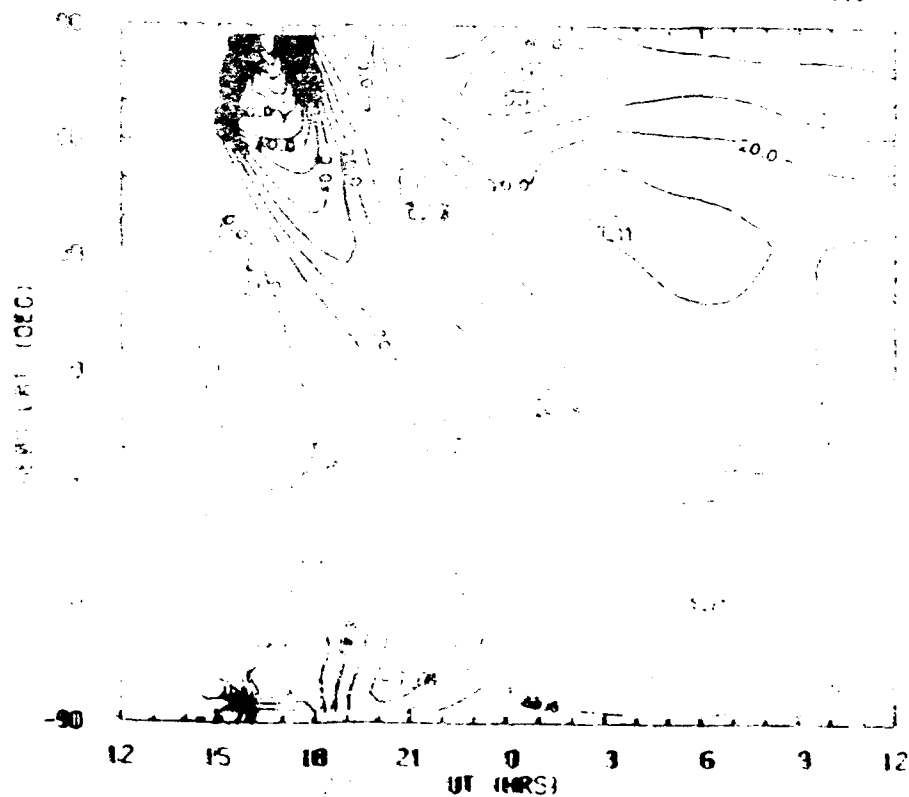
HIGH NEUTRAL MERIDIONAL WIND (M/S) (DIFF)

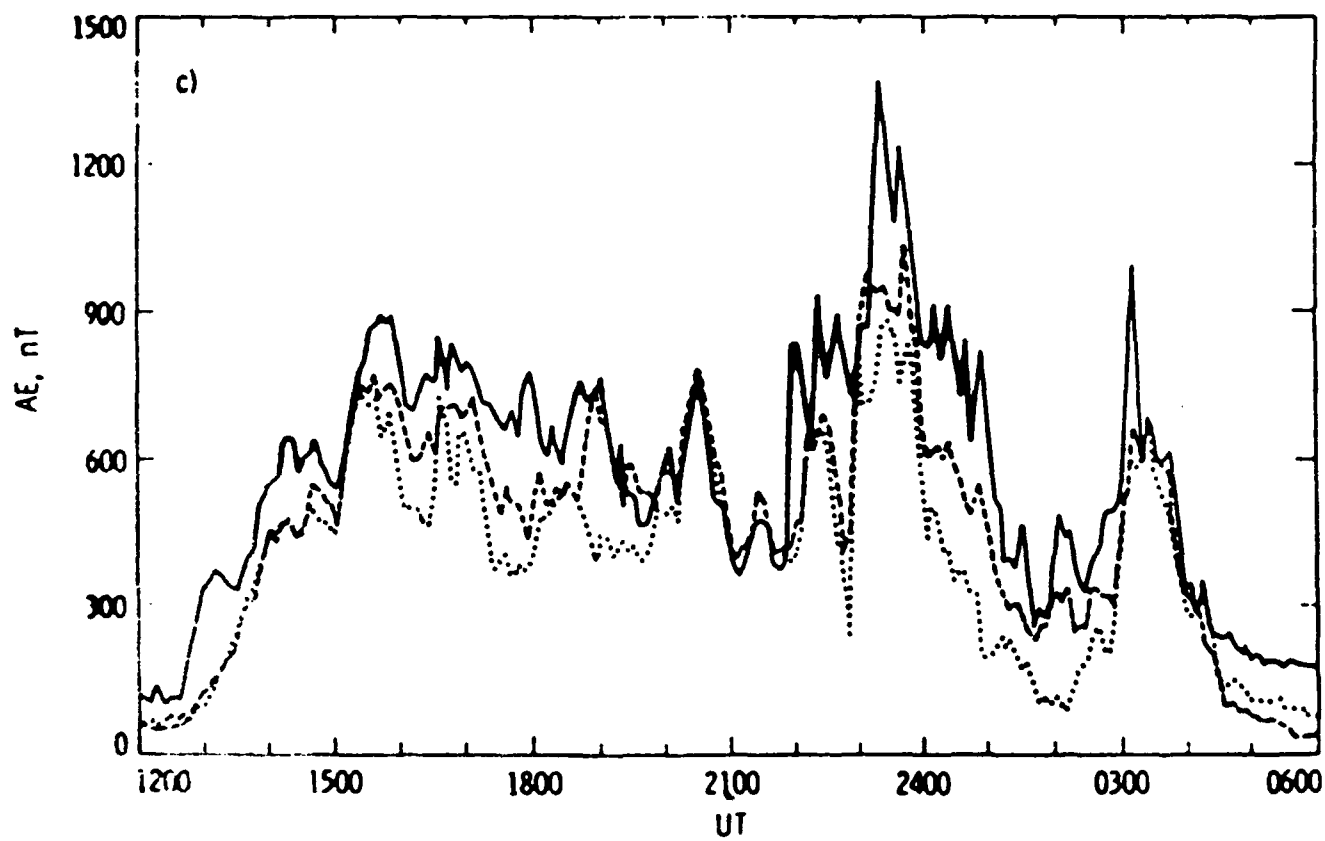
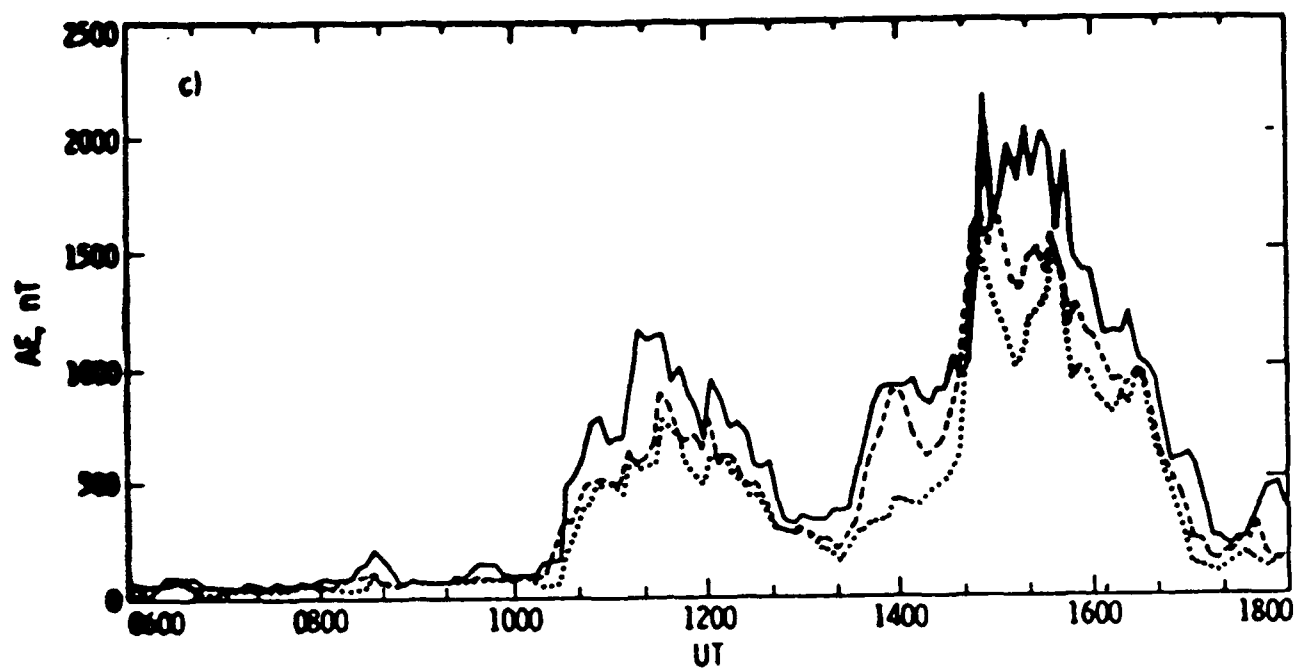
0000 SEP68, 1974 Z = -4.8 AVE HT = 121.7 LON = -70.0



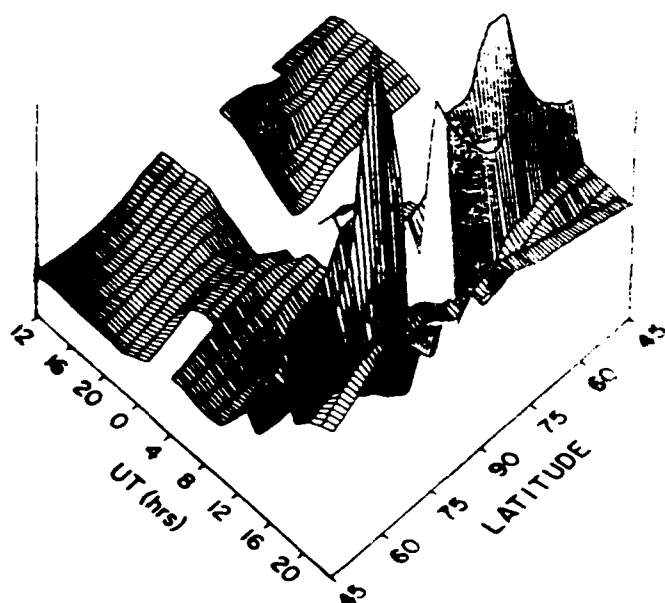
HIGH NEUTRAL TEMPERATURE (°C) (DIFF)

0000 SEP68, 1974 Z = -4.8 AVE HT = 121.7 LON = -70.0

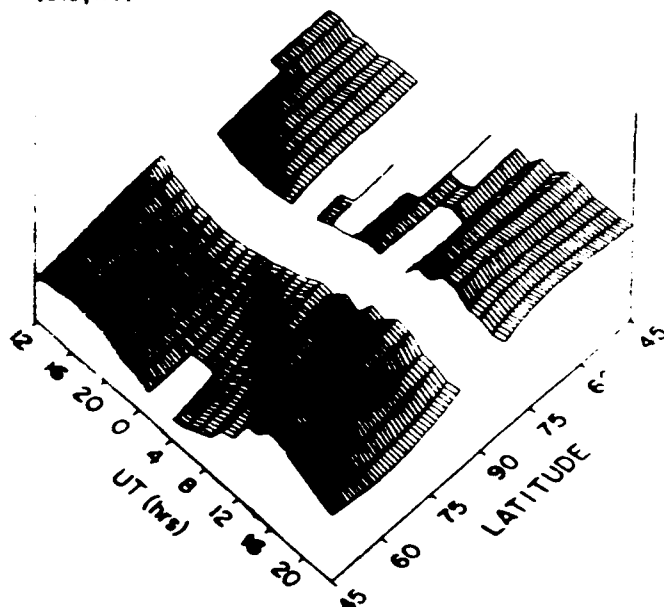




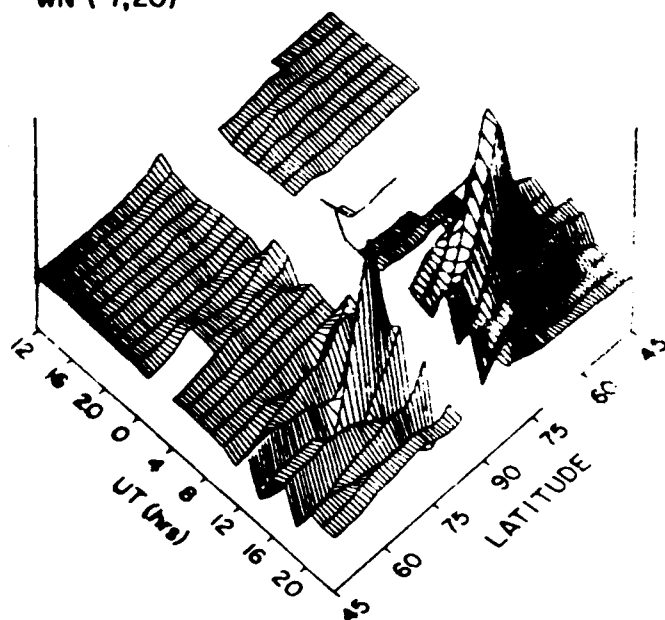
DENSITY RATIO
TSCM AT 200 KM
(0.8, 1.6)



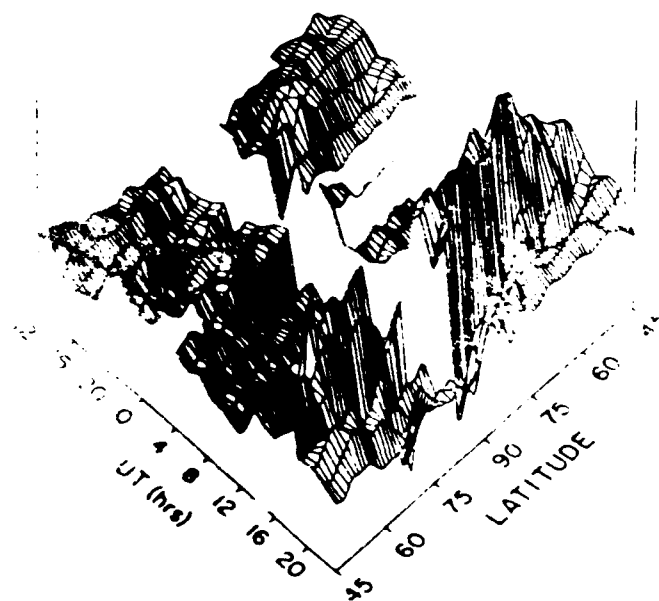
DENSITY RATIO
MSIS AT 200 KM
(0.8, 1.6)



VERTICAL WIND (M/S)
TGCM AT 200 KM
WN (-7, 20)



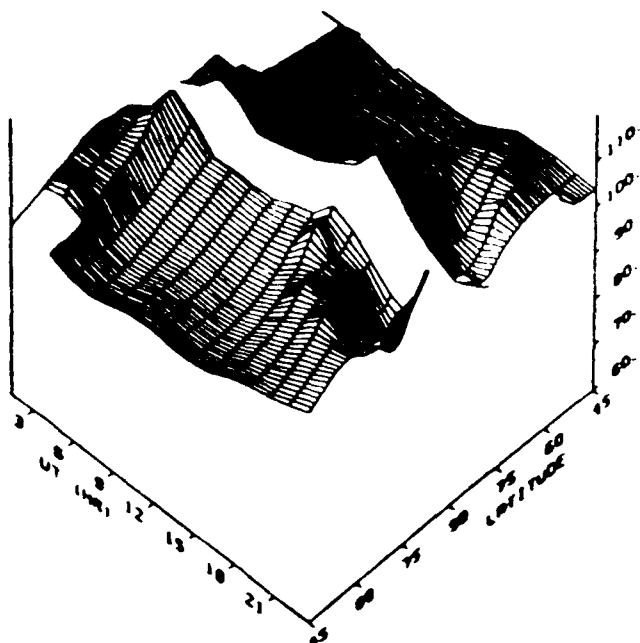
DENSITY RATIO
SAT AT 200 KM
(0.8, 1.6)



WDCM AT 200 KM

AF SAT

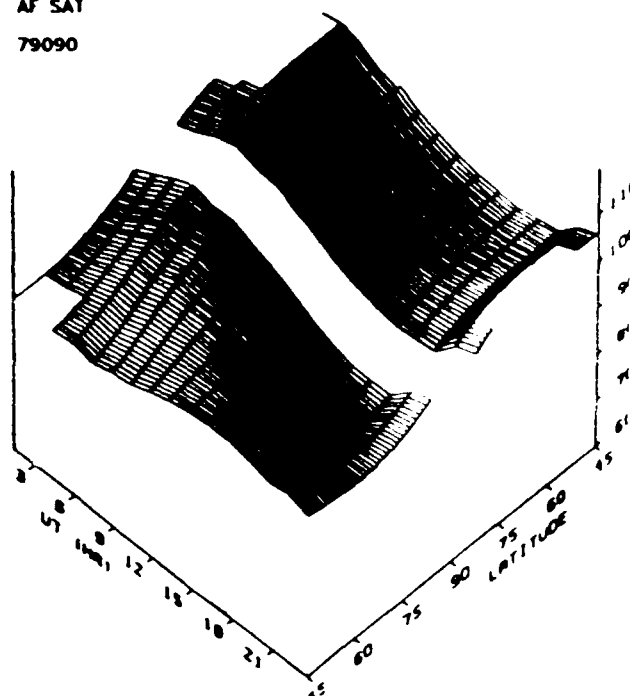
79090



MSIS AT 200 KM

AF SAT

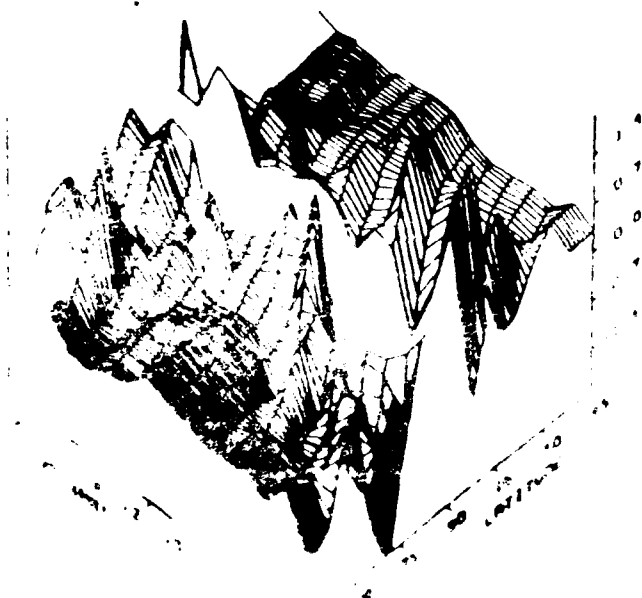
79090



TGCM AT 200 KM

AF SAT

79090



SETA AT 200 KM

AF SAT

79090



Problem Areas

- **Realistic Specification of:**
 - **Solar EUV and UV fluxes**
 - **Aurora particle inputs**
 - **Ionospheric convection patterns**

} **Solar wind
measurements**
- **Lower Boundary Interactions**
 - **Tides, gravity waves, planetary disturbances**
- **Magnetosphere/Ionosphere Interactions**
 - **H^+/O^+ plasma flow**
 - **Plasma heat fluxes**
- **Thermospheric and Ionospheric Measurements**
 - **Old measurements (AE, 1976-1979), (DE, 1981-1982)**
 - **CEDAR campaign**
- **Need Dedicated Satellite**

Future Efforts

- **Refinement of Aeronomical Scheme**
- **Detailed Comparison with MSIS-86 Climatology**
 - **Areas of agreement, disagreement**
 - **Physical cause of differences (instantaneous vs. averaging)**
- **Detailed Comparison with Satellite Data:**
 - **Air Force satellite density and wind measurements**
 - **AE, DE-NASA satellites**
- **VHS analysis and improvements to MSIS, Jacchia**
 - **Development of new empirical model for operational use**
- **Continued Development of TIGCM into an Operational Space Weather Forecasting Model (1990's to 2000's)**

EUV MONITORING AND GEOMAGNETIC STORM FORECASTS USING THE USAF-NOAA SOLAR X-RAY IMAGERS (SXI)

W. J. Wagner

Space Environment Laboratory, NOAA/Environmental Research Laboratories,
Boulder, Colorado 80303

Abstract

Neutral atmosphere density models will require continuous real time information. The histories and prognoses from data on radiant extreme ultraviolet (EUV) solar flux and geomagnetic storm heating are needed for advancing these operational models beyond mere climatology. The USAF-NOAA Solar X-Ray Imagers (SXI) will be providing these data in the 1990's.

Introduction

The Sun is the source of disturbances to the space environment. An upgrading of the present solar remote sensing systems is planned through the implementation of X-ray and EUV imaging of the Sun (Wagner et al. 1987). The use of Solar X-Ray Imagers (SXI) will give important improvements in the prediction of proton flare events, geomagnetic storms, and heating of the Earth's neutral atmosphere. The SXI will permit better performance of USAF missions by providing forecasts of disruptions due to these effects. Forecasts give USAF decision-makers the planning time which allows for shifting to backup systems or for attaching more credibility to other warning systems. The improved space environment services resulting from the SXI will also act as a force multiplier. When forecasts are available for the support of advanced systems, they provide economies in resources such as design complexity, launch weight, and, appropriate to this workshop, satellite orbit lifetime.

The design of the SXI copies that of a telescope on NASA's 1973 Skylab spacecraft. Anomalous orbital drag caused premature re-entry of the Skylab in 1979 before a space shuttle rescue mission could be mounted to save this, the nation's first space station. In a sense, as we will see below, SXI may be considered to be a spin-off from Skylab, whose pathfinding has returned to serve against such future calamities. Already today, early in solar activity cycle 22, scientific spacecraft are being endangered (Speich 1988) and missions are being delayed (Industry Observer 1988) at the same time that DOD launch schedules (Covault 1988) are imperiled by the unpredicted decay of other satellite orbits. I will briefly discuss the SXI instrument and its expected contributions to the neutral density atmospheric models which are intended to mitigate losses from satellite drag.

The Solar X-Ray Imager and its Contributions

The Solar X-Ray Imagers will be flown on the NOAA GOES geostationary satellites at 22000 mile altitude with no day/night cycles (Figure 1). With the SXI, grazing incidence optics will give continuous real time data (Figure 2) consisting of both extreme ultraviolet and soft X-ray images of the complete solar disk. Images will arrive once per ten minutes (at fastest rates, up to one per minute) and will have pixel size of 5 arc-seconds. The passbands to be used include 10 - 20 and 20 - 60 Angstroms in the soft X-ray region, and 255 - 300 Angstroms in the EUV.

To select the optimal EUV band for monitoring the radiant energy input to the thermosphere, previous investigations by AFGL were used (Hinteregger 1981). Additional studies of the AFGL data (Hedin 1984; Hedin and Mayr 1987; Roble 1987) seem to indicate that solar flux in the 255 - 300 Angstrom band best correlates with the density of thermospheric nitrogen (Figure 3). A heat rejection prefilter covers the aperture of the SXI thus preventing passage of wavelengths above approximately 350 Angstroms. Unclear at this time is whether to include the strong but relatively constant contribution of He II 304 Angstroms. However, it appears (Figure 3, from Hedin 1984) that this spectral line would serve only to degrade the data if the intention were to monitor the changing thermospheric densities.

The SXI will measure the EUV flux over an entire solar cycle. With a series of SXIs installed on the GOES satellites, it is expected that long-term variations of these 255 - 300 Angstrom EUV fluxes will be available for comparison with other longer-established solar indices (Figure 4). Although, no overall absolute radiometric calibration will be provided in orbit, any sensitivity changes are expected to be gradual and uniform with time and thus amenable to periodic checks by other space instruments. The SXI detector, a charge-coupled device, will be regularly calibrated onboard in a visible wavelength band.

In addition to monitoring the solar EUV radiant flux for input into thermospheric density models, the SXI will also aid in the prediction of the heating of the Earth's atmosphere that is caused by geomagnetic storms. The location of X-ray coronal holes and the details of their evolution and shape will be used to infer high speed streams in the solar wind structure. Long-duration X-ray events, believed to mark the launch of coronal mass ejections, will also be detected (by the soft X-ray channel) as they leave the Sun.

A Memorandum of Agreement was signed by the USAF and NOAA in June 1987 providing funds in October 1989. At the same time, NASA declined to join the project. GOES launches are now posted for May 1992, February 1997, and December 1997. If funding earlier than FY 90 can be identified, the 1992 launch would carry the first SXI into orbit.

Conclusions

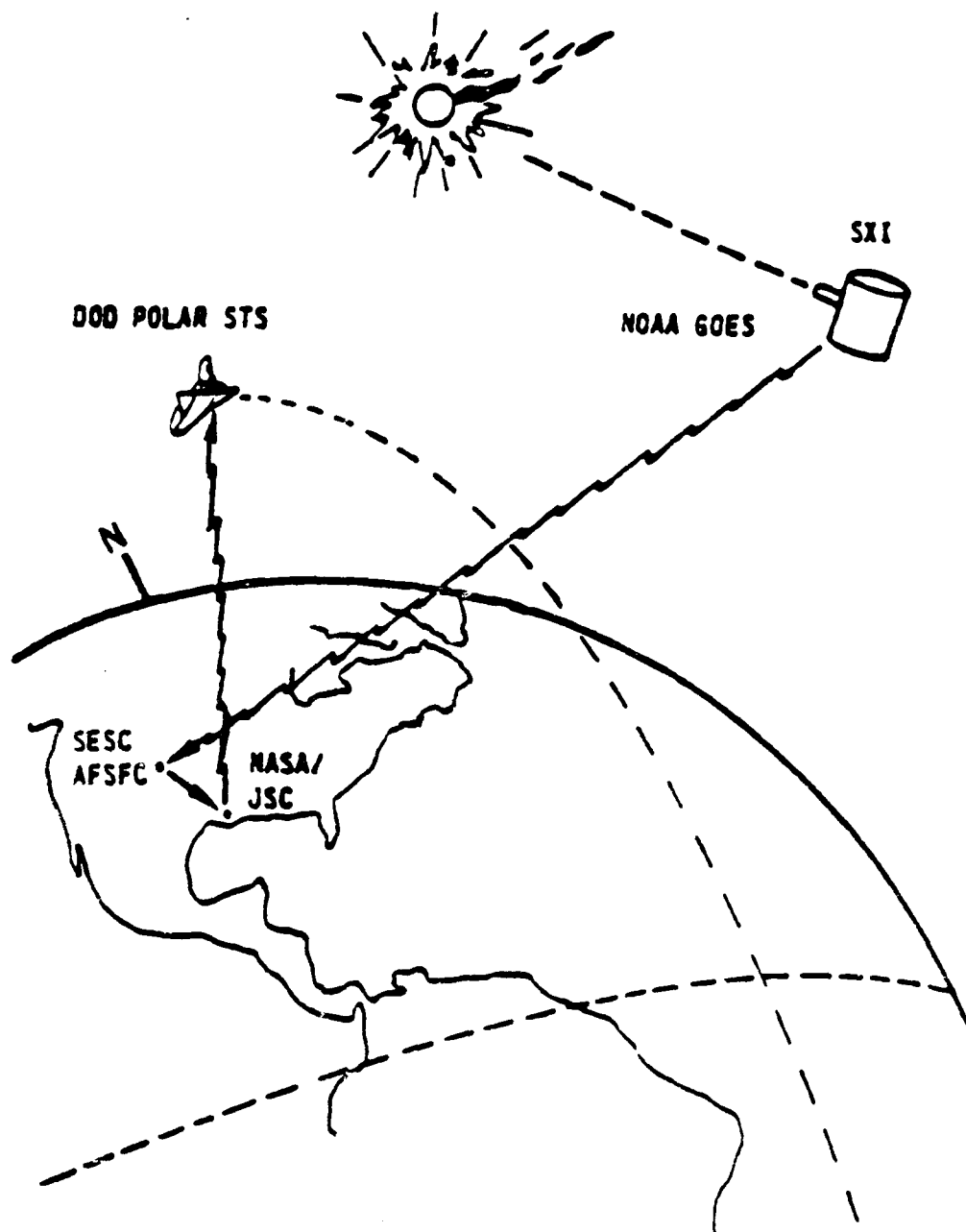
The SXI program will deliver 10 to 15 years of data and prediction services through the USAF and NOAA forecast centers in Colorado (Mulligan and Wagner 1987). Accurate forecasts of satellite drag can save the nation real money. They will permit the coherent and consistent space shuttle mission planning which was advocated by the Rogers Commission on the Challenger accident. Today, circumstances still resemble the situation in 1979 at the time of the inadvertant Skylab re-entry. However, with workshops such as this one and using neutral atmosphere density models supplied with on-going real time EUV input data and with geomagnetic storm forecasts from Solar X-ray Imager, we are likely to minimize losses due to unanticipated orbital decay in the future.

References

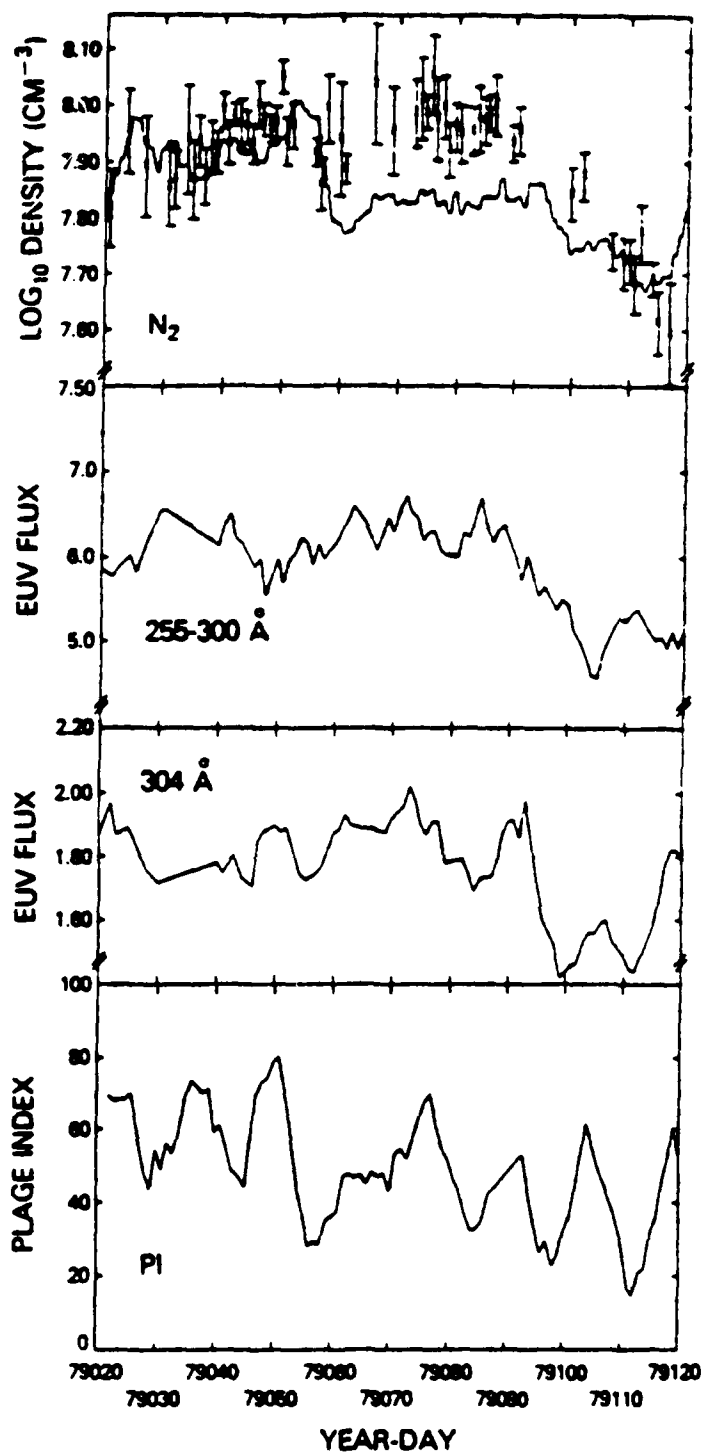
- Covault, C., NASA changing shuttle payloads to retrieve decaying satellite, Av. Week and Space Tech., February 6, 1988, p. 30.
- Donnelly, R. F., submitted to Annales Geophysica, 1988.
- Hedin, A. E., Correlations between thermospheric density and temperature, solar EUV flux, and 10.7-cm flux variations, J. Geophys. Res., 89, 9828-9834, 1984.
- Hedin, A. E., and H. G. Mayr, Solar EUV induced variations in the thermosphere, J. Geophys. Res., 92, 869-875, 1987.
- Hinteregger, H. E., Representations of solar EUV fluxes for aeronautical applications, Adv. Space Res., 1, 39-52, 1981.
- Industry Observer, NASA Hubble Space Telescope scientists, Av. Week and Space Tech., April 11, 1988, p. 9.
- Mulligan, P. J., and W. J. Wagner, Plans for science studies and space environment services from the GOES Solar X-Ray Imagers (SXI), Bull. Amer. Astron. Soc., 19, 944, 1987.
- Speich, D. M., private communication concerning Solar Maximum Mission, 1988.
- Roble, R. G., summary paper in, F. A. Marcos (ed.), Atmospheric Density and Aerodynamic Drag Models for Air Force Operations, workshop held at the Air Force Geophysics Laboratory, 20-22 October 1987, Hanscom AFB, MA.
- Wagner, W. J., and R. N. Grubb, G. R. Heckman, and P. J. Mulligan, The Solar X-Ray Imagers (SXI) on NOAA's GOES, Bull. Amer. Astron. Soc., 19, 923, 1987.

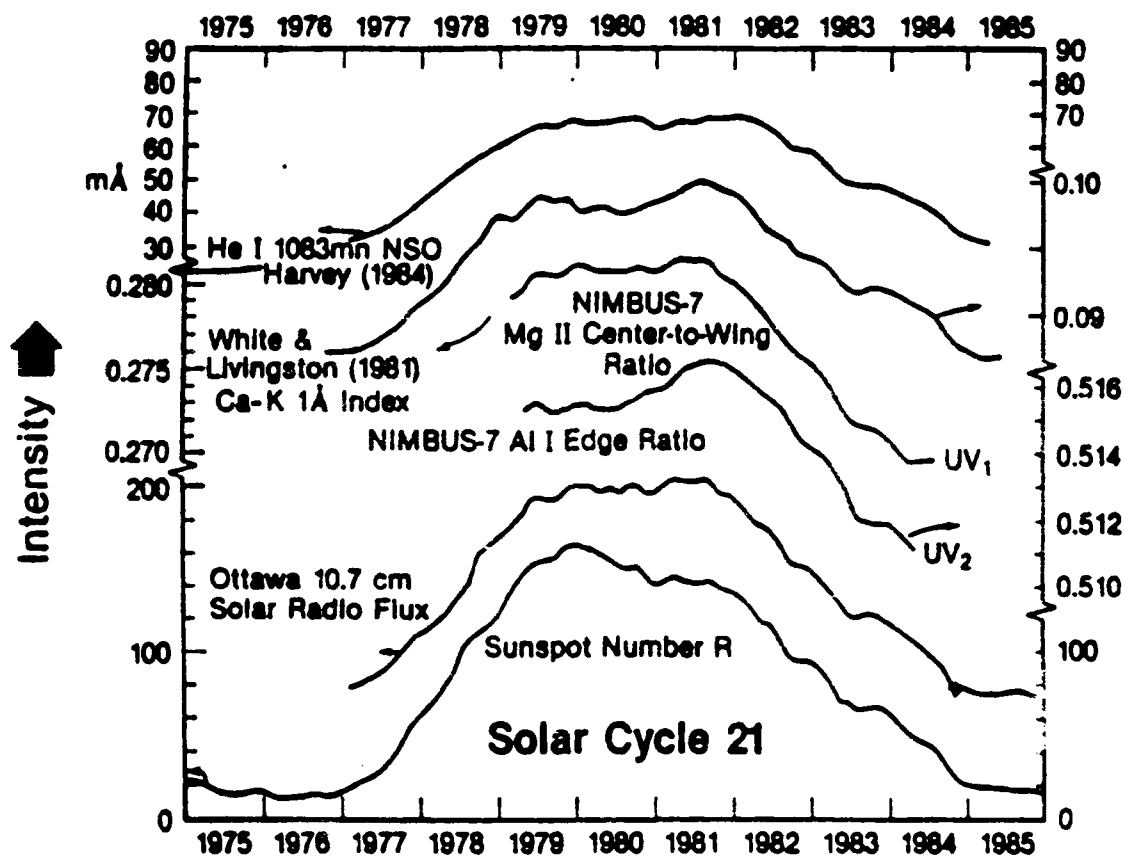
Figure Captions

- Figure 1. Real time SXI EUV and X-ray data will be delivered directly to Air Force and NOAA forecast centers for dissemination to users.
- Figure 2. X-ray image of the Sun from the NASA Skylab mission. Data from the SXI will resemble this. Currently, no image exists which was taken in the 255 - 300 Angstrom band designated for the SXI.
- Figure 3. This work by Hedin (1984) shows that nitrogen densities (error bars in the top panel) correlate better with 255 - 300 Angstrom fluxes (second panel) than they do with (a model driven by) 10-cm radio fluxes which are shown as the solid curve in the top panel. The inclusion of He II 304 Angstroms (third panel) within this EUV band would actually lower the correlation with atmospheric densities.
- Figure 4. Solar cycle variations of various indices that have been used as surrogates for the heating by EUV flux (according to Donnelly 1988). A comparison of their dissimilar solar cycle variations demonstrates the differences among these surrogates.









THE REMOTE ATMOSPHERIC AND IONOSPHERIC DETECTION SYSTEM

R. P. McCoy, K. D. Wolfram, R. R. Meier, L. J. Paxton, D. D. Cleary,
D. K. Prinz, D. E. Anderson, Jr.

E. O. Hulburt Center for Space Research, Naval Research Laboratory,
Washington, DC 20375-5000

and

A. B. Christensen, J. Pranke, G. G. Sivjee, D. Kayser

The Aerospace Corporation, P. O. Box 92957, Los Angeles, CA 90009

Abstract

The Remote Atmospheric and Ionospheric Detection System (RAIDS) experiment, to fly on a TIROS spacecraft in the late 1980's, consists of a comprehensive set of one limb imaging and seven limb scanning optical sensors. These eight instruments span the spectral range from the extreme ultraviolet to the near infrared, allowing simultaneous observations of the neutral and ion composition on the day and night side as well as in the auroral region. The primary objective of RAIDS is to demonstrate a system for remote sensing of the ionosphere to produce global maps of the electron density, peak altitude and critical frequency.

Introduction

The Remote Atmospheric and Ionospheric Detection System (RAIDS) is a satellite experiment designed to perform a comprehensive study of the upper atmospheric airglow emissions. RAIDS observations will be used to develop and test techniques for remote sensing of the neutral atmosphere and ionosphere on a global scale. The RAIDS experiment consists of a set of one limb-imaging and seven limb-scanning optical sensors which sample the altitude interval 75 - 750 km and cover the wavelength range 500 - 8700 Å.

The goal of the RAIDS experiment is to obtain a set of simultaneous airglow profiles at a number of wavelengths which will be used to develop and evaluate techniques for neutral atmospheric and ionospheric remote sensing. The RAIDS instrumentation will acquire a global database of airglow intensities which will be used in conjunction with, and compared to, theoretical models of radiation transport, photochemistry and dynamics to examine in detail the relationships between atmospheric composition and airglow. The primary focus of RAIDS will be on remote sensing of the ionosphere since there is considerable interest by the ionospheric and high frequency propagation communities in monitoring the ionosphere in real-time on a global basis.

RAIDS has been proposed to the U.S. Air Force Space Test Program and is currently being considered for flight on a NOAA TIROS-N series satellite. The planned orbit will be sun-synchronous in the early afternoon at an altitude of 870 km.

Experiment Objectives

The ionospheric electron density on the dayside will be determined from measurements of the extreme ultraviolet (EUV) emissions from ionized oxygen (primarily at 844 Å) in the F2 region of the ionosphere^{1,2}. The ionized oxygen dayglow is produced from ionization-excitation of neutral atomic oxygen and, as the EUV radiation undergoes multiple resonant scattering, the radiation field acquires the signature of the O⁺ ion distribution. Measurements of the O⁺ EUV radiation by limb scanning instruments can be used to infer the electron density profile throughout most of the F2 region where the O⁺ density is largely equal to the electron density.

The nightside electron density will be determined by measurement of the nightglow from neutral oxygen atoms produced by the recombination of O⁺ and O₂⁺ ions and electrons. These emissions have been observed at a number of wavelengths including the EUV 911 Å continuum, the far ultraviolet (FUV) 1304 Å, 1356 Å multiplets, and in the visible and near infrared at 6300 Å and 7774 Å^{3,4,5,6,7}. Scanning through the limb gives the shape of the emission profile which can be used to determine the altitude distribution of the electron density. The magnitude of the nightglow recombination emission has been shown to be proportional to the square of the peak electron density in the F2 region^{1,5}.

Another scheme for ionospheric remote sensing to be explored by RAIDS experiment involves the simultaneous measurement of dayglow emissions from neutral oxygen and molecular nitrogen in the FUV part of the spectrum. The atomic oxygen/molecular nitrogen ratio has been shown to be related to the distribution of O^+ ions.

In addition to the EUV and FUV sensors, the RAIDS experiment will contain sensors to measure airglow emissions in the middle and near ultraviolet (MUV, NUV) and the near infrared (NIR) which will be used to determine the neutral atmospheric composition (O , N_2 and O_2), temperature, energetic electron flux and the densities of minor atmospheric species such as NO , N , Na , H , He and Mg . The major and minor neutral species will provide important inputs into photochemical and dynamical models of the thermosphere and ionosphere. By making airglow observations over an extended spectral range, the RAIDS experiment will provide enough inputs to adequately test the theoretical models. Table 1 summarizes the major scientific objectives of RAIDS and the emission features that will be observed to satisfy the objectives.

TABLE 1. RAIDS SCIENTIFIC OBJECTIVES

<u>SCIENCE OBJECTIVES</u>	<u>METHOD</u>	<u>WAVELENGTHS (\AA)</u>
Dayside Electron Density	O^+ Dayglow	540-834 (O^+)
Nightside Electron Density	O^+ Recombination O_2^- Recombination	911, 1304, 1356, 7774 (O) 6300 (O)
Neutral Composition	N_2 Airglow	1250-2000 (N_2 LBH)
And Temperature	O Airglow	989, 1304, 1356, 1641 (O)
	O_2 Absorption	1750-5350 (O_2 Schumann-Runge) 7400-10000 (O_2 Atmospheric)
	$O+O$ Association	2500-5000 (O_2 Herzberg I)
Energetic Electrons	N_2 , N_2^+ Airglow	1250-2000 (N_2 LBH) 3100-4000 (N_2^+ Second Positive N_2^- First Negative)
Minor Species		
NO	NO Airglow	2000-2800 (NO γ)
N	NO	1900-2400 (NO δ)
Na	Na	5890 (Na "D")
Mg	Mg	2800 (Mg)
H	H	1027 (H Ly α)
He	He	564 (He)

Observing Scheme

Figure 1 is an artist's conception of the RAIDS experiment in orbit aboard a TIROS satellite. The experiment will be mounted to the underside of the spacecraft and the instruments will view along the anti-velocity direction. The instrument compartment is divided into three sections: a fixed central "T" shaped structure housing the spin mechanism and the limb-imaging instrument, and two rotatable side compartments which house the limb-scanning instruments. The primary instrument package has dimensions of 59.3 cm (X) by 63.5 cm (Y) by 83.8 cm (Z) where X is in the nadir direction, Y is opposite the velocity vector and Z is along the long axis of the satellite.



Figure 1. The RAIDS experiment, in an artist's conception, scans the Earth's limb from a NOAA TIROS-N satellite.

The scan platform will rotate the side compartments so that the optical axes of the instruments scan in depression angle from -10 to -16.5 degrees relative to the spacecraft horizontal. These angles correspond to tangent altitudes of 250 to 35 km.

To optimize the science return, a variable scan rate is employed. The nominal scan rate is 0.34 degrees/sec at viewing altitudes near 400 km; the scan rate will slow to 0.1 degrees/sec to provide better altitude resolution in the most important altitude region. The complete cycle of the scan platform requires 17 seconds, 13 seconds of which are in the flyback. A scan rate near zero at tangent altitude was chosen to minimize the horizontal smear of the scan caused by the orbital velocity. The scan rate is zero at the horizon of the spacecraft and at vertical altitude. Since the RAIDS will scan and scan platform are microprocessor controlled, the scan platform can be programmed to scan the lines of greatest interest for a given altitude. For example, the scan rate can be zero at the altitude of interest and the scan rate can be maximum at the altitude of interest.

Instrumentation

The eight RAIDS optical instruments can be divided into three categories: (i) spectrophotometers with microchannel plate (MCP) array detectors, (ii) spectrophotometers with MCP array detectors, and (iii) spectrophotometers with MCP array detectors.

scanning gratings and single photomultiplier detectors, and (3) single channel photometers. The spectrographs record emissions from several wavelengths simultaneously over a fixed spectral interval while the spectrometers can be commanded either to scan across wavelength range, obtaining data at each wavelength in series or stop and record data at a single wavelength. The photometers have fixed bandpasses which isolate a single airglow emission feature. A summary of some of the more important instrument parameters is contained in Table 2.

TABLE 2. RAIDS INSTRUMENT PARAMETERS

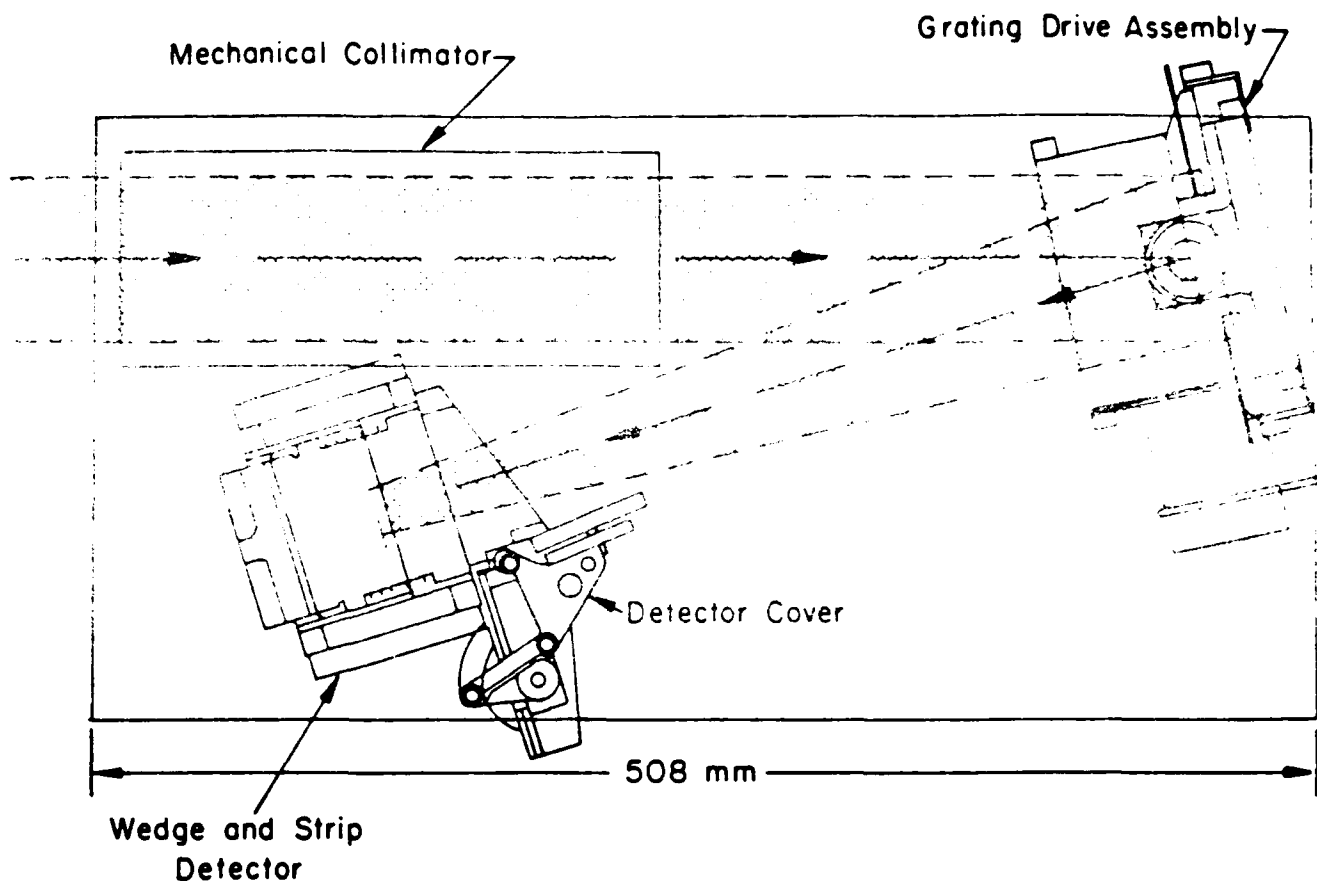
Instrument	Wavelength Range	Bandpass	Field* of View	Integration [®] Time	Aperture Area	Peak Sens.	Telemetry Rate
	(Å)	(Å)	(deg ²)	(sec)	(mm ²)	(C/s/R)	(Bits/s)
EUV Spectrograph	500-1100	12	0.1x2.4	0.5	70x70	0.5	2560
FUV Spectrograph	1300-1700	8	4.0x0.1	87.0	25x25	2.5	4096
MUV Spectrometer	1900-3200	10	0.1x2.1	0.1 or .025	42x50	7.5	800
NUV Spectrometer	2950-4000	7	0.1x2.1	0.1 or .025	21x25	1.8	800
NIR Spectrometer	7250-8700	7	0.1x2.1	0.1 or .025	21x25	2.8	800
5890 Photometer	5890	20	0.2x2.1	0.1	50x50	6.2	200
6300 Photometer	6300	20	0.2x2.1	0.1	50x50	8.0	200
7774 Photometer	7774	20	0.1x2.1	0.1	25x25	4.6	200

* The first and second values of the field-of-view correspond to the vertical and horizontal dimensions respectively.

[®] The integration times of the MUV, NUV, and NIR spectrometers are given for both the fixed-wavelength/altitude-scan and the fixed-altitude/wavelength-scan modes respectively.

EUV and FUV Spectrographs

The EUV instrument is an f/5, Wadsworth concave grating spectrograph (Figure 2). Incident light enters through a mechanical modulation collimator and is focussed on a position sensitive MCP array detector by a spherical reflectance grating used in first order. The grating has a ruled area 72 x 72 mm, a ruling density of 1710 lines/mm with a first order blaze at 700 Å and a 355 mm focal length. The grating can be rotated into one of two positions focussing, 350 Å segments between 500 and 1000 Å on the detector. The two segments overlap so that the O⁺ 844 Å feature is measured in either grating position. The spectral resolution is 12 Å. The field of view defined by the collimator and grating is 0.1 x 2.4 deg. The instrument is mounted on the scan platform so that the long axis of the field of view is parallel to the horizon on orbit.



EUV WADSWORTH

Figure 2. Layout diagram of the RAIDS EUV spectrograph.

The EUV detector consists of a stack of three MCP's in a "Z" stack configuration with a wedge-and-strip type anode. The MCP's are 36 mm diameter rimless plates with a 27 mm active area and 80:1 length/diameter channel ratio. The detector is windowless and a MgF_2 photocathode is deposited directly on the top MCP. The detector can resolve 256×256 pixels but on orbit it will be operated using 128×1 resolution elements aligned along the wavelength dispersion direction. The detector is enclosed in a vacuum housing which is sealed with a DC powered cover assembly which will be opened in flight.

The design of the FUV spectrograph uses an $f/5$ 125 mm focal length imaging Wadsworth configuration. The optical elements in the spectrograph consist of a spherical telescope mirror used off-axis, a collimating mirror, a concave grating and a MCP array detector (Figure 3). The two mirrors and the grating have focal lengths of 125 mm. The 0.25 mm x 9.0 mm entrance slit is at the focus of the telescope mirror defines a field of view of 0.1×4.0 deg. The grating has a ruled area 31 mm x 31 mm, a ruling density of 3600 lines/mm and is blazed at 1400 Å. The FUV spectrograph contains no moving parts and it will be fixed to the mounting surface of the spacecraft. The long axis of the entrance slit will be perpendicular to the horizon during flight and the spectrograph will image vertically along the length of the slit. The wavelength dispersion direction is perpendicular to the slit. The wavelength coverage is 1300 - 1700 Å and the spectral resolution is 6-8 Å.

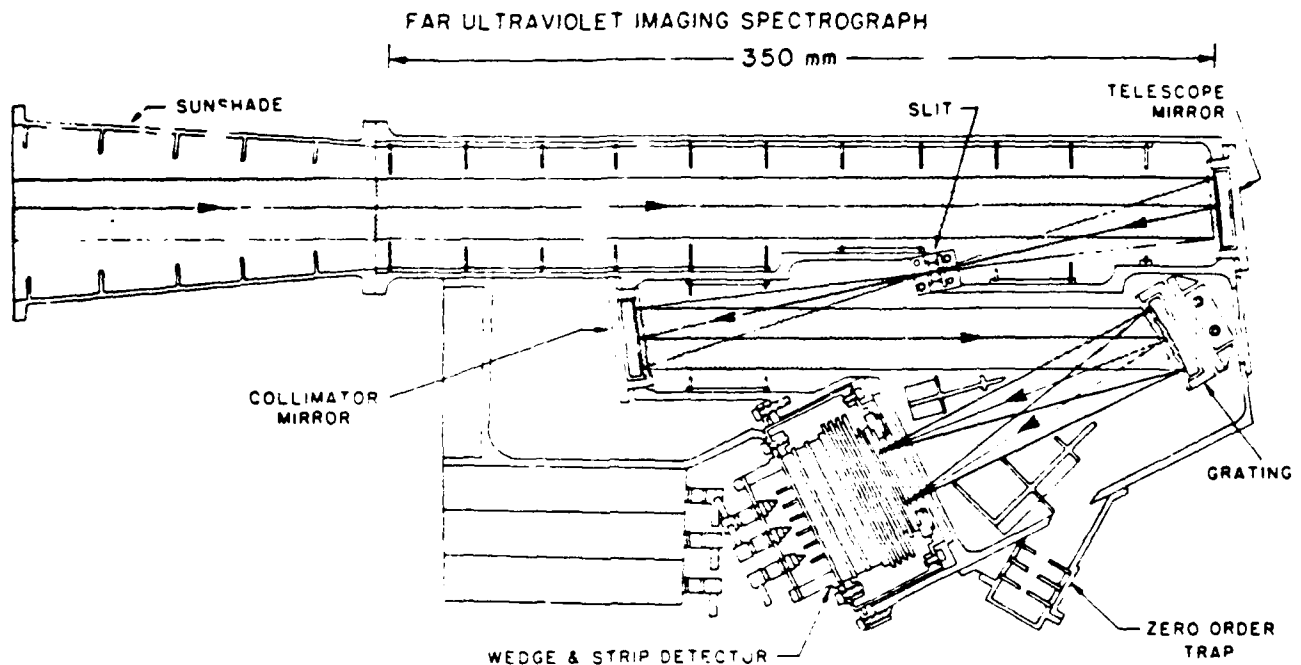


Figure 3. Layout diagram of the RAIDS FUV imaging spectrograph.

The FUV spectrograph detector consists of a permanently sealed evacuated housing enclosing a stack of four MCP's and a wedge and strip anode array. The detector window is MgF_2 and is coated on the inside with a CsI photocathode. The MCP's are 25 mm in diameter and have a length/diameter channel ratio of 40:1. The detector will be operated in a two dimensional mode using 256 pixels along the dispersion direction and 64 pixels along the altitude direction. The altitude resolution is 3.5 km and the minimum ray height point altitude range imaged is 75 km to 285 km.

MUV, NUV and NIR Spectrometers

The MUV, NUV and NIR spectrometers consist of f/5, 125 mm focal length Ebert-Fastie monochromators with off-axis telescopes containing spherical mirrors. The grating positions are determined by stepper-driven cam mechanisms which can be controlled by the flight microprocessor either to scan continuously in wavelength or to step to a particular wavelength position and record data at that fixed wavelength. The grating cams and gear ratios were chosen so that a complete scan of each spectrometer consists of 1974 motor steps and takes approximately 25 seconds. The entrance and exit slits of the monochromators are matched and the fields of view of the three spectrometers are 0.1×2.1 deg. As with the EUV spectrograph, the spectrometers are to be mounted to the scan platform with the long axis of the slit parallel to the horizon in flight.

The telescope of the MUV spectrometer is f/5 with a 250 mm focal length. This instrument uses a 3600 lines/mm grating blazed at 2400 Å. With an entrance slit size of 0.5 mm x 9.0 mm the spectrometer has a resolution of 9.6 Å. The spectral coverage of the MUV spectrometer extends from 1900-3200 Å. The MUV spectrometer detector is a 25 mm diameter photomultiplier with a CsTe photocathode and MgF_2 window and is mounted at the exit slit of the monochromator.

The NUV spectrometer has an f/5, 125 mm telescope and a 0.25 mm by 9.0 mm entrance slit. The grating has 2400 lines/mm and is blazed at 3000 Å. The spectral coverage of the NUV spectrometer extends from 2950-4000 Å and the spectral resolution is 7 Å. The NUV spectrometer detector is a 25 mm diameter photomultiplier with a bi-alkali photocathode and glass window (Figure 4).

Raids 1/8 Meter Spectrometer System

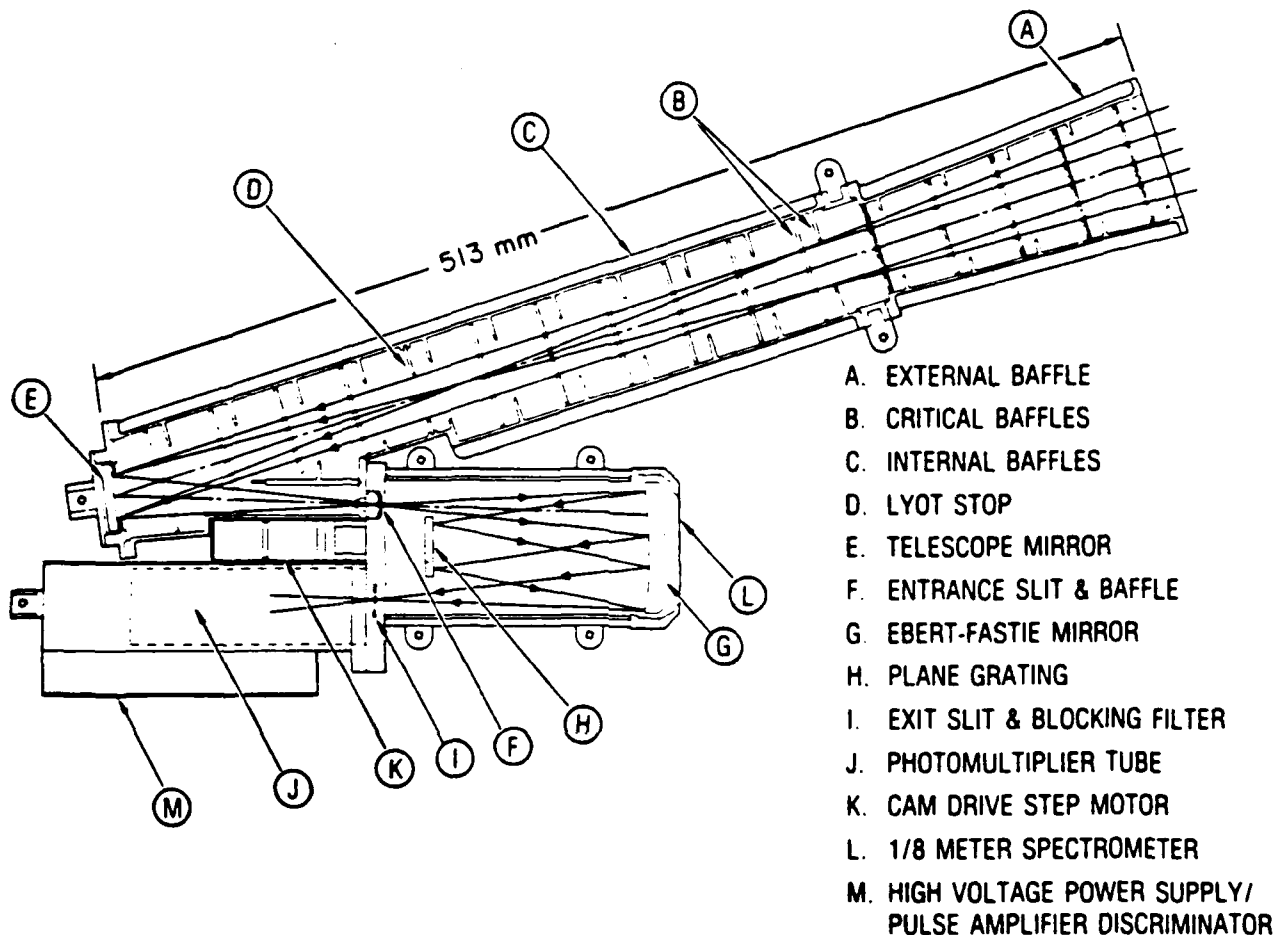


Figure 4. Layout diagram of the NUV spectrometer.

The telescope and slit dimensions of the NIR spectrometer are identical to the NUV instrument. The NIR grating has 1800 line/mm and is blazed at 7500 Å. The wavelength scan range is 7400-8700 Å and the spectral resolution is 7 Å. The detector is a photomultiplier with a GaAs photocathode and glass window. Because detector must be cooled to reduce the dark count to an acceptable level, the photomultiplier tube is housed in a separate box and is radiatively cooled to approximately -20 C. A 3 mm diameter fiber optical bundle is used to deliver the light from the monochromator to the detector. A lens assembly couples light from the monochromator into the fiber bundle.

Photometers

The RAIDS experiment includes three photometers with bandpasses centered at the sodium 5890 Å line, and the oxygen 6300 Å and 7774 Å lines. The photometers use off-axis telescopes identical to those on the spectrometers, and field stops at the foci of the telescopes limit the field-of-view to 0.1 x 2.1 deg. At the field stop an optical coupling assembly collects light, renders it parallel, passes it through an interference filter and refocusses it into a 3 mm diameter fiber optical bundle. The bundle transmits the light to the radiatively cooled (separate) detector box. Each photometer uses a GaAs photomultiplier as a detector.

In addition to providing information on the distribution of the Na D line airglow, the 5890 Å photometer will be used as an independent absolute calibration of the scan platform angle. The height of the peak of the Na airglow is 90 ± 5 km, and limb scans of this

emission feature will provide a check on the accuracy of the instrument look direction. The Na airglow will be measured on both the dayside and nightside.

Flight Microprocessor and Scan Platform

The RAIDS flight microprocessor (FMP), which is based on a Harris HS-8085RH microprocessor, functions primarily as a spacecraft command interpreter and data manager for telemetry. The FMP accepts 8-bit coded commands and executes the associated stored command macros after checking for conflicts. The FMP manipulates the large quantity of data received from the instruments and multiplexes it into the satellite telemetry stream. Other operations performed by the FMP include power sequencing for the instruments and heaters, setting the wavelength positions of the spectrometers, controlling the scan platform, performing analog-to-digital conversions, and controlling data buffers for the instruments.

The electronics have been designed to minimize the microprocessor intervention and to prevent over-tasking. Most subsystems are autonomous except for inputs such as wavelength, power on/off commands, and cross-strapping the various data channels. Analog to digital conversions, discrete digital status, and the positions of the various stepper motors must be read and stored by the microprocessor.

The scan platform is the principal structural unit of the RAIDS instrument. All the instruments except the FUV spectrograph are mounted to the movable section of the platform. The mechanically scanned instruments are located on one of four vertical fins. There are two sets of fins on each side of the platform along with the stationary FUV spectrograph in the center. The fins are coupled in pairs into two integral scanning assemblies that are tilted independently by a pinion and sector gear drive. The scanning assemblies rotate about a ~~point fixed~~ ^{axis} to the chassis base.

A single stepper motor rotates the scanning assemblies. The direction of the motor rotation is determined by the state of microswitches actuated by the platform at the top and bottom of the scan cycle. A counter is used to indicate the position of the platform and is zeroed after each cycle. A linear potentiometer is also attached to the platform to monitor the platform motion.

Acknowledgements

RAIDS is a Naval Research Laboratory experiment in collaboration with the Aerospace Corporation. Support for the development of the NRL portion of the RAIDS experiment is provided by the Office of Naval Research through the Atmospheric and Ionospheric Remote Sensing (AIRS) Accelerated Research Initiative and the Defense Meteorological Satellite Program (DMSP). Spaceflight sponsorship for RAIDS is provided by the Space Test Program (STP). Initial design development and implementation of the RAIDS instruments was carried out by G. H. Mount. D. J. Strickland and Computational Physics, Inc. have provided science support.

References

1. Kumar, S., S. S. Chakrabarti, F. Paresce, and S. Bowyer, The O⁺ 834-Å Dayglow: Satellite Observations and Interpretation With a Radiation Transfer Model, J. Geophys. Res., Vol. 88, pp. 9271-9279, 1983.
2. McCoy, R. P., D. E. Anderson Jr. and S. Chakrabarti, F2 Region Ion Densities from Analysis of O⁺ 834-Å Airglow: A Parametric Study and Comparisons with Satellite Data, J. Geophys. Res., Vol. 90, pp. 12257-12264, 1985.
3. Hicks, G. T., T. A. Chubb, Equatorial Aurora/Airglow in the Far Ultraviolet, J. Geophys. Res., Vol. 75, pp. 6233-6248, 1970.
4. Meier, R. R., C. B. Opal, Tropical UV Arcs: Comparison of Brightness with foF2, J. Geophys. Res., Vol. 78, pp. 3183-3193, 1973.
5. Tinsley, B. A., and J. A. Bittencourt, Determination of F Region Height and Peak Electron Density at Night Using Airglow Emissions from Atomic Oxygen, J. Geophys. Res., Vol. 80, pp. 2333-2337, 1975.
6. Chandra, S., E. I. Reed, R. R. Meier, C. B. Opal, and G. T. Hicks, Remote Sensing of the Ionospheric F Layer by Use of OI 6300-Å and OI 8446-Å Observations, J. Geophys. Res., Vol. 80, pp. 2327-2332, 1975.
7. Anderson, D. E. Jr., R. R. Meier and C. S. Weller, Observations of Far and Extreme Ultraviolet OI Emissions in the Tropical Ionosphere, Planet. Space Sci., Vol. 24, pp. 945-950, 1976.
8. Miller N. J., H. G. Mayr, N. W. Spencer, L. H. Brace, and G. R. Carignan, Observations Relating Changes in Thermospheric Composition to Depletions in Topside Ionization During the Geomagnetic Storm of September 1982, J. Geophys. Res., Vol. 89, pp. 2389-2394, 1984.

ATMOSPHERIC NEUTRAL DENSITY CONFERENCE

MARCH 22-23, 1988

COLORADO SPRINGS, COLORADO

REMOTE SENSING OF THE UPPER ATMOSPHERE:

THE RAIDS PROJECT

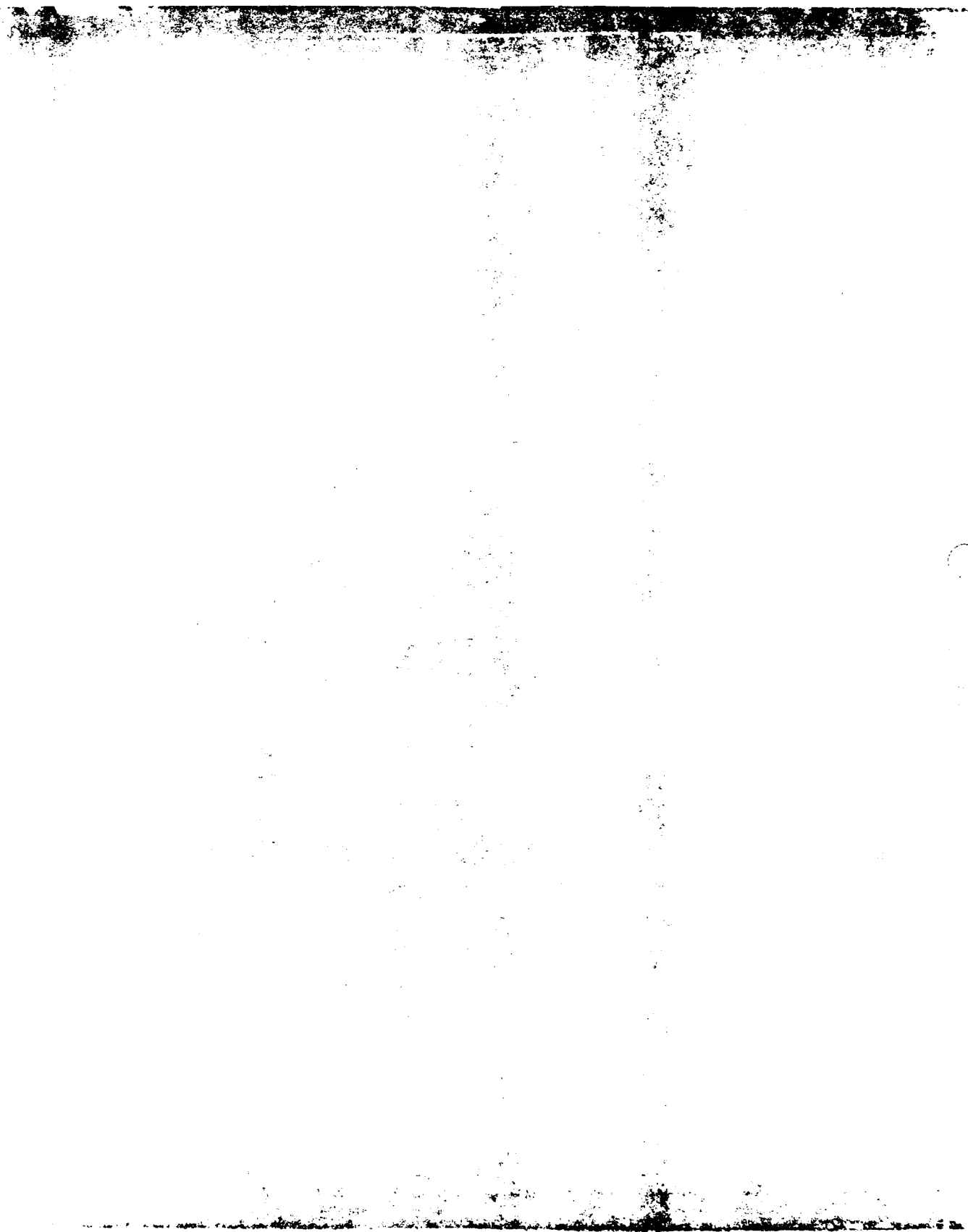
ANDREW B. CHRISTENSEN
SPACE SCIENCES LABORATORY
THE AEROSPACE CORPORATION
EL SEGUNDO, CALIFORNIA

OUTLINE

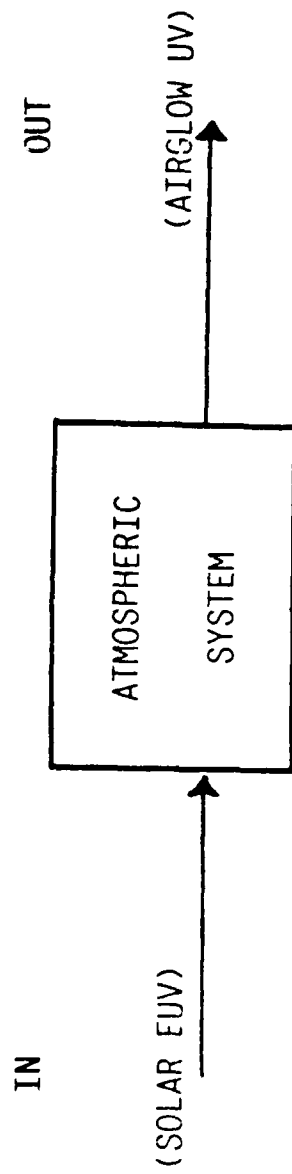
● THE UV ENVIRONMENT OF THE EARTH

● MILITARY REQUIREMENTS

● RAIDS APPROACH

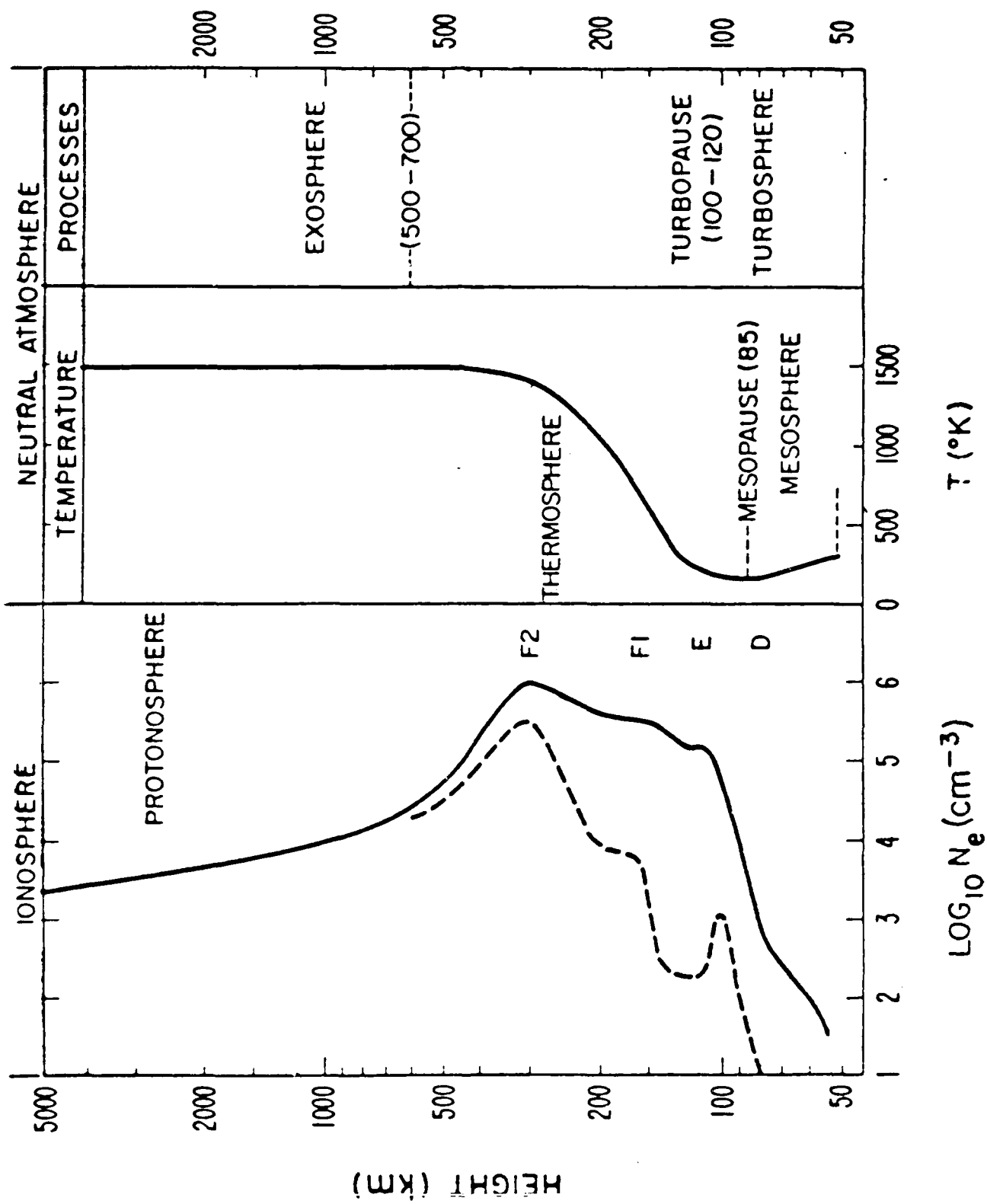


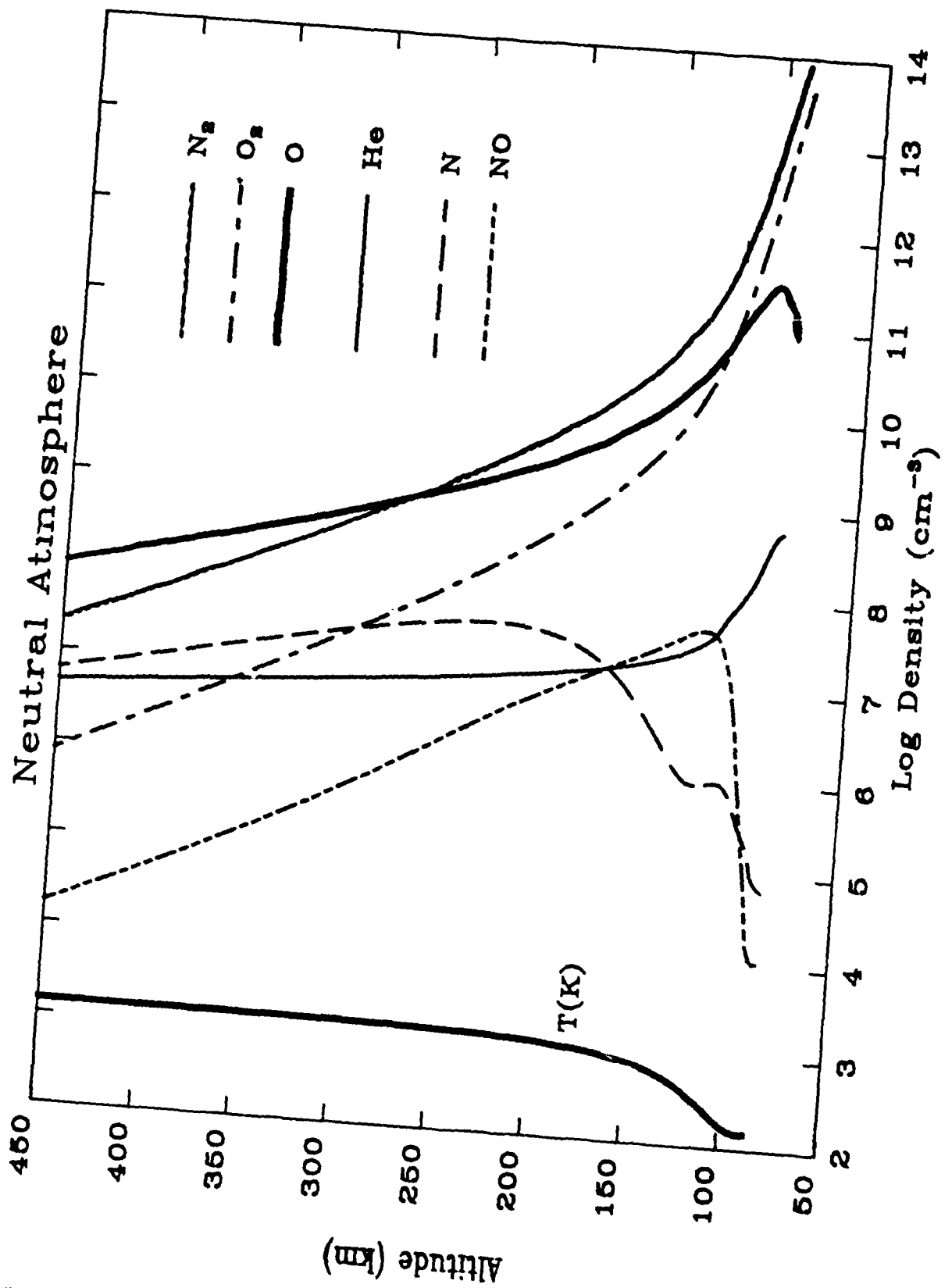
ATMOSPHERE AS A FREQUENCY CONVERTER SYSTEM

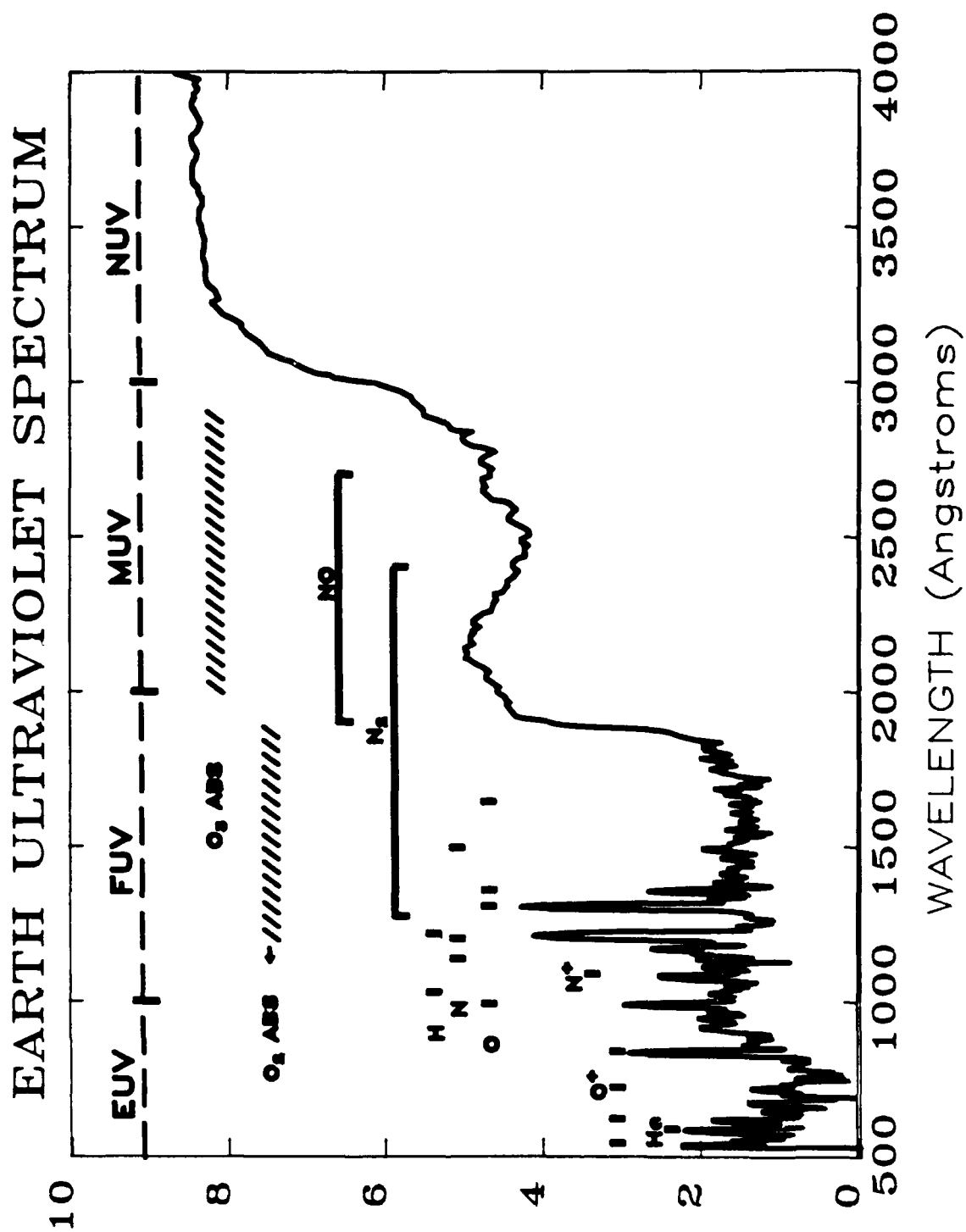


SYSTEM PARAMETERS DETERMINE OUTPUT SPECTRAL AND SPATIAL DISTRIBUTION

- NEUTRAL COMPOSITION
- IONOSPHERIC DENSITIES
- DISTRIBUTION OF MINOR SPECIES
- TEMPERATURE







REMOTE ATMOSPHERIC AND IONOSPHERIC DETECTION SYSTEM

(RAIDS)

- APPLICATION OF NEW TECHNIQUES FOR IONOSPHERIC AND ATMOSPHERIC WEATHER SENSING USING UV DAYGLOW EMISSIONS
- EVOLVING THEORETICAL MODELS STRONGLY SUPPORT UV REMOTE SENSING OF SPACE WEATHER
- STATE-OF-THE-ART SENSORS DEVELOPED
- A MAJOR SPACECRAFT MISSION (RAIDS) HAS BEEN MANIFESTED FOR A TIROS J LAUNCH IN 1991
- RAIDS WILL ACHIEVE NATIONAL SCIENTIFIC PROMINENCE AS THE ONLY IONOSPHERIC-THERMOSPHERIC MISSION IN THE EARLY 1990'S
- A CLEAR TRANSITION TO OPERATIONAL PROGRAM DEFINED: DMSP BLOCK 6 SPACECRAFT (LATE 1990'S)

MILITARY REQUIREMENTS
FOR UPPER ATMOSPHERIC WEATHER CONDITIONS

- MAC 02-80, STATEMENT OF OPERATIONAL NEED (SON) FOR IONOSPHERIC SENSING (IONS)
 - TEC
 - SCINTILLATION
 - ELECTRON DENSITY PROFILES

- MEMORANDUM JOINT CHIEFS OF STAFF (MJCS - 154-86) MILITARY REQUIREMENTS FOR DEFENSE ENVIRONMENTAL SATELLITES

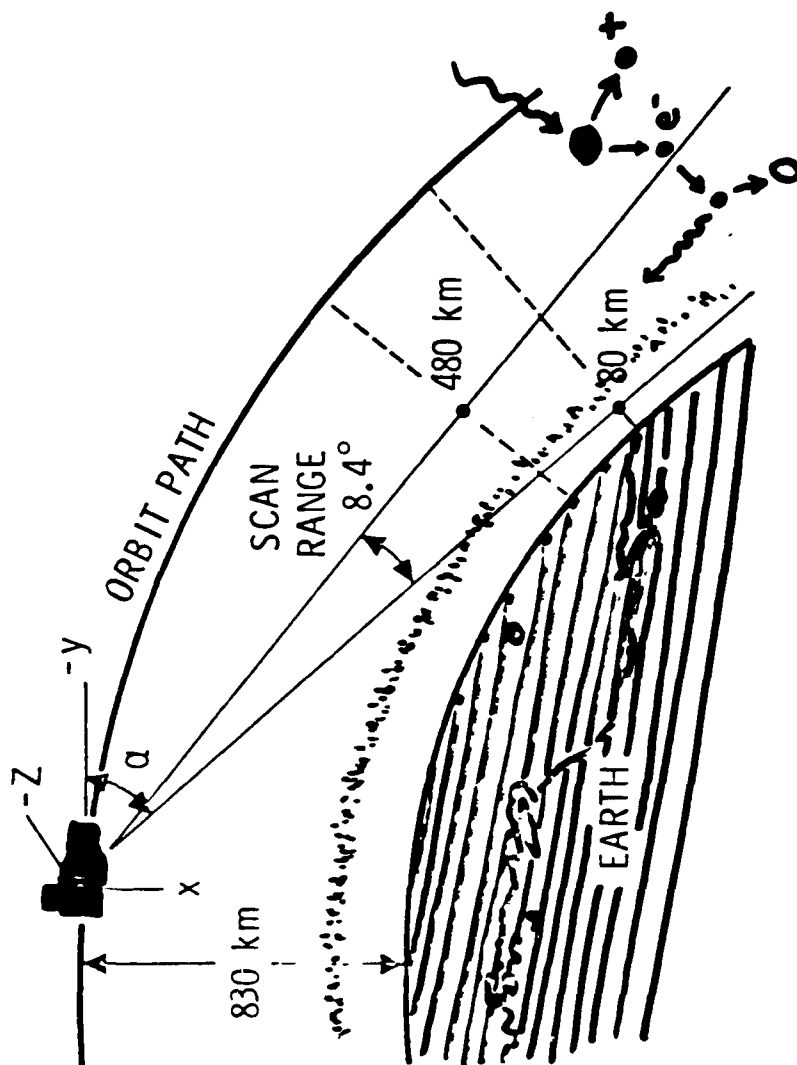
- GEOPHYSICAL REQUIREMENT (GR) 2-87, "NEUTRAL ATMOSPHERIC SPECIFICATION AND PREDICTION"
 - DENSITY, TEMPERATURE, COMPOSITION, WIND
 - ALTITUDE PROFILES 100-1000 KM
 - AURORAL ENERGY INPUT
 - SOLAR DATA
 - OPERATIONAL MODEL

PRIORITIZATION OF MILITARY REQUIREMENTS FOR DEFENSE ENVIRONMENTAL SATELLITES

MJCS 154-86

TO BE MEASURED BY RAIDS:

RANKING	
5	ELECTRON DENSITY PROFILE
12	NEUTRAL DENSITY
18	AURORAL EMISSIONS AND AIRGLOW
24	PRECIPITATING ELECTRONS AND IONS
27	RADIATION BACKGROUNDS
31	IONOSPHERIC SCINTILLATION



ATMOSPHERIC PARAMETERS INFERRED FROM UV DAYGLOW

<u>PARAMETER</u>	<u>EMISSION FEATURE</u>
NEUTRAL COMPOSITION	
N ₂	N ₂ (LBH), 1300 TO 1700 Å (.13-.17 μm)
O ₂	N ₂ (LBH) ABSORPTION
O	OI EMISSIONS, 1356 Å, 1641 Å, 1304 Å, <u>ETC.</u>
NEUTRAL DENSITY, ρ	RAYLEIGH SCATTERING O ₂ (ATMOSPHERIC BAND) 7600 Å
NEUTRAL TEMPERATURE, T	O ₂ (ATMOSPHERIC BAND) N ₂ BANDS (SCALE HEIGHT)
ELECTRON DENSITY PROFILE, N _E	O ⁺ EMISSIONS, 834 Å, 718 Å, <u>ETC.</u>

REMOTE SENSING OBSERVABLES

<u>OBJECTIVE</u>	<u>OBSERVABLE</u>	<u>APPROACH</u>	<u>NEW</u>	<u>SYSTEMS APPLICATIONS</u>
<u>ELECTRON DENSITY</u>				
-DAY	OII 834 A	LIMB SCANS	•	C,P,N,I
-DAY	OII 718,673,617,540 A	LINE RATIOS	•	
-DAY/STORMS	OI 1356, N ₂ LBH	N _e FROM O/N ₂ RATIO	•	
-NIGHT	OI 911,1304,1356 A	N _e FROM I ^{1/2}		
-NIGHT	OI 6300 A	I \propto [O ₂] [N _e]		
-F LAYER HEIGHT	OI 1304,1356 A	HT. FROM LINE RATIO	•	
<u>NEUTRAL COMPOSITION</u>				
-DAY TEMPERATURE	OI 1356,N ₂ LBH,2POS	SCALE HEIGHT		S,R,N,G
-DAY ATOMIC O	OI 1641,1304 A	LINE RATIOS	•	
	OI 1304,1356 A	INTENSITY		
	N ₂ VK BANDS	QUENCHING		
	O ₂ HERZBERG I	O+O	•	
-DAY N ₂	LBH, 2 POS BANDS	EMISSION PEAK	•	
-DAY O ₂	N ₂ LBH BANDS	ABSORPTION		
-NIGHT O	O ₂ HERZBERG I	O+O		
-NIGHT O ₂	OI 6300 A	O ₂ FROM I/N _e	•	
-GLOBAL DYNAMICS	He 584 A	He DENSITY	•	
-AIR DENSITY	RAYLEIGH SCATTERING	LIMB SCANS		
<u>IONIZATION RATES</u>				
-O + h ν	OI 834,617,...	RATE FROM INTENSITY	•	C,P,N,I
-N ₂ + h ν	NI 1085,916 A	RATE FROM INTENSITY		
<u>PHOTOELECTRON FLUXES</u>	N ₂ LBH, 2 POS	COMBINE W. MODEL		
<u>MINOR SPECIES</u>				
	2150 A	NO DENSITY		C,P,S,I,G
	1493, 1743 A	N	•	
	2852, 2798 A	Mg, Mg ⁺	•	
	5890 A	Na		
	IR (NIGHT)	OH		
	NOCTILUCENT CLOUDS	LIMB SCAN		
<u>AURORAS</u>	ALL BANDS	EXCITATION PROCESSES	•	C,P,S,I,N

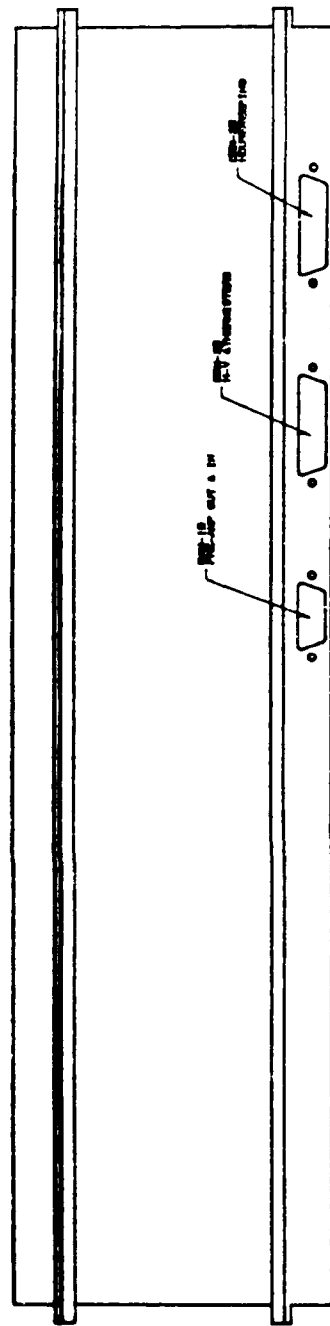
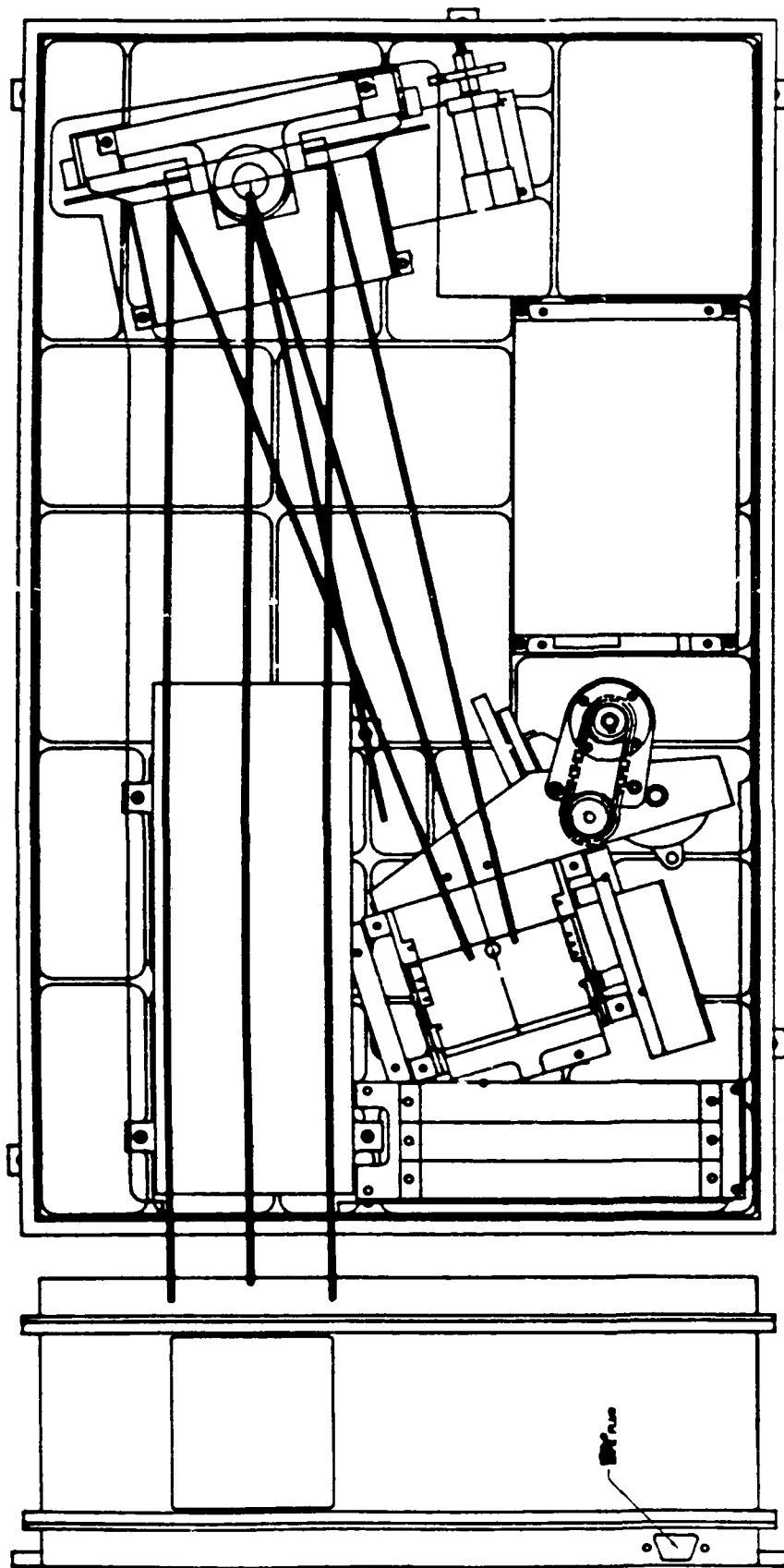
SYSTEMS APPLICATIONS KEY

C - COMMUNICATIONS	R - REENTRY
P - PROPAGATION (OTH,HF)	N - NUCLEAR ENVIRONMENT
S - SURVEILLANCE/BACKGROUNDS	G - GUIDANCE
I - INTELLIGENCE	

RAIDS

EXPERIMENT COMPLEMENT

- MULTISPECTRAL EXTREME UV LIMB IMAGING INSTRUMENT (550-1100 A)
- MULTISPECTRAL FAR UV LIMB IMAGING INSTRUMENT (1250-1700 A)
- MIDDLE UV LIMB SCANNING INSTRUMENT (1900-2971 A)
- NEAR UV LIMB SCANNING INSTRUMENT (3371-4250 A)
- NEAR IR LIMB SCANNING INSTRUMENT (5577-8450 A)
- 3 LIMB SCANNING PHOTOMETERS: 5890, 7774, 6300 A

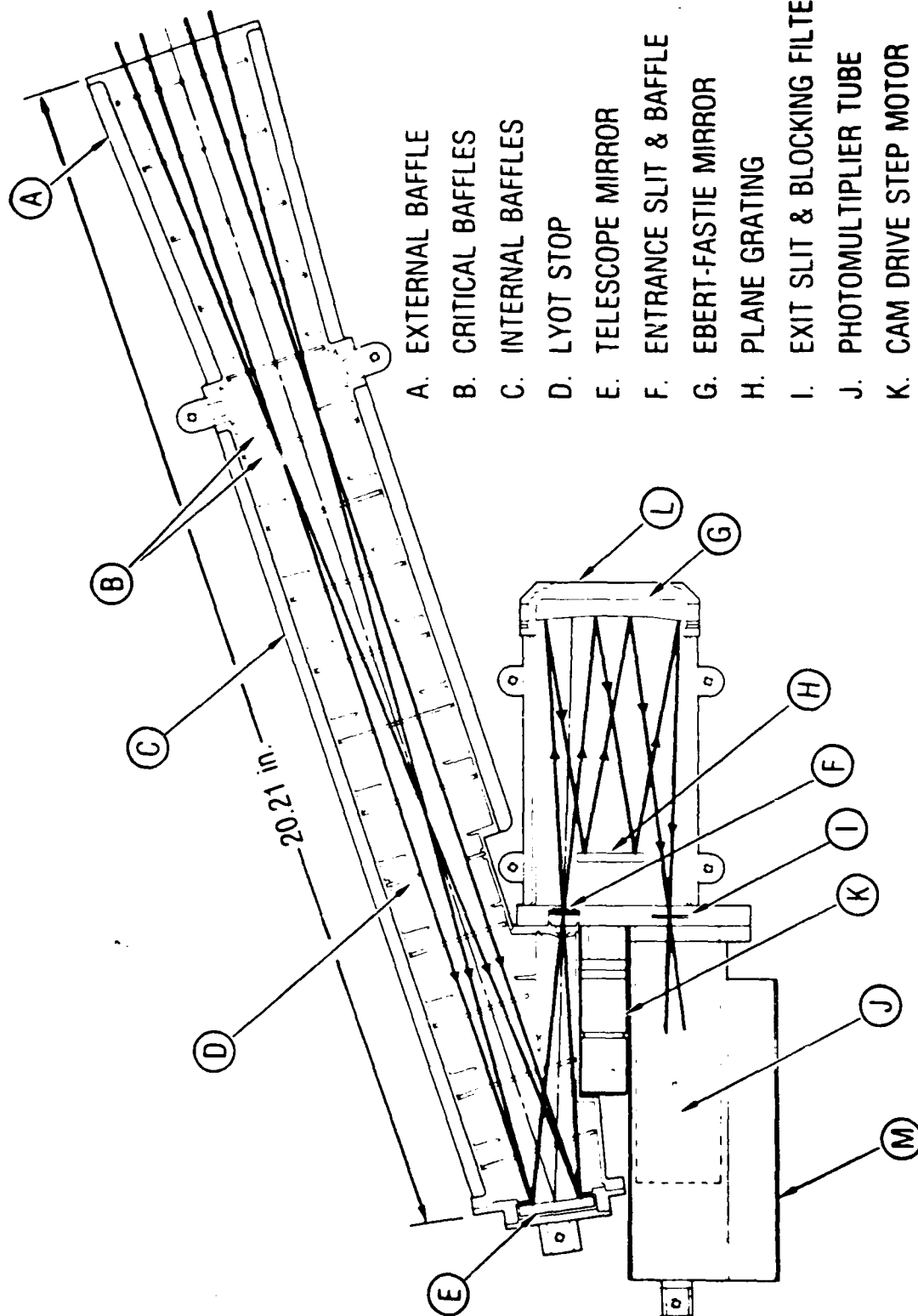


EUVS ASSEMBLY

Reproduced from
best available copy

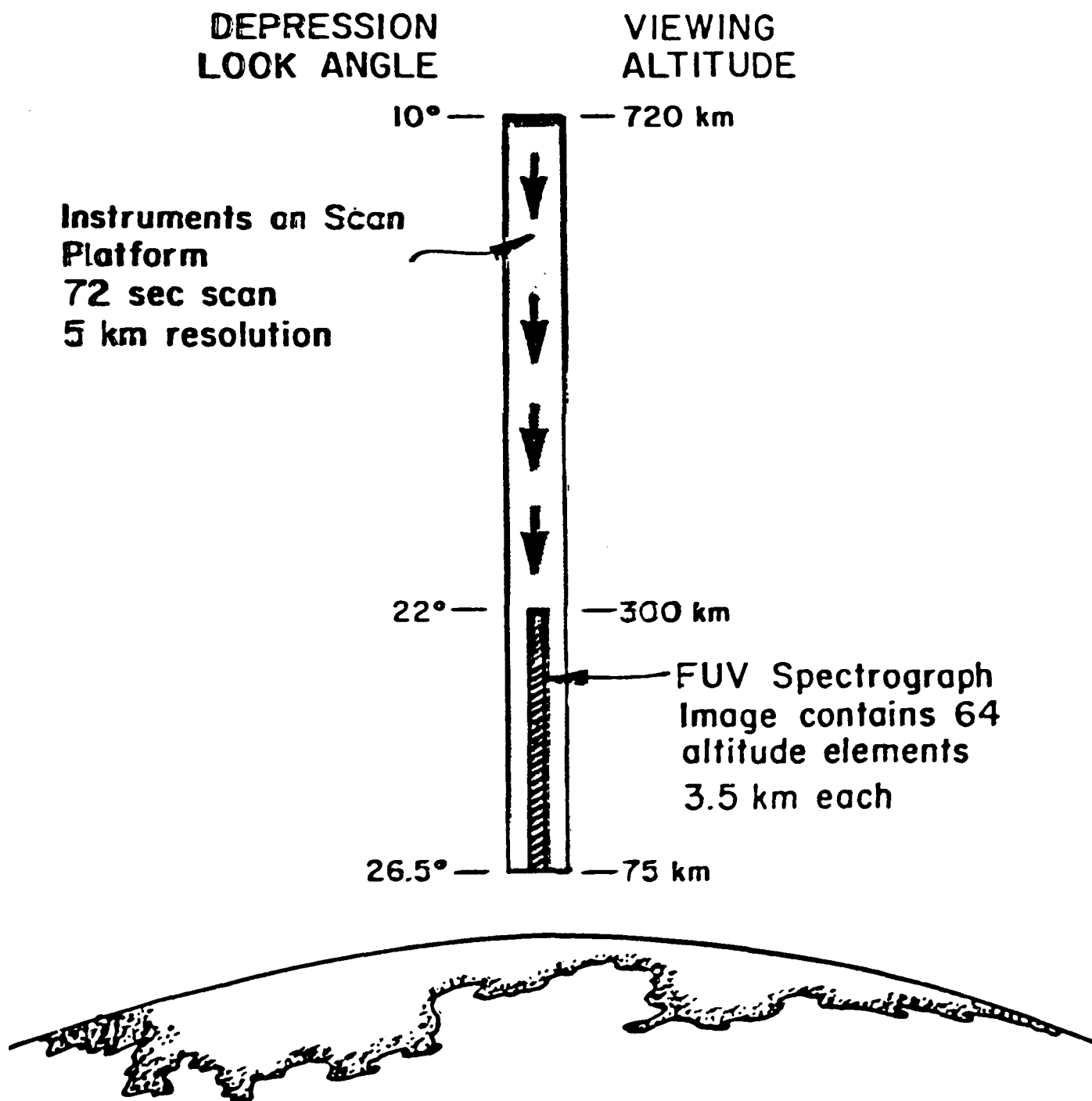


Raids 1/8 Meter Spectrometer System

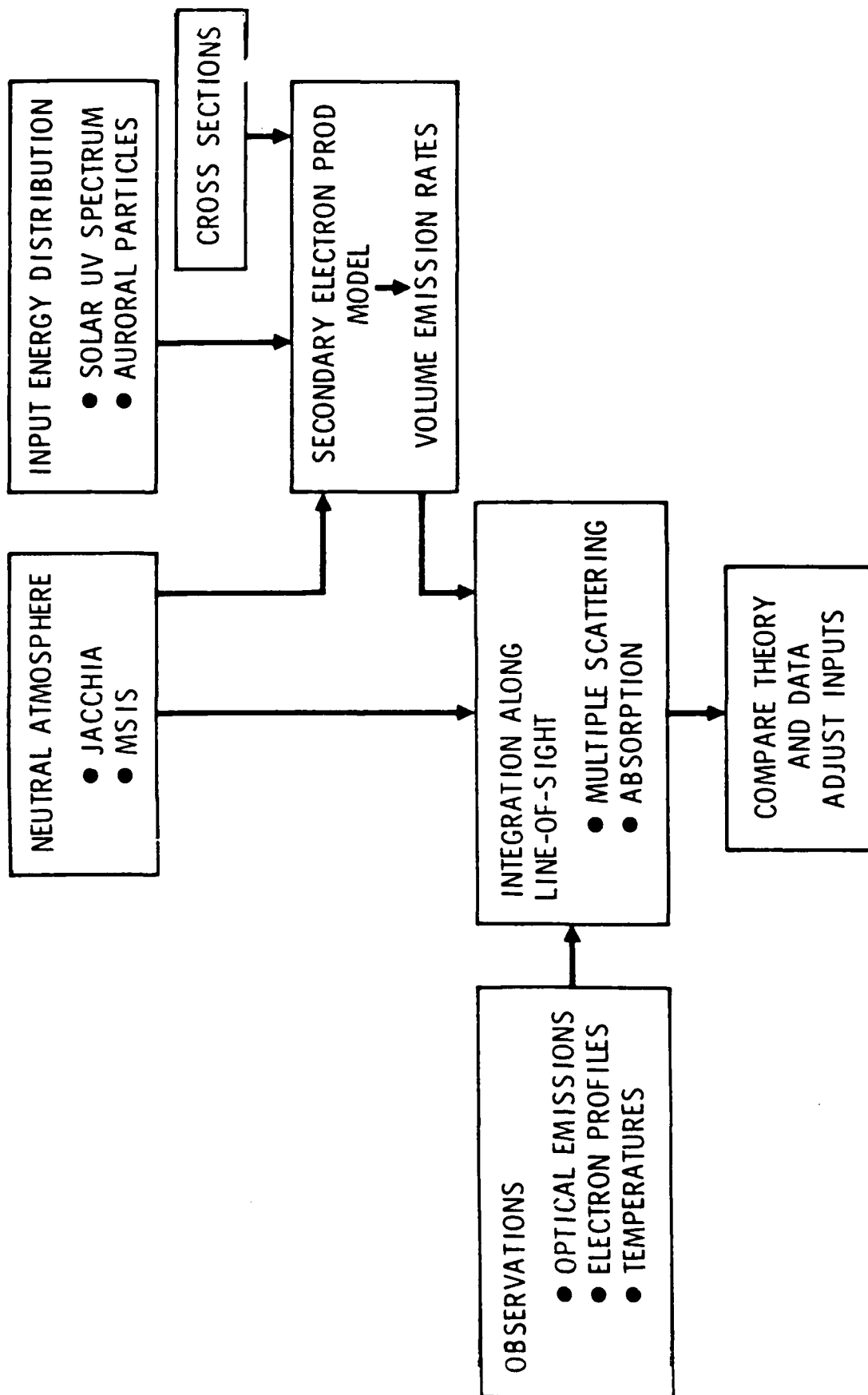


- A. EXTERNAL BAFFLE
- B. CRITICAL BAFFLES
- C. INTERNAL BAFFLES
- D. LYOT STOP
- E. TELESCOPE MIRROR
- F. ENTRANCE SLIT & BAFFLE
- G. EBERT-FASTIE MIRROR
- H. PLANE GRATING
- I. EXIT SLIT & BLOCKING FILTER
- J. PHOTOMULTIPLIER TUBE
- K. CAM DRIVE STEP MOTOR
- L. 1/8 METER SPECTROMETER
- M. HIGH VOLTAGE POWER SUPPLY/
PULSE AMPLIFIER DISCRIMINATOR

RAIDS INSTRUMENTS FIELD-OF-VIEW COMPARISON



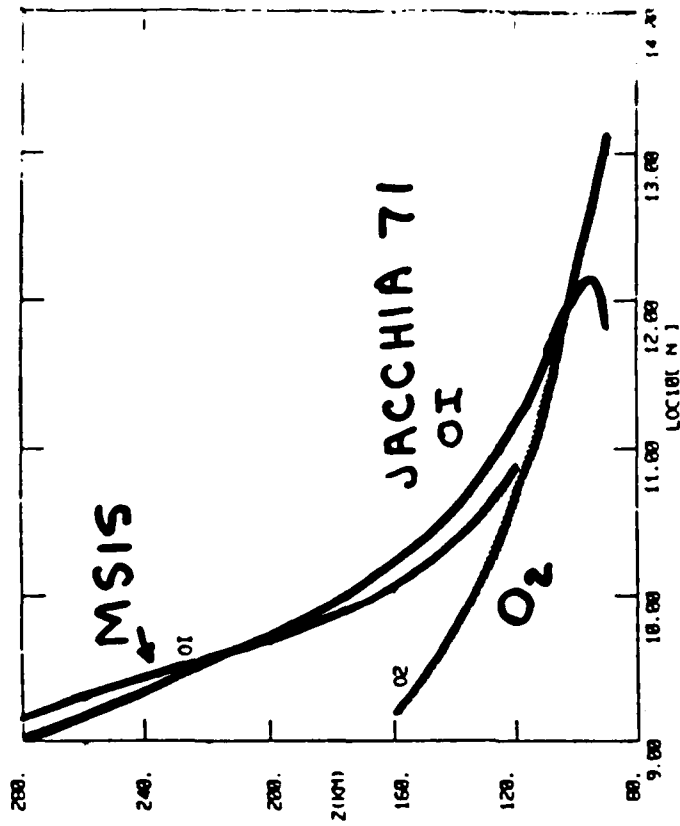
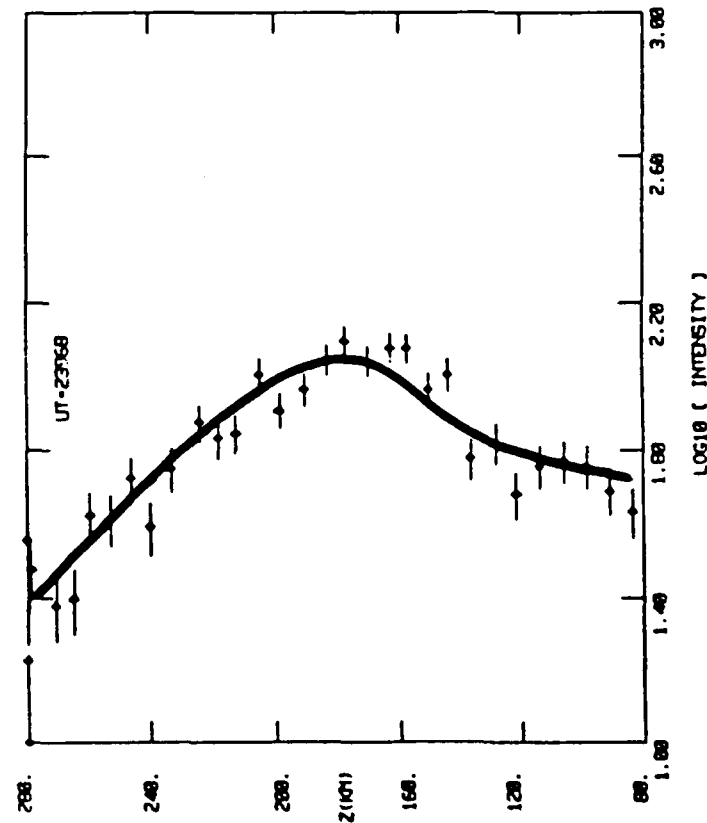
Analysis Scheme



THEORETICAL MODELLING

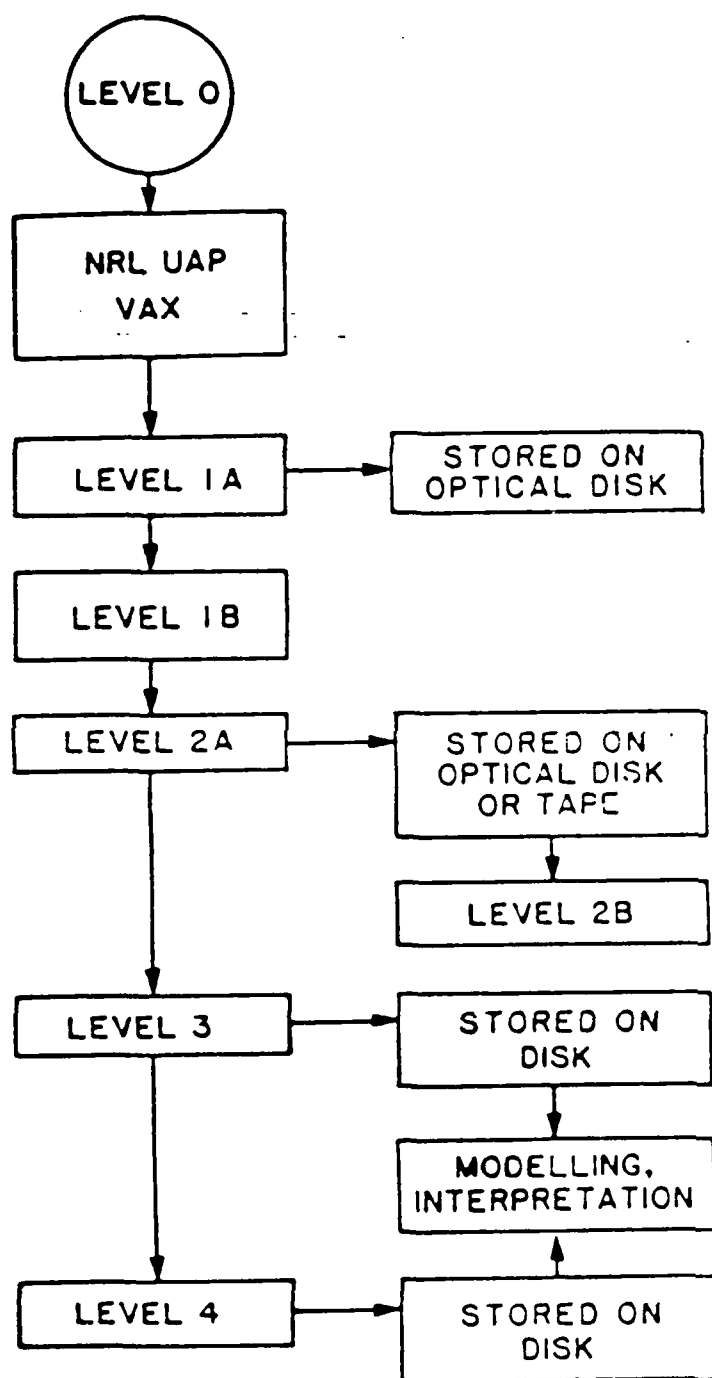
DETAILED PHYSICAL MODELS IN PLACE

- SOLAR SPECTRAL DEFINITION
- EMPIRICAL ATMOSPHERE
- PHOTOELECTRON EXCITATION
- ION CHEMISTRY
- AURORAL ELECTRON TRANSPORT
- INTENSITY/RADIATIVE TRANSPORT
 - OPTICALLY THIN
 - OPTICALLY THICK
 - EXTREMELY THICK
- MOLECULAR SPECTROSCOPY



OXYGEN DENSITIES FROM DMSP-F4 UV DATA

RAIDS DATABASE



- NOAA data tapes stored
- Arrival and timespan (rev#, date, etc.) of NOAA tapes cataloged on a PC AT using Rbase. NOAA tapes converted from IBM format to VAX format.
- Data blocks: Reconstructed time-ordered data
- Averaged, calibrated data (intensity units)
- Maps of observed intensities for selected features: auroral and airglow backgrounds
- 2A may be further condensed to minimize storage space or act as a browse file
- Emission rates, density profiles, atmospheric composition
- Scientific analysis
- "Final" product as maps TEC, f_oF2 , H_{max} , n_{max} , electron, ion and neutral temperatures.

RAIDS ORGANIZATIONS

NRL	-	PRINCIPAL INVESTIGATORS
SSL, AEROSPACE CORPORATION	-	CO-INVESTIGATORS
SPACE TEST PROGRAM	-	INTEGRATION
AEROSPACE CORPORATION	-	THERMAL, MECHANICAL MODELS
NASA	-	SPACECRAFT MANAGERS
NOAA	-	TIROS SPACECRAFT PROGRAM
RCA	-	SPACECRAFT CONTRACTORS
AFSD	-	DMSP SUPPORT AT NRL AND SSL

REMOTE ATMOSPHERIC & IONOSPHERIC DETECTION SYSTEM (RAIDS)

COMBINING:

- RECENTLY DEVELOPED SCIENTIFIC TECHNIQUES

WITH

- AN UNPRECEDENTED ARRAY OF STATE-OF-THE-ART INSTRUMENTATION

AND

- A HIGH-SPEED, IMAGE-BASED DATA ANALYSIS APPROACH

FOR THE RAPID DETERMINATION OF ATMOSPHERIC & IONOSPHERIC DENSITIES & TEMPERATURES

UPPER ATMOSPHERIC DENSITY SPECIFICATION

RECOMMENDATIONS

- ENCOURAGE FURTHER DEVELOPMENT OF DYNAMICAL MODELS
- FOSTER RESEARCH IN SPACE-BASED AND GROUND-BASED TECHNIQUES
- PROMOTE THE SPACE FLIGHT OF REMOTE SENSING AND IN-SITU INSTRUMENTATION
- BEGIN TO CREATE AN UPPER ATMOSPHERIC DATA BASE INCLUDING MEASURED INPUTS OF THE MAJOR ENERGY SOURCES

SESSION 4

SUMMARY AND RECOMMENDATIONS

DR JOSEPH J. F. LIU
CHAIRMAN

SUMMARY OF THE NEUTRAL DENSITY CONFERENCE

by Dr H. Beat Wackernagel
Hq Space Command/Directorate of Operations Analysis

This afternoon Lieutenant Colonel George Davenport and I will summarize what we have heard at this conference. Colonel Davenports summary will be from the perspective of the purveyor of atmospheric data, while I will deal with the same matter from the perspective of the consumer (or user) of atmospheric data. In addition there will be a recapitulation of action-items as we heard them - corrections from the floor are welcome!

The user has the task of calculating satellite orbits, both in terms of determining the orbit on the basis of observations and environmental data (establishing past positions), as well as the task of calculating predictions of future positions of the satellite. For doing this the user needs those data which are called for by the model (or models) for the calculation of both, the past, and future satellite positions.

Computational Efficiency.

In the presentation by Capt de la Barre computational efficiency was mentioned as one of the requirements. Since this aspect is sometimes not fully appreciated by the model-building community, I will take this occasion to elaborate and to provide some numbers.

The total catalog contains some 19,000 satellites of which 7,300 are in orbit today, while the others have decayed. Hence, the number of satellites the computing center has to handle - on a real-time basis - is a thousandfold more than the handful of satellites used in a research project.

The data influx is presently in the vicinity of 50,000 to 60,000 observations per day, seven days per week. For planning purposes use 100,000 per day, which means an average of about one observation per second - 24 hours a day. In a realtime system you may not fall behind - the data must be processed as they flow into the system. In a favorable case each observation is processed twice: a first time to verify the identification, so that it can be placed into the correct data file and a second time for calculating an improved orbit. In the case of an untagged or mistagged observation, the computational effort is vastly higher. Because of computational limitations only about one or two percent of the satellites are maintained with Special Perturbations (including a full atmospheric density model). Density information is required at each integration step for each iteration in the improvement process for each satellite. Conjectures for such numbers are:

2000 x 5 x 100 = a million.

Because many other activities must go on concurrently in a realtime system, only a small fraction, perhaps two percent, of the computing resources can be devoted to neutral atmospheric density calculations; that comes to perhaps 2000 seconds per day during which a million requests must be serviced; that divides out to two milliseconds per request. If the entire catalog is to be serviced, that number is hundred times smaller, namely only 20 microseconds.

Hence, in addition to better accuracy, the software of the next model must be computationally efficient in the way it is operationally implemented. An available option might be to evaluate the model once every few hours and store the results in tables from which the data can be retrieved more rapidly; however there are important limitations as to the size of available storage areas.

Additional, data retrieval algorithms assessing large data bases require non-trivial amounts of machine time. This is clearly an area where some trade-offs have to be studied quite carefully.

SUMMARY, ACTION ITEMS, AND SUBSEQUENT EVENTS

Lt Col George R. Davenport
Headquarters 4th Weather Wing
(Now at Science Applications International Corporation)

The existing procedures for specifying and predicting the atmospheric neutral density at satellite altitudes leave a great deal to be desired. Air Weather Service just reports the observations that describe the environment, and the various customers enter these input data into their own atmospheric neutral density models. Each customer uses these observed data to execute the model that has been installed on its computer system; the model may or may not generate output that really satisfies the customer's needs.

Air Weather Service should be providing customers with the output from the best possible atmospheric neutral density model rather than input observations. Rather than merely relaying observed environmental parameters for the customers to input into their own models, the appropriate procedure would be for Air Weather Service to provide the various customers with the parameters that they really need, the actual specification or prediction of the atmospheric neutral density at satellite altitudes.

For Air Weather Service to assume responsibility for executing the optimum atmospheric neutral density model will require a fundamental change in the way that Air Weather Service and the customer, in this case Air Force Space Command, conduct business. Currently Air Weather Service forwards to Air Force Space Command a standardized message, including the observed and predicted 2800 MHz, 10.7 centimeter wavelength solar radio flux (the Ottawa Flux or F₁₀), the 90-day mean F₁₀, and the observed and predicted geomagnetic index A_p; Air Force Space Command extracts appropriate parameters from the Air Weather Service message for input into the Jacchia 64 atmospheric neutral density model resident on the computer system inside Cheyenne Mountain; finally Air Force Space Command uses the output from the Jacchia 64 model to carry out drag computations. In the future, Air Weather Service will accumulate all of the best possible observed and forecast environmental parameters; these data will be input into a state-of-the-art atmospheric neutral density model that Air Weather Service will execute at the new Space Forecast Center, which is to be established at Falcon AFS; Air Weather Service will transmit relevant model output parameters from the Space Forecast Center to Air Force Space Command in Cheyenne Mountain; and Air Force Space Command will use the atmospheric neutral density output from the Air Weather Service model to compute the drag on its highest interest satellites.

Air Force Space Command is the primary driver for improvements in the capability to specify and predict the atmospheric neutral

density and for the development of an improved atmospheric neutral density model. The Air Force Space Command Directorate of Astrodynamics initially stated the command's requirements in a letter to the 4th Weather Wing Aerospace Sciences Division on 21 May 1986. On 25 May 1988, the Air Force Space Command Deputy Chief of Staff for Plans elevated and reinforced the command's requirements in correspondence to his counterparts at Military Airlift Command and Air Force Systems Command; he forwarded a letter from the United States Space Command Director of Operations that stated refined requirements for improved density models. Such specific articulated requirements motivated Air Weather Service to develop an improved capability to specify and predict the atmospheric neutral density at satellite altitudes.

The Air Force Geophysics Laboratory is about to award a contract for advanced development of the Vector Spherical Harmonics model, a derivative of the highly sophisticated Thermospheric - Ionospheric General Circulation Model that was developed at the National Center for Atmospheric Research. Military Airlift Command will award a contract for operational software development soon after the advanced development effort begins. This operational software development will ensure that the Space Forecast Center can execute the Vector Spherical Harmonics model efficiently and that it will generate products that customers, such as Air Force Space Command, can use effectively.

At this Atmospheric Neutral Density Specialist Conference, representatives from Air Weather Service and Air Force Space Command agreed that they should begin a dialogue to work out the interface between the new model's output and the customer's input. This dialogue has begun and must continue throughout operational software development to ensure that the new model offers a quantifiable improvement over the older Jacchia models and that it is computationally efficient.

Other related studies continue as the new model advanced development and operational software development proceed. For example, Air Weather Service continues to search for an improved capability to predict the solar radio flux, the Ottawa Flux (F_{10}), and the geomagnetic index, A_p , that remain the primary inputs to currently operational atmospheric neutral density models. Air Weather Service also continues to monitor the continued availability of the Ottawa Flux in light of repeated threats by the Canadian National Research Council to close down the Algonquin Observatory where the world standard F_{10} is measured each day.

The conference participants seemed pleased with the presentations, discussion, and progress made during this conference. In fact, during the closing session it was suggested that a meeting or a conference such as this one should be convened on a periodic and recurring basis, perhaps annually. One specific goal for a future meeting of this nature could be to investigate the availability and the possibility of sharing databases.

DISTRIBUTION LIST

22 MARCH 1988

Mr Norm Baker
HQ 4th Weather Wing/DN
Stop 13
Peterson AFB, CO 80914-5001
(719) 554-4856
AV 692-4856

Capt Leslie Belisma
SD/CWDA, OL-F, AWS
PO Box 92960
Los Angeles, CA 90009-2960
AV 833-1732

*Dr Albert Bevan
HQ AFSPACECOM/XP
Stop 7
Peterson AFB, CO 80914-5001
(719) 554-3802
AV 692-3802

*Lt Col John S. Bohlson
OL-F, AWS
PO Box 92960
Los Angeles, CA 90009-2960
AV 833-2482

Capt Stacy Brodzik
HQ USSPACECOM/J3SOS
Stop 4
Peterson AFB, CO 80914
(719) 473-4010 x3185
AV 834-1211 x3185

*Mr Jerry W. Brown
HQ USSPACECOM/AND
Stop 7
Peterson AFB, CO 80914-5001
(719) 554-3945
AV 692-3945

*Capt Mark Clausen
Air Force Global Weather Central
AFGWC/WSE
Offutt AFB, NE 68113
AV 271-2968

*Dr Rich Chappel
MSFC
Huntsville, AL 35812
(205) 544-3033

Dr Andrew B. Christensen
The Aerospace Corporation
Mail Stop M2-255
PO Box 92957
Los Angeles, CA 90009

*Mr John Clark
HQ AFSPACECOM/DOAA
Stop 7
Peterson AFB, CO 80914
(719) 554-5196
AV 692-5196

*Capt Matteo Colello
AFSCF/WE, Det 3, AWS
PO Box 3430
Sunnyvale AFS, CA 94088-3430
AV 359-3902

*Maj Marv Coleman
AFGWC/WSE
Offutt AFB, NE 68113

Maj David Cooke
HQ AFSPACECOM/DOS
Stop 7
Peterson AFB, CO 80914-5001
(current address not available)

Dr Anthea Coster
Millstone Hill Radar
MIT Lincoln Laboratory
PO Box 73
Lexington, MA 02173-0073
AV 757-2270

*Col Harry Culbertson
HQ USSPACECOM/J3S
Stop 4
Peterson AFB, CO 80914-5001
(719) 473-4010 ext 3004
AV 834-1211 ect 3004

Lt Col George Davenport (Ret)
SAIC
2860 South Circle Drive, Suite 2400
Colorado Springs CO 80906
(719) 576-2181

Capt Colette de la Barre
USAFA/DFAS
Department of Astrodynamics
USAFA, CO 80840-5701

*Col John W. Dierks
AFGWC/CC
Offutt AFB, NE 68113

*Col David L. Donley
AWS/DN
Scott AFB IL 62225-5008
AV 576-5879

Capt Richard L. Fennessey
HQ AFSPACECOM/DOAS
Stop 7
Peterson AFB, CO 80914-5001
(719) 554-5464
AV 692-5464

Dr Michael Ganoschkin
MIT Lincoln Laboratory
PO Box 73
Lexington, MA 02173
AV 757-2270

Lt Reynal Guillen
HQ 4 WW/WL, Stop 4
Peterson AFB, CO 80914-5001
(719) 473-4010 x3377
AV 834-1211 x3377

*Col Peter J. Havanac
Det 3, AWS/CC
PO Box 3430
Sunnyvale AFS, CA 94088-3430
AV 359-3902

*Dr Paul B. Hays
Space Physical Research Laboratory
University of Michigan
2455 Hayward
Ann Arbor, Michigan 48109-2143
(313) 764-7220

Mr Gary Heckman
NOAA R/E/SE2
(Space Environment Services Center
Space Environment Laboratory)
325 Broadway
Boulder, CO 80303
(303) 497-5687

Dr Al Hedin
Code 614
GSFC
Greenbelt, MD 20771
(301) 286-8393

*Dr Ernest Hildner
Space Environment Laboratory
325 Broadway
Boulder, CO 80303
(303) 497-3311

Dr Jack Horvath
The University of Michigan
Space Physics Research Laboratory
Space Research Building
2455 Hayward
Ann Arbor, Michigan 48109-2143

Mr Dale Johnson/Dr Robert Smith/Dr Mike Hickey
MSFC/ED44
Huntsville, AL 35812
(205) 544-1665

Maj Kaneshiro
Det 1, 4 WW/CC
Stop 82
Falcon AFB, 80912-5000
(719) 550-4685
AV 560-4685

*Mr Bernard Kaufman
Code 8103
Advanced Concept Office
Naval Research Laboratory
Washington, D.C. 20375
(202) 767-2611,
AV 297-2611

Mrs Denise Kaya
HO AFSPACECOM/DOAS
Stop 7
Peterson AFB, CO 80914-5001
(719) 554-5851
AV 692-5851

Dr David Kayser
The Aerospace Corporation
Mail Stop M2-256
PO Box 92957
Los Angeles, CA 90009

Dr Stephen H. Knowles
Code 02, NAVSPASUR
Dahlgren, VA 22448
AV 249-8191

Dr Joseph J. F. Liu
HQ AFSPACECOM/DOAS
Stop 7
Peterson AFB, CO 80914-5001
(719) 554-5467
AV 692-5467

Mr Frank Marcos
AFGL/LIS
Hanscom AFB, MA 01731
(617) 377-3037
AV 478-3037

*Col James McDonough
HQ AFSPACECOM/DOS
Stop 7
Peterson AFB, CO 80914-5001
(719) 554-5486
AV 692-5486

*Mr Robert Morris
HO AFSPACECOM/DOA
Stop 7
Peterson AFB, CO 80914-5001
(719) 554-5462
AV 692-5462

*Col Vito Pagano
HO AFSPACECOM/XPS
Stop 7
Peterson AFB, CO 80914-5001

Capt Stephen Patterson
HO AWS/XTPP
Scott AFB, IL 62225-5008
AV 576-4858

Maj Jeanine Paul
HO USSPACECOM/J3SO
Stop 4
Peterson AFB, 80914-5001
(719) 473-4010 x3290
AV 834-1211 x3290

Col Gene J. Pfeffer
HQ 4 WW/CC
Stop 13
Peterson AFB, CO 80914-5001

Dr Russ C. Philbrick
Prof, Electric Engineering
Communication and Space Sciences Laboratory
315 Electrical Engineering East
The Pennsylvania State University
University Park, PA 16802
(814) 865-6337

Dr Ray G. Roble
HAO/NCAR
Box 3000
Boulder, CO
(303) 497-1562

*Lt Col Sharkey
HO USSPACECOM/J3SOS
Stop 4
Peterson AFB, CO 80914-5001

Dr Paul W. Shumacher
Code 02, NAVSPASUR
Dahlgren, VA 22448
AV 249-8191

Mr Robert Skrivanek
AFGL/LI
Hanscom AFB, MA

*Mr Jack Slowey
SAO
60 Garden St
Cambridge, MA 02138
(617) 495-7214

Mr Daniel Snow
HQ AFSPACECOM/DOA
Stop 7
Peterson AFB, CO 80914-5001
(719) 554-5866
AV 692-5866

Dr Joe Straus
The Aerospace Corporation
Mail Stop M2-256
PO Box 92957
Los Angeles, CA 90009
(213) 336-8182

CAPT John L. Sullivan, USN
HO USSPACECOM/J3S
Stop 35
Peterson AFB, CO 80914-5001

Col Eric Sundberg
Space Chair AWC/DFX
Maxwell AFB, AL 36112-5522
(205) 293-2407
AV 875-2407

Capt Mark F. Storz
Det 1, 4 WW/CC
Stop 82
Falcon AFB, CO 80912-5000

*Col John H. Taylor
3WW/CC
Offutt AFB, NE 68113-5000
AV 271-3706

Maj Howard Tilton
HQ USSPACECOM/J3SO
Stop 4
Peterson AFB, CO 80914-5001

Capt Christopher Tschan
AWS/DNXP
Scott AFB, IL 62225-5008
AV 576-4781

Mr E. S. Van Inwegen
TRW
1 Ocean Park (R-112313)
Redondo Beach, CA 90278

Dr H. Beat Wackernagel
HQ AFSPACECOM/DOA
Stop 7
Peterson AFB, CO 80914-5001
(719) 554-3594
AV 692-3594

Dr William J. Wagner
Space Environment Laboratory
R/E/SE
325 Broadway
Boulder, CO 80303
(303) 497-3274

Dr Richard Walterscheid
The Aerospace Corporation
Mail Stop M2-256
PO Box 92957
Los Angeles, CA 90009
(213) 336-7352

Dr J. H. Yee
The University of Michigan
Space Physics Research Laboratory
Space Research Building
2455 Hayward
Ann Arbor, Michigan 48109-2143
(313) 747-3590

Lt Col Thomas Yechout
USAFA/DFAN
Department of Aeronautics
USAFA, CO 80840-5701
(719) 472-4010

Mr C. T. Yue
HQ AFSPACECOM/DOAS
Stop 7
Peterson AFB, CO 80914-5001
(719) 554-5785
AV 692-5785

* Did not attend conference